

This item was submitted to Loughborough University as a PhD thesis by the author and is made available in the Institutional Repository (<https://dspace.lboro.ac.uk/>) under the following Creative Commons Licence conditions.



For the full text of this licence, please go to:  
<http://creativecommons.org/licenses/by-nc-nd/2.5/>

**Pilkington Library**

Author/Filing Title ..... SWEETLAND, L.A. .....

Accession/Copy No. .... 040160737 .....

Vol. No. ....

Class Mark .....

LOAN COPY

0401607372






**Adsorption of Organic Micropollutants from Water  
Using Hypersol-Macronet™ Polymers**

by

Lee A. Sweetland

A Doctoral Thesis submitted in partial fulfilment of the requirements  
for the award of Doctor of Philosophy of Loughborough University

September 1997

|                                                                                     |                                    |
|-------------------------------------------------------------------------------------|------------------------------------|
|  | <b>Loughborough<br/>University</b> |
| P.                      rary                                                        |                                    |
| Date                                                                                | Mar 98                             |
| Class                                                                               |                                    |
| Acc<br>No                                                                           | 060160737                          |

K 0630802

## ABSTRACT

Hypersol-Macronet™ polymers have been evaluated for the adsorption of organic pollutants from aqueous solution. The adsorption performance of the polymers was compared with a commercial activated carbon, Chemviron F-400. Investigation into the physical structure of the adsorbents was performed using microscopy and the adsorption of nitrogen at liquid nitrogen temperatures. A critical analysis of the adsorption isotherm data reduction models is given. The polymers possess a bimodal pore size distribution of micropores, approximately 13Å in diameter, and macropores, greater than 200Å. The surface functionality of the Macronets, determined by diffuse reflectance IR, <sup>13</sup>C NMR and X-ray photoelectron spectroscopy, is presented. Elemental analysis and direct titration techniques were also investigated. Relatively high concentrations of oxygen containing functional groups were observed on the polymers, attributed to ethers, alcohols and ketones formed during polymer production. Adsorption isotherms are given for the removal of phenol and three chlorophenols substituted in the ortho, meta and para position. The greater hydrophobicity of the chlorinated phenols resulted in stronger interaction energies and larger adsorption capacities. Batch kinetic data for the above adsorbates was modelled using the homogeneous surface diffusion correlations.

Analytical techniques were developed and validated for the determination of trace levels (0.1 parts per billion) of five pesticides; atrazine, simazine, isoproturon, diuron and chlorotoluron. Single and multi-component adsorption isotherms are presented for trace concentrations of pesticides in aqueous solution. Mini-column breakthrough curves are presented for MN-200 and F-400. Selectivity of the polymers for the various pesticides was explained by differences in molecular size and the hydrophobicity of the adsorbates. The primary adsorption mechanism is hydrophobic interaction enhanced by hydrogen bonding. The negative influence of natural organic matter (NOM) on the removal of pesticides was investigated using batch and column techniques. The uptake of NOM on activated carbon is much greater than that on MN-200. Total regeneration of MN-200 using a variety of organic solvents was achieved for high and low solid phase concentrations of pesticides. Regeneration of F-400 was ineffective. The breakthrough point of a regenerated mini-column containing MN-200 was identical to the virgin polymer data. The potential commercial application of the resin for the purification of drinking water is discussed.

## ACKNOWLEDGEMENTS

The completion of this thesis in less than three years reflects upon the excellent support and encouragement of my supervisor, Michael Streat. His discussions and guidance were greatly appreciated. My sincerest thanks go to my father for his advice during my studies.

I would like to thank Jim Dale and Kevin Blaxall, of Purolite International Ltd, for their financial support of the project and enabling me to spend an invaluable eight week period working at the production facility in Pontyclun. I also acknowledge the financial support of EPSRC.

Thanks to my colleagues in the adsorption technology group who have made my studies an enjoyable experience. Special thanks go to Daniel Horner who continued the mini-column experimentation during the last three months of my studies. Thanks also to Andrzej Trochimeczuk, with whom I had many invaluable discussions.

Finally, I would like to acknowledge the following people

- Ian Sutherland of the Chemistry Department for the use of their infra-red spectrophotometer.
- Bob Bradley, formally of ISST, for the XPS data.
- David Sherrington from the University of Strathclyde for the elemental analysis data.
- Barbara Gore from UMIST for the solid state  $^{13}\text{C}$  NMR data.
- The academic and technical staff in the Chemical Engineering Department.

# CONTENTS

|                            |                                                           |           |
|----------------------------|-----------------------------------------------------------|-----------|
| Abstract                   |                                                           | i         |
| Acknowledgements           |                                                           | ii        |
| Certificate of Originality |                                                           | iii       |
| List of Figures            |                                                           | vii       |
| List of Tables             |                                                           | x         |
| <b>CHAPTER 1</b>           | <b>INTRODUCTION</b>                                       | <b>1</b>  |
| Section 1.1                | General Introduction                                      | 1         |
| Section 1.2                | Research Objectives                                       | 2         |
| Section 1.3                | Hypersol-Macronet Polymers                                | 3         |
| Section 1.4                | References                                                | 7         |
| <b>CHAPTER 2</b>           | <b>PHYSICAL CHARACTERISATION</b>                          | <b>9</b>  |
| Section 2.1                | Introduction                                              | 9         |
| Section 2.2                | Literature Review                                         | 9         |
| Section 2.3                | Experimental Parameters                                   | 19        |
|                            | Microscopy                                                | 19        |
|                            | Surface Area and Pore Size Distributions                  | 19        |
| Section 2.4                | Results and Discussions                                   | 20        |
|                            | Microscopy                                                | 20        |
|                            | Nitrogen Adsorption Isotherms and Pore Size Distributions | 28        |
| Section 2.5                | Conclusions                                               | 41        |
| Section 2.6                | References                                                | 42        |
| <b>CHAPTER 3</b>           | <b>CHEMICAL CHARACTERISATION</b>                          | <b>47</b> |
| Section 3.1                | Introduction                                              | 47        |
| Section 3.2                | Theory and Literature Review                              | 47        |
| Section 3.3                | Experimental Parameters                                   | 53        |
|                            | Diffuse reflectance infra red spectroscopy                | 53        |
|                            | X-ray photoelectron spectroscopy                          | 54        |
|                            | Solid State Nuclear Magnetic Resonance Spectroscopy       | 54        |
|                            | Direct Titration                                          | 54        |
|                            | Elemental Analysis                                        | 55        |
|                            | Zeta Potential Analysis                                   | 55        |
| Section 3.4                | Results and Discussions                                   | 56        |
|                            | Diffuse reflectance infra red spectroscopy                | 56        |
|                            | X-ray photoelectron spectroscopy                          | 62        |
|                            | Elemental Analysis                                        | 63        |
|                            | Solid State Nuclear Magnetic Resonance Spectroscopy       | 65        |
|                            | Direct Titration                                          | 69        |
|                            | Zeta Potential Analysis                                   | 71        |
|                            | General Discussion                                        | 71        |
| Section 3.4                | Conclusions                                               | 73        |
| Section 3.5                | References                                                | 74        |
| <b>CHAPTER 4</b>           | <b>PHENOLS ADSORPTION</b>                                 | <b>77</b> |
| Section 4.1                | Introduction                                              | 77        |
| Section 4.2                | Theory of Adsorption and Literature Review                | 77        |
|                            | Phenols Adsorption                                        | 85        |
| Section 4.3                | Experimental Parameters                                   | 90        |



|                  |                                                                               |            |
|------------------|-------------------------------------------------------------------------------|------------|
|                  | Equilibrium and kinetic sorption studies                                      | 93         |
|                  | Effect of the agitation rate on the kinetics of removal for phenol            | 93         |
|                  | Effect of the adsorbent particle size on the kinetics and capacity for phenol | 94         |
|                  | Effect of the adsorption temperature on the kinetics and capacity for phenol  | 94         |
| Section 4.4      | Results and Discussion                                                        | 95         |
|                  | Adsorption Isotherms                                                          | 95         |
|                  | Adsorption Kinetics                                                           | 100        |
| Section 4.5      | Conclusions                                                                   | 109        |
| Section 4.6      | References                                                                    | 111        |
| <b>CHAPTER 5</b> | <b>PESTICIDES ADSORPTION</b>                                                  | <b>115</b> |
| Section 5.1      | Introduction                                                                  | 115        |
| Section 5.2      | Background Information and Literature Review.                                 | 116        |
|                  | Pesticides                                                                    | 116        |
|                  | Natural Organic Matter                                                        | 119        |
|                  | Adsorption                                                                    | 121        |
| Section 5.3      | Analysis Method Development                                                   | 127        |
|                  | HPLC and Solid Phase Extraction Method Development                            | 127        |
| Section 5.4      | Experimental                                                                  | 136        |
|                  | Batch Experiments                                                             | 136        |
|                  | Mini-column Experiments                                                       | 137        |
|                  | Humic and Fulvic Acid Purification                                            | 140        |
|                  | Ultrafiltration                                                               | 141        |
|                  | High concentration column experiments                                         | 142        |
| Section 5.5      | Results and Discussion                                                        | 143        |
|                  | Batch Studies                                                                 | 143        |
|                  | Humic and Fulvic Acid Adsorption                                              | 154        |
|                  | Mini-column Experiments                                                       | 156        |
|                  | High concentration kinetic trials                                             | 159        |
|                  | Influence of Fulvic acid on Mini-column breakthrough                          | 161        |
| Section 5.7      | References                                                                    | 164        |
| <b>CHAPTER 6</b> | <b>REGENERATION</b>                                                           | <b>169</b> |
| Section 6.1      | Introduction                                                                  | 169        |
| Section 6.2      | Background and Literature Review                                              | 170        |
| Section 6.3      | Experimental                                                                  | 173        |
|                  | Trial Regeneration                                                            | 173        |
|                  | Ethanol Washout                                                               | 174        |
|                  | Regeneration of Adsorption Column                                             | 174        |
| Section 6.4      | Results and Discussions                                                       | 175        |
|                  | Trial Regeneration                                                            | 175        |
|                  | Ethanol Washout                                                               | 179        |
|                  | Adsorption columns regeneration                                               | 179        |
| Section 6.5      | Conclusions                                                                   | 189        |
| Section 6.6      | References                                                                    | 190        |
| <b>CHAPTER 7</b> | <b>GENERAL CONCLUSIONS</b>                                                    | <b>192</b> |
| Section 7.1      | Conclusions                                                                   | 192        |
| Section 7.2      | Future Work                                                                   | 195        |
| Section 7.3      | Commercial Implications                                                       | 196        |
| Appendix 1       |                                                                               | 199        |
| Appendix 2       |                                                                               | 200        |

## LIST OF FIGURES

|            |                                                                                                                                                                                           |    |
|------------|-------------------------------------------------------------------------------------------------------------------------------------------------------------------------------------------|----|
| Fig. 1.1.  | Scheme of the synthesis of polymers [13].                                                                                                                                                 | 5  |
| Fig. 2.1.  | A schematic representation of the structure of active carbons and Macronet polymers.                                                                                                      | 10 |
| Fig. 2.2.  | Optical Photographs of MN-200 at 15× and 45× magnification.                                                                                                                               | 21 |
| Fig. 2.3.  | Optical Photographs of F-400 at 15× and 45× magnification.                                                                                                                                | 21 |
| Fig. 2.4.  | SEM of Crushed F-400, 53-75μm, at two different magnifications.                                                                                                                           | 22 |
| Fig. 2.5.  | SEM of Crushed MN-150, 53-75μm, at two different magnifications.                                                                                                                          | 23 |
| Fig. 2.6.  | SEM of Washed F-400, 500-600μm, at two different magnifications.                                                                                                                          | 24 |
| Fig. 2.7.  | SEM of MN-200, cross-section, at 10,000× magnification.                                                                                                                                   | 26 |
| Fig. 2.8.  | SEM of MN-200, cross-section, at 50,000× magnification.                                                                                                                                   | 26 |
| Fig. 2.9.  | SEM of MN-200, outer surface, at 10,000× magnification.                                                                                                                                   | 27 |
| Fig. 2.10. | SEM of MN-200, outer surface, at 50,000× magnification.                                                                                                                                   | 27 |
| Fig. 2.11. | Nitrogen Adsorption/Desorption Isotherms for MN-100, MN-150, MN-200, F-400 and the Styrene Copolymer.                                                                                     | 29 |
| Fig. 2.12. | Comparison of the Nitrogen Adsorption Isotherms for MN-100, MN-150, MN-200, F-400 and the Styrene Copolymer.                                                                              | 30 |
| Fig. 2.13. | Logarithmic Comparison of the Nitrogen Adsorption Isotherms for MN-100, MN-150, MN-200, F-400 and the Styrene Copolymer.                                                                  | 30 |
| Fig. 2.14. | Langmuir and B.E.T. Plots for MN-200, 53-75μm.                                                                                                                                            | 31 |
| Fig. 2.15. | Effect of The Interaction Parameter on the Pore Size Distribution of MN-200, 53-75μm, calculated using the Slit Pore Horvath and Kawazoe Model.                                           | 34 |
| Fig. 2.16. | Effect of Pore Geometry on the Pore Size Distribution of MN-200, 53-75μm, calculated using the Horvath and Kawazoe (Slit), Saito and Foley (Cylinder) and Cheng and Yang (Sphere) Models. | 34 |
| Fig. 2.17. | Pore Size Distributions of MN-100, MN-150, MN-200 and F-400.                                                                                                                              | 36 |
| Fig. 2.18. | DFT Pore Size Distributions of MN-100, MN-150, MN-200, F-400 and the Styrene Precursor                                                                                                    | 38 |
| Fig. 2.19. | Fractional Approach to Equilibrium Curves for the Adsorption of Nitrogen onto MN-200, 53-75μm.                                                                                            | 40 |
| Fig. 3.1.  | IR-active functionalities on carbon surfaces (Fanning <i>et al</i> ) [8].                                                                                                                 | 50 |
| Fig. 3.2.  | Diffuse reflectance FT-IR spectra of MN-100.                                                                                                                                              | 57 |
| Fig. 3.3.  | Diffuse reflectance FT-IR spectra of MN-150.                                                                                                                                              | 58 |
| Fig. 3.4.  | Diffuse reflectance FT-IR spectra of MN-200.                                                                                                                                              | 59 |
| Fig. 3.5.  | Diffuse reflectance FT-IR spectra of Styrene Precursor and Atactic Polystyrene.                                                                                                           | 60 |
| Fig. 3.6.  | Diffuse reflectance FT-IR spectra of F-400.                                                                                                                                               | 60 |
| Fig. 3.7.  | Subtraction spectra of MN-200 and the styrene copolymer                                                                                                                                   | 61 |
| Fig. 3.8.  | Comparison of the FT-IR spectra of MN-150 and MN-200.                                                                                                                                     | 61 |
| Fig. 3.9.  | X-ray photoelectron spectra of the C1s orbital.                                                                                                                                           | 63 |
| Fig. 3.10. | <sup>13</sup> C NMR Spectra of MN-100.                                                                                                                                                    | 66 |
| Fig. 3.11. | <sup>13</sup> C NMR Spectra of MN-150 at Spinning Speeds of 4811 and 3938Hz.                                                                                                              | 67 |
| Fig. 3.12. | <sup>13</sup> C NMR Spectra of MN-200.                                                                                                                                                    | 68 |
| Fig. 3.13. | Zeta Potential of MN-100, MN-150 and MN-200.                                                                                                                                              | 71 |
| Fig. 4.1.  | Types of hydrogen bonds.                                                                                                                                                                  | 78 |
| Fig. 4.2.  | Binding of phenol and s-triazine by complexation.                                                                                                                                         | 80 |
| Fig. 4.3.  | Adsorption Isotherm Classifications.                                                                                                                                                      | 81 |
| Fig. 4.4.  | Mechanisms for the process of adsorption.                                                                                                                                                 | 83 |
| Fig. 4.5.  | Adsorption isotherms of various adsorbents for phenol (Vliet <i>et al</i> [23]).                                                                                                          | 87 |
| Fig. 4.6.  | Photograph of Batch Adsorption Experimental Apparatus.                                                                                                                                    | 91 |
| Fig. 4.7.  | Photograph of Batch Adsorption Reactor.                                                                                                                                                   | 92 |
| Fig. 4.8.  | Phenol sorption isotherms for MN-100, MN-150, MN-200 and F-400 at 25±1°C.                                                                                                                 | 96 |
| Fig. 4.9.  | 4-chlorophenol sorption isotherms for MN-100, MN-150 and MN-200 at 25±1°C.                                                                                                                | 96 |
| Fig. 4.10. | 2-chlorophenol sorption isotherms for MN-100, MN-150 and MN-200 at 25±1°C.                                                                                                                | 97 |

|            |                                                                                                                                                                                            |     |
|------------|--------------------------------------------------------------------------------------------------------------------------------------------------------------------------------------------|-----|
| Fig. 4.11. | 3-chlorophenol sorption isotherms for MN-100, MN-150, MN-200 and F-400 at $25\pm 1^\circ\text{C}$ .                                                                                        | 97  |
| Fig. 4.12. | Fractional approach to equilibrium curves for MN-200 adsorbing phenol, 2-chlorophenol, 3-chlorophenol and 4-chlorophenol. 200mg of adsorbent.                                              | 101 |
| Fig. 4.13. | Fractional approach to equilibrium curves for MN-100, MN-150, MN-200 and F-400 adsorbing phenol. 200mg of adsorbent.                                                                       | 101 |
| Fig. 4.14. | Molecular structure of phenol, 2-chlorophenol, 3-chlorophenol and 4-chlorophenol.                                                                                                          | 102 |
| Fig. 4.15. | Comparison of experimental and theoretical concentration decay curves for MN-200 adsorbing phenol. $25^\circ\text{C}$ , 350rpm.                                                            | 106 |
| Fig. 4.16. | Arrhenius plots for MN-100, MN-150 and MN-200 sorbing phenol.                                                                                                                              | 108 |
| Fig. 4.17. | Effect of temperature on the equilibrium conc. for MN-100, MN-150 and MN-200.                                                                                                              | 108 |
| Fig. 5.1.  | Annual use of atrazine, simazine and diuron in 1992 [9].                                                                                                                                   | 118 |
| Fig. 5.2.  | Surface area distribution of the F300 and F400 activated carbons, showing available surface area for different commercial humic acid mass fractions [29].                                  | 124 |
| Fig. 5.3.  | Stages of Method Development.                                                                                                                                                              | 127 |
| Fig. 5.4.  | Isoabsorbance plot for HPLC analysis of a pure pesticides mix.                                                                                                                             | 129 |
| Fig. 5.5.  | Isoabsorbance plot for HPLC analysis of a fulvic acid and pesticides mix. (No guard column).                                                                                               | 129 |
| Fig. 5.6.  | HPLC calibration graph for Atrazine, Simazine, Isoproturon, Chlorotoluron and Diuron.                                                                                                      | 130 |
| Fig. 5.7.  | Recovery efficiency of pesticides at a concentration of 0.1ppb.                                                                                                                            | 133 |
| Fig. 5.8.  | HPLC chromatogram of pesticide mix at a concentration of 0.1 $\mu\text{g/l}$ .                                                                                                             | 135 |
| Fig. 5.9.  | Simplified flow diagram of experimental apparatus.                                                                                                                                         | 137 |
| Fig. 5.10. | Photograph of column experimental apparatus.                                                                                                                                               | 139 |
| Fig. 5.11. | Photograph of the ultrafiltration cell.                                                                                                                                                    | 141 |
| Fig. 5.12. | Single component adsorption isotherms for MN-200 sorbing simazine, chlorotoluron, isoproturon, atrazine and diuron.                                                                        | 144 |
| Fig. 5.13. | Single component adsorption isotherms for MN-100, MN-150 and MN-200 sorbing atrazine                                                                                                       | 144 |
| Fig. 5.14. | Multi-component adsorption isotherms for MN-100.                                                                                                                                           | 145 |
| Fig. 5.15. | Multi-component adsorption isotherms for MN-150.                                                                                                                                           | 145 |
| Fig. 5.16. | Multi-component adsorption isotherms for MN-200.                                                                                                                                           | 146 |
| Fig. 5.17. | Comparison of multi-component adsorption isotherms for MN-100, MN-150, MN-200 and single component isotherms for MN-200 sorbing simazine, chlorotoluron, isoproturon, atrazine and diuron. | 147 |
| Fig. 5.18. | Molecular structure of simazine, chlorotoluron and isoproturon.                                                                                                                            | 148 |
| Fig. 5.19. | Molecular structure of atrazine and diuron.                                                                                                                                                | 149 |
| Fig. 5.20. | Possible cooperative and normal hydrogen bonding of atrazine.                                                                                                                              | 151 |
| Fig. 5.21. | UV-visible scan of humic and fulvic acid.                                                                                                                                                  | 154 |
| Fig. 5.22. | Adsorption isotherms for the removal of humic and fulvic acid.                                                                                                                             | 155 |
| Fig. 5.23. | Multi-component adsorption isotherms for MN-200 in the presence of 20mg/l fulvic acid.                                                                                                     | 157 |
| Fig. 5.24. | Mini-column breakthrough curves for MN-200 sorbing simazine, chlorotoluron, atrazine, diuron and isoproturon.                                                                              | 158 |
| Fig. 5.25. | Adsorption kinetics for the sorption of atrazine and fulvic acid.                                                                                                                          | 160 |
| Fig. 5.26. | Aldrich humic acid sodium salt breakthrough curves for MN-200 and F-400.                                                                                                                   | 160 |
| Fig. 5.27. | Mini-column breakthrough curves for MN-200 sorbing simazine, chlorotoluron, atrazine, diuron and isoproturon in the presence of 10mg/l fulvic acid.                                        | 162 |
| Fig. 5.28. | Mini-column breakthrough curves for F-400 sorbing simazine, chlorotoluron, atrazine, diuron and isoproturon in the presence of 10mg/l fulvic acid.                                         | 162 |
| Fig. 6.1.  | Regeneration of MN-200 using HPLC grade ethanol.                                                                                                                                           | 176 |
| Fig. 6.2.  | Regeneration of MN-200 using azeotropic ethanol.                                                                                                                                           | 176 |
| Fig. 6.3.  | Regeneration of MN-200 using HPLC grade acetone.                                                                                                                                           | 177 |
| Fig. 6.4.  | Regeneration of MN-200 using HPLC grade methanol.                                                                                                                                          | 177 |
| Fig. 6.5.  | Regeneration of MN-200 using HPLC grade 1-propanol.                                                                                                                                        | 178 |
| Fig. 6.6.  | Regeneration of MN-200 using various organic solvents.                                                                                                                                     | 178 |
| Fig. 6.7.  | Ethanol wash out curves for MN-200.                                                                                                                                                        | 179 |
| Fig. 6.8.  | Elution curves for the regeneration of the MN-200 adsorption column.                                                                                                                       | 180 |

|            |                                                                                                                                        |     |
|------------|----------------------------------------------------------------------------------------------------------------------------------------|-----|
| Fig. 6.9.  | Elution curves for the regeneration of the F-400 adsorption column.                                                                    | 180 |
| Fig. 6.10. | HPLC chromatograms of regenerant solutions.                                                                                            | 181 |
| Fig. 6.11. | Isoabsorbance plot for the regeneration solution in vial 3.                                                                            | 186 |
| Fig. 6.12. | Mini-column breakthrough curves for MN-200 sorbing simazine, chlorotoluron, atrazine, diuron and isoproturon. Second adsorption cycle. | 188 |
| Fig. A1.1. | Types of physisorption isotherms.                                                                                                      | 199 |
| Fig. A1.2. | Types of hysteresis loops.                                                                                                             | 199 |

## LIST OF TABLES

|             |                                                                                                                                                                                                               |     |
|-------------|---------------------------------------------------------------------------------------------------------------------------------------------------------------------------------------------------------------|-----|
| Table 1.1.  | Hypersol-Macronet™ Sorbent Resins [10].                                                                                                                                                                       | 4   |
| Table 2.1.  | Surface Area Results for MN-100, MN-150, MN-200, F-400 and the Styrene Copolymer Based Upon Different Models. (53-75µm and 500-600µm adsorbents).                                                             | 32  |
| Table 2.2.  | Effect of the Interaction Parameter on the Mean Pore Size of MN-200, 53-75 calculated using Horvath and Kawazoe Slit Pore Model.                                                                              | 33  |
| Table 2.3.  | Effect of Pore Geometry and Interaction Parameter on the Mean Pore Size of MN-200.                                                                                                                            | 33  |
| Table 2.4.  | Mean Pore Size of MN-100, MN-150, MN-200 and F-400 (53-75µm).                                                                                                                                                 | 35  |
| Table 3.1.  | Elemental composition of Calgon F-400 Activated Carbon.                                                                                                                                                       | 52  |
| Table 3.2.  | Concentration of Surface functional groups on F-400 (meq/g).                                                                                                                                                  | 52  |
| Table 3.3.  | Atomic composition of MN-150 determined by X-ray photoelectron spectroscopy.                                                                                                                                  | 62  |
| Table 3.4.  | Peak assignments for Fig. 3.9.                                                                                                                                                                                | 63  |
| Table 3.5.  | Elemental Analysis of the Macronet Polymers.                                                                                                                                                                  | 64  |
| Table 3.6.  | Base Consumption of Various Adsorbents.                                                                                                                                                                       | 70  |
| Table 3.7.  | Concentration of Surface Functional Groups of Various Adsorbents.                                                                                                                                             | 70  |
| Table 3.8.  | Weak base volume and weight capacities of the Macronet polymers.                                                                                                                                              | 70  |
| Table 4.1.  | Relationship between pH, $pK_b$ , and the percentage of the molecule in the cationic form.                                                                                                                    | 79  |
| Table 4.2.  | Approximate bond energies and equilibrium lengths for various types of interactions.                                                                                                                          | 80  |
| Table 4.3.  | Freundlich parameters for the sorption of phenol onto F-400 activated carbon.                                                                                                                                 | 88  |
| Table 4.4.  | Freundlich and correlation coefficients.                                                                                                                                                                      | 95  |
| Table 4.5.  | Langmuir and correlation coefficients.                                                                                                                                                                        | 95  |
| Table 4.6.  | Physical properties of phenols.                                                                                                                                                                               | 99  |
| Table 4.7.  | Average external mass transfer coefficients for MN-100, MN-150, MN-200, and F-400 sorbing phenol, 2-chlorophenol, 3-chlorophenol and 4-chlorophenol. 25°C, 350rpm, 500-600µm particles, $C_0=50\text{mg/l}$ . | 104 |
| Table 4.8.  | Surface Diffusivities for MN-100, MN-150, MN-200 and F-400 sorbing phenol and ortho, meta, para substituted chlorophenols. 25°C, 350rpm, 500-600µm particles, $C_0=50\text{mg/l}$ .                           | 105 |
| Table 4.9.  | Effect of particle size on the external film and surface diffusivity coefficients for MN-100, MN-150 and MN-200 sorbing phenol. 25°C, 350 rpm, $C_0=50\text{mg/l}$ .                                          | 107 |
| Table 4.10. | External mass transfer coefficients for MN-200 using different agitation speeds. 25°C, 500-600µm particles, $C_0=50\text{mg/l}$ .                                                                             | 109 |
| Table 5.1.  | Concentration of pesticides in drinking water sources and supplies in 1993 (µg/l).                                                                                                                            | 117 |
| Table 5.2.  | Usage data for frequently detected pesticides.                                                                                                                                                                | 117 |
| Table 5.3.  | Chemical characteristics of humic and fulvic acid [13].                                                                                                                                                       | 120 |
| Table 5.4.  | GAC performance evaluation methodologies in comparison to field scale columns [14].                                                                                                                           | 121 |
| Table 5.5.  | Procedure for solid phase extraction.                                                                                                                                                                         | 131 |
| Table 5.6.  | Means, relative standard deviations and recoveries for the determination of simazine, chlorotoluron, isoproturon, atrazine and diuron at a concentration of 0.1µg/l.                                          | 132 |
| Table 5.7.  | Recovery efficiency for the determination of simazine, chlorotoluron, isoproturon, atrazine and diuron at a concentration range of 1-8µg/l.                                                                   | 134 |
| Table 5.8.  | Limits of determination for analytical method.                                                                                                                                                                | 134 |
| Table 5.9.  | Determination of pesticides in waters by reversed phased HPLC.                                                                                                                                                | 135 |
| Table 5.10. | Freundlich and correlation coefficients for the adsorption of pesticides.                                                                                                                                     | 143 |
| Table 5.11. | Physical properties of simazine, chlorotoluron, isoproturon, atrazine and diuron.                                                                                                                             | 150 |
| Table 6.1.  | Solubility of pesticides in various organic solvents.                                                                                                                                                         | 175 |
| Table 6.2.  | Concentration of pesticides in regenerant solution for MN-200.                                                                                                                                                | 184 |
| Table 6.3.  | Concentration of pesticides in regenerant solution for F-400.                                                                                                                                                 | 187 |

## CHAPTER 1

### INTRODUCTION

#### SECTION 1.1      GENERAL INTRODUCTION

Activated carbon is used extensively in the purification of water due to its ability to remove taste and odour organic species, and more recently to reduce the levels of pesticides. Despite the increasing use of activated carbon there are problems with the technology including high regeneration costs and the generation of carbon fines due to the brittle nature of the carbons used. This has stimulated research into speciality adsorbents using naturally occurring starting materials and synthetic polymeric materials that may facilitate cheap and effective chemical regeneration processes.

The XAD series of polymeric adsorbents produced by Rohm and Haas have been widely studied in the literature as potential replacements to activated carbon. Suffet *et al* [1] conducted a pilot scale experiment comparing the sorptive performance of XAD-2 with the carbon Filtrasorb-400 for the removal of trace organics from treated drinking water. They concluded that the carbon was much more effective for the removal of non-polar trace organic compounds.

The resins have found application for the cleanup of wastewater streams, especially phenolic streams, due to their ability to be regenerated. Fox [2] presented examples of phenol, para-nitrophenol, dichlorophenols and phenoxy acid pesticide removal and recovery using XAD-2, XAD-4 and XAD-7. No degradation of XAD-4 was apparent after two years of operation and 1300 cycles, for the sorption and recovery of phenol from a waste stream. Extraction of humic and fulvic acids from natural waters is commonly achieved by sorption onto XAD resins followed by elution using sodium hydroxide [3]. However, wide scale commercial application of polymeric resins has not been achieved for drinking water treatment.

In 1969, Davankov and Tsyurupa first disclosed their new series of hypercrosslinked polymeric networks [4]. The polymers were originally described as macro reticulated, offering different characteristics to other polymeric resins. Purolite International Ltd, in collaboration with the Russian inventors, has developed an optimal series of 'Hypersol Macronet™' sorbent resins for industrial application. The polymers are based on a spherical styrene-divinylbenzene copolymer that is crosslinked while the polymer is in a swollen state. Their manufacture is based upon the Davankov-Tsyurupa technology producing polymers with various pore structures and functionalities.

In 1990 and 1992 Dow Chemical patented their new series of methylene bridged styrene-divinylbenzene hypercrosslinked polymeric adsorbents, based on the Davankov-Tsyurupa technology [5]. Dow Chemical have patented a number of different applications for gas and liquid phase adsorption. Their polymeric adsorbents have been applied to adsorption and recovery of volatile organic compounds such as methyl ethyl ketone (MEK) [6], an area where activated carbon cannot be used due to the catalytic oxidation of MEK on activated carbon. Processes for decolourising aqueous sugar solutions using the resin and the subsequent desorption of the colour bodies have also been patented [7], demonstrating the potential of such adsorbents.

Macronet polymers possess higher surface areas, 800-1000m<sup>2</sup>/g, than those offered by conventional polymeric adsorbents such as the XAD series of resins, 500-800m<sup>2</sup>/g. They are also mechanically stronger than activated carbons suggesting a possible application for the drinking water industry. Tsyurupa *et al* [8] have investigated the use of the hypercrosslinked polymers for the sorption of organic compounds such as synthetic organic dyes, *n*-valeric acid, lipids, tributylphosphate and petroleum spirit. They concluded that the adsorptive performance of the Macronet polymers MN-100 and MN-150 was superior to the common macroreticular polystyrene sorbent XAD-4. Work has also been performed on the possibilities of using the sorbent as a solid phase extraction material for phenolic compounds [9].

## SECTION 1.2 RESEARCH OBJECTIVES

The objectives of this research were to evaluate the adsorption of organic species onto Hypersol

Macronet™ polymers and their subsequent regeneration efficiency using organic solvents. Two porosity classes of Macronet polymers were selected, namely MN-150 and the group MN-100 and MN-200. MN-100 and MN-150 contain weakly basic functional groups whereas MN-200 has no added functionality. The adsorbates chosen for the study were; phenol, 2-chlorophenol, 3-chlorophenol, 4-chlorophenol and the pesticides, atrazine, simazine, diuron, isoproturon and chlorotoluron. All of these compounds are considered as priority pollutants by the European Union.

Adsorption using high concentrations of single solute phenols in solution were performed to study the adsorption capacity and kinetics of the polymers compared to the commercial activated carbon F-400, manufactured by Chemviron. Studies using trace levels of pesticides in the parts per billion range were performed to assess the polymers' potential for industrial application in the water industry. Multi-component adsorption was investigated including the influence of naturally occurring organic matter on the adsorption to make the trials more realistic.

Investigations into the physical and chemical surface characteristics of the polymers were performed by several techniques in an attempt to describe the process and mechanism of adsorption for the various adsorbates.

### **SECTION 1.3      HYPERSOL-MACRONET POLYMERS**

Hypersol-Macronet polymers are produced by Purolite International Limited with a wide variety of pore sizes and chemical functionalities. The development of an optimal series of Macronets was performed in collaboration with Davankov and Tsyurupa, the inventors of the novel polymeric networks, see Table 1.1.

Little work has been published on the characterisation and application of the Macronet polymers produced by Purolite International due to their recent invention. However, Davankov, Tsyurupa and co-workers have carried out numerous investigations into the diverse synthetic routes, performance and characterisation of their Macronet polymers which are reviewed briefly. Further



details regarding the characterisation of the polymers can be seen in the individual chapters.

**Table 1.1. Hypersol-Macronet™ Sorbent Resins [10].**

| Characteristic                      | Group I  |        |         |         |         |         | Group II |        | Group III |
|-------------------------------------|----------|--------|---------|---------|---------|---------|----------|--------|-----------|
|                                     | MN-100   | MN-200 | MN-300  | MN-400  | MN-500  | MN-600  | MN-150   | MN-250 | MN-170    |
| Functionality                       | WBA      | -      | WBA     | SBA     | SAC     | WAC     | WBA      | -      | WBA       |
| $d_{50}$ , Å, meso-macropores       | 850-950  |        |         |         |         |         | 300-400  |        | (nil)     |
| $d_{50}$ , Å, micropores            | 15       |        |         |         |         |         | 14       |        | 25        |
| Weight Capacity, eq/kg              | 0.6-0.8  | -      | 1.2-1.4 | 0.6-0.8 | 2.2-2.4 | 0.4-0.8 | 0.4-0.7  | -      | 0.7-1.0   |
| BET Surface Area, m <sup>2</sup> /g | 800-1000 |        |         |         |         |         | 800-1000 |        | ~1200     |

WBA-Weak Base Anion,

SBA-Strong Base Anion,

WAC-Weak Acid Cation,

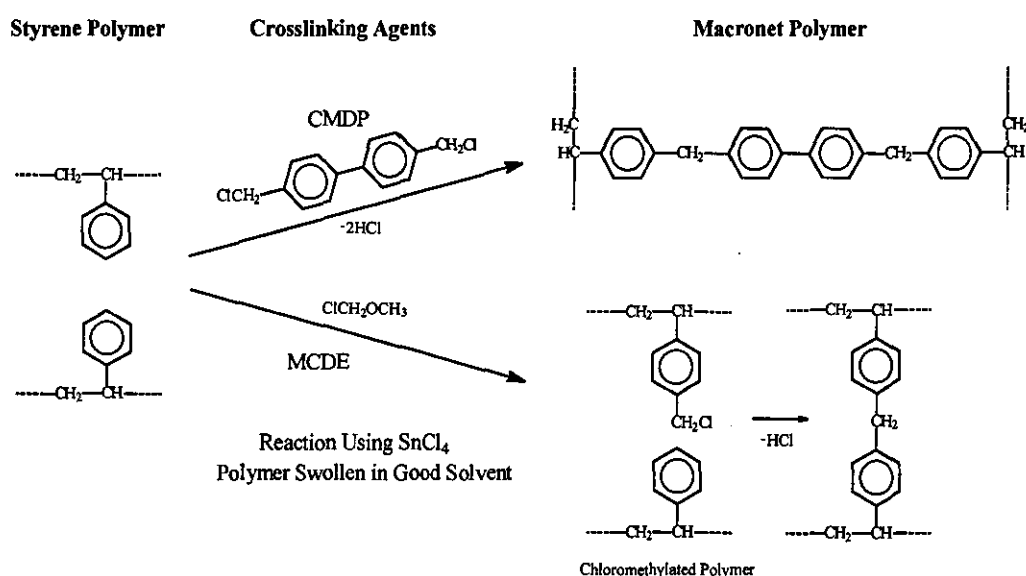
SAC-Strong Acid Cation

Davankov and Tsyurupa first disclosed the method for manufacture of macroreticular polystyrene structures for ion-exchange resins in 1969. Insoluble crosslinked polystyrenes were prepared by treating polystyrenes or styrene-divinylbenzene copolymers, in the swollen state, with crosslinking agents in the presence of a Friedel-Crafts catalyst. The resulting gel was ground with acetone and sulphonated to produce a cation exchange resin with a capacity of 5.35meq/g. In the US patent the polymers were simply termed Macronet [11].

Prior to the development of Macronet polymers ion exchange or sorbent resins were categorised into gel type and macroporous resins. Gel type styrene-divinylbenzene resins are made by a copolymerisation reaction carried out in the absence of a porogen. The products are homogeneous and non-porous in the dry state and so they can only be used in media that causes the polymeric network to swell. Macroporous resins are produced by the copolymerisation of styrene with a large proportion of divinylbenzene in the presence of a porogen that precipitates the growing polystyrene chains. XAD-16 and XAD-4 produced by Rohm and Haas are good examples of macroporous sorbent resins [12]. The distinguishing difference between Macronet polymers and the traditional gel and macroporous resins is that crosslinking in the structure occurs in a solution where the polystyrene chains are in a highly swollen state. When the solvent is removed the extensive crosslinking prevents the collapse of the structure, resulting in the development and rapid growth of inner strains in the polymer network.

Macronet polymers have been produced using a large number of different crosslinking agents including p, p'-bis-chloromethyl-1,4-diphenylbutane (DBP) [13], p-xylylene-dichloride (XDC) [14], 4,4-bis-chloromethyldiphenyl (CMDP), monochlorodimethyl ether (MCDE) [15], dimethylformal (DMF) [16] and tris-(chloromethyl)-mesitylene (CMM) [13]. Fig 1.1 presents a schematic for the synthesis of Macronet polymers based upon two different crosslinking agents.

Fig. 1.1. Scheme of the synthesis of polymers [13].



The crosslinking agents undergo a Friedel-Crafts reaction with the phenyl rings of the polymer producing a bridge between the polystyrene chains. The length of the bridge is two phenyl rings greater than the crosslinking agent. Conformational mobility of the polymer network can be adjusted by varying the length of the bridges, with the diphenylmethane type having the most rigid structures. The degree of crosslinking was controlled by varying the amount of crosslinking agent, e.g. 'if 0.5mol of bifunctional crosslinking reagent is involved in the reaction of 1 mole styrene practically all the initial phenyl rings should be incorporated into cross bridges in the final polymer and the crosslinking degree of the latter would be 100%' [17]. When more than 0.5 mole of bifunctional reagent is used for the reaction it is likely that all phenyl rings of the polymer chain undergo crosslinking. Also, the crosslinking agent may slowly chloromethylate the phenyl rings on which a bridge has already formed.

Davankov and Tsyurupa crosslinked styrene swollen in a variety of solvents including

dichloroethane, tetrachloroethane, nitrobenzene and cyclohexane [18]. Polymers produced in dichloroethane and tetrachloroethane were virtually identical with respect to their final properties. Nitrobenzene caused the gel to form too quickly causing a heterogeneity in the reaction mixture, resulting in a low overall degree of crosslinking. Polymerisation in cyclohexane, which from the thermodynamic point of view is a bad solvent for polystyrene, introduced mesopores into the microporous gel structure.

Two different classes of Macronet polymer were developed by Davankov and Tsyurupa termed Styrosorb I and II [19]. Styrosorb 1 polymers were typically produced by the crosslinking of linear atactic polystyrene, molecular weight of 300,000, dissolved in a good solvent such as dichloroethane. The volume concentration of all constituents of the reaction in the solvent was in the range 10-11%. Sorbent resin was obtained by crushing the single gel block into irregularly shaped particles. Styrosorb Type II polymer beads were obtained by crosslinking small spherical copolymers of styrene with 0.3-2% divinylbenzene. The initial polymer was typically swollen using dichloroethane prior to crosslinking using MCDE. Stannic chloride was used as the Friedel-Crafts catalyst for Styrosorb type I and II polymers at a concentration of 0.2-3.0 mol/mol of crosslinking agent. The time of synthesis varied between 1 and 11 hours at a temperature of 50-80°C. The reaction mixtures were protected from air moisture to prevent the degradation of the catalyst during the reaction.

The introduction of amine functional groups onto the surface of the polymers was achieved by a chloromethylation reaction followed by an amination reaction [20]. Chloromethylation of 100% crosslinked Styrosorbs, pre-swollen in dichloroethane or tetrachloroethane, was achieved with 5M of MCDE per 1M of polymer aromatic rings at room temperature. The amount of stannic chloride catalyst was varied between 0.06 and 0.2M per 1M of MCDE which resulted in an increase in the amount of chlorine in the polymer from 7.3 to 13.6%. Attempts to increase the amount of chlorine to the theoretical 23% were unsuccessful; this was attributed to further crosslinking of phenyl rings. Basic capacities of between 1 and 4.4meq/g were achieved. However 1.3% of unreacted chlorine was still present in the polymer.

Sulphonation of the Styrosorbs was readily achieved by swelling the polymers in dichloroethane

prior to being placed in concentrated sulphuric acid. The reaction mixture was stirred for three hours at 80°C. Capacities for the 100% crosslinked polymers were around 4-5meq/g [21].

For further information regarding the structure and properties of hypercrosslinked polystyrene networks I refer the reader to the review paper by Davankov and Tsyurupa published in 1990 [22].

## SECTION 1.4 REFERENCES

- [1] I.H. Suffet, L. Brenner, J.T. Coyle and P.R. Cairo, Evaluation of the Capacity of Granular Activated Carbon and XAD-2 Resin to Remove Trace Organics from Treated Drinking Water., *Environmental Science and Technology*, 12, (12), (1978), p1315-1322.
- [2] C.R. Fox, Plant Uses Prove Phenol Recovery with Resins., *Hydrocarbon Processing*, November, (1978), p269-273.
- [3] S.A. Daignault, D.K. Noot, D.T. Williams and P.M. Huck, Review of the use of XAD resins to concentrate organic compounds in water., *Water Research*, 22, (7), (1988), p803-813.
- [4] V.A. Davankov, S.V. Rogozhin and M.P. Tsyurupa, Patent USSR 299165, Sept 12, (1969).
- [5] H.P. Schneider, Y.M. Görlach-Doht, M.A. Kümin, U.S. Patent 5,079,274, Jan 7, (1992).
- [6] P.G. Blystone, H.R. Goltz and J. Springer (Jr), Recovery and Reuse of MEK from Paint Stripping Operation Emissions Using Specialized Adsorbents., *Air & Waste Management Association*, presented at 87th Annual Meeting & Exhibition, Cincinnati, Ohio, June 19-24, (1994).
- [7] R.T. Stringfield, H.R. Goltz, S.I. Norman, U.J. Bharwada, R.L. LaBrie, U.S. Patent 4,950,332, Aug 21, (1990).
- [8] M.P. Tsyurupa, L.A. Maslova, A.I. Andreeva, T.A. Mrachkovskaya, V.A. Davankov, Sorption of Organic Compounds from Aqueous Media by Hypercrosslinked Polystyrene Sorbents 'Styrosorb'., *Reactive Polymers*, 25, (1995), p69-78.
- [9] M.P. Tsyurupa, M.M. Ilyin, A.I. Andreeva, V.A. Davankov, Use of the Hyper-crosslinked Polystyrene Sorbents "Styrosorb" for Solid Phase Extraction of Phenols from Water., *Fresenius' Journal of Analytical Chemistry*, 352, (1995), p672-675.

- [10] Purolite Technical Bulletin, Hypersol-Macronet™ Sorbent Resins, The Purolite Company, (1995).
- [11] V.A. Davankov, S.V. Rogozhin and M.P. Tsyurupa, U.S. Patent 3,729,457, Apr 24, (1973).
- [12] Amberlite XAD Polymeric Adsorbents, Rohm and Haas, (1995).
- [13] M.P. Tsyurupa, V.V. Lalaev and V.A. Davankov, On Reasons Determining Unusual Properties of Hypercrosslinked Styrene Polymers., Dokladi Academi Nauk SSSR, 279, (1), (1984), p156-159.
- [14] V.A. Davankov, S.V. Rogozhin and M.P. Tsyurupa, Über Faktoren, die das Quellvermögen von vernetzten Polymeren bestimmen., Die Angewandte Makromolekulare Chemie, 32, (1973), p145-151.
- [15] V.A. Davankov, M.P. Tsyurupa and S.V. Rogozhin, On Factors Determining the Swelling Ability of Cross-linked Polymers, II\*, Die Angewandte Makromolekulare Chemie, 53, (1976), p19-27.
- [16] M.P. Tsyurupa, V.V. Lalaev and V.A. Davankov, Synthesis and some Physico-chemical Properties of Macronet Isoporous Styrene Polymers with Cross-bridges of biphenylmethane type, Acta Polymerica, 35, (6), (1984), p451-455.
- [17] V.A. Davankov and M.P. Tsyurupa, Structure and Properties of Porous Hypercrosslinked Polystyrene Sorbents 'Styrosorb', Pure and Applied Chemistry, 61, (11), (1989), p1881-1888.
- [18] V.A. Davankov and M.P. Tsyurupa, Rigid Hypercrosslinked Polystyrene Networks with Unexpected Mobility., Paper provided by M.P. Tsyurupa.
- [19] L.D. Belyakova, T.I. Schevchenko, V.A. Davankov and M.P. Tsyurupa, Sorption of Vapors of Various Substances by Hypercrosslinked "Styrosorb" Polystyrenes., Advances in Colloid and Interface Science, 25, (1986), p249-266.
- [20] L.D. Belyakova, V.A. Davankov, A.V. Kiselev, E.I., G.G. Muttik, M.P. Tsyurupa and T.I. Schevchenko, The Study of Sorption of Different Substance Vapors by Macronet Isoporous Ionites., Kolloidn. zh., XL, N 6, (1978), p1059-1064.
- [21] R.V. Martsyinkewich, V.S. Soldatov, V.A. Davankov, M.P. Tsyurupa and S.V. Rogozhin, Some Sorption and Selective Properties of Macronet Isoporous Ionites Based on Polystyrene., Zh. Physich. Khim., 51, (6), (1977), p1465. Translation into English by V.A. Davankov.
- [22] V.A. Davankov and M.P. Tsyurupa, Structure and Properties of Hypercrosslinked Polystyrene-The First Representative of a New Class of Polymer Networks., Reactive Polymers, 13, (1990), p27-42.

## CHAPTER 2

### PHYSICAL CHARACTERISATION

#### SECTION 2.1 INTRODUCTION

Macronet polymers and activated carbon possess large internal surface areas that make them suitable for the removal of organic species from aqueous solution. The porous nature of the adsorbents influences their ability and capacity for adsorption of differently sized adsorbates. Relationships between the size of the pores in carbons and the size of the adsorbates have been investigated by many authors, including Summers *et al* [1], Newcombe *et al* [2] and Hopman *et al* [3]. This chapter investigates the porous nature of the adsorbents by optical and nitrogen adsorption techniques to assess the possibility of size exclusion of adsorbates, and to explain the kinetics of adsorption in the aqueous phase.

#### SECTION 2.2 LITERATURE REVIEW

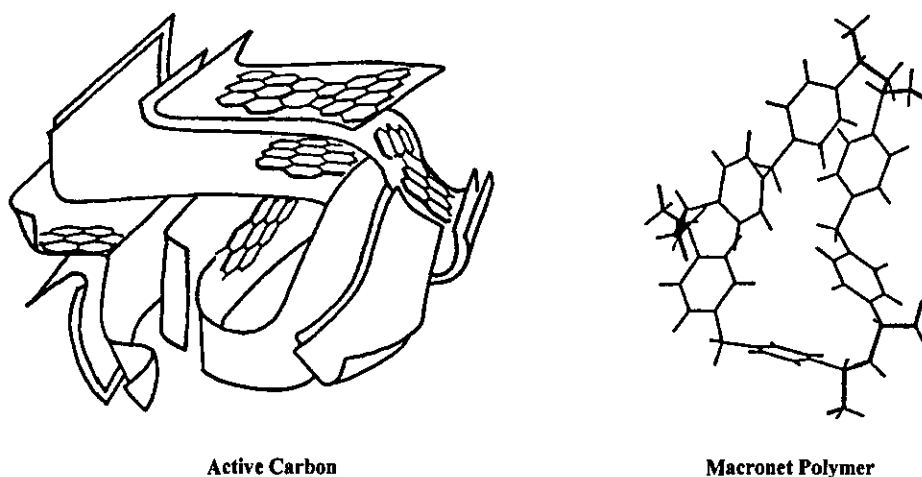
A wide distribution of pores, from the micron to Angstrom range, exist in porous media. The International Union of Pure and Applied Chemistry (IUPAC) physical chemistry division have recommended that pores, with width  $w$ , are classified as micropores ( $w < 2\text{nm}$ ), mesopores ( $2\text{nm} < w < 50\text{nm}$ ) and macropores ( $w > 50\text{nm}$ ) [4]. The specific surface area for adsorption provided by the different sizes of pores varies between  $0.5$  and  $2\text{m}^2/\text{g}$  for macropores,  $10$  and  $400\text{m}^2/\text{g}$  for mesopores and greater than  $400\text{m}^2/\text{g}$  for micropores [5]. Hence, although the macropore size distribution provides useful information regarding the speed of transport of the adsorbates to the microporous region, their adsorption capacity is negligible.

The study of macro and mesopores is often performed by scanning electron microscopy or mercury intrusion porosimetry. However, both techniques are limited to the characterisation of pores greater than approximately  $30\text{\AA}$  in size. A number of direct and indirect techniques are

available for the determination of micropores.

High-Resolution Transmission Electron Microscopy (HRTEM) is a direct technique for the determination of the micropore size. Endo *et al* [6] used the technique to investigate the pore structure of activated carbon fibres and clearly showed the distribution of pore sizes as well as the apparent disorder in the structure. Similar investigations have been completed by Innes *et al* [7] and Oshida *et al* [8]. Economy *et al* [9] used Scanning Tunnelling Microscopy (STM) to investigate the micropore size and shape of activated carbon fibres and suggested that the pore structure had fractal characteristics. Generally, most observations suggest that activated carbon has slit shaped micropores. Fig. 2.1 presents a schematic representation of the structure of activated carbon presented by Stoeckli [10] and a computer simulation of the most probable structure of the Macronet polymer presented by Davankov and Tsyurupa [1.18].

Fig. 2.1. A schematic representation of the structure of active carbons and Macronet polymers.



Ito and Fraissard [11] used nuclear magnetic resonance, using a  $^{129}\text{Xe}$  probe, to correlate chemical shift to pore sizes. As the pore size decreased they observed an increase in the chemical shift, thus allowing a qualitative measure of the pore size distribution. Conner *et al* [12] applied the method to mesoporous silica which showed the opposite chemical shift dependency with the pore size distribution. Small angle X-ray scattering (SAXS) techniques have also been applied with limited success for activated carbon adsorbents. Davankov and Tsyurupa studied their Styrosorb polymers using SAXS. However little information regarding the microporous nature of the materials was obtained [13].

Tsyurupa and Davankov used gel permeation chromatography to study the micropore size distribution of Macronet Isoporous Styrene polymers [14]. The technique consisted of passing narrow fractions of polystyrene, with a molecular weight of 362-2,000,000, through a chromatography column prepared with the adsorbent material swollen in chloroform, and looking at their retention. They found that the polymers, produced using dichloroethane as the swelling solvent, possessed a narrow pore distribution with a mean pore size of approximately 7 Å. Investigations into the structure of polymers made using cyclohexane revealed a bidisperse structure containing meso and micropores [1.19].

Jeřábek and Setínek [15] studied the structure of Macronet styrene polymer, prepared by Tsyurupa, by inverse steric exclusion chromatography, which allows the characterisation of pore sizes for swollen polymers. Jeřábek *et al* used fifteen solutes with an effective molecular size of <10nm for the tetrahydrofuran environment and six solutes for the water trials. They concluded that the polymer contained 10-15% of highly expandable polymer mass and the rest was formed by a much more dense polymer skeleton.

Quinson *et al* [16] applied thermoporosimetry to evaluate the pore size distribution of wet silica gels. The technique is based upon the dependance of the solidification temperature of liquid produced in pores on the pore width, measured by a differential scanning calorimeter. However, the technique was limited to the determination of pores greater than 1nm. Yenkie and Natarajan [17] used the adsorption of phenol from aqueous solution to assess the surface area of six carbons which were then compared to nitrogen surface areas, thus allowing rough estimates of pore sizes to be determined.

The adsorption of molecules such as benzene and nitrogen on to the surface of the porous media has been used extensively for the characterisation of porous materials by carbon and polymer scientists. Davankov, Tsyurupa and co-workers have investigated their Macronet polymers extensively using the sorption of molecules including nitrogen, argon, cyclohexane, methanol, water, n-perfluorooctane and many other hydrocarbons [1.17, 1.19-20][18]. They observed that the pore volume calculated from the difference in the apparent and true density of the material was different to the value suggested by nitrogen adsorption. This was attributed to swelling of



the Styrosorbs in nitrogen which is recognised as a distinctive property of hypercrosslinked polymers. The adsorption isotherm data produced a straight line in the coordinates of the BET equation (discussed later) in the range of relative pressure 0-0.35 with surface areas of approximately  $1000\text{m}^2/\text{g}$  for 100% crosslinked polymers. Despite presenting a large number of adsorption isotherms little pore size distribution data has been presented by Davankov, Tsyurupa and co-workers.

Pore size distribution and surface area measurements can be extracted from adsorption isotherm data by modelling. This has become the standard method for the determination of the microporous nature of adsorbents due to the simplicity in generating the adsorption isotherm; however, the results are extremely dependent on the model used to derive the distribution, which has resulted in many different modelling techniques. The following text provides a review of the models from the well established theory of Langmuir to the modern molecular dynamics models.

In 1916, Langmuir presented a paper regarding the mechanism of adsorption of molecules [19] which was followed by a paper in 1918 that described the adsorption of gases onto plane surfaces of glass, mica and platinum [20]. According to his theory, gaseous molecules impinging on solid, or liquid surfaces do not in general rebound elastically from the surface, but condense, and are held or adsorbed on the surface by forces similar to those holding the atoms or group molecules of solid bodies. The degree of adsorption was related to the strength of the forces resulting in monolayer coverage of the surface if the forces were large enough. Langmuir performed experiments where he observed that relatively large amounts of gases could be adsorbed by mica and glass at a temperature of  $-118^\circ\text{C}$  compared with negligible adsorption at room temperature. At higher pressures the surface tended to become saturated with gas resulting in monolayer coverage, which is a requirement for his theory. Other investigators working on porous bodies often used saturated vapours so that condensation of liquid occurred in capillary spaces.

In 1938, Brunauer, Emmett and Teller (B.E.T.) [21] extended the work of deBoer and Zwicker [22], and later work by Bradley [23], who proposed isotherm equations to account for multi-layer adsorption. They suggested that the forces responsible for the binding energy of multimolecular

adsorption were the same forces that produce condensation. This was in contrast to the previous theories which assumed that the forces were due to polarisation of the adsorbed layers causing induced dipole interactions, thus allowing for multi-layers. The B.E.T. theory explained nearly all of the 'S' shaped curves observed for the low temperature van der Waals adsorption isotherms of gases including nitrogen, oxygen, argon, carbon dioxide, carbon monoxide, sulphur dioxide and butane on some 30 samples of catalysts, catalyst supports, and various miscellaneous materials. The beginning of the approximately linear portion of the experimentally determined low temperature adsorption isotherms, termed the point B, corresponded to the covering of the surface of the adsorbent by a complete uni-molecular layer of adsorbed gas. At relative pressures below 0.05, B.E.T. observed that their theory broke down since at these pressures, adsorption was occurring on the most active parts of the surface. They also observed that at relative pressures greater than 0.35 there was significant deviation from their model. Special forms of the B.E.T. equation, where the number of molecular layers equalled one, were shown to account for the absence of 'S' shaped isotherms for charcoal. Details of the equations for the Langmuir and B.E.T. theories are covered extensively in the literature. Hence, rather than repeating the equations I refer the reader to the excellent text by Gregg and Sing [24].

The Langmuir and B.E.T. theories allow the determination of the surface area of the adsorbent from the calculated monolayer capacities and the cross-sectional area of the adsorbate, which for nitrogen is assumed to be  $16.2\text{\AA}^2$ . In 1943, Harkins and Jura [25] proposed a method for the determination of the area of a solid without the assumption of a molecular area, and the area occupied by nitrogen molecules on the surfaces of solids. The surface areas derived from their calculations were remarkably close to those calculated using the B.E.T. theory. Also, for the one charcoal they tested the surface area agreed with the Langmuir model whereas the B.E.T. theory failed. However, despite the apparent improvement of their isotherm equations the Langmuir and B.E.T. equations were still preferred by many authors due to their theoretical derivation. Halsey [26], 1948, also criticised the isotherm equation of the B.E.T. theory. He believed it to be untenable that an isolated adsorbed molecule can adsorb a second molecule on top, yielding the full energy of liquefaction, and that in turn the second molecule can adsorb a third and so on. For isotherms that did not suggest capillary condensation, Schüll and co-workers [27] showed that the ratio between the adsorbed volume and the volume of the uni-molecular layer, if plotted as

a function of relative pressure, could be represented approximately by a single curve. This function allowed the thickness of the adsorbed layer,  $t$ , to be calculated, if for one point on the curve the thickness was known. Schüll assumed that the thickness of the monolayer was equal to the diameter of the nitrogen molecule and proposed a value of  $4.3\text{\AA}$ , based on a close packing arrangement of spheres.

In 1951, Barrett, Joyner and Halenda (B.J.H.) [28] presented a paper that enabled the determination of pore volume and area distributions in porous substances based upon nitrogen adsorption data. The model was derived from the work of Wheeler [29] who assumed that equilibrium between the gas phase and the adsorbed phase during desorption, is determined by two mechanisms: (1) physical adsorption on the pore walls, the thickness of which was calculated based on the theories of Schüll and (2) capillary condensation, modelled by the Kelvin equation. The B.J.H. method allowed mesoporous materials to be characterised; however, the model could not characterise pores below  $15\text{\AA}$  since the extension of the Kelvin equation to pores of very small radius cannot be made.

Crankston and Inkley [30] derived an improved method for the determination of pore size distributions from adsorption isotherms, based upon the theories presented by B.J.H.. Their method provided an estimate of the surface area which was almost independent of the B.E.T. value and could be applied to the adsorption and desorption branch of the isotherm. However, vast improvements in computational power have lead to exact solutions to the B.J.H. equations and so little attention is currently paid to the improved method by Crankston and Inkley.

The concept of the  $t$ -curve was extended in a series of papers by deBoer *et al* [31-36]. Contrary to Schüll, deBoer *et al* assigned the same density to the adsorbed layer as to the capillary condensed liquid, which is taken to have the density of normal liquid nitrogen, to calculate their statistical thickness,  $t$ . A plot of the volume of nitrogen adsorbed versus the statistical thickness,  $t$ , of the adsorbed layer enabled deBoer *et al* to investigate the micropore region. For non porous adsorbents the  $t$ -plot is linear and passes through the origin. However,  $t$ -plots for microporous materials were curved, caused by the filling of the micropores with the adsorbate. At higher relative pressures deviations from the straight line occurred. The slope of the linear portion of

the t-plot, that passes through the origin, was a measure of the specific surface area of the adsorbent. Dollimore and Heal [37] also formulated solutions based on capillary condensation, modelled by the Kelvin equation, and the thickness correlation of Halsey [26]. Their method simplified the solution to the equation by the use of tables that they presented.

In 1968 Mikhail *et al* [38] extended the work of deBoer and co-workers which only allowed for the determination of surface areas and volumes of the totality of narrow pores and the totality of wide pores. Their model, termed the Micropore model (MP-method), allowed the determination of the pore surface and pore volume distributions of narrow pores. The MP-method was still based on the t-curve using the statistical thickness equation proposed by deBoer. However, they determined the slope at each point on the t-plot which gives the surface area accessible to nitrogen molecules at that particular thickness, or pressure.

In the 1960's, Dubinin [39][40] took a different approach to the modelling of microporous materials. He proposed that microporous adsorbents undergo volume filling instead of the formation of successive adsorption layers on the surface of nonporous adsorbents. The model was called the theory of volume filling of micropores (TVFM) [41]. Dubinin assumed that the adsorbed molecules have an adsorption potential which governed the fractional filling of the micropores, based on Polanyi's potential theory of adsorption. The Dubinin-Radushkevich (DR) [42] equation was used to describe the local isotherm, which provided an approximate description of pore filling for adsorbents composed of uniformly sized capillaries. The equation leads to the calculation of the micropore volume and the isosteric heat of adsorption by fitting a straight line through a plot of *log volume adsorbed* versus the transformed pressure ( $\log(p_0/p)^2$ ). However, for a system with a distribution of pore sizes it is necessary to base the calculation on the sum of the contributions from individual pore groups. Stoeckli [43] proposed a solution based on an adsorption integral for a system with polydisperse pore sizes, using the DR equation to describe the local isotherm. Calculation of the pore size distribution required the correlation between the characteristic adsorption energy of a reference substance (conventionally benzene) and the pore's slit width. One correlation was proposed by Dubinin and Stoeckli [44]. The integral contained the term  $f'(B)$  which described the distribution of the micropore volume with a structural parameter ( $B$ ). Stoeckli chose a Gaussian distribution for  $f'(B)$ . However, other

distributions have been used such as the gamma distribution proposed by Jaroniec and Madey [45]. For some activated carbon isotherms, deviations from the DR equation were observed which lead to the derivation of the Dubinin-Astakhov (DA) equation [46], incorporating a different exponent power,  $n$ , to transform the pressure.

In 1983, Horvath and Kawazoe (HK) [47] presented a method for the calculation of the effective pore size distribution in molecular sieve carbon based upon the slit potential model of Everett and Powl [48]. The model considered the micropores of molecular sieve materials to be slits between two graphitised carbon planes. Mathematical descriptions were developed for the potential function, the interaction energy between a gas molecule and an infinite surface between two parallel layers filled with adsorbates. The functions were dependent on the polarizability and the magnetic susceptibility of the adsorbent and the adsorbate molecule. After integration they had an equation which related the pressure to the distance between the nuclei of the two layers, thus providing a micropore size distribution. However, their model gave poor values for larger pores and so Horvath and Kawazoe recommended the use of the Dollimore and Heal [37] model for pores greater than 15Å.

The average potential approach of HK was extended to the evaluation of cylindrical micropore size distributions by Saito and Foley [49], using the cylindrical potential equations of Everett and Powl [48]. They tested the geometric sensitivity of the calculated pore size for commercial fluidised cracking catalyst containing zeolite Y, based on the adsorption of argon at 87°C, and concluded that the cylindrical model provides a more accurate description of the mean pore size. In addition to geometric sensitivity, Saito and Foley demonstrated some parametric sensitivity with the variation in the physical constants of the adsorbate-adsorbent pair. Cheng and Yang [50] extended the idea to enable spherical pores to be modelled, and also proposed improvements to the original Horvath-Kawazoe equations by including the provision for non-linearity of the adsorption isotherm. Horvath and Kawazoe formulated their solution based on linear isotherms, the ideal Henry's law, despite most isotherms of microporous materials demonstrating the Langmuir type relationship. The result of the inclusion of non-linearity was a sharpening of the pore size distribution and a reduction of the mean pore size.

Advancement in computing power has led to the whole adsorption isotherm being modelled by techniques such as Monte Carlo simulations, the approach of molecular dynamics and density functional theory. In 1989, Seaton, Walton and Quirke [51] presented a new analysis method for the determination of pore size distributions, based on a molecular model of the adsorption of nitrogen in porous carbon. Their method considered experimentally measured adsorption isotherms to be the aggregate of the isotherms for individual pores that make up the pore structure of the solid. Using this approach, they mathematically described the isotherm as the integral of the single pore isotherm multiplied by the pore size distribution. The molecular model for nitrogen was based upon mean-field theory, an approximate theory of inhomogeneous fluids in which the interactions between the fluid molecules are divided up into a short-ranged, repulsive part and a long-ranged, attractive part. Each interaction is treated separately, with the long range forces determined by mean-field theory and the short-range forces modelled by an equivalent array of hard spheres. The nitrogen-nitrogen and nitrogen-carbon interactions were modelled by a Lennard-Jones potential with the pore described as a parallel sided slit bound by semi-infinite graphite. Seaton *et al* chose a bimodal log normal distribution to represent the pore size distribution since they believed it to be sufficiently flexible to represent the pore structure of a wide variety of carbons.

Olivier and Conkin [52] extended the ideas of Seaton *et al* and showed that it was feasible to extract the pore size distribution from experimental data by a deconvolution technique without the restriction of assuming a functional form for the distribution. Both Seaton *et al* and Olivier *et al* generated their model isotherms based on the local density approximation to the repulsive forces between molecules which ignored the short range forces. In 1993, Lastoskie, Gubbins and Quirke [53] improved the modelling technique by introducing the non-local mean-field theory calculations into the model. The non-local theory enabled quantitative accurate descriptions of even ultra-microporous structures to be modelled correctly compared to the underestimates of the pore size distributions by the local form of the model. Olivier [54] and Quirke *et al* [55] have also demonstrated the improvements of the non-local mean-field theory, or non-local Density Functional Theory. The big advantages of the simulation approach to the whole of the isotherm is that it allows a pore size distribution from the smallest micropore to macropores to be calculated.

The connectivity of pores within a porous solid are also important parameters with respect to the transport of molecules to the adsorption surface. In 1991, Seaton [56] presented a technique to determine the connectivity of porous solids from the observed hysteresis in nitrogen adsorption-desorption measurements. Originally deBoer [57] proposed five types of hysteresis loops, three of which were used to describe mesopore geometries. In 1985, the IUPAC [4] recommended a new classification using the symbols H1, H2, H3, and H4 (a graphical representation of the isotherms can be seen in Appendix 1). Seaton used percolation theory to determine the mean coordination number of the pore network for type H1 and H2 hysteresis. No connectivity information could be obtained for type H4 hysteresis, exhibited by many microporous carbons, and there were limitations on the applicability of the method for type H3 hysteresis. Liu, Zhang and Seaton [58] improved the original percolation model, enabling the prediction of effective diffusivities, using effective medium theory. Their results suggested that the calculated effective diffusivities were relatively insensitive to the assumed pore shape.

## SECTION 2.3      EXPERIMENTAL PARAMETERS

### *Microscopy*

Optical photographs of the polymers and carbon were taken using a Leica microscope at a variety of magnifications. Low magnification electron micrograph pictures, 100-20,000 $\times$ , of the adsorbents were taken by Mr. F. Page using a Cambridge Stereoscan 360 scanning electron microscope at an accelerating voltage of 20kV. High magnification pictures, 10,000-50,000 $\times$ , were taken by Mr. J. Bates using a Jeol 100CX scanning electron microscope at an accelerating voltage of 100kV.

All samples were dried in a vacuum oven for 24 hours at 70°C and stored in a desiccating jar over silica gel. The adsorbents were glued to aluminium platforms prior to gold coating. Investigations were made into whole, dissected and crushed MN-100, MN-150, MN-200 and F-400.

### *Surface Area and Pore Size Distributions*

Surface area and pore size distributions were obtained using a Micromeritics ASAP 2010C automatic analyser fitted with an optional high stability 1 torr pressure transducer. Samples of the polymers and carbon, in the particle size range 53-75 $\mu\text{m}$  and 500-600 $\mu\text{m}$ , were prepared by outgassing for a minimum of 24 hours at 60°C on the degas ports of the analyser. The adsorbent mass was determined by subtracting the weight of the empty sample tube from the nitrogen backfilled degassed adsorbent/sample tube. Seal frits, inserted into the top of the sample tubes, prevent the degassed samples from being contaminated by exposure to air.

Adsorption isotherms were generated by dosing nitrogen, >99.99% purity, onto the adsorbent contained within a bath of liquid nitrogen at approximately 77K. The analysis and cold trap Dewars were filled using liquid nitrogen to approximately 5cm from the top, measured using a dipstick. An isothermal jacket was then placed over the sample tube before connection to the analysis port of the analyser. Insulated Dewar covers were then placed on the top of both



Dewars.

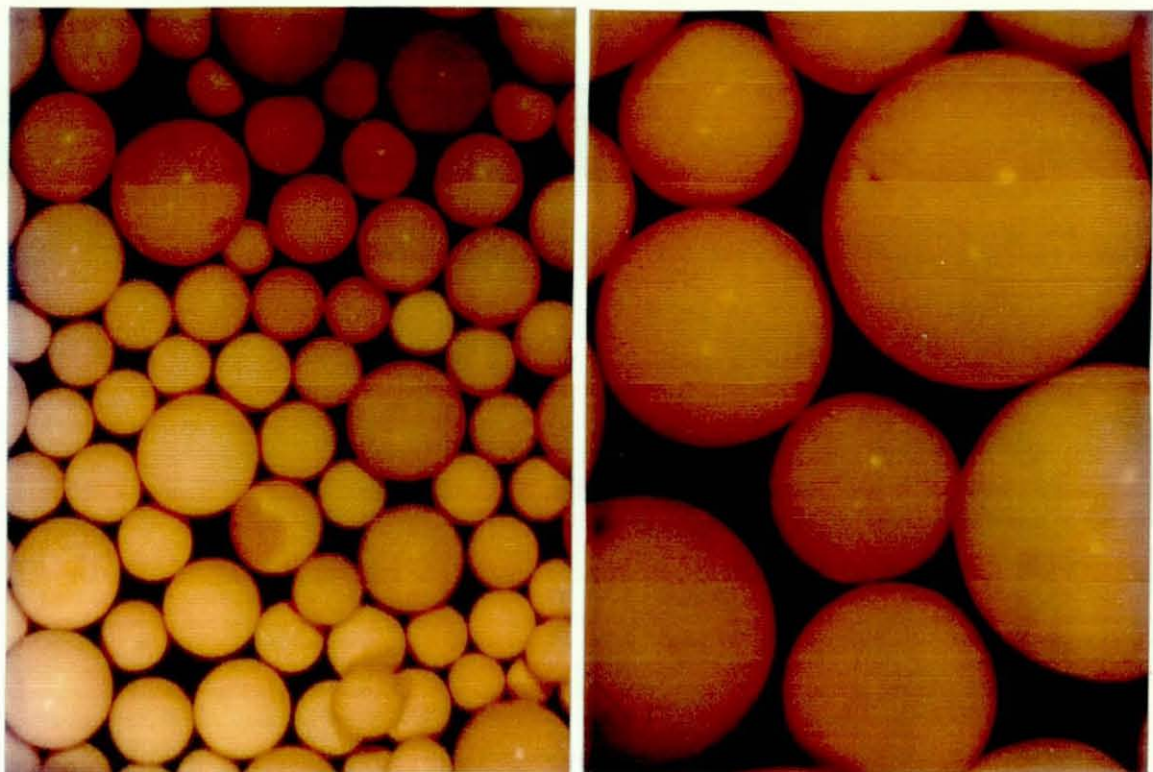
The ASAP 2010 software contains a number of input files which define the instrument parameters for a number of different types of data measurement. The option chosen for all the samples was “High Resolution Nitrogen Adsorption/Desorption”. However a number of parameters were varied according to the sample being analysed (e.g. slow evacuation for fine particles). The dose mode of “Rate of Adsorption” was selected to enable kinetic effects to be investigated prior to data collection which was defined in the high resolution adsorption/desorption pressure table. The equilibration interval was initially set at 45 seconds so as to enable adequate diffusion of the nitrogen into the micropores. However, this selection led to excessive analysis times. The effect of equilibration interval was investigated by analysing samples at intervals of 5, 10, and 45 seconds. An interval of 10 seconds was finally selected since no observable effect was seen on the pore size distribution or the isotherm with the reduction in the equilibration time. The microporous nature of the adsorbents necessitated the free space determination to be measured after the nitrogen adsorption isotherm, since helium is sometimes retained. The molecular drag pump was turned on for all measurements. The subsequent data reduction parameters are described in the results and discussion section.

## SECTION 2.4 RESULTS AND DISCUSSIONS

### *Microscopy*

Figs. 2.2 and 2.3 present the optical microscopy photographs (15 and 45 times magnification) of MN-200 and F-400 respectively. The polymers are perfectly spherical orange/brown beads. Their colouration is probably caused by residual iron introduced during the Friedel-Crafts reaction, since the styrene copolymer is white. The top lighting of the activated carbon causes a significant amount of reflection which explains the golden colour. However, the photographs illustrate the irregular particle shape of the carbon. Low magnification scanning electron micrographs of crushed carbon and polymer can be seen in Figs. 2.4 and 2.5. Crushing of the polymers and carbon causes irregularly shaped particles to be generated and a significant quantity

**Fig. 2.2.**            **Optical Photographs of MN-200 at 15× and 45× magnification.**



**Fig. 2.3.**            **Optical Photographs of F-400 at 15× and 45× magnification.**

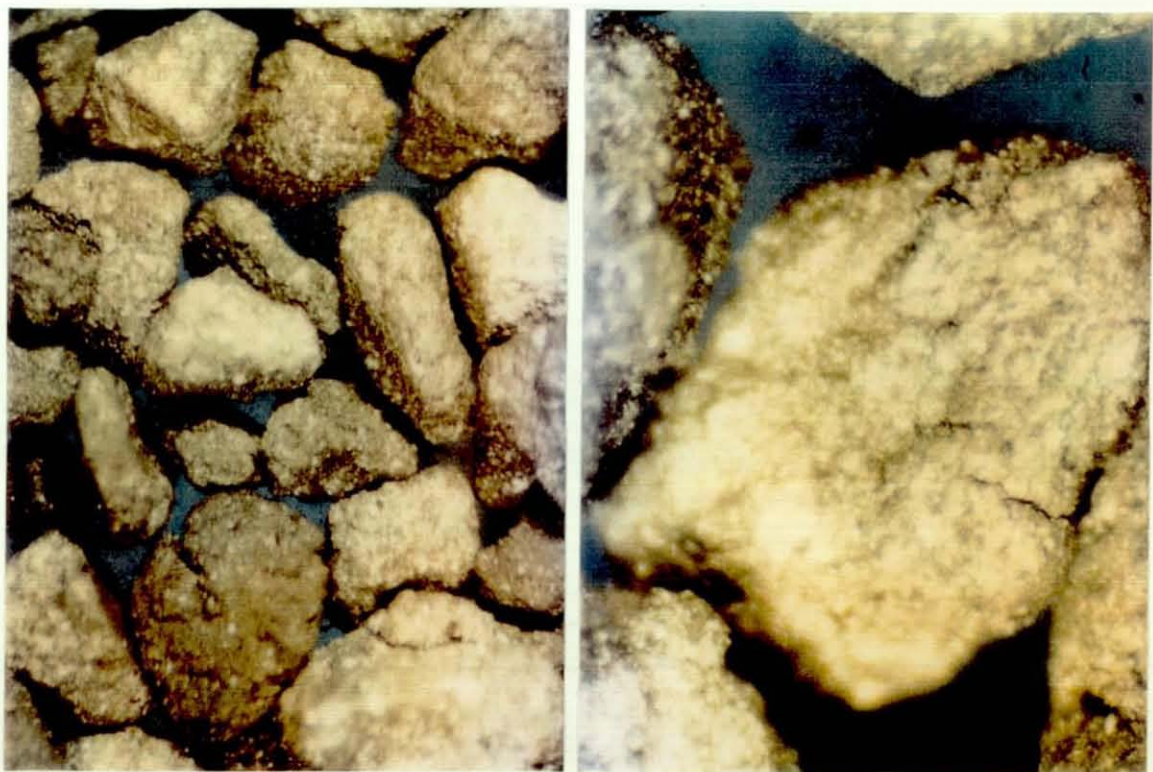




Fig. 2.4. SEM of Crushed F-400, 53-75 $\mu$ m, at two different magnifications.

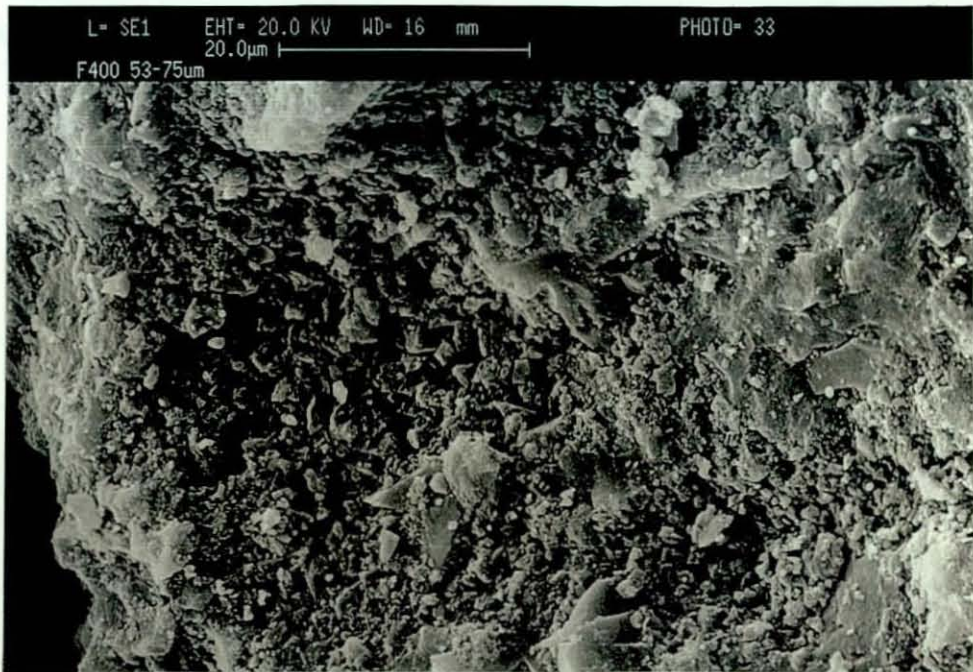
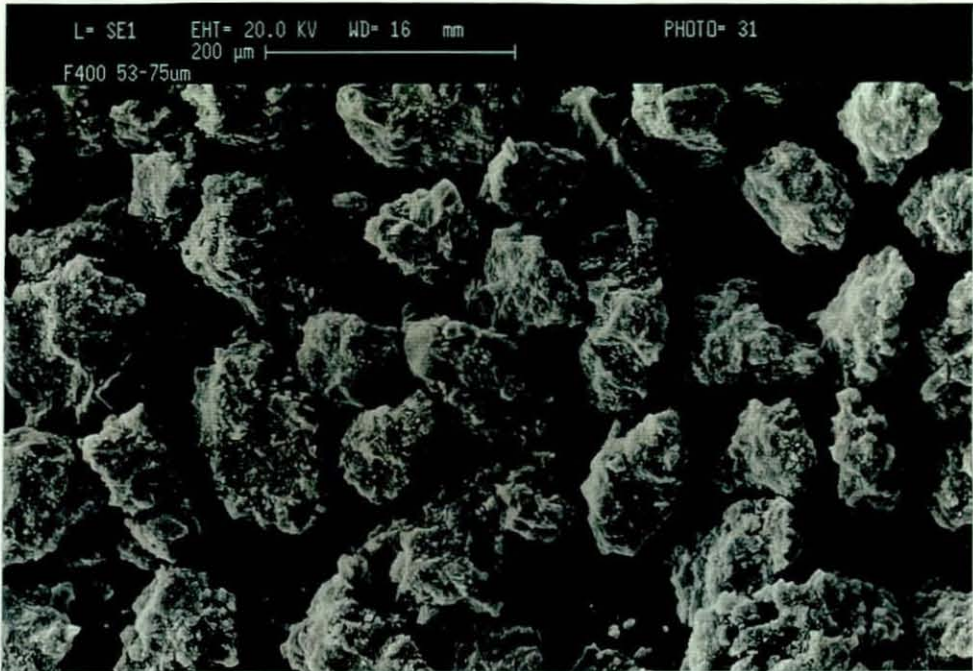


Fig. 2.5. SEM of Crushed MN-150, 53-75 $\mu$ m, at two different magnifications.

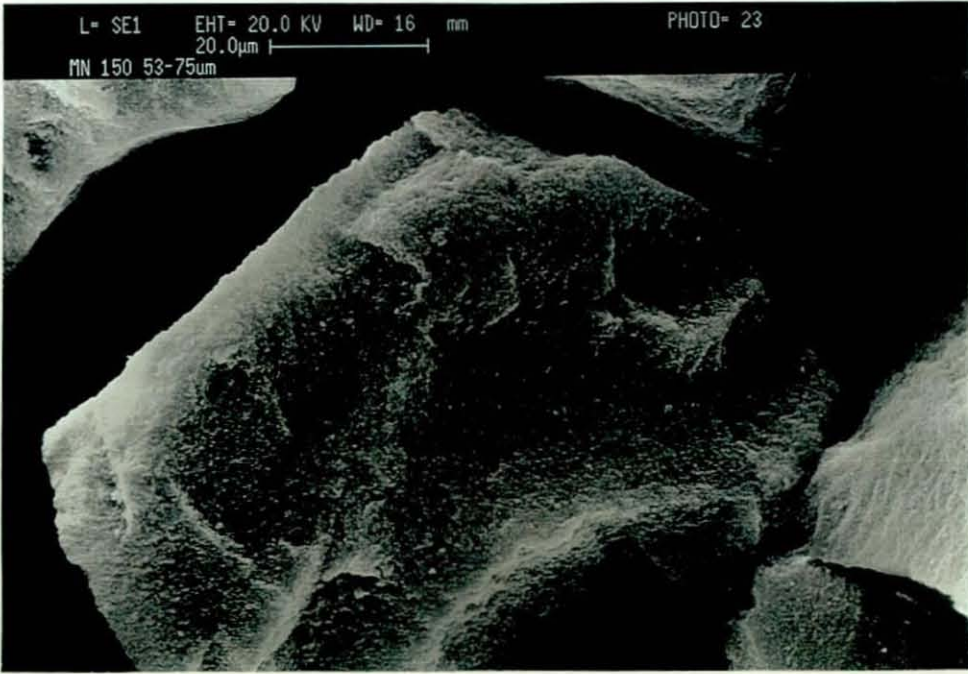
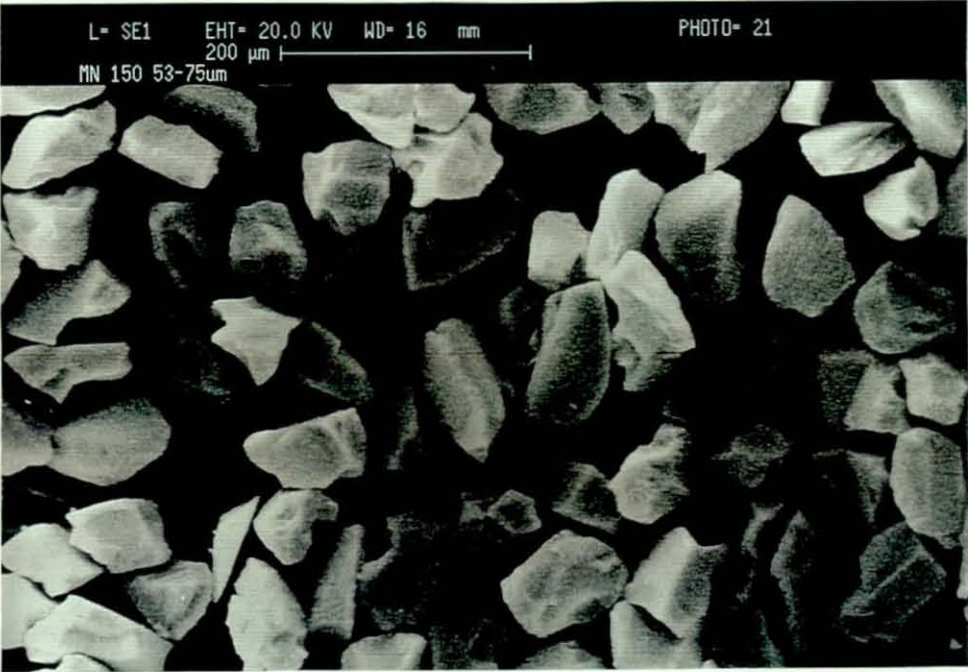
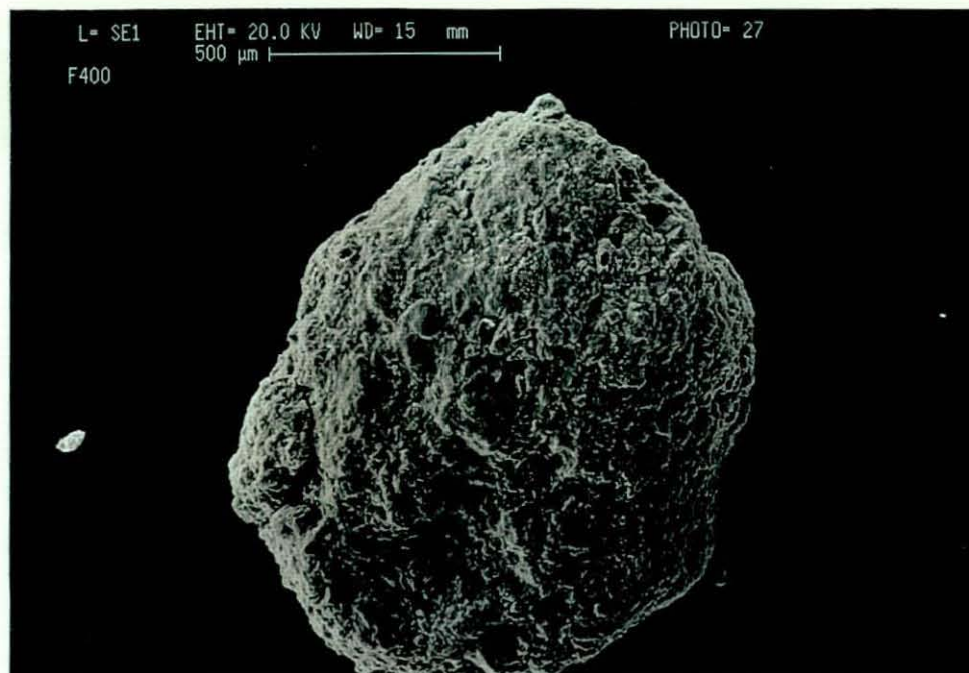




Fig. 2.6. SEM of Washed F-400, 500-600 $\mu$ m, at two different magnifications.



of fines. The adsorbents were wet sieved in an attempt to remove the fines. However, the micrographs clearly demonstrate that fines remain attached to the surface of the carbon whereas the polymer surface is perfectly clean. The brittleness of F-400 and the jagged shape of the particles may cause large quantities of fines to be released. The surface texture of the polymer is sponge like in appearance which indicates the presence of large macropores. However, F-400 appears to be graphite like in structure with flat planes of carbon connected together.

Fig. 2.6 illustrates the scanning electron micrograph of a 500-600 $\mu\text{m}$  particle of F-400. The particle shape appears to be more regular than the crushed material. However, there is still a significant quantity of fines attached to the surface. Operational experience with activated carbon suggests that the fines gradually migrate through adsorption columns into water distribution systems. The fines are a good host for biological media, which may necessitate the installation of post carbon bed filtration at many water facilities.

High resolution scanning electron micrographs, presented in Figs. 2.7-10, show the uniform globular structure of the polymers. The globule diameter is approximately 120-160nm for all the Macronets thus creating large pores that will enable rapid diffusion of adsorbates. A surface texture is apparent on the SEM at 50,000 $\times$  magnification, possibly indicating the presence of large mesopores (around 20nm). However, the surface texture is most likely caused by the gold sputtering process. The external surface of whole polymer beads, illustrated in Figs. 2.9 and 2.10, appears to be partially glazed in comparison with the cross sectional views. The glazed surface may inhibit diffusion into the polymer matrix. The resolution of scanning electron instruments is limited to approximately 20 $\text{\AA}$  which prevents the detection of micropores.



Fig. 2.7. SEM of MN-200, cross-section, at 10,000 $\times$  magnification.

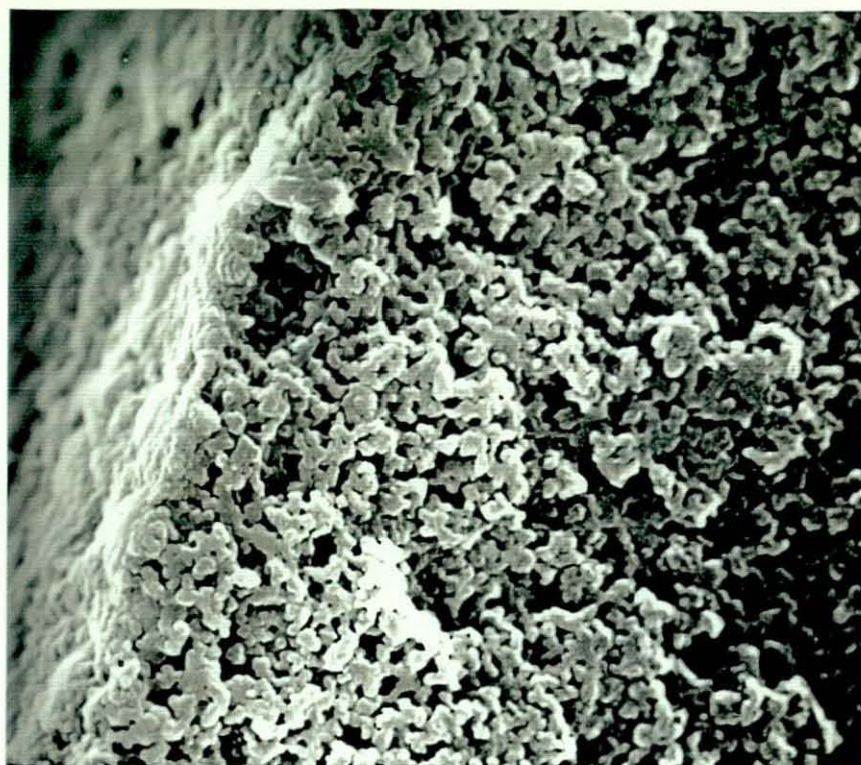


Fig. 2.8. SEM of MN-200, cross-section, at 50,000 $\times$  magnification.

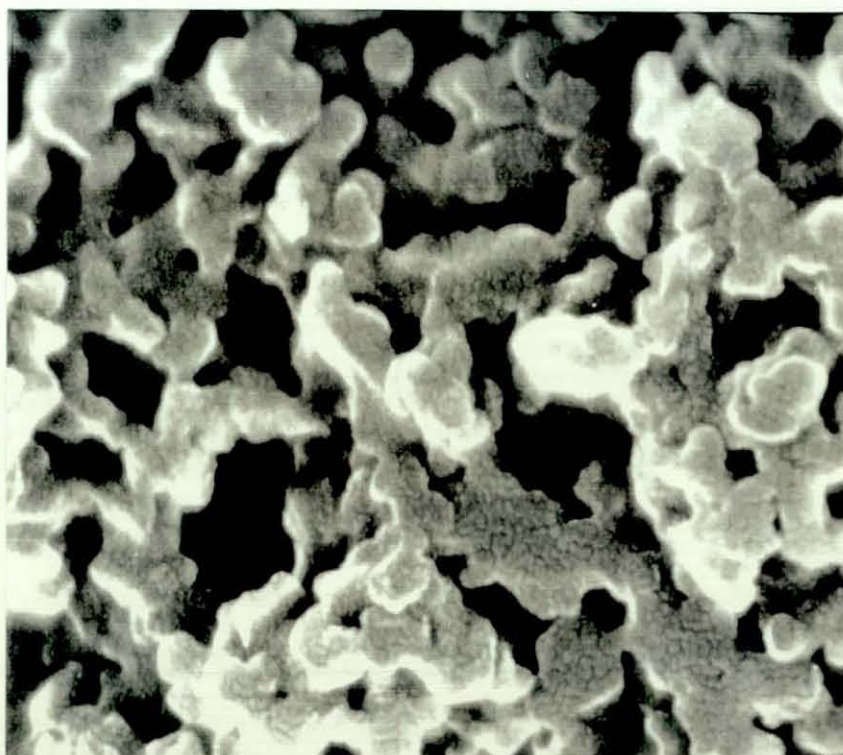




Fig. 2.9. SEM of MN-200, outer surface, at 10,000 $\times$  magnification.

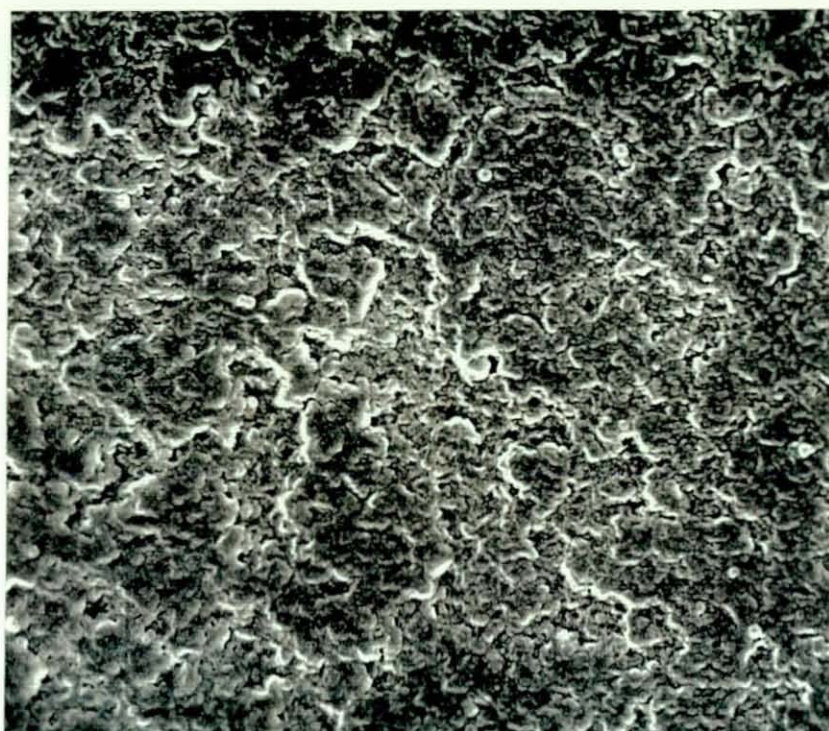
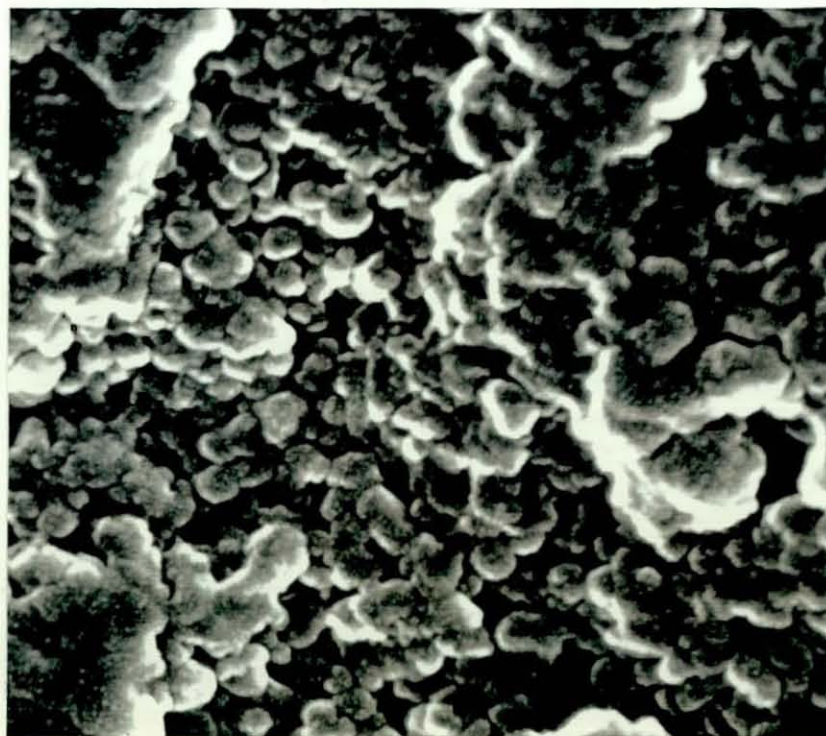


Fig. 2.10. SEM of MN-200, outer surface, at 50,000 $\times$  magnification.





### ***Nitrogen Adsorption Isotherms and Pore Size Distributions***

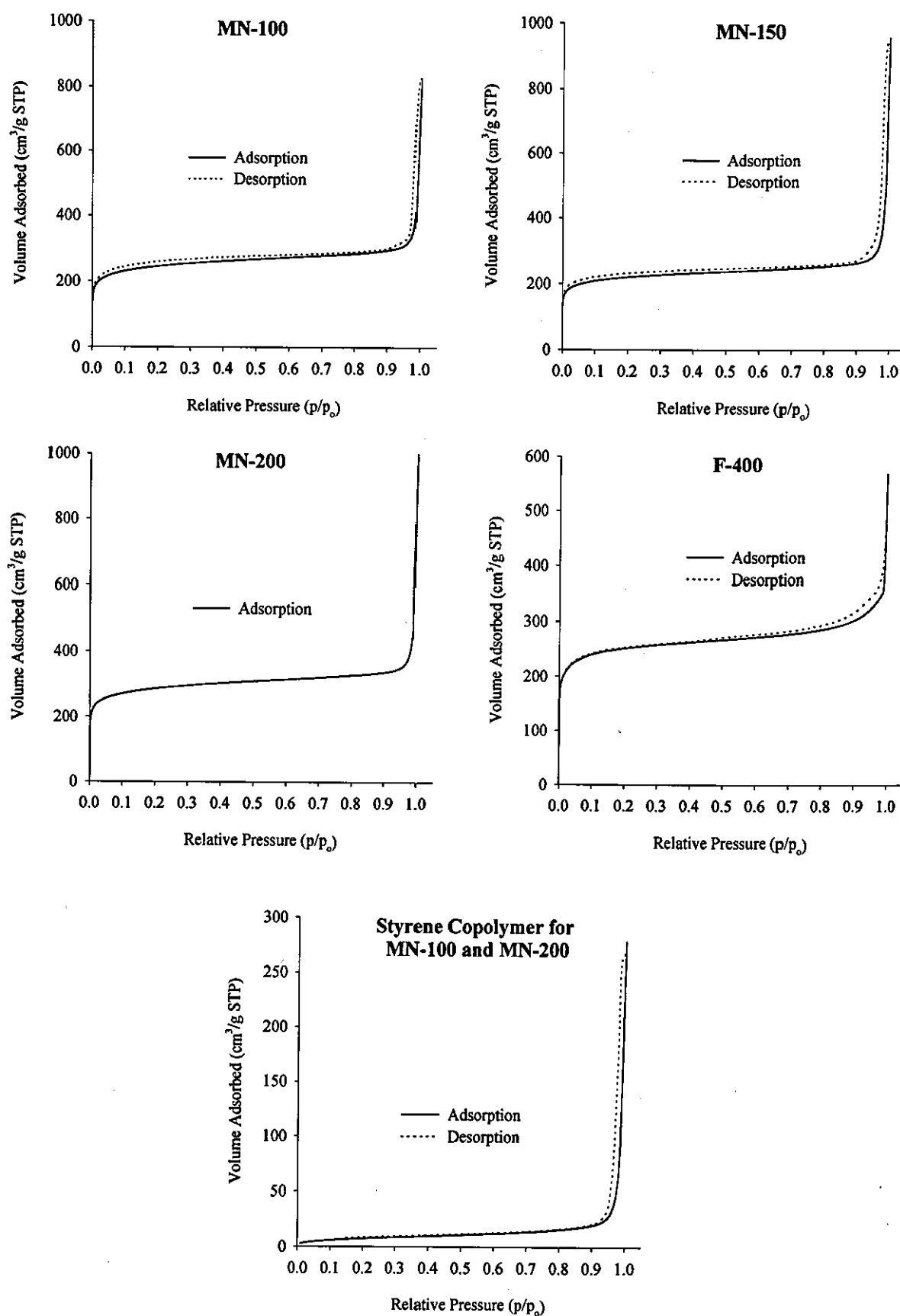
The nitrogen adsorption/desorption isotherms for MN-100, MN-150, MN-200, F-400 and the styrene copolymer are shown in Fig. 2.11. All of the isotherms, except the styrene copolymer, have the classical *Type I* shape indicating the microporous nature of the adsorbents. The styrene copolymer has a *Type II* shape which is characteristic of the multi-layer adsorption onto non-porous or macroporous solid. (Appendix 1 presents the IUPAC classification of the different shapes of isotherms)

The hysteresis in the isotherms provides information about the mesoporous structure of the adsorbents. According to the IUPAC classification [4] the Macronet polymers and the styrene copolymer have type  $H_1$  hysteresis. This shape is often associated with porous materials which consist of agglomerates or compacts of approximately uniform spheres in a fairly regular array, and hence tend to have a narrow pore size distribution. The scanning electron micrographs of the Macronet polymers confirm their agglomerate nature. The ability of Macronet polymers to swell in nitrogen is demonstrated by the low pressure hysteresis observed on the isotherms. The hysteresis of F-400 is best characterised as  $H_4$  behaviour which is often associated with narrow slit-shaped pores or microporosity in the case of *Type I* isotherms. Linares-Solano *et al* [59] provided evidence that microporous carbon with mesopores exhibits such behaviour.

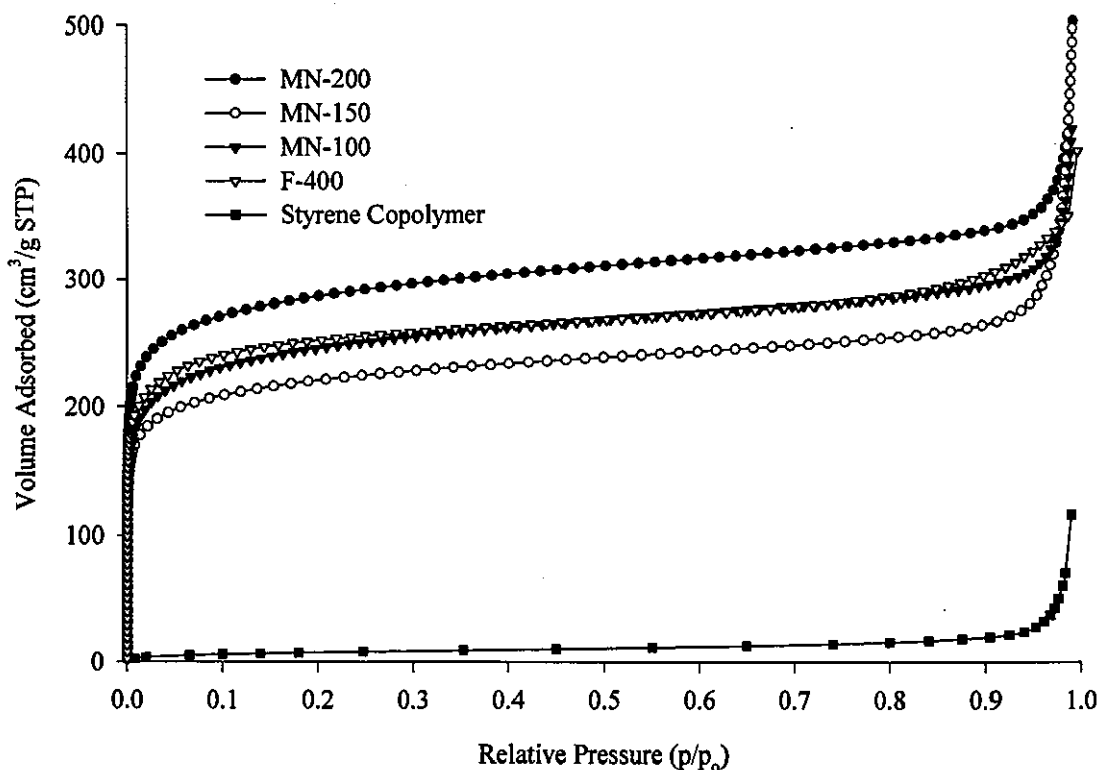
Figs. 2.12 and 2.13 present the overlaid adsorption isotherms for all the adsorbents. Every other data point has been excluded from the graph to simplify the picture. Overall, MN-200 has the greatest capacity for nitrogen with the styrene copolymer having the lowest. However, analysis of the low pressure region in Fig. 2.13 suggests that the carbon has a slightly larger micropore capacity. The overall capacity of MN-100 and MN-150 is lower than that of MN-200 and F-400.

Characterisation of the macropores from isotherm data near  $p/p_0=1$  is not practical since serious condensation on the apparatus walls begins near the saturated vapour pressure. The most common technique for the determination of macropores is mercury intrusion porosimetry which is studied briefly.

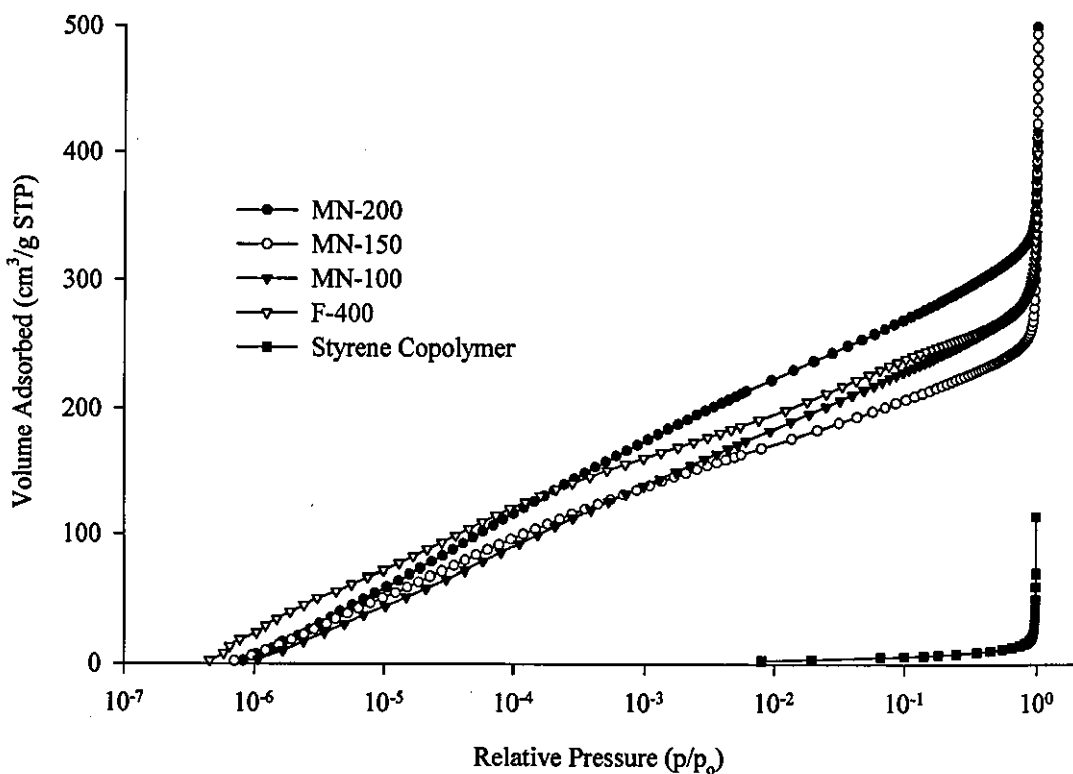
**Fig. 2.11.** Nitrogen Adsorption/Desorption Isotherms for MN-100, MN-150, MN-200, F-400 and the Styrene Copolymer.



**Fig. 2.12.** Comparison of the Nitrogen Adsorption Isotherms for MN-100, MN-150, MN-200, F-400 and the Styrene Copolymer.

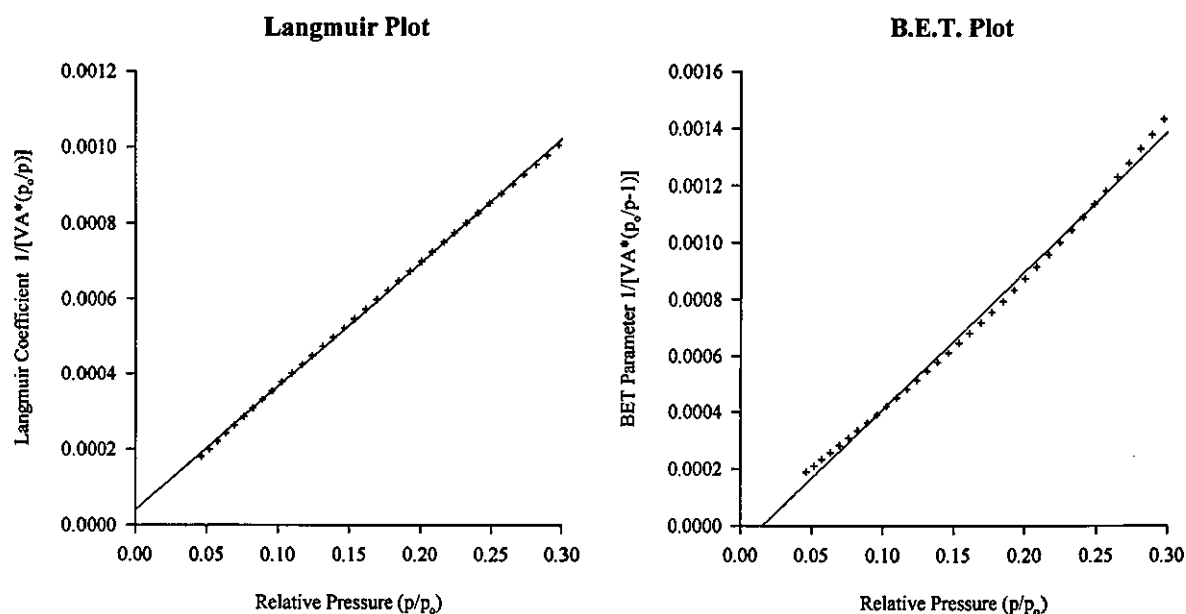


**Fig. 2.13.** Logarithmic Comparison of the Nitrogen Adsorption Isotherms for MN-100, MN-150, MN-200, F-400 and the Styrene Copolymer.



A large number of models can be applied to the experimental adsorption isotherm data to enable the surface area and pore size distributions to be determined. Fig. 2.14 illustrates the Langmuir and B.E.T. plots used for the calculation of the surface area for MN-200, 53-75 $\mu\text{m}$ .

Fig. 2.14. Langmuir and B.E.T. Plots for MN-200, 53-75 $\mu\text{m}$ .



The B.E.T. plot has significant curvature over the pressure range 0.05-0.3. It is possible to obtain a straight line over a limited section of the data. However the differing tangents to the curve result in surface areas that vary by up to 200 $\text{m}^2/\text{g}$ . In order to obtain a positive y-intercept on the B.E.T. plot, the linear range of 0.05-0.10 was selected for the surface area results presented in Table 2.1. However, this results in large values of the B.E.T. coefficient 'C' ( $\gg 200$ ) which indicates that micropore filling occurred. The B.E.T. analysis does not take into account the possibility of micropore filling or penetration into cavities of molecular size. Hence, these effects may falsify the B.E.T. surface areas for the microporous adsorbents MN-100, MN-150, MN-200 and F-400. The theory is however valid for the copolymer which demonstrates a linear relationship over the relative pressure range of 0.05-0.30.

The Langmuir isotherm is linear over the full range of 0.05-0.30 for all of the adsorbents which suggests that the analysis is applicable. However, the results may be slightly higher than the true surface area results due to monolayer-multilayer formation occurring in the meso-macropores of the adsorbents.

**Table 2.1. Surface Area Results for MN-100, MN-150, MN-200, F-400 and the Styrene Copolymer Based Upon Different Models. (53-75 $\mu$ m and 500-600 $\mu$ m adsorbents).**

| Surface Area<br>(m <sup>2</sup> /g) | 53-75 $\mu$ m Adsorbent |        |        |       | 500-600 $\mu$ m Adsorbent |        |        |        |           |
|-------------------------------------|-------------------------|--------|--------|-------|---------------------------|--------|--------|--------|-----------|
|                                     | MN-100                  | MN-150 | MN-200 | F-400 | MN-100                    | MN-150 | MN-200 | F-400  | Copolymer |
| Langmuir                            | 1144                    | 1018   | 1331   | 1150  | 1029                      | 968    | 1306   | 1254   | 43.4      |
| B.E.T.*                             | (922)                   | (825)  | (1072) | (950) | (827)                     | (785)  | (1086) | (1182) | 28.4      |
| DFT                                 | 719                     | 698    | 868    | 852   | 630                       | 645    | 852    | 850    | 29.9      |

\* Results in brackets indicate uncertainty in the figures presented

The Langmuir surface areas for the 500-600 $\mu$ m adsorbent are slightly lower for all the adsorbents compared to the 53-75 $\mu$ m material which is probably due to slower diffusion of the nitrogen molecules into the micropores. The slow diffusion tricks the surface area instrument into taking the equilibrium pressure before the true equilibrium is reached, causing the volume adsorbed to be under predicted. MN-200 has a larger surface area than MN-100, MN-150 and F-400. Since MN-200 and MN-100 are produced from the same polymer backbone it appears as if the amine functional group may block or occupy a percentage of the micropores, resulting in the lower surface area. The surface area values calculated using Density Functional Theory, see page 37, are lower than both the Langmuir and B.E.T. results. However similar trends are observed.

In recent times the Horvath and Kawazoe model has been widely used and accepted for the characterisation of micropores. Valladares *et al* [60] tested the validity of the model by Monte Carlo Simulation and concluded that the HK model gave good results when the microporosity was confined to a pore size lower than approximately 13Å. Russell *et al* [61] concluded that the simplicity of the HK model made it extremely attractive. However, the pore size distributions obtained show a strong dependency on the input parameters; the diameter, density of atoms and polarizability of the adsorbent under investigation. These parameters exist in the literature for well defined pore structured materials such as zeolites since their molecular dimensions can be measured by techniques such as X-ray diffraction. Cheng and Yang [50] proposed enhanced Horvath and Kawazoe equations. However, they were unable to demonstrate the improvements of their model due to the uncertainty in the physical parameters currently available. The problem of parameter estimation becomes more difficult for novel materials such as the Macronet

polymers. Fig. 2.15 illustrates the micropore size distribution for MN-200, 53-75 $\mu\text{m}$ , calculated using the original Horvath and Kawazoe slit pore model, based on different interaction parameters found in the literature. The data clearly shows the strong dependency of the model on the interaction parameter. Table 2.2 presents the mean pore sizes calculated.

**Table 2.2. Effect of the Interaction Parameter on the Mean Pore Size of MN-200, 53-75 calculated using Horvath and Kawazoe Slit Pore Model.**

| Porous Material                       | Interaction Parameter (ergs.cm <sup>4</sup> ) | Mean Pore Size (Å) |
|---------------------------------------|-----------------------------------------------|--------------------|
| Carbon-Graphite (Horvath and Kawazoe) | $6.53 \times 10^{-43}$                        | 9.9                |
| Zeolite                               | $3.49 \times 10^{-43}$                        | 7.2                |
| Carbon-Graphite (Ross/Olivier)        | $2.84 \times 10^{-43}$                        | 5.5                |
| Aluminophosphate                      | $1.85 \times 10^{-43}$                        | 5.5                |
| Aluminosilicate                       | $1.70 \times 10^{-43}$                        | 4.9                |
| Other (Micromeritics)                 | $1.39 \times 10^{-43}$                        | 3.9                |

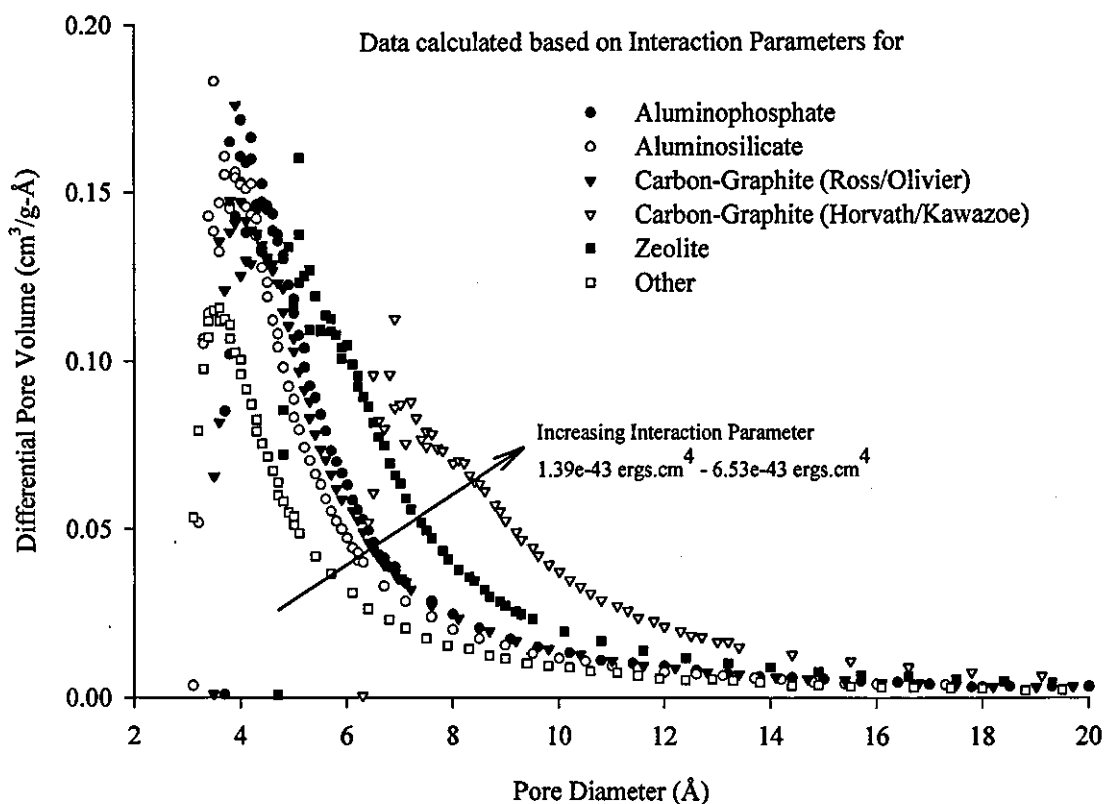
The geometry assumed for the shape of the pore also has a significant effect on the resulting pore size distribution. Fig. 2.16 presents the effect of the pore geometry on the pore size distribution for MN-200, 53-75 $\mu\text{m}$ . The models were calculated using two different interaction energies which demonstrates the different distributions that can be generated. Table 2.3 presents the mean pore sizes based upon the different geometries.

**Table 2.3. Effect of Pore Geometry and Interaction Parameter on the Mean Pore Size of MN-200.**

| Interaction Parameter               | Mean Pore Size Based Upon |                    |                     |
|-------------------------------------|---------------------------|--------------------|---------------------|
|                                     | Slit Pores (Å)            | Cylinder Pores (Å) | Spherical Pores (Å) |
| Carbon-Graphite (Horvath & Kawazoe) | 9.9                       | 18.2               | 35.5                |
| Other                               | 3.9                       | 6.6                | 7.9                 |

Such a wide variation in the mean pore sizes and distributions means that quantitative pore sizes for the adsorbents in this study cannot be achieved. However, the data does allow for comparisons between similar adsorbents since the pore geometry and interaction energies may be comparable.

**Fig. 2.15.** Effect of The Interaction Parameter on the Pore Size Distribution of MN-200, 53-75 $\mu$ m, calculated using the Slit Pore Horvath and Kawazoe Model.



**Fig. 2.16.** Effect of Pore Geometry on the Pore Size Distribution of MN-200, 53-75 $\mu$ m, calculated using the Horvath and Kawazoe (Slit), Saito and Foley (Cylinder) and Cheng and Yang (Sphere) Models.

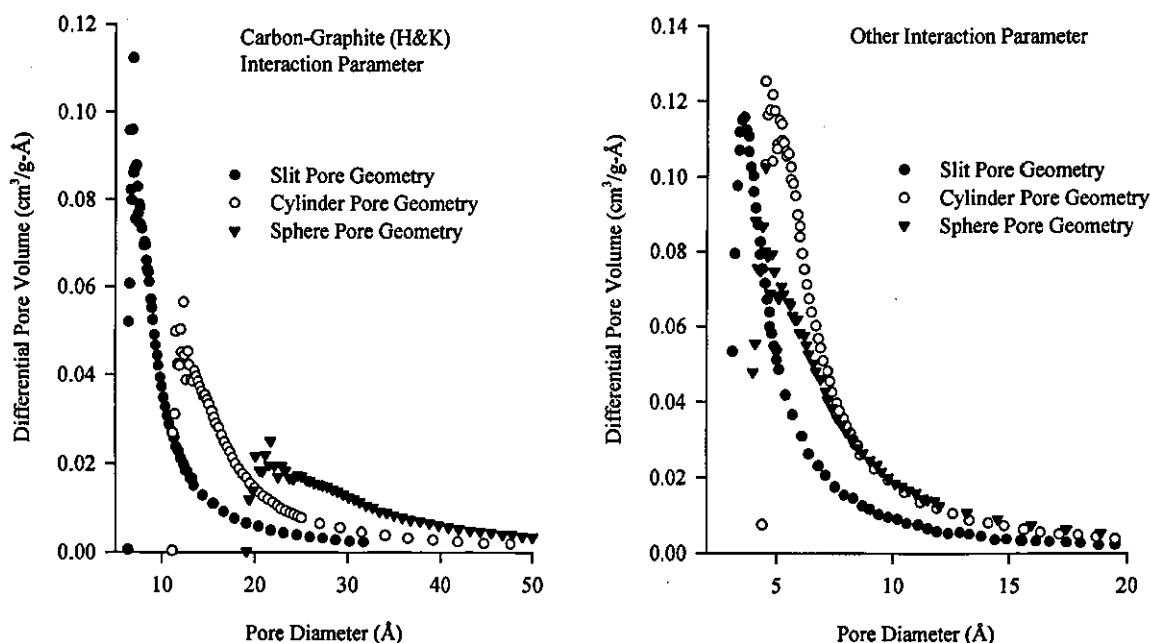


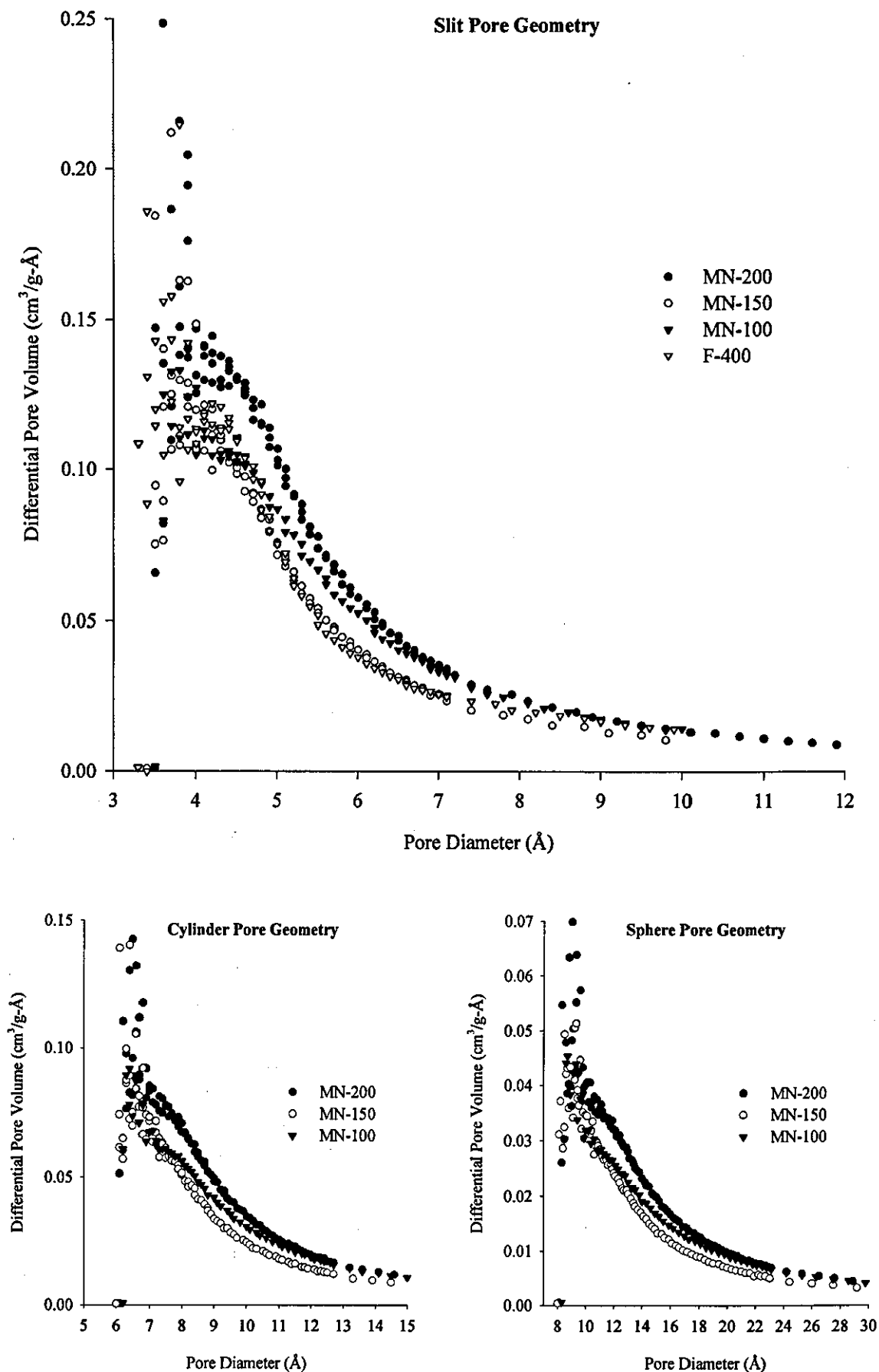
Fig. 2.17 presents the pore size distributions for MN-100, MN-150, MN-200 and F-400 based on the carbon-graphite interaction parameter. The parameter was as a compromise between the interaction energies of the carbon and the lower interactions of the polymers. The slit pore geometry of carbons, derived from natural materials, is well accepted in the literature. However, the polymers are unlikely to have such a geometry due to the random crosslinking that occurs during their production. Ogston [62] described the pores in swollen polymer gels as spaces between randomly oriented rigid rods, such as might be occupied by a spherical object placed within the network or might allow free rotation to an elongated one. The effective mean pore sizes for three different pore geometries; slit pores (the original Horvath and Kawazoe correlation), cylindrical pores (Saito and Foley extension to H&K model) and spherical pores (L. Cheng and R. Yang extension to the H&K model) are presented in Table 2.4. (Interaction Parameter of  $2.84 \times 10^{-43}$  ergs.cm<sup>4</sup>).

**Table 2.4. Mean Pore Size of MN-100, MN-150, MN-200 and F-400 (53-75 $\mu$ m).**

| Pore Geometry  | Mean Pore Size (Å) |        |        |       |
|----------------|--------------------|--------|--------|-------|
|                | MN-100             | MN-150 | MN-200 | F-400 |
| Slit Pores     | 5.0                | 4.8    | 5.5    | 4.6   |
| Cylinder Pores | 8.7                | 8.2    | 9.5    | -     |
| Sphere Pores   | 13.7               | 12.6   | 15.6   | -     |

The backbone polymer matrix of MN-100 and MN-200 is the same. However the addition of the amine functional group appears to reduce the micropore size slightly. The greater degree of weak base functionality for MN-150 may provide a reason for its lowest effective mean pore size. However, the amine functional groups on the surface of MN-100 and MN-150 may necessitate the use of different interaction parameters, since the groups may induce a dipole on the nitrogen causing an increase in the adsorbent/adsorbate interaction energy. The resultant distributions would be shifted to larger pore sizes, perhaps providing distributions which are identical to those of MN-200. This theory was investigated by conducting an adsorption isotherm using argon as the adsorbate at liquid argon temperatures for MN-100. Argon is a totally inert gas, no dipoles can be induced, and it is also slightly smaller than nitrogen (a molecular cross section of  $14.2\text{\AA}^2$  compared to  $16.2\text{\AA}^2$  for nitrogen). The small molecular size enables more pores to be accessed,



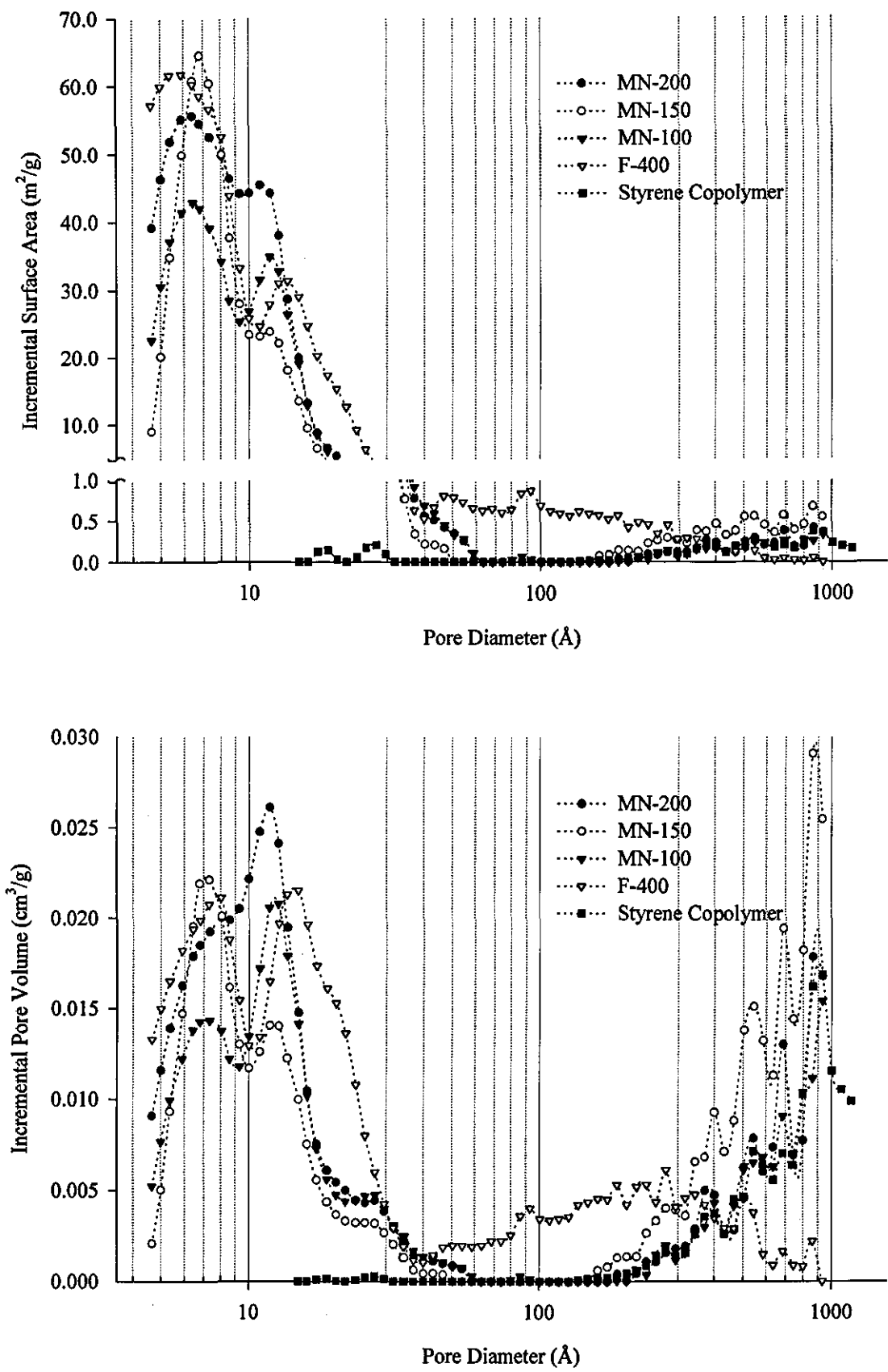
**Fig. 2.17. Pore Size Distributions of MN-100, MN-150, MN-200 and F-400.**

which is demonstrated by the slightly higher Langmuir surface area of 1170m<sup>2</sup>/g. The mean pore diameters were 5.5Å, 9.7Å and 16.2Å for slit, cylindrical and spherical pores geometries respectively (based upon the carbon-graphite/argon (Ross/Olivier) interaction parameter of  $2.61 \times 10^{-43}$  ergs.cm<sup>4</sup>). The results are virtually identical to those of MN-200 presented in Table 2.4, thus confirming that the nitrogen in the amine group affects the interaction parameter. There are a number of advantages of argon as the adsorbate. However the cost of liquid argon prevented the routine analysis. The mean pore diameter of F-400 appears to be exceptionally low although this may be due to the incorrect selection of the interaction parameter. The Horvath and Kawazoe carbon graphite interaction parameter would yield a mean pore diameter of nearer 9Å.

A number of other models are widely used for the determination of the micropore size distribution including the MP-method and solutions based upon the theory of micropore filling method presented by Dubinin and co-workers. The MP-method is based upon the differentiation of the  $t$  plot which does not take into account the enhancement of the adsorptive interaction in small pores, due to interactions among molecules in the adsorbed films on opposing walls and the superposition of the wall potentials. Thus, at a given pressure the statistical thickness, approximated using the Halsey or the Harkins-Jura equation, of the adsorbed layer would be greater in the pore than the non porous material. The TVFM, using the Dubinin-Radushkevich or the Dubinin-Astakhov equations to represent the local isotherm, requires the shape of the pore size distribution, often Gaussian, to be assumed. This tends to unduly constrain the resultant pore size distribution calculated by the technique. At low pressures, or volume fillings, the TVFM is not applicable which restricts the use of the method.

Density Functional Theory (DFT) is a new technique that is based upon the adsorbate-adsorbate and adsorbate-adsorbent interactions, similar to the HK technique. However, the HK model assumes that the density of fluid near the walls of micropores is constant whereas the DFT models actually calculate the density. DFT is applicable for a broad spectrum of pore sizes up to 4000Å which makes it an attractive model. However, as with the original Horvath and Kawazoe correlations, the DFT model is based upon slit pores with graphite interaction energies. Fig. 2.18 illustrates the DFT distributions for MN-100, MN-150, MN-200, F-400 and the styrene copolymer. The model demonstrates the bimodal nature of the Macronet polymers, micropores

Fig. 2.18. DFT Pore Size Distributions of MN-100, MN-150, MN-200, F-400 and the Styrene Precursor



and meso/macropores. The effect is more apparent on the pore volume plot since larger pores contribute very little to the overall incremental surface area of the adsorbent. The pore size distribution of MN-100 and MN-200 is virtually identical over the entire range of pore sizes. However, the incremental surface area and pore volume of MN-100 is slightly lower which seems to confirm that the functional groups block the access to a percentage of the micropores. MN-150 has a significant pore volume from about 200Å upwards which is lower than that for MN-100 and MN-200. This would suggest that the diffusion into MN-150 may be slower.

The pore size distribution of the polystyrene precursor to MN-100 and MN-200 indicates no appreciable microporous volume or surface area. Prior to the crosslinking reaction the macroporous styrene copolymer is swollen in a good solvent. The solvation of the polymer creates a freedom in the gel type structure. When the solvent is removed, after the Friedel-Crafts reaction, the polymer is prevented from returning to its original state by the rigid crosslinking bridges. This creates a structure that is strained when it is in dried form and develops the high micropore surface area and pore volume. The macropore distribution is identical to MN-100 and MN-200.

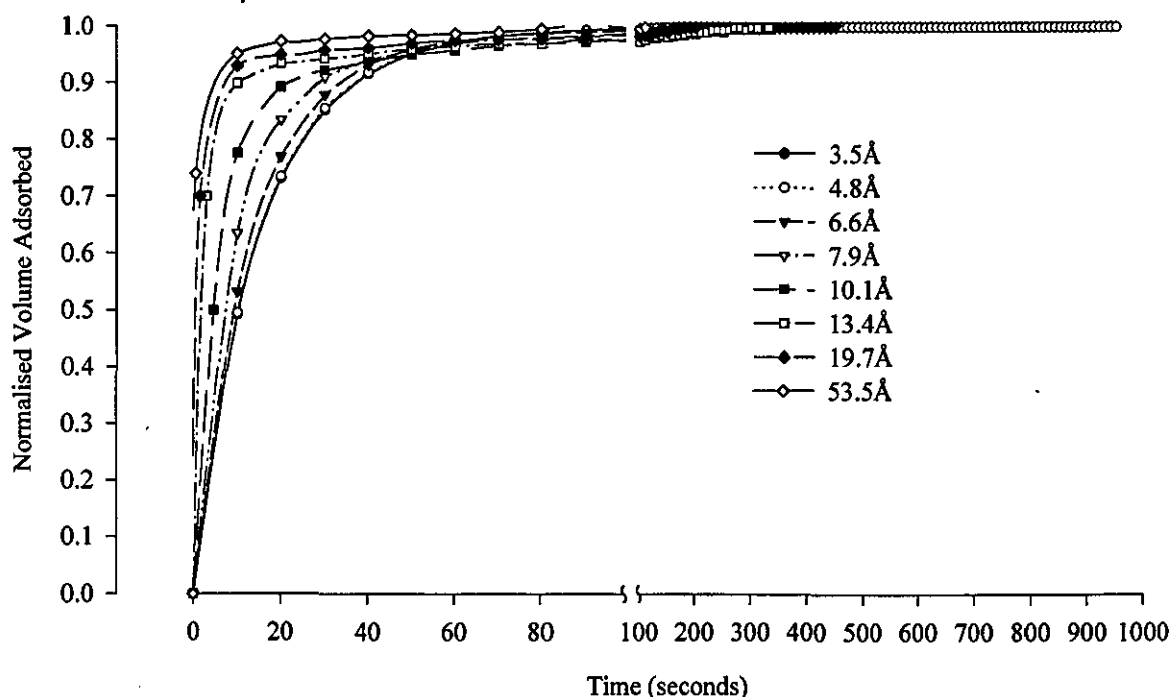
The pore size distribution of F-400 is significantly different to the Macronet Polymers in the meso/macropore region. The carbon has a significant quantity of pores in the mesoporous range, 20-500Å, which may enhance the diffusion of organic species into the micropores. However, these pores may also suffer from being blocked by large organic molecules such as fulvic and humic acids. The Macronet polymers show few mesopores in the range 30-200Å. The distribution of micropores within F-400 appears broader than with the Macronet polymers, 3-20Å compared to 4-14Å.

The apparent bimodal distribution of pores in the microporous region is caused by deficiencies in the Density Function Theory model. The theory is incapable of modelling pores in the 8-10Å region which causes the smoothed data to have a slight dip in the distribution. The pore size distributions of the 500-600µm adsorbents were virtually identical and showed similar trends to the results presented above. The microporous distribution appeared to be marginally larger than for the crushed material which is due to kinetics effects.

The B.J.H equations enable the size of mesopores and small macropores to be modelled. However, the polymers do not show any mesoporosity and so the model has not been applied. The mean macropore sizes of the polymers were measured at Purolite International Ltd using mercury intrusion porosimetry. MN-150 had a mean macropore size of  $532\text{\AA}$  compared to the value of  $880\text{\AA}$  for MN-200 and MN-100. These values are in reasonable agreement with the values suggested by the nitrogen adsorption. The specified contact angle used for the mercury porosimetry size distribution calculations has a dramatic effect on the meso/macropore size distribution. A  $20^\circ$  change in the contact angle causes variations of up to  $200\text{\AA}$  in the mean pore size.

The collection mode for the isotherm data allowed the rate of nitrogen adsorption to be investigated. Fig. 2.19 presents the equilibrium curves at different relative pressures for MN-200 53-75 $\mu\text{m}$ .

**Fig. 2.19.** Fractional Approach to Equilibrium Curves for the Adsorption of Nitrogen onto MN-200, 53-75 $\mu\text{m}$ .



The pore sizes presented were calculated from the equilibrium relative pressure using the Horvath and Kawazoe slit pore model using the carbon-graphite (Ross-Olivier) interaction parameter.

The data illustrates the rate of adsorption dependency on the pore size distribution. A comparison between the different adsorbents indicated no differences with respect to the rate of adsorption. There was also no significant difference between the rate of adsorption of the two size fractions 53-75 $\mu\text{m}$  and 500-600 $\mu\text{m}$ . The curves demonstrate the quick kinetics for small probe molecules such as nitrogen. More meaningful rate of adsorption studies require the use of larger molecules such as benzene.

## SECTION 2.5 CONCLUSIONS

The measurement of pore sizes is extremely subjective on the data reduction that is applied to the experimentally derived information. This is true for the two techniques used for porosity measurement, mercury intrusion porosimetry and nitrogen adsorption. Despite these inadequacies the techniques allow for reasonable comparisons to be made between similar adsorbents whose pore geometry and energy of the adsorbent/adsorbate interaction are similar.

The Macronet polymers contain both macropore and micropores. MN-100 and MN-200 are virtually identical in pore size distribution with a mean macropore and micropore diameters of approximately 900 $\text{\AA}$  and 12 $\text{\AA}$  respectively. MN-150 has a similar microporous structure. However it exhibits a smaller mean macropore diameter of 532 $\text{\AA}$ . Subtle differences in the microporous structure of the polymers are observed. However, the amine functional groups on MN-100 and MN-150 increase the adsorbent/nitrogen interaction. An argon pore size distribution for MN-100 indicated that the mean pore sizes are virtually identical. The activated carbon has a similar microporous size distribution to the polymers. However there are a number of mesopores in the range 20-500 $\text{\AA}$ .

**SECTION 2.6 REFERENCES**

- [1] R.S. Summers and P.V. Roberts, Activated Carbon Adsorption of Humic Substances. II. Size Exclusion and Electrostatic Interactions, *Journal of Colloid and Interface Science*, 122, (2), (1988), p382-397.
- [2] G. Newcombe, C. Donati, M. Drikas and R. Hayes, Adsorption Onto Activated Carbon: Electrostatic and Non-electrostatic Interactions., *Water Supply*, 14, (2), (1996), p129-144.
- [3] R. Hopman, W.G. Siegers and J.C. Kruithof, Organic Micropollutant Removal by Activated Carbon Filter Filtration., *Water Supply*, 13, (3-4), (1995), p257-261.
- [4] K.S.W. Sing, D.H. Everett, R.A.W. Haul, L. Moscou, R.A. Pierotti, J. Rouquerol and T. Siemieniewska, Reporting Physisorption Data For Gas/Solid Systems with Special Reference to the Determination of Surface Area and Porosity., *Pure and Applied Chemistry*, 57, (1985), p603-619.
- [5] M.M. Dubinin, Physical Adsorption of Gases and Vapors in Micropores., in 'Progress in Surface and Membrane Science', D.A. Cadenhead, J.F. Danielle and M.D. Rosenberg ed, 9, Academic Press, New York, (1975), p1-70.
- [6] M. Endo, K. Oshida, K. Kogiso, K. Matsubayashi, K. Takeuchi, S. Kobayashi and M.S. Dresselhaus, Pore Analysis of Activated Carbon Fibres by High Resolution Transmission Electron Microscope Combined Image Analyser., *Materials Research Society Symposium Proceedings*, 371, (1995), p511-515.
- [7] R.W. Innes, J.R. Fryer and H.F. Stoeckli, On the Correlation Between Micropore Distribution Obtained From Molecule Probes and From High Resolution Electron Microscopy, *Carbon*, 27, (1), (1989), p71-76.
- [8] K. Oshida, K. Kogiso, K. Matsubayashi, K. Takeuchi, S. Kobayashi, M. Endo, M.S. Dresselhaus and G. Dresselhaus, Analysis of Pore Structure of Activated Carbon Fibres Using High Resolution Transmission Electron Microscopy and Image Processing., *Journal of Materials Research*, 10, (10), (1995), p2507-2517.
- [9] J. Economy, M. Daley, E.J. Hippo and D. Tandon, Elucidating the Pore Structure of Activated Carbon Fibres Through Direct Imaging Using Scanning Tunnelling Microscopy (STM)., *Carbon*, 33, (3), (1995), p344-345.
- [10] H.F. Stoeckli, Microporous Carbons and Their Characterisation: The Present State of the Art., *Carbon*, 28, (1), (1990), p1-6.
- [11] T. Ito and J. Fraissard,  $^{129}\text{Xe}$  Nuclear Magnetic Resonance Study of Xenon Adsorbed on Zeolite NaY Exchanged with Alkali-metal and Alkaline-earth Cations, *Journal of the Chemical Society. Faraday Transactions. 1.*, 83, (1987), p451-462.

- [12] W.M. Curtis Conner, E.L. Weist, T. Ito and J. Fraissard, Characterisation of the Porous Structure of Agglomerated Microspheres by  $^{129}\text{Xe}$  NMR Spectroscopy., *Journal of Physical Chemistry*, 93, (1989), p4138-4142.
- [13] V.A. Davankov and M.P. Tsyurupa, Macronet Isoporous Styrene Copolymers: Unusual Structure and Properties., *Die Angewandte Makromolekulare Chemie*, 91, (1980), p127-142.
- [14] M.P. Tsyurupa and V.A. Davankov, The Study of Macronet Isoporous Styrene Polymers by Gel Permeation Chromatography., *Journal of Polymer Science: Polymer Chemistry Edition*, 18, (1980), p1399-1406.
- [15] K. Jeřábek and K. Setínek, Structure of Macronet Styrene Polymer as Studied by Inverse Steric Exclusion Chromatography and by Selective Sulfonation., *Journal of Polymer Science: Part A: Polymer Chemistry*, 27, (1989), p1619-1623.
- [16] J.F. Quinson, J. Dumas and J. Serughetti, Alkoxide Silica Gel: Porous Structure by Thermoporometry., *Journal of Non-Crystalline Solids*, 79, (3), (1986), p397-404.
- [17] M.K.N. Yenkie and G.S. Natarajan, Determination of Specific Surface Area of Granular Activated Carbon by Aqueous Phase Adsorption of Phenol and from Pore Size Distribution Measurements., *Separation Science and Technology*, 28, (5), (1993), p1177-1190.
- [18] V.N. Marsheva, V.S. Moryakov, A.C. Schabaeva, L.M. Kozlov, V.A. Davankov, M.P. Tsyurupa, Method of Purification of Gases from Hydrocarbons, Alcohols and Ketones., *USSR Patent 860,832*, July 5, (1981).
- [19] I. Langmuir, The Evaporation, Condensation, and Reflection of Molecules and The Mechanism of Adsorption., *The Physical Review, Second Series*, VIII, 4, (1916), p149-176.
- [20] I. Langmuir, The Adsorption of Gases on Plane Surfaces of Glass, Mica and Platinum, *Journal of the American Chemical Society*., 40, (1918), p1361-1403.
- [21] S. Brunauer, P.H. Emmett and E. Teller, Adsorption of Gases in Multimolecular Layers., *Journal of the American Chemical Society*, 60, (1938), p309-319.
- [22] DeBoer and Zwicker, *Zeitschrift für Physikalische Chemie*., B3, (1929), p407. cited in ref 21.
- [23] R. Stevenson Bradley, Polymolecular Adsorbed Films. Part I. The Adsorption of Argon on Salt Crystals at Low Temperatures, and the Determination of Surface Fields., *Journal of the Chemical Society, Part II*, (1936), p1467-1474.
- [24] S.J. Gregg and K.S.W. Sing, *Adsorption, Surface Area and Porosity*., Academic Press, London, (1982).



- [25] W.D. Harkins and G. Jura, An Adsorption Method for the Determination of the Area of a Solid without the Assumption of a Molecular Area, and Area Occupied by Nitrogen Molecules on the Surfaces of Solids., *The Journal of Chemical Physics*, 11, (9), (1943), p431-432.
- [26] G. Halsey, Physical Adsorption on Non-Uniform Surfaces., *The Journal of Chemical Physics*, 16, (10), (1948), p931-937.
- [27] C.G. Schüll, The Determination of Pore Size Distribution from Gas Adsorption Data., *The Journal of the American Chemical Society*, LXX, April-August, (1948), p1405-1410. and C.G. Schüll, P.B. Elkin and L.C. Roess, *Journal of the American Chemical Society*, LXX, April-August, (1948), p1410-1414.
- [28] E.P. Barrett, L.G. Joyner and P.P. Halenda, The Determination of Pore Volume and Area Distributions in Porous Substances. I. Computations from Nitrogen Isotherms., *Journal of the American Chemical Society*, 73, (1951), p373-380.
- [29] A. Wheeler, discussed at American Association for the Advancement of Science Conference on Catalysis, Gibson Island, (1945). cited in ref 28.
- [30] R.W. Cranston and F.A. Inkley, The Determination of Pore Structures from Nitrogen Adsorption Isotherms., *Advances in Catalysis*, 9, (1957), p143-154.
- [31] B.C. Lippens, B.G. Linsen and J.H. deBoer, Studies on Pore Systems in Catalysis I. The Adsorption of Nitrogen; Apparatus and Calculation., *Journal of Catalysis*, 3, (1964), p32-37.
- [32] J.H. deBoer and B.C. Lippens, Studies on Pore Systems in Catalysis II. The Shapes of Pores in Aluminium Oxides Systems., *Journal of Catalysis*, 3, (1964), p38-43.
- [33] B.C. Lippens and J.H. deBoer, Studies on Pore Systems in Catalysis III. Pore-Size Distribution Curves in Aluminium Oxide Systems., *Journal of Catalysis*, 3, (1964), p44-49.
- [34] B.C. Lippens and J.H. deBoer, Studies on Pore Systems in Catalysis V. The  $t$  Method, *Journal of Catalysis*., 4, (1965), p319-323.
- [35] J.H. deBoer, B.G. Linsen and TH.J. Osinga, Studies on Pore Systems in Catalysis VI. The Universal  $t$  Curve., *Journal of Catalysis*, 4, (1965), p643-648.
- [36] J.H. deBoer, B.G. Linsen, TH. van der Plas and G.J. Zondervan, Studies on Pore Systems in Catalysis VI. Description of the Pore Dimensions of Carbon Blacks by the  $t$  Method., *Journal of Catalysis*, 4, (1965), p649-653.
- [37] D. Dollimore and G.R. Heal, An Improved Method for the Calculation of Pore Size Distribution From Adsorption Data., *Journal of Applied Chemistry*, 14, (March), (1964), p109-114.

- [38] R.SH. Mikhail, S. Brunauer and E.E. Bodor, Investigations of a Complete Pore Structure Analysis 1. Analysis of Micropores., *Journal of Colloid and Interface Science*, 26, (1968), p45-53.
- [39] M.M. Dubinin, The Potential Theory of Adsorption of Gases and Vapors for Adsorbents With Energetically Nonuniform Surfaces, *Chemical Review*, 60, (1), (1960), p235-241.
- [40] M.M. Dubinin, In *Chemistry and Physics of Carbon*, P. Walker. *ed.* , Vol 2, (1966), p51-120.
- [41] M.M. Dubinin, Microporous Structures and Absorption Properties of Carbonaceous Adsorbents., *Carbon*, 21, (4), (1983), p359-366.
- [42] M.M. Dubinin, Adsorption in Micropores., *Journal of Colloid and Interface Science*, 23, (1967), p487-499.
- [43] H.F. Stoeckli, A Generalisation of the Dubinin-Radushkevich Equation for the Filling of Heterogeneous Micropore Systems., *Journal of Colloid and Interface Science*, 59, (1), (1977), p184-185.
- [44] M.M. Dubinin and H.F. Stoeckli, Homogeneous and Heterogeneous Micropore Structures in Carbonaceous Adsorbents., *Journal of Colloid and Interface Science*, 75, (1), (1980), p34-42.
- [45] M. Jaroniec and R. Madey, *Physical Adsorption on Heterogeneous Solids.*, Elsevier, Amsterdam, (1988), Chapter 8.
- [46] M.M. Dubinin, V.A. Astakhov, *Izv. Akad. Nauk SSSR. Ser. Khim.*, (1971), p5. cited in ref 5.
- [47] G. Horvath and K. Kawazoe, Method for the Calculation of Effective Pore Size Distribution in Molecular Sieve Carbon., *Journal of Chemical Engineering of Japan*, 16, (6), (1983), p470-475.
- [48] D.H. Everett and J.C. Powl, Adsorption in Slit-like and Cylindrical Micropores in the Henry's Law Region., *Journal of the Chemical Society, Faraday Transactions 1*, 72, (1976), p619-636.
- [49] A. Saito and H.C. Foley, Curvature and Parametric Sensitivity in Models for Adsorption in Micropores., *AIChE Journal*, 37, (3), (1991), p429-436.
- [50] L.S. Cheng and R.T. Yang, Improved Horvath-Kawazoe Equations Including Spherical Pore Models for Calculating Micropore Size Distributions., *Chemical Engineering Science*, 49, (16), (1994), p2599-2609.
- [51] N.A. Seaton, J.P.R.B. Walton and N. Quirke, A New Analysis Method for the Determination of the Pore Size Distribution of Porous Carbons from Nitrogen Adsorption

- Measurements., Carbon, 27, (6), (1989), p853-861.
- [52] J.P. Olivier and W.B. Conkin, presented at 7th International Conference on Surface and Colloid Science, Compiègne, France, (1991). cited in Micromeritics DFT Manual
- [53] C. Lastoskie, K.E. Gubbins and N. Quirke, Pore-size Distribution Analysis of Microporous Carbons - A Density-Functional Theory Approach., Journal of Physical Chemistry, 97, (18), (1993), p4786-4796.
- [54] J.P. Olivier, Modelling Physical Adsorption on Porous and Nonporous Solids Using Density Functional Theory., Journal of Porous Materials, 2, (1995), p9-17.
- [55] N. Quirke and S.R.R. Tennison, The Interpretation of Pore Size Distributions of Microporous Carbons., Carbon, 34, (10), (1996), p1281-1286.
- [56] N.A. Seaton, Determination of the Connectivity of Porous Solids From Nitrogen Sorption Measurements., Chemical Engineering Science, 46, (8), (1991), p1895-1909.
- [57] J.H. deBoer, The Shape of Capillaries, in 'The Structure and Properties of Porous Materials', D.H. Everett and F.S.Stone *ed.* , Butterworth, London, (1958).
- [58] H. Liu, L. Zhang and N.A. Seaton, Determination of the Connectivity of Porous Solids From Nitrogen Sorption Measurements-II. Generalisation., Chemical Engineering Science, 47, (17/18), (1992), p4393-4404.
- [59] A. Linares-Solano, F. Rodriguez-Reinoso, J.M. Martin-Martinez and J. De D.Lopez-Gonzalez, Adsorption of Hydrocarbons on Air-Reacted Activated Carbons. II. High and Low Pressure Hysteresis., Adsorption Science and Technology, 1, (4), (1984), p317-327.
- [60] D. Valladares and G. Zgrablich, Test of the Horvath-Kawazoe Method by Monte Carlo Simulation., Adsorption Science and Technology, 15, (1), (1997), p15-24.
- [61] B.P. Russell and M. Douglas LeVan, Pore Size Distribution of BPL Activated Carbon Determined by Different Methods., Carbon, 32, (5), (1994), p845-855.
- [62] A.G. Ogston, The Spaces in a Uniform Random Suspension of Fibres., Transactions of the Faraday Society, 54, (1958), p1754-1757.

## CHAPTER 3

### CHEMICAL CHARACTERISATION

#### SECTION 3.1 INTRODUCTION

The adsorption of organic species from aqueous solution is influenced by the functional groups present on the surface of the adsorbent. Functional groups may directly interact with organic species by an ion exchange mechanism or by hydrogen bonding. Also, the acidic or basic nature of the groups govern the surface electrostatic charge of the adsorbents allowing for an attraction or repulsion of charged organic species. Davankov and Tsyurupa [1.18] studied the chemical functionality of their hypercrosslinked polymers and concluded that the polymers contained no polar or halogen functional groups. However, Law *et al* [1] observed that 10% of aromatic groups of the hypercrosslinked resins they analysed, using  $^{13}\text{C}$  CP/MAS NMR, retained a chloromethyl group. These groups can be hydrolysed, thus enabling hydrogen bonding with suitable organics. Numerous studies have been presented into the chemical functionality of carbon surfaces, and their modification by oxidation and heat treatment. A brief review of the determination of carbon surface functional groups will be presented due to their widespread use as adsorbents for organic species.

The chemical characteristics of the surface of the Macronet polymers and F-400 activated carbon have been studied by a variety of techniques in an attempt to understand the mechanisms for the adsorption of different adsorbates and to provide an insight into the polymer's manufacture.

#### SECTION 3.2 THEORY AND LITERATURE REVIEW

A wide variety of techniques can be applied to the determination of functional groups on the surfaces of polymers and carbons, or the bulk composition of the material including; elemental

analysis, Fourier Transform Infra Red (FT-IR) spectroscopy,  $^{13}\text{C}$  Nuclear Magnetic Resonance (NMR) spectroscopy, X-ray Photoelectron Spectroscopy (XPS) or Electron Spectroscopy for Chemical Analysis (ESCA), Static Secondary Ion Mass Spectroscopy (SSIMS), chemical derivatisation and direct titration. Numerous other techniques are available. However, the following discussion will be restricted to the techniques that have been applied for the characterisation of the adsorbents used in this study.

IR spectra of various Macronet polymers, presented by Davankov and Tsyurupa [1.22], suggested that there were only bands attributable to the characteristic vibrations of CH and  $\text{CH}_2$  groups and benzene rings. They observed that the crosslinking reagents caused bridges to be formed at the para position on the phenyl rings, with no evidence for ortho or meta substituted rings. The IR spectra of polymers with a theoretical 100% crosslinking demonstrated a band at  $765\text{cm}^{-1}$ , often associated with non-planar deformational vibrations of a mono-substituted phenyl group. However, the absence of tri-substituted phenyl vibrations made it difficult for Davankov and Tsyurupa to assign the band. Qualitatively, the polymers were described as having spectra identical to that of a styrene copolymer with 60% p-divinyl benzene. Polymers crosslinked using methylal instead of monochlorodimethyl ether contained a band at  $1700\text{-}1705\text{cm}^{-1}$ , characteristic of an aromatic aldehyde group [1.16]. The concentrations of these groups did not exceed  $0.27\text{meq/g}$ , equivalent to an aldehyde functional group substituted on 3% of the phenyl rings. Little evidence was found for the  $-\text{CH}_2\text{-O-CH}_3$  group which might have occurred if the methylal had reacted with polystyrene as a mono-functional reagent. Their method of IR analysis is not described.

Joseph *et al* [2] used  $^{13}\text{C}$  NMR analysis to investigate the chemical properties of Macronet resins produced by Davankov and Tsyurupa. Deconvolution of the quaternary aromatic signals enabled the percentage of un-substituted rings to be calculated. They observed that a resin with a theoretical crosslinking percentage of 100% contained 32-42% of phenyl rings that were not involved in the crosslinking reaction. Common values of the proton spin-lattice relaxation times in the rotating frame suggested that hypercrosslinked samples are homogeneous down to dimensions of less than  $10\text{nm}$ .

Law *et al* [1] studied Macronet polymers produced by Purolite International using FT-IR,  $^{13}\text{C}$  MAS NMR and elemental analysis. No peaks were observed at  $765\text{cm}^{-1}$  in their FT-IR analysis which suggested that the polymers were 100% crosslinked. Contrary to the investigations of Davankov and coworkers, carbonyl peaks at  $1699$  and  $1678\text{cm}^{-1}$  were observed which were associated with an ester or carboxylic functionality. Large amounts of chlorine were observed in all the techniques investigated suggesting that up to 10% of the phenyl rings contained an unreacted chloromethyl group. Small amounts of vinyl groups were also suggested. Quantitative structural analysis of the polymer was achieved, using single-pulse excitation (SPE)  $^{13}\text{C}$  NMR, by considering the ratio of areas of the peaks. They suggested that trialkyl-substituted aromatic rings accounted for the low ratio of the aromatic to aliphatic groups.

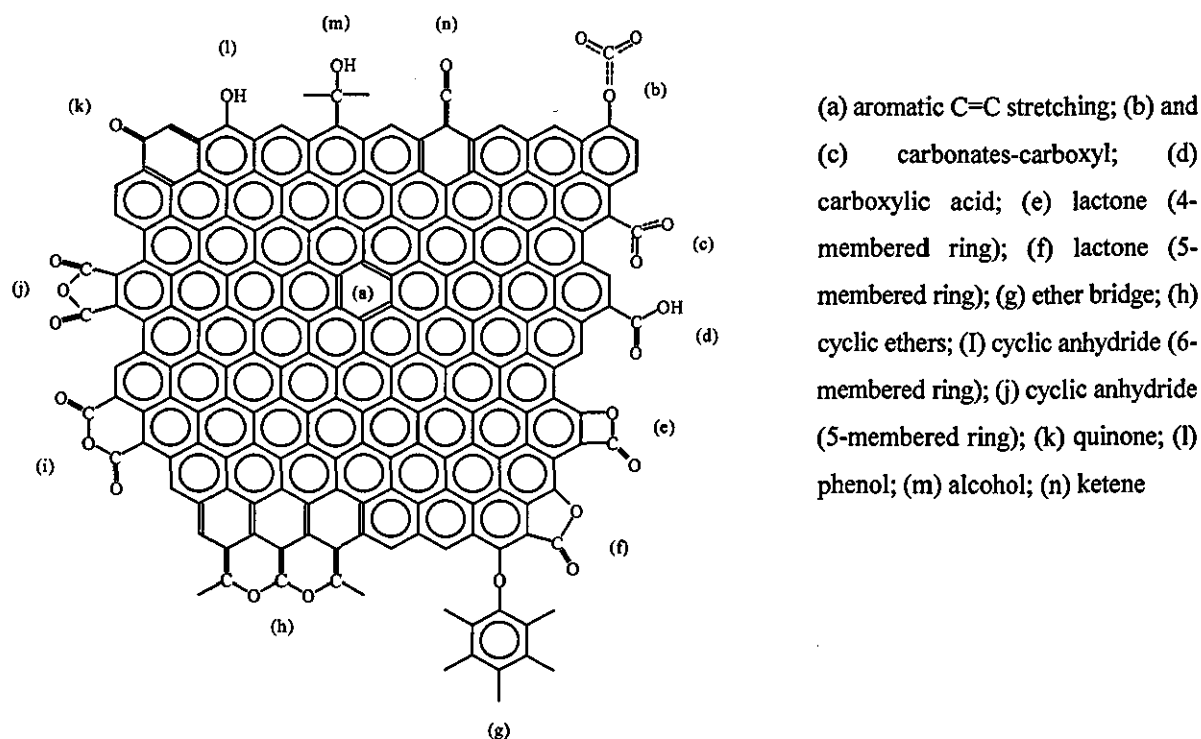
IR spectroscopy of activated carbon is more problematical since many carbons act as black body absorbers, thereby markedly diminishing or completely attenuating the beam energy. Early work by Mattson *et al* [3] identified surface functional groups by a technique known as attenuated total reflection infra-red (ATR) spectroscopy. The ATR technique has also been useful in the study of surface oxidation in polymers [4]. Direct transmission IR, probably the most common form, has also been applied for the study of carbonaceous materials [5-7]. However, varying degrees of success have been achieved, depending on the nature of the sample. Recently, diffuse reflectance FT-IR (DRIFT) spectroscopy has been used for the determination of carbon spectra [8-9]. The technique overcomes some of the contamination and reflection problems experienced with the other techniques and is simpler in operation.

Infra-red studies have suggested a wide variety of functional groups on the surface of carbonaceous materials, since bands tend to be broad and unresolved. Also the graphitic planes tend to shift the frequencies of vibrations of various functional groups which causes uncertainty in their assignment. Fanning *et al* [8] conducted a survey of the literature regarding functional groups on activated carbon. The groups determined by 69 different investigations using IR spectroscopy are summarised in Fig. 3.1.

Improvements in the resolution of X-ray Photoelectron Spectrometers has led to better quantification of functional groups. Briggs *et al* [10] studied the spectra of 43 aliphatic

homopolymers containing C, H, and O plus two copolymers (styrene/maleic anhydride and ethylene/maleic anhydride). They presented the primary and secondary chemical shift data for the C1s envelope associated with the different types of oxygen functionality. Detailed studies

Fig. 3.1. IR-active functionalities on carbon surfaces (Fanning *et al*) [8].



into the surface functional groups on oxidised polyolefins were performed by Popat [4]. He used variable take-off angles to enable depth profiling of the functional groups. Bradely *et al* [11] used XPS to investigate the surface functionality of two carbon blacks and two porous carbons. He was able to correlate the concentration of oxygen on the surface of carbon to the heat of immersion of the carbons for n-heptane and water. Jansen *et al* [12] used XPS to determine nitrogen functional groups on several nitrogen containing activated carbons. They observed that the nitrogen content of a series of modified carbons varied from 2.9 to 7.9% with a range in oxygen concentration of 4.2-16.0%. Elemental analysis produced compositions of nitrogen and oxygen that were generally higher than obtained from XPS. The difference was attributed to a non-uniform distribution of surface groups throughout the carbon. The type of modification appeared to govern the type of nitrogen functional group. Amides, lactams, imides and aromatic nitrogen (e.g. pyridine and pyrrole) groups were identified.

Direct titration of oxygen and nitrogen containing groups has been performed for many years. Early work was performed by Kruyt and De Kadt [13] in 1929 who postulated the presence of carboxylic functional groups, determined by titration with sodium hydroxide. Phenolic groups and lactones were also suggested by titration and specific reactions by many authors. In 1964, Boehm *et al* [14] presented a paper discussing the surface oxides of carbon by neutralisation of the acidic functional groups. They used four bases of different strength,  $\text{NaHCO}_3$ ,  $\text{Na}_2\text{CO}_3$ ,  $\text{NaOH}$  and  $\text{NaOC}_2\text{H}_5$ , to differentiate acidic groups of various strengths.  $\text{NaHCO}_3$  neutralised only 'strongly' acidic groups such as  $\text{COOH}$ . Lactones were could be identified by the difference in the number of groups titrated by  $\text{Na}_2\text{CO}_3$  and  $\text{NaHCO}_3$  whereas weakly acidic groups (phenols) were neutralised by  $\text{NaOH}$  but not by  $\text{Na}_2\text{CO}_3$ . Sodium ethoxide in ethanol was able to titrate more groups than sodium hydroxide which was ascribed to carbonyl functionality. It is believed that the sodium ethoxide reacts with the surface to form sodium salts of hemi-acetals [15]. Equal quantities of each group were observed. Verification of the type of functional groups, suggested by titration, was performed by chemical modification of the acidic functional groups. Later work by Boehm [16][17] validated the accuracy and assumptions of the titration method. Boehm's titrations are still commonly performed to provide an assessment of the functional group concentrations. Basic functional groups on the surfaces of activated carbons have also been studied using titration and specific reactions. The functional groups that have been hypothesised are chromene, pyrone and isoviolanthrene-like structures. An excellent review of the literature regarding the determination of functional groups on carbon is presented in the book of Bansal, Donnet and Stoeckli [18]. I refer the reader to this book, Chapter 2, for a more detailed review.

Activated carbons often contain elements other than carbon. hydrogen, oxygen and nitrogen. Alben *et al* [19] used scanning electron microscopy combined with energy dispersive X-ray fluorescence (EDXRF) to identify the trace element distributions of F-400 granular activated carbon. They presented distributions for Al, Si, K, S, Cl, Ca, Ti and Fe. Table 3.1 presents the elemental composition of F-400 presented by the Calgon corporation, the manufacturer of F-400 in the US [20]. The total concentration of elements accounts for 4.4% of the carbon weight although the percentage ash was measured at 7.4%.

Ishizaki *et al* [7] studied the surface oxide structures of F-200 by titration and transmission IR.



**Table 3.1. Elemental composition of Calgon F-400 Activated Carbon.**

| Element              | Al   | Si   | S   | Cl | K   | Ca  | Ti   | Mn   | Fe  | Cu   |
|----------------------|------|------|-----|----|-----|-----|------|------|-----|------|
| Concentration (mg/g) | 12.3 | 15.5 | 8.3 | -  | 0.3 | 1.6 | 0.74 | 0.01 | 5.0 | 0.03 |

They suggested that the main oxides present were lactones, quinones, phenols and carboxylates. Also 0.08 meq/100m<sup>2</sup> of hydrochloric acid was neutralised suggesting the presence of basic groups. The total sodium hydroxide acidic capacity was 0.11 meq/100m<sup>2</sup> (approximately 1 meq/g). Mazet *et al* [21] and Hazourli [22] have studied the surface functional groups of F-400 by Boehm's titration, the concentrations of which are presented in Table 3.2.

**Table 3.2. Concentration of Surface functional groups on F-400 (meq/g).**

| Type of Functionality | Carboxylic | Lactone | Phenol | Carbonyl | ∑Acidic Groups | ∑Basic Groups |
|-----------------------|------------|---------|--------|----------|----------------|---------------|
| Mazet <i>et al</i>    | 0.33       | 0.23    | 0.10   | 0.49     | 1.05           | 0.26          |
| Hazourli              | 0.13       | 0.19    | 0.10   | 0.87     | 1.29           | -             |

The oxygen and nitrogen functionality of surfaces alters the surface charge of adsorbents, often assessed by measurement of the zeta potential of the material at different pH values. Summers *et al* [23] used pH drift experiments, a technique where carbon is added to 0.1M NaCl solutions at different pH values, to determine the surface charge. The point of zero charge (pH<sub>PZC</sub>) occurs when there is no change in the pH after contact with the carbon. They observed that the pH<sub>PZC</sub> for F-400 was greater than nine indicating that at the pH in normal waters, around pH 7, the surface charge would be positive. Ulmer [24] investigated the zeta potential of F-400 under different pH conditions and observed a pH<sub>PZC</sub> of 5.3. The pH<sub>PZC</sub> tended to decrease to values around 2-3 in the presence of humic acid adsorbed on the carbon thus suggesting that the surface would be negative in natural waters.

## SECTION 3.3      EXPERIMENTAL PARAMETERS

### *Diffuse reflectance infra red spectroscopy*

All spectra were recorded on a Nicolet 20-DXC FT-IR spectrometer with a dry air purge, liquid nitrogen cooled MCT (mercury-cadmium-telluride) detector, and a Spectra-Tech diffuse reflectance accessory. The diffuse reflectance accessory consisted of a hemispherical mirror which split into two halves, with the sample mounted on the central platform. The accessory was aligned to provide maximum infra red signal intensity using a stainless steel mirrored platform. The height of the sample on the platform was adjusted to minimise the gain of the detector.

A number of different techniques of diffuse reflectance spectroscopy were attempted to enable whole polymer beads to be examined. Spectra recorded using 300-400 $\mu\text{m}$  polymer were slightly unresolved and gave absorbance values of greater than one. Attempts were also made to enable a study of the external surface of the polymer by grating the surface of a polymer bead with a steel grating pad. This technique also produced unresolved spectra necessitating the use of crushed material for the analysis.

Samples of MN-100, MN-150, MN-200, F-400 and the styrene copolymer were crushed using an agate mortar and pestle to provide a particle size range of 8-30 $\mu\text{m}$ . The size range was achieved by sedimenting the larger particles out in ultrapure water followed by recovery of the fines using micro filtration. Polymer samples that had undergone a Soxhlet extraction using toluene were also analysed to try to identify any differences. Finely divided spectroscopic grade potassium bromide, obtained from Fisher Scientific, was ground and stored in a desiccator prior to use. The samples were mixed with the KBr in the ratio 1:50 to enable absorbance values of less than one to be recorded.

Background spectra of KBr and water vapour were recorded every 100 minutes. Spectra were recorded at a resolution of 4 $\text{cm}^{-1}$  using a minimum of 200 scans and an aperture setting of 15. The samples were allowed to equilibrate in the instrument for 10 minutes prior to recording the spectra to ensure their dryness.

### ***X-ray photoelectron spectroscopy***

A VG ESCALAB MK 1 spectrometer employing a monoenergetic Al  $k_{\alpha}$  X-ray source (1486.6 eV) at a pressure of  $\sim 10^{-7}$  mbar was used for the analysis of whole and crushed beads of MN-150. Survey spectra were obtained at a pass energy of 100eV using a 0-1100eV scan (0.3eV step size) and a dwell time of 50ms. Subsequent analysis of the C1s peak, over the range 285-295eV, used an analyser pass energy of 35eV and a step size of 0.025eV. All spectra were obtained using an anode power of 200W (10kV, 20mA). The analysis was performed by Dr. R.H.Bradley in the Institute of Surface Science and Technology at Loughborough University.

### ***Solid State Nuclear Magnetic Resonance Spectroscopy***

Samples of MN-100, MN-150 and MN-200 were sent to the EPSRC  $^{13}\text{C}$  solid state NMR facility based in the Department of Chemistry at UMIST. The analysis was performed by Ms B.E.Gore using a Bruker spectrophotometer. Spectra for the polymers were recorded using a spinning speed of 4811Hz. However the spectra for MN-150 were also recorded at 3938Hz. The instrument parameters used in the analysis can be seen in the results section.

### ***Direct Titration***

Samples of MN-100, MN-150, MN-200 and F-400, in protonated form, were contacted with 0.1M solutions of sodium hydroxide, sodium hydrogen carbonate, sodium carbonate and sodium ethoxide. The sodium hydroxide and sodium carbonate were volumetric standards purchased from Aldrich Chemicals. The sodium hydrogen carbonate and sodium ethoxide solutions were prepared from analytical reagents also from Aldrich. The sodium ethoxide solution was dissolved in HPLC grade ethanol to prevent degradation of the compound caused by a reaction with water. 250mg quantities of dried adsorbents, in the particle size range 75-100 $\mu\text{m}$ , were weighed into 100ml conical flasks prior to the addition of 25ml of the different bases. The flasks were then sealed using parafilm and agitated using an orbital shaker at 150rpm for 72 hours. Each base/adsorbent mixture was prepared in duplicate. Blank solutions of each base were also shaken.

The equilibrated solutions were filtered, using 0.2 $\mu$ m PTFE syringe top filters, to remove the adsorbent particles. Aliquots of 10ml were then titrated with a 0.1M volumetric HCl standard using methyl red as the indicator.

The weight, volume, and strong base capacity of MN-100 and MN-150 were determined whilst working in the quality control laboratory of Purolite International Ltd. The procedure used is confidential to the company and so only the results will be presented.

### ***Elemental Analysis***

An elemental analysis of MN-100, MN-150 and MN-200 was performed in the polymer chemistry department at the University of Strathclyde. The samples were analysed on a Perkin Elmer Series II 2400 elemental micro analyser. The estimated error for each element analysed was  $\pm 0.5\%$ .

### ***Zeta Potential Analysis***

The zeta potential of MN-100, MN-150 and MN-200 was determined using a Zetamaster from Malvern Instruments. The polymers were crushed using an agate mortar and pestle and added to ultrapure water to allow the larger particles to sediment out. The suspended particles of the polymer were added to the reaction flask of the autotitrator and diluted with ultrapure water to provide a concentration of approximately 4000 counts/sec. The suspension was titrated using volumetric standards of 0.1M hydrochloric acid and 0.1M sodium hydroxide respectively. An equilibration time of 30 minutes, after the addition of base or alkali, was allowed before measurement of the zeta potential. Data was recorded at pH intervals of 0.5.

## SECTION 3.4      RESULTS AND DISCUSSIONS

### *Diffuse reflectance infra red spectroscopy*

Infra red spectra of all three Macronet polymers, the styrene precursor and F-400 can be seen in Figs. 3.2-6 respectively. The spectra of F-400 does not indicate any sharp peaks which are caused by the carbon absorbing the infra-red beam. Transmission FT-IR has also been attempted. However, the results showed little improvement. It is possible to obtain excellent spectra using a photo acoustic spectrophotometer. However, this equipment was not available.

A comparison of the spectra of the styrene copolymer to a reference sample of atactic polystyrene, illustrated in Fig. 3.5, indicates that the percentage of cross linking agent, divinyl benzene, used in the initial polymerisation stage is low due to the similarity in their spectra.

The Macronet polymers, MN-100, MN-150 and MN-200, have characteristic bands attributable to the vibrations of CH, CH<sub>2</sub>, benzene rings and oxygen functionality. The aromatic out-of-plane C-H vibrations and ring out-of-plane vibrations in the region 900-650cm<sup>-1</sup> provide a means of determining the type of aromatic substitution [25]. The strong absorption bands at 816cm<sup>-1</sup> and 700 cm<sup>-1</sup> are indicative of p-substituted benzene rings suggesting that most of the crosslinking bridges are in the para position. Evidence of mono-substituted rings, e.g. uncrosslinked polystyrene, is shown by the two medium absorptions, one at 760cm<sup>-1</sup> and the other at 700cm<sup>-1</sup>, the first being smaller than the second. These two adsorption bands are also represented in the spectra of 1,2,3-tri-substituted and 1,2,4-tri-substituted benzene rings. However, the absence of a strong band in the 720-685cm<sup>-1</sup> region eliminates the possibility of 1,2,3 tri-substituted rings. The size of the phenyl peak might suggest that a proportion of the band is attributable to tri-substituted benzene rings. A subtraction spectrum of MN-200 and the polystyrene precursor, shown in Fig. 3.7, indicates a small peak at 893cm<sup>-1</sup> that appears to confirm the presence of 1,2,4-tri-substituted benzene rings. Davankov and Tsyurupa [1.22], did not observe any bands attributable to m- and o-substitution and found it difficult to assign the 765±5cm<sup>-1</sup>. The lack of evidence may be due to a lack of sensitivity in their detection.

Fig. 3.2.

Diffuse reflectance FT-IR spectra of MN-100.

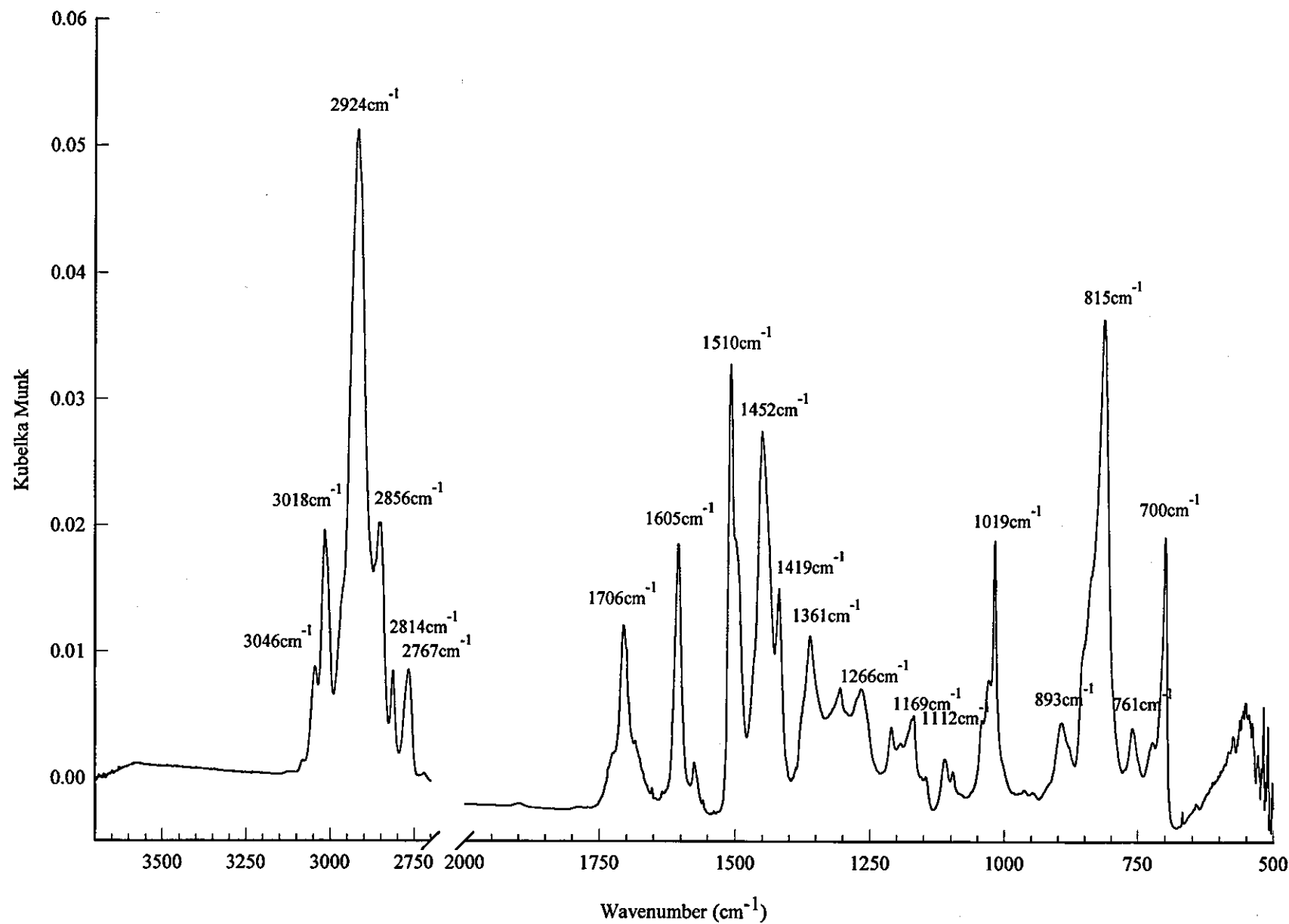


Fig. 3.3. Diffuse reflectance FT-IR spectra of MN-150.

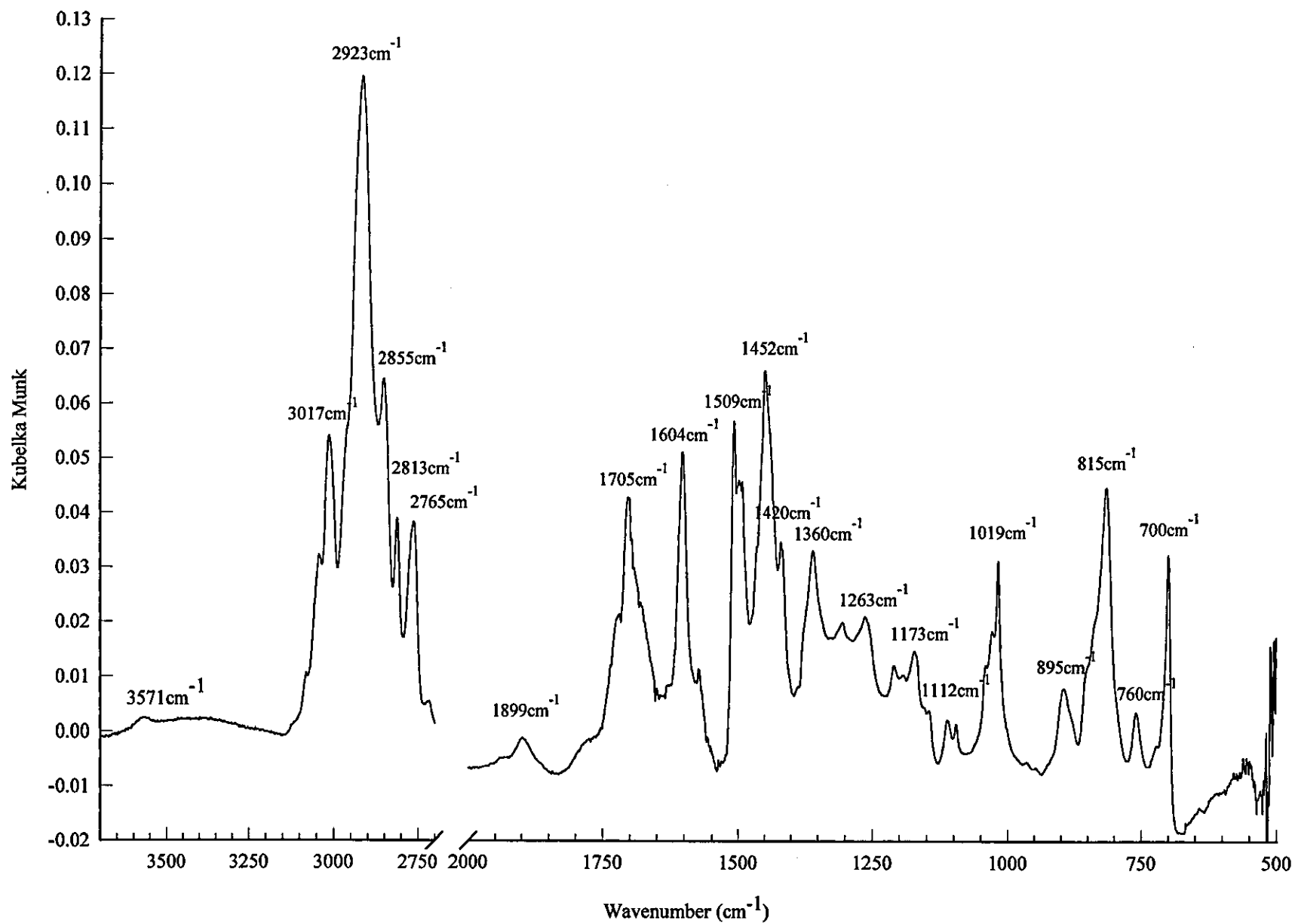
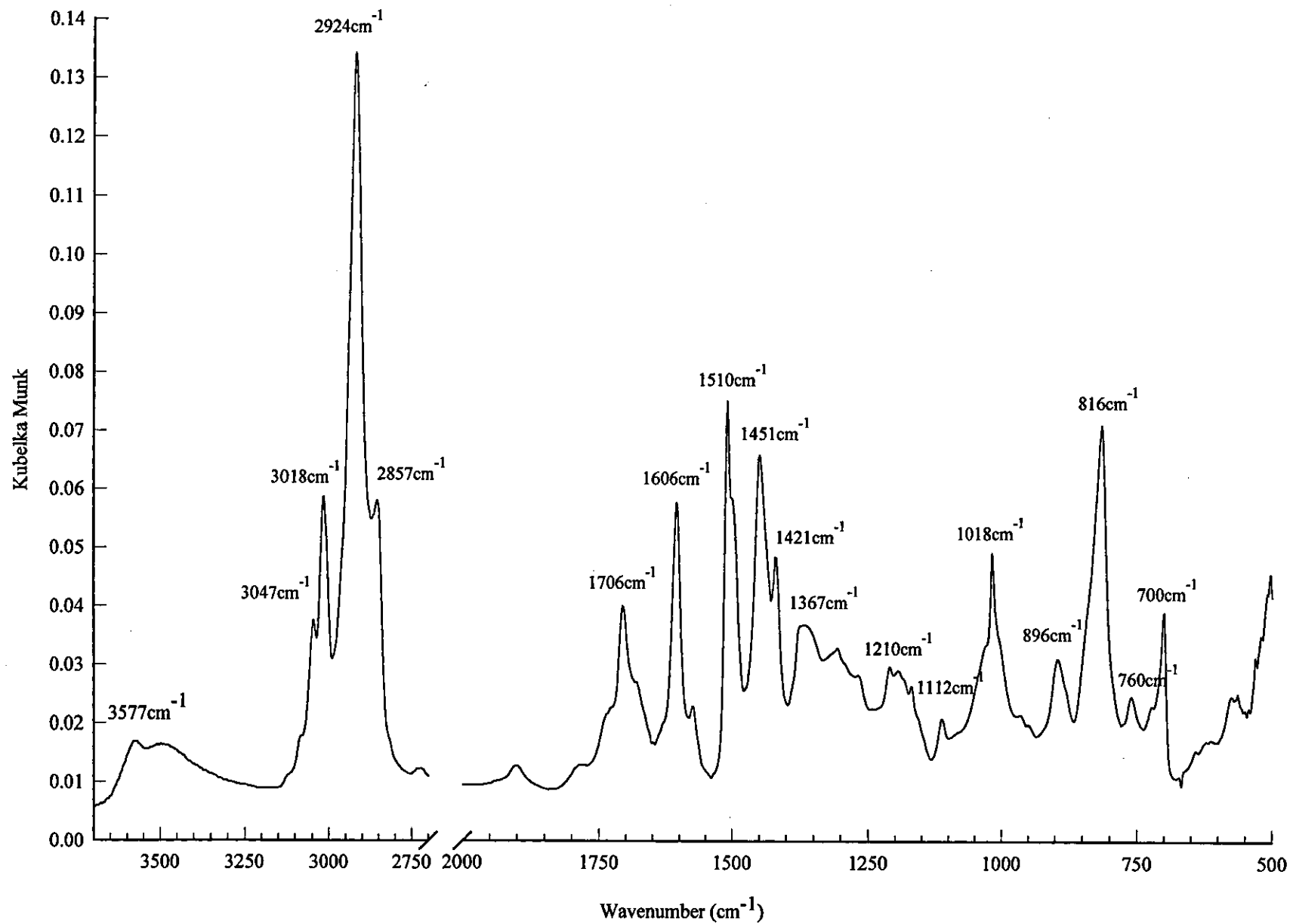
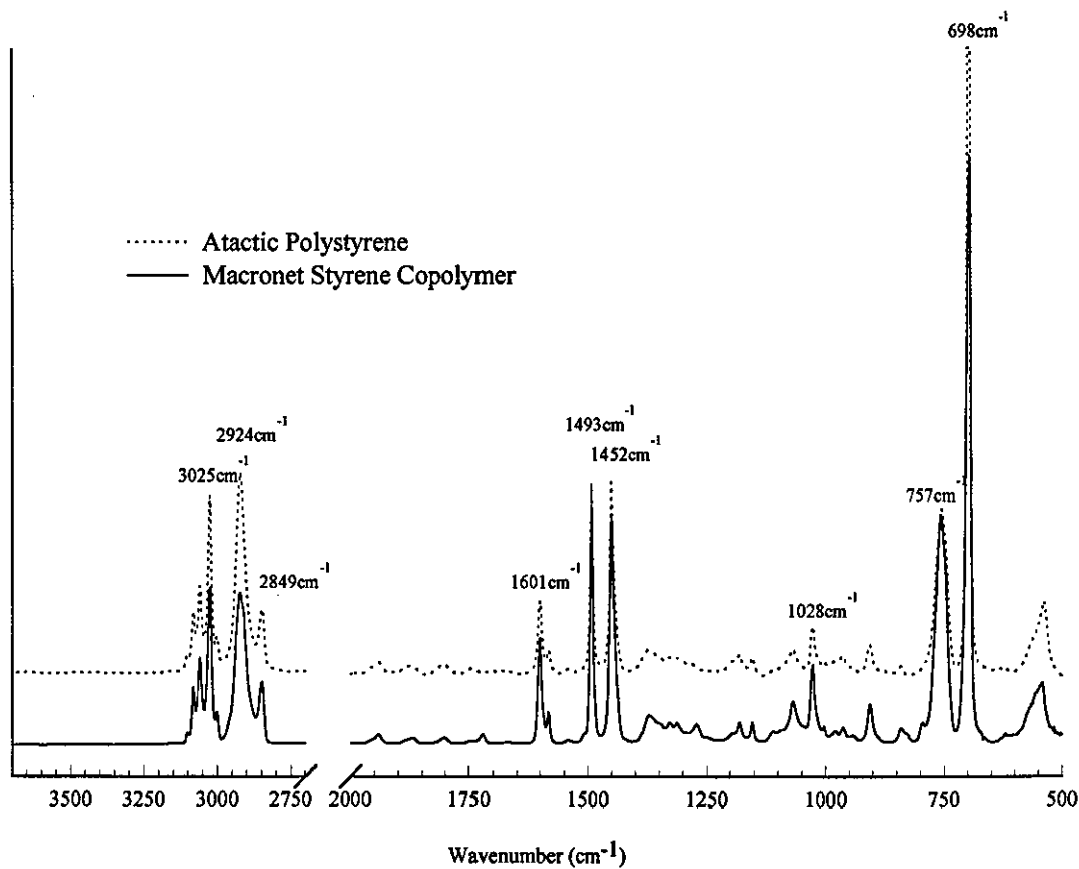


Fig. 3.4. Diffuse reflectance FT-IR spectra of MN-200.





**Fig. 3.5. Diffuse reflectance FT-IR spectra of Styrene Precursor and Atactic Polystyrene.**



**Fig. 3.6. Diffuse reflectance FT-IR spectra of F-400.**

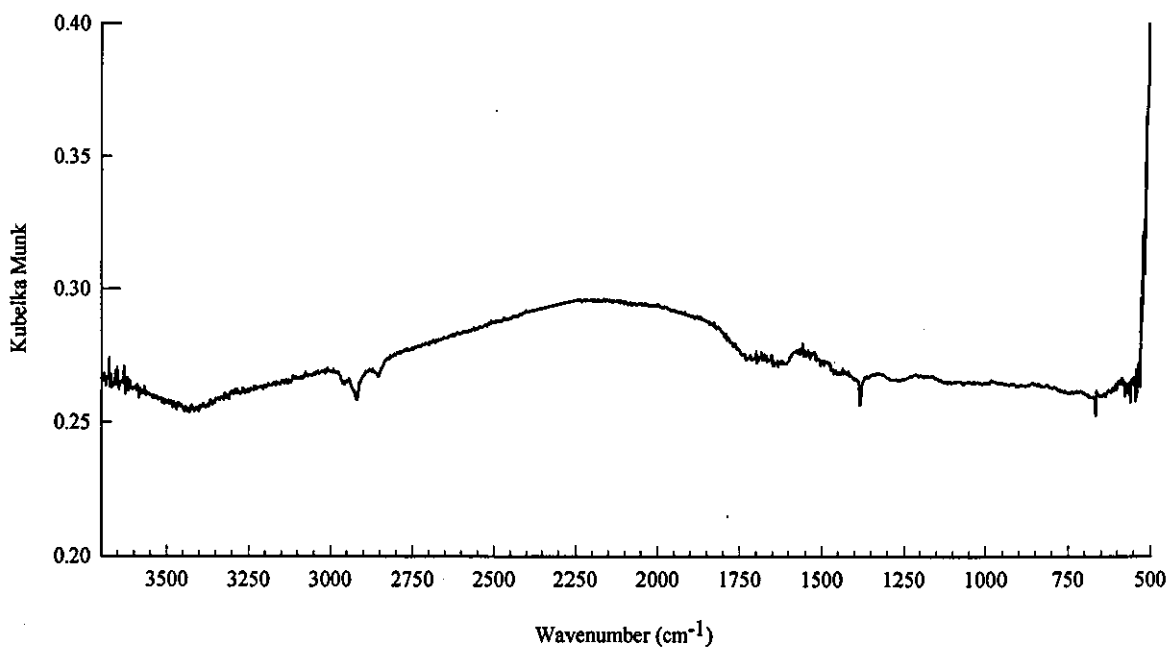
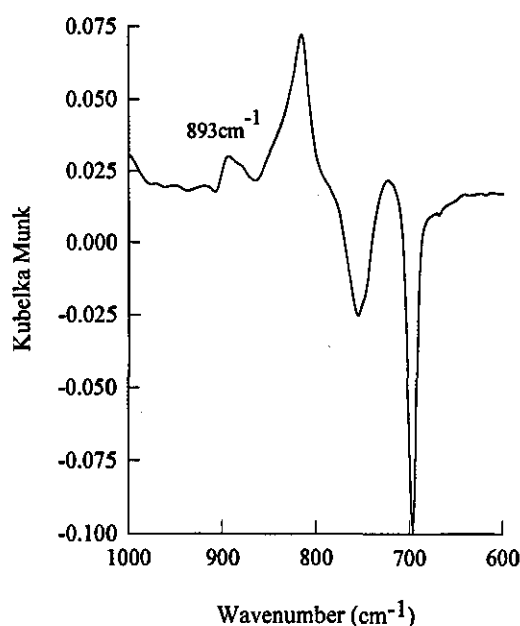
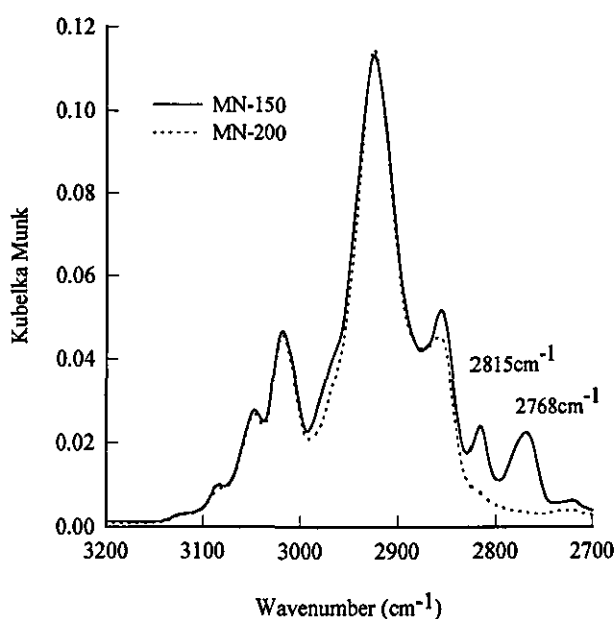


Fig. 3.8 shows the tertiary amine functional groups that are present on MN-150 indicated by additional peaks, at  $2815\text{cm}^{-1}$  and  $2768\text{cm}^{-1}$ , when compared to the unfunctionalised MN-200. A peak at  $1361\text{cm}^{-1}$  in the spectra of MN-150 and MN-100 confirms the amine functional group.

**Fig. 3.7.** Subtraction spectrum of MN-200 and the styrene copolymer.



**Fig. 3.8.** Comparison of the FT-IR spectra of MN-150 and MN-200.



A strong peak at  $1706\text{cm}^{-1}$  is present on the spectra of MN-100, MN-150 and MN-200 suggesting the presence of carbonyl ( $\text{C}=\text{O}$ ) functional groups. Carbonyl peaks are observed in a wide variety of compounds including ketones, aldehydes, carboxylic acids, esters, peroxides etc. Further analysis of the spectra using other characteristic peaks suggested that the  $\text{C}=\text{O}$  may be attributed to a combination of aryl and alkyl ketones. Evidence of aryl ketones is shown by the presence of an absorption band at  $1210\text{cm}^{-1}$ , the phenyl carbon stretch, and several medium intensity bands around  $1300\text{cm}^{-1}$ , due to  $\text{C}-\text{C}-\text{C}$  bending and  $\text{C}-\text{CO}-\text{C}$ . Similarly bands at  $1304\text{cm}^{-1}$  and several bands around  $1100\text{cm}^{-1}$  suggest the possible presence of an alkyl ketone. The methylene scissoring vibration of the  $-\text{CH}_2-\text{CO}-$  group occurs in the range  $1435-1405\text{cm}^{-1}$  which is lower than that for  $\text{CH}_2$  in aliphatic hydrocarbons which occurs in the range  $1480-1440\text{cm}^{-1}$ . Analysis of the IR spectra eliminates the possibility of an aldehyde since a sharp band at  $2720\text{cm}^{-1}$  is not represented. Aryl ethers absorb strongly in the region  $1270-1230\text{cm}^{-1}$  whereas alkyl aryl ethers have two strong absorptions, the most intense of which is at  $1270-1230\text{cm}^{-1}$ , and

the other being at 1120-1020 $\text{cm}^{-1}$ . Bands at these frequencies are present in the spectra of the Macronets. However, bands due to ketonic compounds also occur in this region, preventing positive determination.

The presence of such a strong carbonyl band was unexpected and required verification by other analytical techniques.

### *X-ray photoelectron spectroscopy*

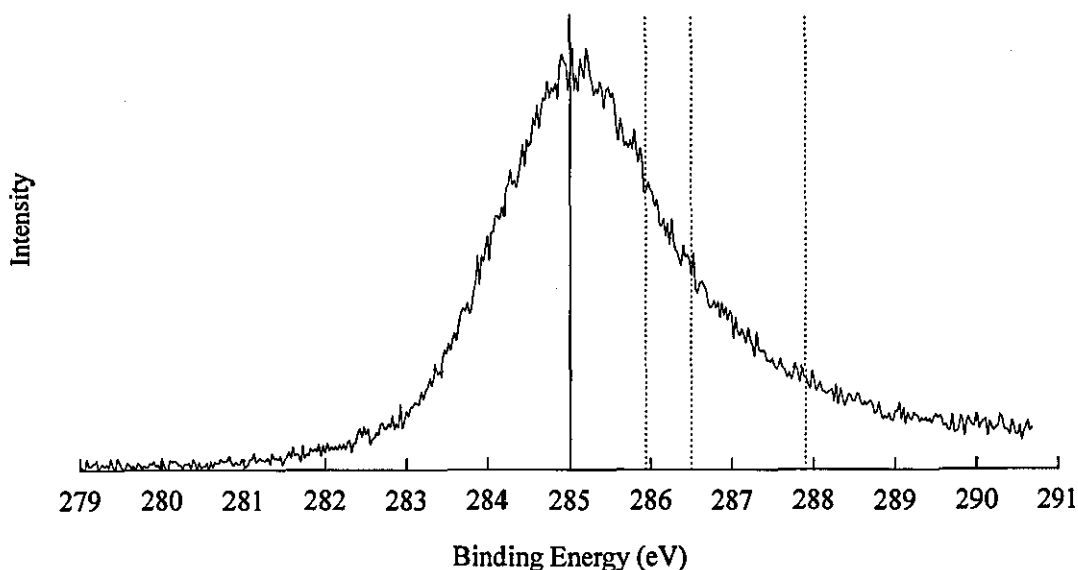
X-ray photoelectron spectroscopy (XPS) was conducted on MN-150 to identify the surface concentration and the chemical state of the oxygen in the polymer matrix, identified by the IR analysis. The spectra confirmed that the oxygen was part of the polymeric matrix and not just physically adsorbed onto it. Table 3.3 presents the atomic composition of the polymer determined by some survey spectra of the polymer.

Table 3.3. Atomic composition of MN-150 determined by X-ray photoelectron spectroscopy.

| Polymer                      | Carbon (%) | Oxygen (%) | Nitrogen (%) |
|------------------------------|------------|------------|--------------|
| MN-150 500-600 $\mu\text{m}$ | 83.5       | 12.6       | 3.9          |
| MN-150 ground                | 94.1       | 4.6        | 1.3          |

The concentration of oxygen is greater at the external surface of the polymer (depth <10nm) in comparison with the bulk material leading to a concentration gradient in the polymer. The higher surface oxygen concentrations may be attributed to heterogeneity of the polymer. A similar profile is apparent for the nitrogen functional groups showing slow diffusion of the tertiary amine during the addition reaction.

Subsequent analysis of the C1s peak, Fig. 3.9, illustrates the chemical shift ( $\Delta E$ ) caused by the oxygen. The quality of the spectra is extremely poor due to a low number of scans.

**Fig. 3.9.** X-ray photoelectron spectra of the C1s orbital.

It was possible to extract some chemical shift information which was performed by Dr. R.H.Bradley. The peak assignment of MN-150 is given in Table 3.4.

**Table 3.4.** Peak assignments for Fig. 3.9.

| Peak | Binding Energy (eV) | Chemical Shift (eV) | Carbon Assignment<br>Beamson & Briggs [26] |
|------|---------------------|---------------------|--------------------------------------------|
| 1    | 285.00              | -                   | -C-C- saturated ( $\text{CH}_n$ )          |
| 2    | 285.94              | 0.94                | -C-N<                                      |
| 3    | 286.50              | 1.50                | -C-O-R / -C-O-H                            |
| 4    | 287.90              | 2.90                | >C=O                                       |

The chemical shift information confirmed the amine functionality of MN-150 and provided further evidence of oxygen functionality in the form of ethers or alcohols.

### *Elemental Analysis*

The elemental analysis results of the MN-100, MN-150, and MN-200 can be seen in Table 3.5. The analytical technique prevents the accurate determination of oxygen since it is calculated by the residual. Note: Data presented in mass percent.

Table 3.5. Elemental Analysis of the Macronet Polymers.

| Adsorbent        | Carbon % | Hydrogen % | Chlorine % | Nitrogen %   | [Oxygen]* |
|------------------|----------|------------|------------|--------------|-----------|
| MN-100           | 85.67    | 7.32       | 0.98       | 1.17         | 4.86      |
| MN-150           | 83.58    | 7.27       | 1.02       | 1.73         | 6.40      |
| MN-200           | 85.61    | 6.87       | 1.09       | Trace or Nil | 6.43      |
| Law <i>et al</i> | 82.7     | 5.8        | 3.8        | nil          | 7.7       |

\* Note: oxygen is determined by residual

The percentage of nitrogen in MN-100 and MN-150 correlates quite well with the values obtained by direct titration of 1.03% and 1.48% respectively, shown later. Law *et al* assumed that the majority of oxygen was due to trapped moisture in the polymers [1]. The aromatic ratio of C:H was calculated as 1.43:1.00 based on the subtraction of hydrogen associated with trapped water or 1.20 as a direct ratio. The ratios for MN-100, MN-150 and MN-200 are 0.98, 0.96 and 1.05 respectively. The theoretical C:H ratio for linear polystyrene is 1:1 and 1.06 for the methylene bridged structure. XPS analysis of MN-150 suggested an oxygen concentration of 4.6% which allows the amount of trapped water to be hypothesised, since XPS is an ultra-high vacuum technique which should remove any trapped moisture. Hence, the C:H ratio, correcting for trapped moisture, becomes 1.00:1.00. The dependance of the ratio on the trapped moisture prevents further meaningful discussion.

All three polymers contain a significant mass of chlorine, although significantly less than that observed by Law *et al*. Some of the chlorine may be attributed to chloromethyl groups that did not undergo crosslinking, suggested by the higher concentrations that are present on MN-200 compared to MN-100 and MN-150. However, the amine functional groups added to MN-100 and MN-150 should displace the chlorine during the amination reaction, resulting in a significantly lower concentration of chloromethyl groups. Since this appears not to be the case, the chlorine is probably due to a chlorinated solvent used in the Macronet production or residuals of Friedel-Crafts catalysts. Law *et al* conducted a combustion analysis of the polymer which indicated no significant inorganic residue. They suggested that the chlorine was probably due to 10% of aromatic groups containing unreacted  $\text{CH}_2\text{Cl}$  groups.

### ***Solid State Nuclear Magnetic Resonance Spectroscopy***

The solid state  $^{13}\text{C}$  NMR for MN-100, MN-150 and MN-200 can be seen in Figs. 3.10, 3.11 and 3.12 respectively. The spectra of MN-150 was recorded at two different spinning speeds to enable the spinning side bands to be identified, since the bands shift as the spinning frequency is changed. The side spinning bands on all the spectra are indicated by an asterisk placed next to the peaks.

The spectra of all three polymers show similar characteristics. The broad band, at approximately 129ppm, is due to the aromatic carbon of the polymers. However, the type of substitution on the benzene ring is difficult to determine for the small chemical shifts ( $\delta=\pm 5$ ) around 128.5ppm due to the complicated nature of the polymer. Other bands at 142ppm and 114ppm are also attributable to the aromatic carbon chemical shifts of the substituent groups. The band at 142 represents a shift of +13.5ppm which may be due to  $-\text{CH}_2\text{-OH}$  ( $\delta=+13$ ) [26] groups attached to the benzene ring. The spectrum of MN-200 shows a stronger band at this chemical shift possibly suggesting that the remaining chloromethyl groups, after the crosslinking stage, have been hydrolysed to the alcohol. The band is weaker for MN-100 and MN-150 since the amine functional groups attach in this position. The spectra of MN-100 and MN-150 show additional peaks at 40ppm and at 63ppm which are due to the amine functionality of the polymers. The intensity of the C-N bands are greater for MN-150 suggesting a high weak base capacity. Esters, ethers and alcohols have bands around 44ppm representing C-O [27]. All three Macronet polymers have bands in this region. However, it is not possible to differentiate between these groups and other carbonyl groups due to the side spinning bands masking other characteristic bands around 150-220ppm. The more intense bands at 62 and 65ppm on the spectra of MN-200 suggest a greater concentration of C-O groups.

Spectra of Macronet polymers presented by Law *et al* are similar to those presented in this study although they observed no peaks in the range 90-120ppm. They suggested that the small peak at 43.7ppm, accompanied by the methylene-methine peak at 40.9ppm, was due to chloromethyl carbon. The peak at 43.7ppm disappeared upon amination of the resin which seemed to confirm their hypothesis, as well as the reduction in the chlorine content from 3.8 to 0.7% for the

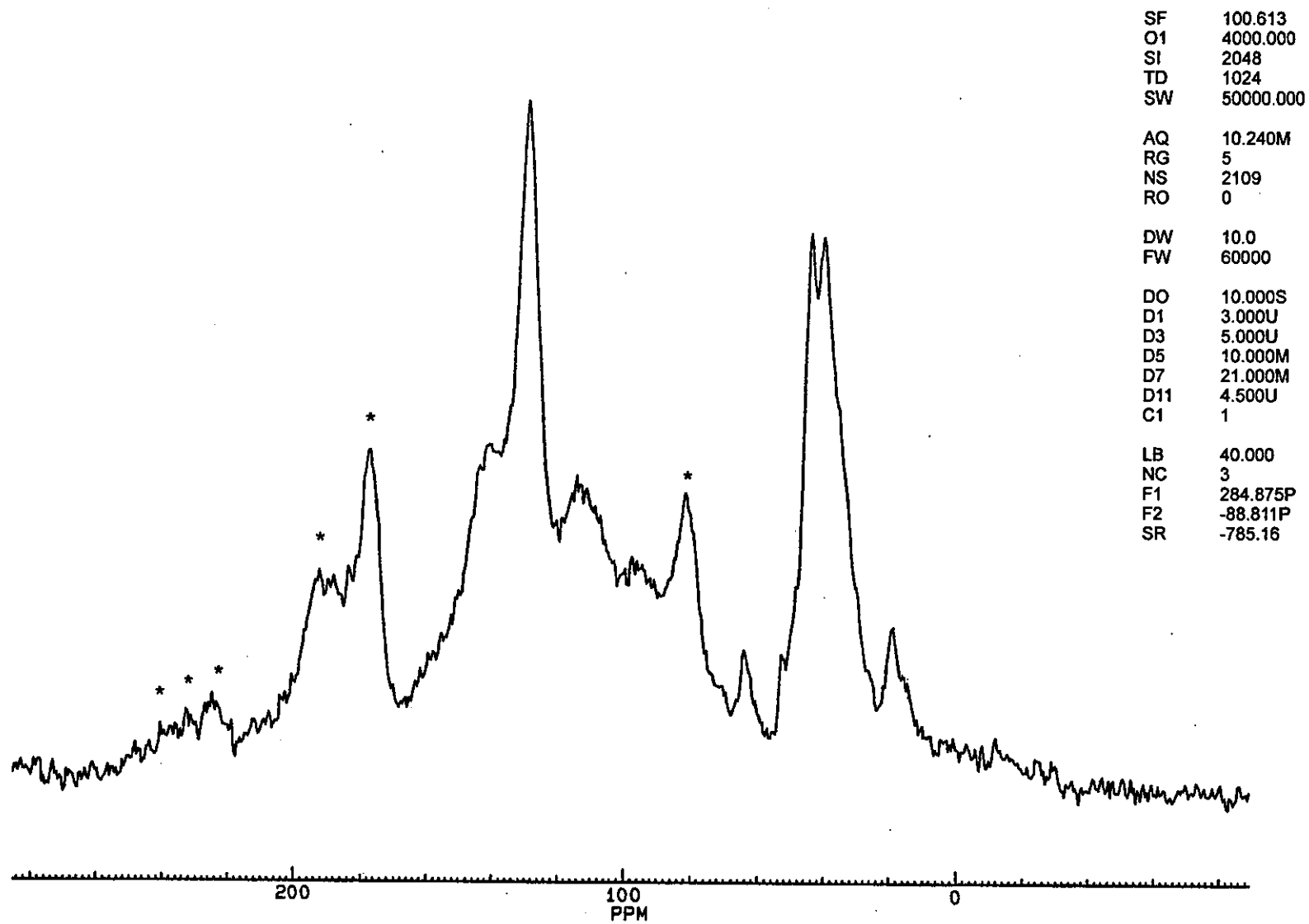
Fig. 3.10.  $^{13}\text{C}$  NMR Spectra of MN-100.

Fig. 3.11.  $^{13}\text{C}$  NMR Spectra of MN-150 at Spinning Speeds of 4811 and 3938Hz.

| Spinning Speed<br>= 3938Hz |           | Spinning Speed<br>= 4811Hz |           |
|----------------------------|-----------|----------------------------|-----------|
| SF                         | 100.613   | SF                         | 100.613   |
| O1                         | 4000.000  | O1                         | 4000.000  |
| SI                         | 2048      | SI                         | 2048      |
| TD                         | 1024      | TD                         | 1024      |
| SW                         | 50000.000 | SW                         | 50000.000 |
| AQ                         | 10.240M   | AQ                         | 10.240M   |
| RG                         | 5         | RG                         | 5         |
| NS                         | 968       | NS                         | 1282      |
| RO                         | 0         | RO                         | 0         |
| DW                         | 10.0      | DW                         | 10.0      |
| FW                         | 60000     | FW                         | 60000     |
| DO                         | 10.000S   | DO                         | 10.000S   |
| D1                         | 3.000U    | D1                         | 3.000U    |
| D3                         | 5.000U    | D3                         | 5.000U    |
| D5                         | 10.000M   | D5                         | 10.000M   |
| D7                         | 21.000M   | D7                         | 21.000M   |
| D11                        | 4.500U    | D11                        | 4.500U    |
| C1                         | 1         | C1                         | 1         |
| LB                         | 40.000    | LB                         | 40.000    |
| NC                         | 2         | NC                         | 3         |
| F1                         | 284.996P  | F1                         | 284.996P  |
| F2                         | -88.690P  | F2                         | -88.690P  |
| SR                         | -797.36   | SR                         | -797.36   |

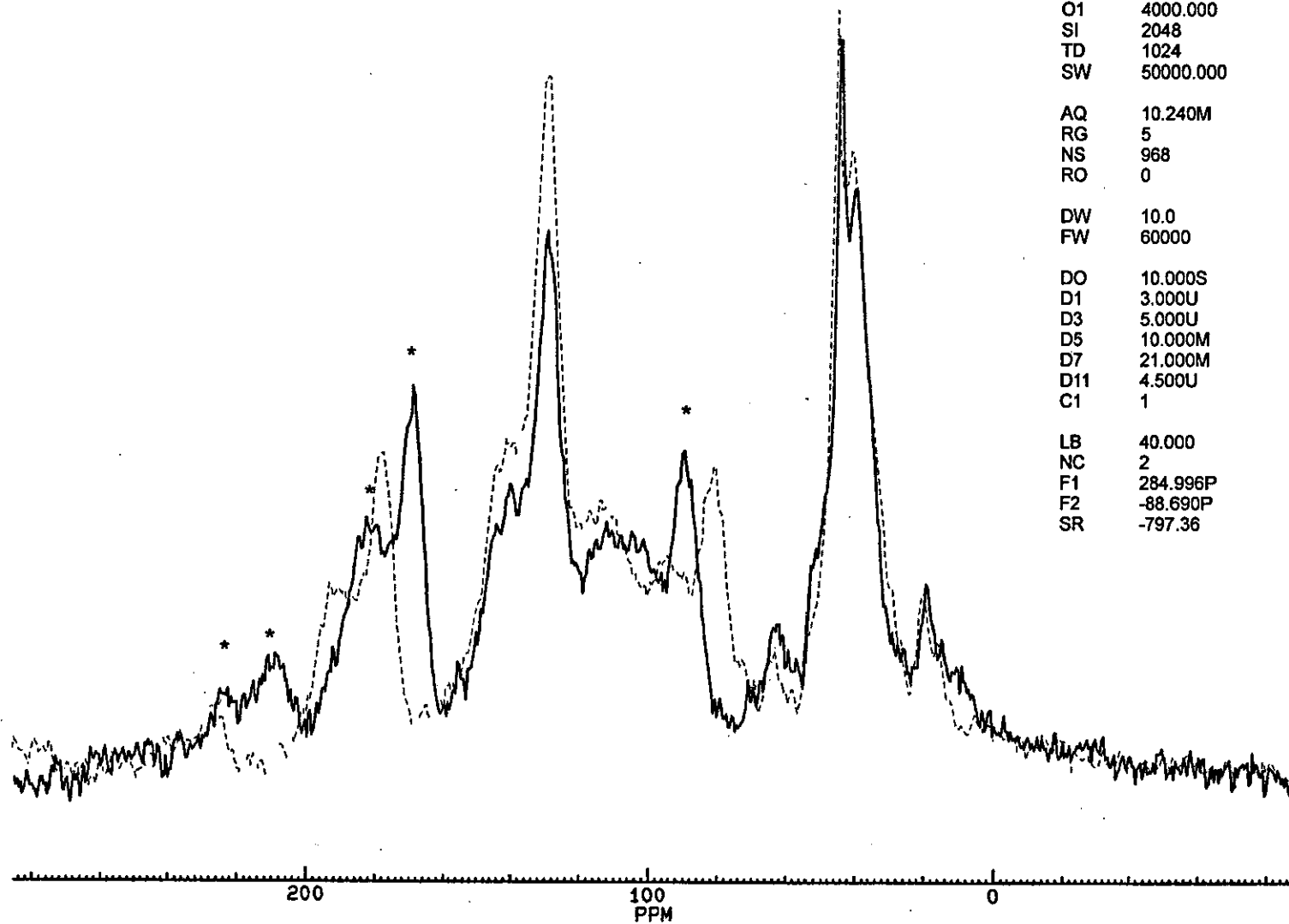
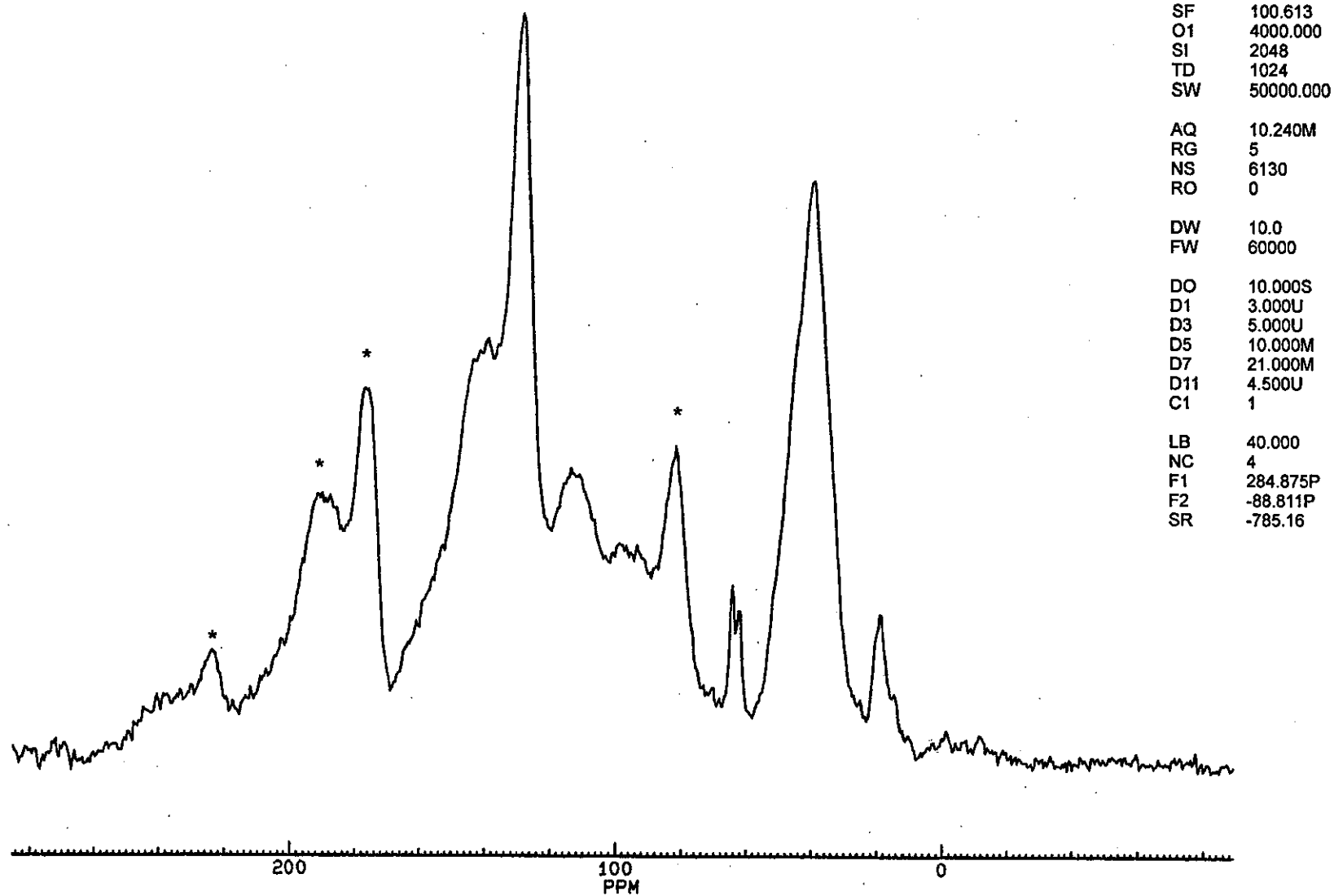




Fig. 3.12.  $^{13}\text{C}$  NMR Spectra of MN-200.

aminated resin. However, the polymers were ground and soaked in ethanol prior to amination which may have enabled any trapped chlorinated solvents to diffuse out of the structure. A simple mass balance on their data suggests that the ratio Cl:N is 1.53:1.00 assuming that the nitrogen containing groups exist as  $\text{CH}_2^+\text{N}(\text{CH}_3)_3\text{Cl}^-$ . Hence, it would appear that some of the chlorine in the polymers was actually due to trapped chlorinated solvent and not chloromethyl groups. FT-IR and  $^{13}\text{C}$  NMR spectroscopy would show similar peaks for the solvent dichloroethane, a solvent commonly used by Davankov and Tsyurupa, as chloromethyl groups. Law *et al* did observe that there were differences in the chemical shifts they observed for chloromethyl groups compared to those previously found in chloromethylated resins. However, they associated this difference with the different proportions of di- and tri-substituted aromatic rings in hypercrosslinked resins.

### ***Direct Titration***

The quantities of base consumed and the concentration of functional groups at the surface of the adsorbents are presented in Tables 3.6 and 3.7 respectively. All of the adsorbents have an extremely low base capacity which limits the accuracy of determination. The end point change of the sodium carbonate and the sodium hydrogen carbonate was difficult to detect which may cause the distribution of the non-carbonyl groups to be rearranged. The titration results show that all of the polymers have oxygen functionality in the form of carbonyl and non-carbonyl groups. The total capacity of each polymer is within 7% of the mean of 0.22meq/g. This makes it difficult to infer any real differences between the polymers. A capacity of 0.22meq/g corresponds to an oxygen mass percent of approximately 1.3. The XPS data indicates a significantly higher oxygen concentration (approx. 5-6% when converted into mass units). It is hypothesised that the significant difference can be attributed to ether groups which act as crosslinking bridges and alcohol functional groups, produced by hydrolysed chloromethyl groups.

The capacity of F-400 activated carbon is significantly higher than that for the polymers. However, the observed capacity is significantly lower than the figures of 1.05meq/g presented by Mazet *et al* [21]. The difference may be due to the different chemical composition of the powdered F-400 activated carbon titrated by Mazet. Three other researchers in our laboratory

have repeated the titration of F-400 and have observed identical results to this work.

**Table 3.6. Base Consumption of Various Adsorbents.**

| Adsorbent | Base consumption (meq/g) |       |                                 |                    |
|-----------|--------------------------|-------|---------------------------------|--------------------|
|           | NaOEt                    | NaOH  | Na <sub>2</sub> CO <sub>3</sub> | NaHCO <sub>3</sub> |
| MN-100    | 0.207                    | 0.110 | 0.032                           | 0.030              |
| MN-150    | 0.237                    | 0.104 | 0.097                           | 0.045              |
| MN-200    | 0.220                    | 0.090 | 0.080                           | 0.055              |
| F-400     | 0.358                    | 0.123 | 0.120                           | 0.047              |

**Table 3.7. Concentration of Surface Functional Groups of Various Adsorbents.**

| Adsorbent | Surface Groups (meq/g) |                  |          |          |                   |
|-----------|------------------------|------------------|----------|----------|-------------------|
|           | Strongly<br>Acidic     | Weakly<br>Acidic | Phenolic | Carbonyl | Total<br>Capacity |
| MN-100    | 0.03                   | 0.00             | 0.08     | 0.10     | 0.21              |
| MN-150    | 0.05                   | 0.05             | 0.01     | 0.13     | 0.24              |
| MN-200    | 0.06                   | 0.03             | 0.01     | 0.13     | 0.23              |
| F-400     | 0.05                   | 0.07             | 0.00     | 0.24     | 0.36              |

The concentration of amine functional groups is presented in Table 3.8. The titration results confirm that the majority of the amine functionality is in the form of weak base anion groups. However, there is a percentage of strong base groups also present.

**Table 3.8. Weak base volume and weight capacities of the Macronet polymers.**

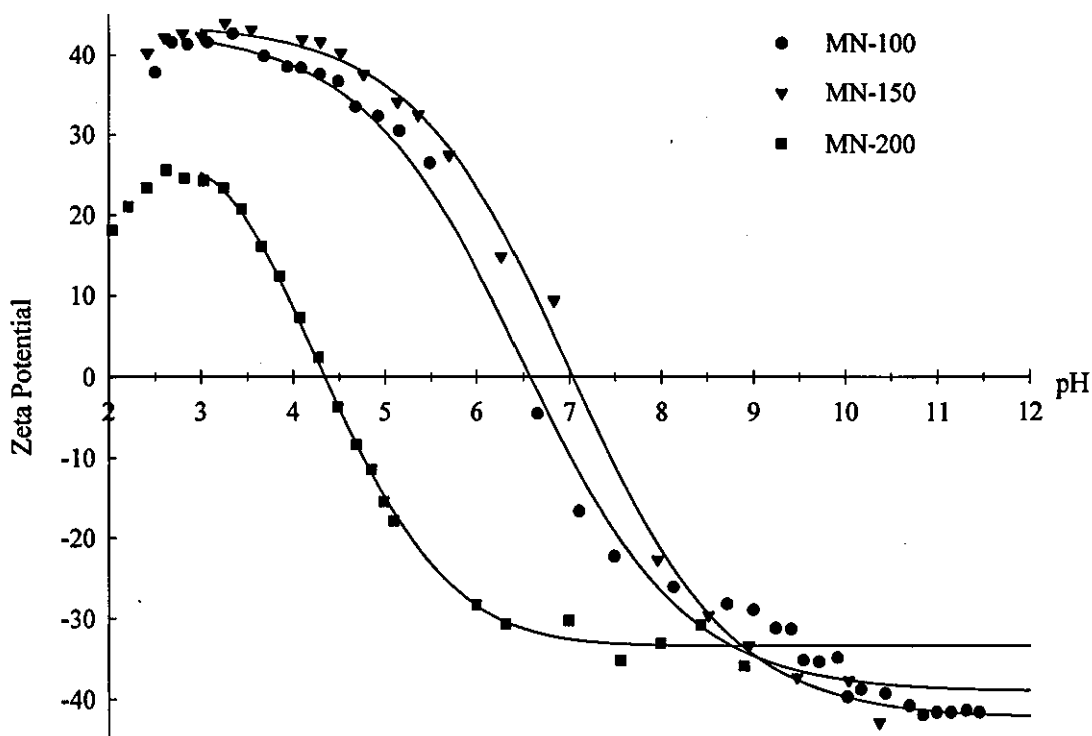
| Adsorbent | Vol. Capacity<br>(OH <sup>-</sup> ) meq/ml | Weight capacity<br>(OH <sup>-</sup> ) meq/g | Strong base<br>capacity % |
|-----------|--------------------------------------------|---------------------------------------------|---------------------------|
| MN-100    | 0.20                                       | 0.74                                        | 7.7                       |
| MN-150    | 0.34                                       | 1.06                                        | 13.5                      |

(OH<sup>-</sup>) indicates that the resin was converted to the OH form before titration

### *Zeta Potential Analysis*

The zeta potential of the polymers at different pH values is illustrated in Fig. 3.13 indicating zero crossover points at a pH of 5.1, 7.4 and 7.8 for MN-200, MN-100 and MN-150 respectively. The surface charge of the polymer at a pH of around those of natural waters (pH 6-7) indicates that MN-200 will have a negatively charged surface. However, the tertiary amine functionality of MN-100 and MN-150 may enable the surface to be either positive, neutral or negative with a small shift in pH. The tertiary amine functional groups may also enable the sorption of anionic species such as humic acid by an ion exchange mechanism.

**Fig. 3.13** Zeta Potential of MN-100, MN-150 and MN-200.



### *General Discussion*

The Macronet polymers are derived from a copolymer of divinyl benzene (DVB) and styrene which is then further crosslinked. The infra red spectra of the copolymer indicates that the percentage of crosslinking agent (DVB) used is low, due to the similarity in its spectra with

atactic polystyrene. Chloromethyl groups are then introduced onto the styrene rings, normally in the para position. Some benzene rings appear to be tri-substituted, in the ortho and para position, whilst others remain unchanged. Hypercrosslinking of the polymer is achieved by swelling the polymer in a good solvent before the introduction a Friedel-Crafts catalyst. The elemental analysis indicated relatively high concentrations of chlorine in all three polymers suggesting that the solvent may be chlorinated. The crosslinking stage does not enable all of the chloromethyl groups to bridge since there is evidence of a small percentage of residual chloromethyl groups in MN-200, the unfunctionalised polymer. The weak base amine functional groups present on MN-100 and MN-150 displace the chlorine at the chloromethyl group.

A detailed study into the surface functionality of the polymers suggested a rather complex mixture of oxygen functional groups. The concentration of such groups appeared to be higher at the external surface of the polymer compared to the bulk material, indicated by the XPS analysis of a whole bead of MN-150. However, most of the analytical techniques used required the polymers to be ground, thus preventing any detailed studies of the external functional groups. The oxygen containing groups that are hypothesised are ketones, ethers, alcohols and carboxylic acids. These groups have been identified by a combination of spectroscopy and titration. However, a mechanism for the production of such groups needs to be identified. The groups appear to be introduced during the crosslinking stage since the spectra of the copolymer indicates no oxygen functionality. Alcohols may originate from the hydrolysis of the chloromethyl group. This mechanism would also explain how ether groups can be introduced since the alcohol could crosslink with chloromethyl groups during the Friedel-Crafts reaction.

Stahlbush [28] presented mechanisms for the decomposition of cationic exchange resins which introduced ketones and acid groups into the decomposition products. However, the oxidising species which would allow the mechanism to proceed is unknown at present.

The limited investigations into the surface chemistry of F-400 also suggested a mixture of oxygen functional groups determined by direct titration. The concentration of these groups was much larger than those present on the polymers. The discussion of the oxygen functional groups on carbon surfaces is extremely well documented in the literature and is still uncertain at present.

The main functionality appears to be carboxyl, phenol, lactone and quinone. However, spectroscopic techniques have proved inadequate in confirming these hypotheses derived from direct titration.

The oxygen functional groups will enable the sorption of organic species by a variety of mechanisms. Carboxyl and phenolic groups may allow sorption by an ion exchange mechanism, so long as the pH of the solution enables dissociation of the functions groups. Other functionality such as ketones, quinones, ethers etc. may enhance sorption due to hydrogen bonding with the oxygen. A more detailed discussion of the influence of surface groups on the sorption of selected organic species will be given in Chapters 4 and 5.

## SECTION 3.4 CONCLUSIONS

Spectroscopic analysis and titration of the Macronet polymers and the activated carbon F-400 have indicated a number of different oxygen functional groups at the surface of the adsorbents. Direct titration, which identifies groups such as carbonyl, carboxyl and phenolic, suggested an oxygen concentration of 0.22meq/g and 0.36meq/g for the polymers and carbon respectively. XPS and elemental analysis suggested a higher concentration of oxygen of between 5 and 6 mass percent for the polymers. The exact nature of the functionality on the polymers was determined using spectroscopic techniques. This suggested that the major functional groups were ketones, ethers and alcohols. However, the complex mixture of groups prevent their quantification. The weak base anion weight capacity of MN-100 and MN-150 was 0.76 and 1.06 respectively. The relatively high percentage of oxygen functional groups present on the polymers and carbon is expected to influence the mechanism and strength of adsorption of organic species.

**SECTION 3.5 REFERENCES**

- [1] R.V. Law, D.C. Sherrington and C.E. Snape, Solid State  $^{13}\text{C}$  MAS NMR Studies of Hyper-Cross-Linked Polystyrene Resins., *Macromolecules*, 29, (1996), p6284-6293.
- [2] R. Joseph, W.T. Ford, S. Zhang, M.P.Tsyurupa, A.V. Pastukhov, V.A. Davankov, Solid State  $^{13}\text{C}$ -NMR Analysis of Hypercrosslinked Polystyrene., *Journal of Polymer Science Part A Polymer Chemistry*, 35, (4), (1997), p695-701.
- [3] J.S. Mattson, H.B. Mark (Jr.) and W.J. Weber (Jr.), Identification of Surface Functional Groups on Active Carbon by Infrared Internal Reflection Spectrophotometric., *Analytical Chemistry*, 41, (2), (1969), p355-358.  
  
J.S. Mattson, L. Lee, H.B. Mark (Jr.) and W.J. Weber (Jr.), Surface Oxides of Activated Carbon: Internal Reflectance Spectroscopic Examination of Activated Sugar Carbons., *Journal of Colloid and Interface Science*, 33, (2), (1970), p284-293.
- [4] R. Popat, Functionalisation of Polyolefins and its Effects on Surface Chemistry and Energetics., PhD Thesis, Loughborough University, (1995).
- [5] R.A. Friedel and L.J.E. Hofer, Spectral Characterisation of Activated Carbon., *The Journal of Physical Chemistry*, 74, (15), (1970), p2921-2922.
- [6] R.A. Friedel and G.L. Carlson, Difficult Carbonaceous Materials and Their Infra-red and Raman Spectra. Reassignments for Coal Spectra., *Fuel*, 51, (1972), p194-198.
- [7] C. Ishizaki and I. Martí, Surface Oxide Structures on a Commercial Activated Carbon., *Carbon*, 19, (6), (1981), p409-412.
- [8] P.E. Fanning and M.A. Vannice, A DRIFTS Study of the Formation of Surface Groups on Carbon by Oxidation., *Carbon*, 31, (5), (1993), p721-730.
- [9] B. J. Meldrum and C.H. Rochester, In Situ Infrared Study of the Surface Oxidation of Activated Carbon in Oxygen and Carbon Dioxide., *Journal of the Chemical Society. Faraday Transactions*, 86, (5), (1990), p861-865.  
  
B. J. Meldrum and C.H. Rochester, In Situ Infrared Study of the Surface Oxidation of Activated Carbon Dispersed in Potassium Bromide., *Journal of the Chemical Society. Faraday Transactions*, 86, (17), (1990), p2997-3002.
- [10] D. Briggs and G. Beamson, Primary and Secondary Oxygen-Induced C1s Binding Energy Shifts in X-ray Photoelectron Spectroscopy of Polymers., *Analytical Chemistry*, 64, (1992), p1729-1736.
- [11] R.H. Bradley, I. Sutherland and E. Sheng, Carbon Surface: Area, Porosity, Chemistry and Energy., *Journal of Colloid and Interface Science*, 179, (1996), p561-569.

- [12] R.J.J. Jansen and H. van Bekkum, XPS of Nitrogen-Containing Functional Groups on Activated Carbon., *Carbon*, 33, (8), (1995), p1021-1027.
- [13] H.R. Kruyt and G.S. de Kadt, *Kolloid Chem.*, 32, (1931), p249. Cited in ref 18.
- [14] H.P. Boehm, E. Diehl, W. Heck and R. Sappok, *Surface Oxides of Carbon.*, *Angewandte Chemie International Edition*, 3, (10), (1964), p669-677.
- [15] H.P. Boehm, Some Aspects of the Surface Chemistry of Carbon Blacks and Other Carbons, *Carbon*, 32, (5), (1994), p759-769.
- [16] H.P. Boehm, Functional Groups on the Surface of Solids., *Angewandte Chemie International Edition*, 5, (6), (1966), p533-622.
- [17] H.P. Boehm, Chemical Identification of Surface Groups., *in Advances in Catalysis*, D.D. Eley, H. Pines and P.B. Weisz (ed), Vol 16, Academic Press. New York. London. (1966), p179-274.
- [18] R.C. Bansal, J-B. Donnet and F. Stoeckli, *Active Carbon*, Marcel Dekker, inc., (1988), p27-118.
- [19] K. T. Alben, Trace Element Distributions of a Granular Activated Carbon., *Carbon*, 24, (2), (1986), p177-183.
- [20] Calgon Corporation, Pittsburgh, PA (August 1978). Cited in ref 19.
- [21] M. Mazet, B. Farkhani and M. Baudu, Influence of Heat or Chemical Treatment of Activated Carbon onto the Adsorption of Organic Compounds., *Water Research*, 28, (7), (1994), p1609-1617.
- [22] S. Hazourli, Adsorption et électrosorption de composés organiques sur charbon actif en grains., PhD Thesis, l'université de Pau et des Pays de l'Adour, (1991).
- [23] R.S. Summers and P.V. Roberts, Activated Carbon Adsorption of Humic Substances II. Size Exclusion and Electrostatic Interactions., *Journal of Colloid and Interface Science*, 122, (2), (1988), p382-397.
- [24] M. Ulmer, Technologiezentrum Wasser (TZW), Karlsruhe University, Germany, Work due to be published in PhD Thesis, (1997-98).
- [25] G. Socrates, *Infrared Characteristic Group Frequencies Tables and Charts*, Second Edition, Wiley, Chichester, (1994), Chap. 11
- [26] G. Beamson and D. Briggs, High Resolution XPS of Organic Polymers, The Scienta ESCA300 Database., John Wiley & Sons, (1992), Appendix 1, 2 and 3.
- [27] Lide, D. R., *CRC Handbook of Chemistry and Physics*, 74th Edition, CRC Press,



London, (1993), p9-160

- [28] J.R. Stahlbush and R.M. Strom, A decomposition mechanism for cation exchange resins, *Reactive Polymers*, 13, (1990), p233-240.

## CHAPTER 4

### PHENOLS ADSORPTION

#### SECTION 4.1 INTRODUCTION

Liquid phase adsorption of phenolic compounds has been studied extensively for the characterisation of new adsorbent materials. Phenolic compounds are produced with a wide variety of functional groups which allow fundamental studies regarding the mechanisms of adsorption to be made.

This chapter investigates the adsorption of phenol, 2-chlorophenol, 3-chlorophenol and 4-chlorophenol onto Macronet polymers and F-400 activated carbon. Kinetic data for batch adsorption are modelled using the homogeneous surface diffusion correlation.

#### SECTION 4.2 THEORY OF ADSORPTION AND LITERATURE REVIEW

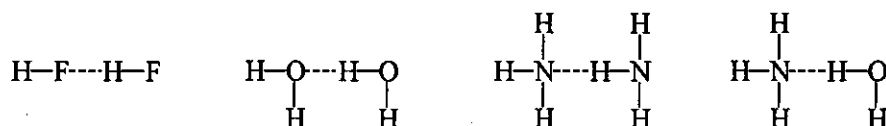
Adsorption of a substance involves its accumulation at the interface between two phases, such as a liquid and a solid, or a gas and a solid. Several mechanisms are involved in the adsorption of organic compounds from aqueous solution which may be generalised as physical adsorption, or van der Waals forces and electrostatic attraction or chemical adsorption.

Physical adsorption forces result from the electric charge density of individual atoms. Non polar molecules are attracted to one another by weak induced dipole-dipole interactions called London forces (hydrophobic bonding). As electrons move, at any instant, the distribution of charge in a molecule is distorted, and a small dipole exists. The negative end of the momentary dipole tends to repel electrons of a second molecule. Thus, an oppositely oriented dipole is induced in the neighbouring molecule, resulting in an attraction between the two molecules. The hydrophobicity of organic pollutants is often assessed by the logarithm of the octanol-water

partition coefficient,  $k_{ow}$ . Most organic pollutants have positive values, gradually increasing as the compounds become more hydrophobic. The solubility of the compound in water is also used as a measure of hydrophobicity.

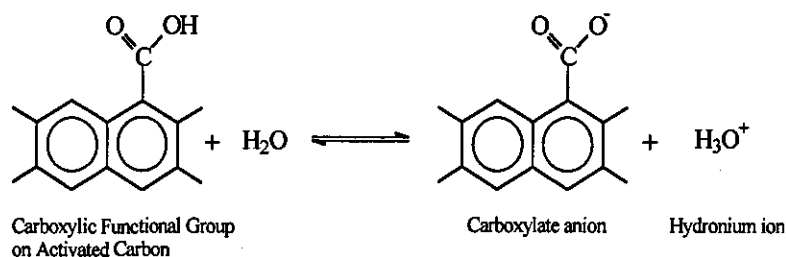
In polar substances there is an attraction between the positive end of one polar molecule for the negative end of another polar molecule. Such attractions are a result of dipole-dipole interactions. A special kind of dipole-dipole attraction is hydrogen bonding, in which 'a hydrogen atom serves as a bridge between two electronegative atoms, holding one by a covalent bond and the other by purely electrostatic forces' [1]. Hydrogen bonding occurs between molecules containing fluorine, oxygen and nitrogen due to the concentrated negative charge of their small atoms. When hydrogen is bonded to one of these atoms its electron cloud is distorted towards the highly electronegative atom, thus exposing the positively charged hydrogen nucleus. The charged hydrogen atom is then strongly attracted to the electronegative atom of a second molecule resulting in an attraction which is much stronger than dipole-dipole interactions. Fig. 4.1 illustrates a variety of hydrogen bonds.

Fig. 4.1. Types of hydrogen bonds.



Hydrogen bonds represented by dashed lines

Electrostatic bonding occurs through the process of ion exchange or coordination. In ion exchange, ions of a given charge (either cations or anions) in a solution are sorbed on a solid material (the ion exchanger) and are replaced by equivalent quantities of other ions of the same charge released by the solid. Ion exchange can only occur when the functional groups on the adsorbent and the organic species are dissociated. Dissociation of the carboxylic acid functionality contained on many activated carbons can be described by the reaction:



Since the concentration of water, the solvent, remains essentially constant in the above reaction the equilibrium relationship can be described by:

$$K_a = \frac{[RCOO^-][H_3O^+]}{[RCOOH]} \quad (1)$$

where  $R$  is the activated carbon surface and  $K_a$  is the acidity constant. The  $pK_a$  is often used to describe the dissociation of functional groups which is defined as the negative logarithm of  $K_a$ . When the concentration of the undissociated carboxylic acid equals the concentration of the dissociated acid, the pH of the solution equals the  $pK_a$  of the carboxylic acid. Similar equations can be derived for weakly basic compounds leading to the basicity constant,  $K_b$ . The equilibrium constant is often expressed in terms of the appropriate acid dissociation constant using the relationship:

$$pK_a = 14 - pK_b \quad \text{at } 25^\circ\text{C} \quad (2)$$

As mentioned previously, the organic molecules have to be dissociated to enable sorption by an ion exchange mechanism. Phenol, for instance, has a  $pK_a$  of 9.99. At pH values around 7, phenol will exist as a neutral molecule and so will not be removed by an anion exchange mechanism. Conversely, weakly basic organic compounds, such as aniline  $pK_b$  of 9.4 ( $pK_a=4.6$ ) will occur in cationic forms only at pH values near or below their respective  $pK_b$  values (molecule in protonated form as  $C_6H_5NH_3^+$ ). The approximate relationship between pH,  $pK_b$ , and the percentage of the molecule in the cationic form is shown in Table 4.1.

**Table 4.1. Relationship between pH,  $pK_b$ , and the percentage of the molecule in the cationic form.**

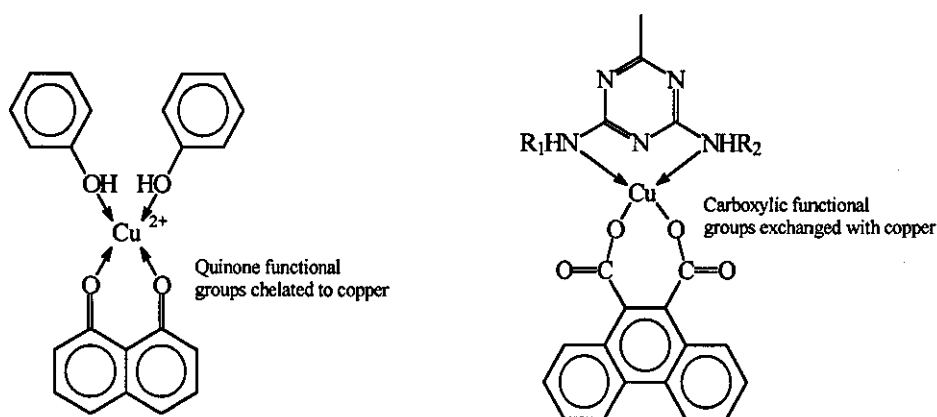
| Relationship  | Percentage of Molecule as |           |
|---------------|---------------------------|-----------|
|               | $RNH_2$                   | $RNH_3^+$ |
| $pH=pK_b$     | 50                        | 50        |
| $pH=pK_b + 1$ | 90                        | 10        |
| $pH=pK_b - 1$ | 10                        | 90        |

Hence, weakly basic pollutants in waters around pH 6-7 may be sorbed to carboxylic acid functionality on the surface of activated carbons by a cation exchange mechanism. Whether or not ion exchange takes place will depend on the presence of stronger cations in solution, since

these would be preferentially removed.

Organic compounds, containing a ligand, can also be removed by forming a complex with metal ions bound to the surface of the adsorbent. Each ligand is bonded to the metal by the overlap of an empty orbital on the metal with a filled orbital on the ligand, thus creating a coordination bond. Some ligand molecules have more than one electron pair to share with the metal, i.e. more than one binding site. Binding of this type is called chelation. Figure 4.2 shows an example of the removal of phenol and the s-triazine by complexation.

**Fig. 4.2.** Binding of phenol and s-triazazine by complexation.



The strength of the different types of bonding varies tremendously. Table 4.2 presents the approximate ranges of interaction energies for various types of force [3.4].

**Table 4.2.** Approximate bond energies and equilibrium lengths for various types of interactions.

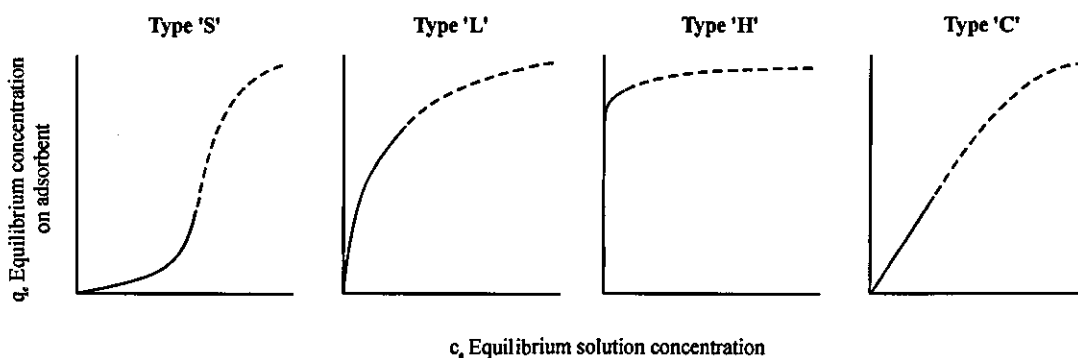
|                         | Chemical Bonds |          |          | Intermolecular Forces |               |           |
|-------------------------|----------------|----------|----------|-----------------------|---------------|-----------|
|                         | Ionic          | Covalent | Metallic | London                | Dipole-Dipole | H-Bonding |
| Bond Energy (kJ/mol)    | 590-1200       | 60-800   | 100-350  | <40                   | <20           | <60       |
| Equilibrium Length (nm) | 0.2-0.4        | 0.08-0.3 | 0.2-0.6  | 0.4-0.6               | 0.2-0.4       | ~0.3      |
| Directional             | No             | Yes      | No       | No                    | No            | Yes       |

Many authors use the term 'adsorption' to describe interactions which are both physical and chemical in nature. Strictly speaking, ion exchange and complexation should be termed

'sorption' since the processes involve the sharing of electrons. However, for simplicity this study will use the terms interchangeably since it is often difficult to assess the extent, if any, of ion exchange.

The capacity of adsorbents is generally proportional to the amount of surface area within the pores that is accessible to the adsorbate, since hydrophobic forces are dominant. As the organic pollutants become more hydrophobic in nature the hydrophobic adsorbent interacts more strongly with the adsorbate, giving rise to an increased capacity. The surface functional groups on the adsorbent can either increase or decrease the capacity, dependent on the their functionality and that of the adsorbate. Adsorption can be enhanced by hydrogen bonding or by ion exchange. However, the dissociated or protonated adsorbent's functional groups can cause the surface charge to be the same as the adsorbing species, thus repelling the molecule. The ability of adsorbents to remove organic compounds from water are often presented graphically, in the form of adsorption isotherms. The adsorption isotherm shows the constant temperature equilibrium relationship between the quantity of adsorbate per unit of adsorbent ( $q_e$ ) and the equilibrium concentration of the adsorbate in solution ( $c_e$ ). Fig. 4.3 presents the four main types of isotherms that are observed in liquid phase adsorption [2].

Fig. 4.3. Adsorption Isotherm Classifications.



The L-type (Langmuir) is the most common and generally represents the high affinity of the adsorbent for the adsorbate. As the initial sites are filled it becomes increasingly difficult for the adsorbate molecules to find a vacant site resulting in the formation of a monolayer. At high solid phase concentrations the curve can bend upwards suggesting multi-layer formation. The H-type (high affinity) isotherm is a special case of the 'L' curve, where the adsorbent has such affinity for the adsorbate that, in dilute solutions, it is completely removed. Such uptake is often

characteristic of sorption of the adsorbate by an ion exchange mechanism. The linearity of the C-type (constant partition) isotherm shows that the number of sites for adsorption remains constant, thus new sites must become available as the solute is adsorbed. The S-type occurs when the solid has a higher affinity for the solvent compared to the adsorbate (i.e. water competes strongly for the adsorption sites). Electrostatic repulsion of negatively charged humic and fulvic acid molecules with negatively charged carbon surfaces often show this type of isotherm [3].

Isotherms of the L-type are often modelled using the Langmuir or Freundlich correlations. The Langmuir equation [2.20] assumes an energetically homogeneous sorbent surface and hence a constant energy of adsorption for all sites. This results in monolayer adsorption on the sorbent surface and the formation of a 'plateau' or constant sorbent capacity. The Langmuir equation can be described by the equation:

$$q_e = \frac{q_{\max} b c_e}{1 + b c_e} \quad (3)$$

The  $q_{\max}$  constant corresponds to the surface concentration at monolayer coverage and represents the maximum value of  $q_e$  that can be achieved as  $c_e$  is increased. The constant  $b$  is related to the energy of adsorption and increases as the strength of the adsorbate/adsorbent bond increases. A plot of  $1/q_e$  versus  $1/c_e$  should yield a straight line with a gradient  $1/q_{\max}b$  and intercept  $1/q_{\max}$ , thus facilitating the calculation of the constants. Deviations often occur from the Langmuir correlation due to multi-layer formation at higher adsorbate surface concentrations. The Freundlich model overcomes some of the limitations of the Langmuir model since it describes equilibrium at heterogeneous surfaces, which allows for multi-layer formation. Although the Freundlich equation is an empirical correlation, a theory of adsorption that leads to the equation has been presented by Halsey *et al* [4]. The Freundlich correlation is described by the equation:

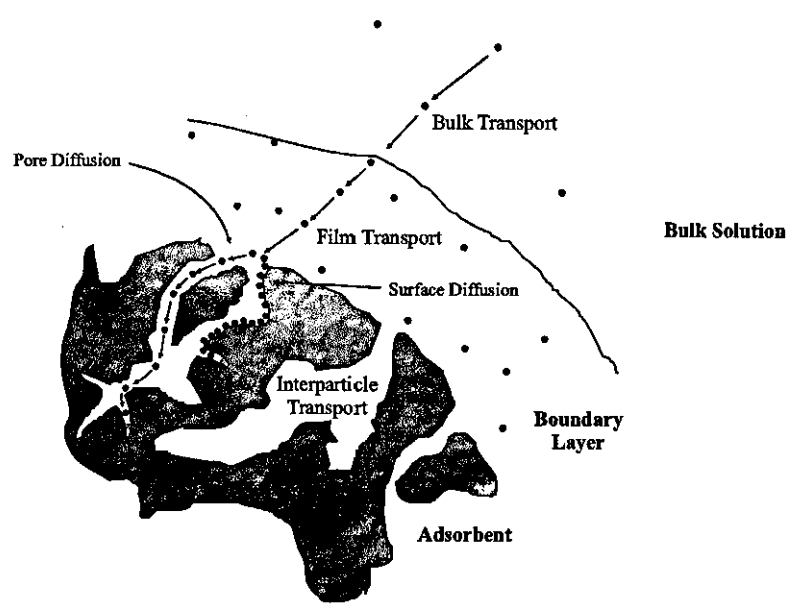
$$q_e = K c_e^{1/n} \quad (4)$$

where  $K$  and  $1/n$  are the Freundlich constants obtained by linearising the above equation. Hence, a plot of  $\log q_e$  versus  $\log c_e$  should yield a straight line with a gradient  $1/n$  and intercept  $\log K$ . The constant  $K$  is primarily related to the capacity of the adsorbent for the adsorbate and  $1/n$  is a function of the strength of adsorption. Low values of  $1/n$  suggest a strong interaction between

the adsorbent surface and the adsorbate, often resulting in irreversible adsorption. The Freundlich isotherm, has a wide range of application. However, it does not converge to Henry's law at low surface coverage ( $q_e \rightarrow 0$ ). Al-Duri *et al* [5] proposed an extrapolation technique to overcome the problem. However, their theory is not widely used. Many other adsorption isotherm correlations exist in the literature. However, these are often only used when application of the Langmuir and Freundlich models fail. I refer the reader to the book by Ruthven [6], Chapter 4, which discusses the theoretical basis of models including the Dubinin-Polanyi characteristic curve and the virial correlation. Theories relating to multi-component adsorption are discussed in Chapter 5.

In order to design adsorption processes a knowledge of the adsorbent's capacity for the given adsorbates and the kinetics of adsorption is required. The overall adsorption process may be considered as three consecutive steps, see Fig. 4.4. The initial stage is the external mass transfer of the solute from the solution bulk, followed by diffusion through the boundary layer to the particle surface. Internal diffusion of the adsorbate then occurs by pore and/or a homogeneous surface diffusion mechanism.

**Fig. 4.4. Mechanisms for the process of adsorption.**





In surface diffusion, molecules migrate by a surface hopping mechanism; i.e. when an adjacent adsorption site is available, and the molecule has enough energy to leave the site it is presently occupying, it will hop from one to the other. Pore diffusion occurs when the adsorbate molecule diffuses in the liquid filling the pore. The surface diffusion flux is many times greater than the pore diffusion flux for strongly adsorbed species. This enables the contribution of pore diffusion to the adsorbate transport to be neglected [7].

The Homogeneous Surface Diffusion Model (HSDM) considers the diffusional process to be controlled surface diffusion sometimes combined with film diffusion. The model has been developed and analysed by several researchers for batch systems, from the 1950's to the present day, to describe the process of adsorption onto granular activated carbon. Solutions to the model, containing non-linear equations, were often solved numerically. However, a number of authors were able to solve the model equations algebraically assuming that film resistance was negligible and that the isotherm was linear. Solutions for systems with non-linear isotherms were also developed. Weber *et al* [8] (1974) provides a good review of the literature concerning the development of solutions to the HSDM for both batch and fixed column systems. Kim *et al* [9] selected the method of quasilinearization in conjunction with the orthogonal collocation method to estimate the model parameters from batch experimental data. Hand *et al* [7] experimentally eliminated the contribution of film diffusion ( $k_f$ ) to the kinetics and so were able to determine the surface diffusion coefficient ( $D_s$ ) by comparing their batch adsorption data with empirical solutions to the HSDM. Traegner *et al* [10] (1989) developed a method to simultaneously estimate both coefficients without the experimental restrictions. They used the Levenberg-Marquardt algorithm to search for the kinetic parameters that minimised the difference between the HSDM solution and the data collected from batch adsorption experiments. Dipak Roy *et al* [11,12] presented a simplified solution technique for the HSDM by discretizing the partial differential equations using the orthogonal collocation method. The ordinary differential equations were then transferred into algebraic equations using Laplace transform, rather than the Runge-Kutta method of integration. The mathematical manipulation resulted in a set of five non-linear algebraic equations and five unknowns. The equations become linear on the input of the value of the dimensionless liquid phase concentration at the interface, refined by iteration of the five equations. The input parameters required for the model are; the adsorbent's particle size,

its apparent density, the Freundlich isotherm coefficients, the initial solution concentration and the adsorbent mass. Rather than repeating the derivation and final equations in this text, I refer the reader to the original papers.

Numerous solutions to the pore diffusion model have also been proposed. As with the HSDM, most solutions involved numerical techniques to solve the equations for systems that considered film resistance and non linear isotherms [8]. Deviations were often observed between the theoretical decay curves generated by the two-resistance models with experimental data. The effect was most evident at long time periods suggesting that another mass transfer step becomes rate controlling at these times. Peel *et al* [13] suggested subdividing the pore diffusional parameter into macropore diffusion and micropore diffusion, thus allowing the slow approach to equilibrium (diffusion into the micropores) to be modelled. McKay *et al* [14] used the equations proposed by Peel *et al* to model various adsorbent/adsorbate systems.

A reasonably comprehensive literature review, containing 30 references was given by McKay [15] (1984). He discussed pore and surface diffusion models for batch and fixed bed liquid phase adsorption. McKay and coworkers have conducted numerous studies into modelling adsorption kinetic data, for various organic compounds onto F-400 activated carbon, using external mass transfer coefficients and various pore diffusion models. [16-20].

Al-Duri *et al* [5] compared the coefficients obtained by the Film-Pore and Branched Pore models with the HSDM for the adsorption of three basic dyes onto F-400 activated carbon. All the models, for a given set of conditions, yielded congruent curves. They also proposed models that combined film, pore and solid diffusion into one diffusion model to provide a more "true" description of the sorption mechanism. However, solutions to such a model would be mathematically complex for batch systems. (Note: models do exist for fixed bed adsorption termed the dispersed flow, pore-surface-diffusion model [5.16, 5.17, 5.39]).

### ***Phenols Adsorption***

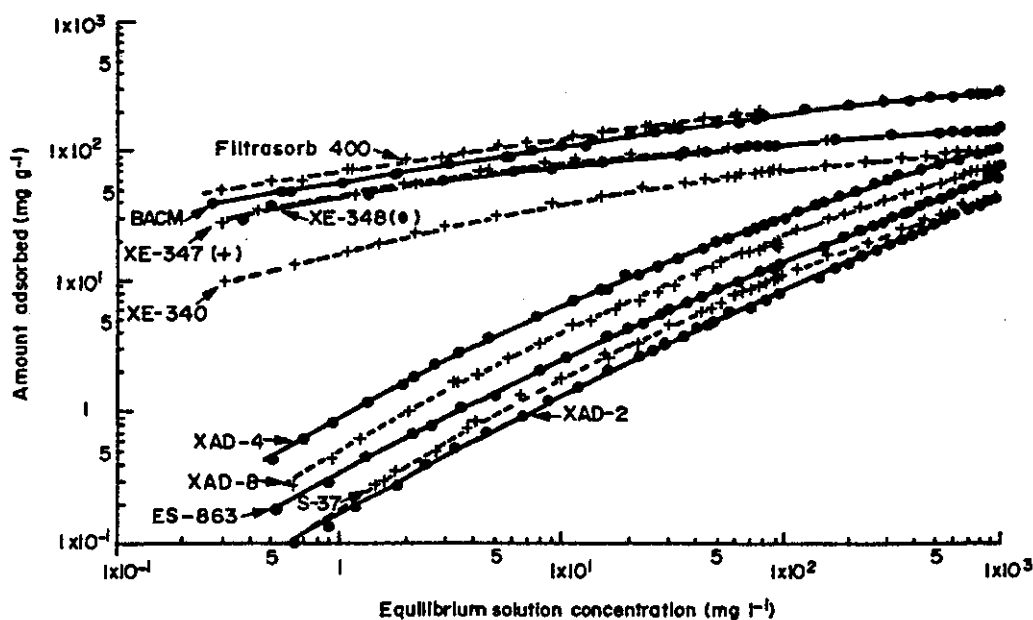
Tsyurupa *et al* [1.8-9] have investigated the sorption of phenol onto Macronet polymers. They

observed that a column packed with 100ml of MN-100 could treat 100 bed volumes (BV's) of a solution containing 100-200mg/l of phenol compared to 25BV's for the polymer Amberlite XAD-4. The isotherms produced for MN-100 and MN-150, in the concentration range 0.1-4 g/l, could not be modelled using either the Langmuir or Freundlich correlations. The amount of phenol removed, approximately 0.4g/g, exceeded the amount of swelling water which is contained in the polymer structure. This was attributed to additional swelling of the polymers when the phenol replaced the swelling water.

Kim *et al* [21] investigated the adsorption of phenols onto macroreticular resins produced with various surface areas and functionalities. Experiments using p-chlorophenol showed that a linear relationship existed between the surface area of the adsorbent and its adsorption capacity. Differences in the adsorption of phenol and phenols containing substituent groups of NO<sub>2</sub> and Cl were explained by the resonance effect of the functional group and the compound's solubility. Existence of functional groups at the ortho position appeared to enhance the adsorption capacity and accelerated intraparticle mass transfer. Itaya *et al* [22] investigated the adsorption of phenol, p-chlorophenol and p-cresol onto two macroporous resins, XAD-4 and XAD-7. Adsorption isotherms, plotted in log form, were also curved over the concentration range 10-1000mg/l. They investigated a number of adsorption isotherm correlations and concluded that the equation of Jossens *et al* proved to be the most satisfactory over the entire range of concentration. In all systems the Freundlich and Langmuir equations showed a very poor fit to the data over the entire concentration range. van Vliet *et al* [23] compared the adsorption capacity for phenol of eight commercial synthetic adsorbents with F-400 activated carbon. The isotherm data was mathematically described by the isotherm equation of Weber & van Vliet, due to the broad range of concentrations investigated. Fig. 4.5 presents the adsorption isotherms generated by van Vliet *et al*. In general, the activated carbons offered the highest capacity, followed by the carbonised polymers and the polymeric adsorbent resins. At high concentrations, the capacity of the polymeric adsorbents, XAD series, was similar to that of the activated carbons suggesting possible uses in waste water treatment. The external mass transfer coefficients were related to the surface topography and shape of the adsorbents. Surface diffusion coefficients were larger for XAD-4 ( $2.06 \times 10^{-8}$  cm<sup>2</sup>/s) compared to F-400 ( $1.29 \times 10^{-9}$  cm<sup>2</sup>/s). Costa *et al* [24] and Huang *et al* [25] also studied the intraparticle diffusion of phenol and its derivatives onto polymeric

resins. Gauntlet [26] compared the adsorption capacity for 2,4-dichlorophenol of a number of ion exchange resins and adsorbent resins with activated carbon. He concluded that the resins would not be used as an alternative to activated carbon due to their low capacity. Fox [1.2] discussed the advantages of XAD resins for the recovery of phenolic compounds from waste streams, due to their simple regeneration.

Fig. 4.5. Adsorption isotherms of various adsorbents for phenol (Vliet *et al* [23]).



F-400, BACM are activated carbons; XE-340, XE-347, XE-348 are carbonised polymers; XAD-2, XAD-4, XAD-8, ES-863 are polymeric adsorbents; S-37 is a WBA resin.

The adsorption of phenolic pollutants has been studied extensively for activated carbons. A review paper, Radovic [27], into the adsorption of phenol and benzoic acid onto activated carbons contains over 360 references, which illustrates the quantity of literature on the subject. Adsorption onto F-400 has been studied by numerous authors. Table 4.3 presents a cross section of some of the Freundlich parameters obtained by a number of authors.

The exact mechanism for the adsorption of phenolic compounds onto carbon is still under debate in the literature [27]. Coughlin *et al* [35] modified the surface of activated carbon to provide an insight into the mechanism for the removal of phenol, nitrobenzene and sodium benzene sulphonate. He considered that most of the functional groups on carbons, introduced by oxidation

of the carbon, were attached to the edges of the layer planes, thus they would not directly interfere with the adsorption of the molecule onto the basal planes. However, a reduction in the amount of phenol adsorbed was apparent for the modified carbon. This was attributed to the oxygen chemically bound on the edges localising electrons, thereby removing them from the  $\pi$ -electron system of the basal planes. This would then reduce the attractive forces between the phenol  $\pi$ -electron system and the  $\pi$  band of the graphitic planes of the carbon responsible for adsorption.

**Table 4.3. Freundlich parameters for the sorption of phenol onto F-400 activated carbon.**

| Authors                     | Freundlich Coeff.  |       | Temp.<br>(°C) | pH              | Particle Size<br>( $\mu\text{m}$ ) | Additional Comments                                                                                                        |
|-----------------------------|--------------------|-------|---------------|-----------------|------------------------------------|----------------------------------------------------------------------------------------------------------------------------|
|                             | K                  | 1/n   |               |                 |                                    |                                                                                                                            |
| Seidel <i>et al</i> [28,29] | 2.32               | 0.216 | 20            | ~6              | 1000-2000                          | Also considered multi-component adsorption with indole, p-nitrophenol and p-chloraniline. Kinetics data presented          |
| Johansson <i>et al</i> [30] | 1.746 <sup>‡</sup> | 0.281 | 25            | 4.7-5.7         | 40-90                              | Investigated kinetics by using fixed columns                                                                               |
| Yenki <i>et al</i> [31]     | 1.209 <sup>+</sup> | 0.345 | 35            | ~6 <sup>+</sup> | 1000-1400                          | Also presented data on aniline, benzoic acid, o-cresol and p-methoxyphenol.                                                |
| Sorial <i>et al</i> [32]    | 2.281              | 0.177 | 23            | 7               | 850-1000                           | Also presented multi-component adsorption data for phenol with o-cresol and 3-ethylphenol under oxic and anoxic conditions |
|                             | 1.415 <sup>+</sup> | 0.214 | 23            | 7               | 850-1000                           |                                                                                                                            |
| Vidic <i>et al</i> [33]     | 1.96               | 0.201 | 35            | 7               | 1180-1400                          | Also presented single-component adsorption data for o-cresol and 3-ethylphenol under oxic and anoxic conditions            |
|                             | 1.26 <sup>+</sup>  | 0.239 | 35            | 7               | 850-1000                           |                                                                                                                            |
| McKay <i>et al</i> [34]     | 1.73               | 0.260 | -             | ~6 <sup>+</sup> | 500-710                            | Also presented data for p-chlorophenol                                                                                     |

‡ values determined from adsorption isotherm presented

\* isotherms conducted in the absence of oxygen

+ Solutions made in distilled water resulting in an approximate pH.

Note: Differences in *K* and *1/n* values are probably due to differences in batches of F-400.

They also suggested that water molecules, accumulated around oxygen functional groups, could prevent the diffusion of organic molecules into the planes, thus reducing the capacity. Mattson *et al* [36], in a similar study to Coughlin *et al*, suggested that hydrogen bonding by the phenolic protons with oxygen functional groups was one possible surface interaction. This hypothesis was verified by FT-IR spectroscopy, since the O-H stretch band disappeared for p-nitrophenol adsorbed onto the carbon. However, the interaction was found to be small. They suggested that

aromatic compounds adsorb by a donor-acceptor complex mechanism, where the carbonyl oxygen of the carbon surface acts as the electron donor and the aromatic ring of the adsorbate as the acceptor. After all of the available sites for complexation were used they suggested that adsorption then takes place on the basal planes. Ma *et al* [37] demonstrated that phenol uptake decreased rapidly at pH values greater than 10, around the pKa value. At a pH of less than 10, where the phenol molecule will be in the undissociated form, the adsorption capacity remained constant. Oda [38][39] investigated the effect of surface acidity on the uptake of phenol and several substituted phenols. The acidic carbon surfaces appeared to reduce the uptake of phenol and o-chlorophenol. The effect of molecular oxygen on the adsorption of o-cresol onto F-400 was investigated by Vidic *et al* [40]. They observed an increase in capacity of almost 200% in the presence of molecular oxygen compared with that attainable under anoxic conditions. Magne *et al* [41] investigated the desorption of phenol adsorbed onto activated carbon by thermogravimetric analysis (TGA). They observed four shoulders in the TGA curves suggesting different binding energies. The first shoulder was assigned to the desorption of phenol molecules physically adsorbed on the surface, weak binding energies. Chemisorbed phenol accounted for the three other shoulders, with the phenol decomposing on the surface rather than desorbing directly. They proposed that activated carbons contained three different types of adsorption site: carbon atoms in the basal planes, carbon groups on the edges of the basal planes and inorganic impurities. The adsorption of organic compounds onto the functional groups and impurities was thermally irreversible.

### SECTION 4.3      EXPERIMENTAL PARAMETERS

The information below describes the on-line batch reactor apparatus used to generate adsorption isotherms and kinetics for the adsorbates phenol, 2-chlorophenol, 3-chlorophenol and 4-chlorophenol. A brief discussion of the apparatus development is also given.

The experimental apparatus consisted of an agitated batch reactor, with a capacity of 1 litre, from which fluid was extracted and pumped through a flow cell in a UV-Vis spectrophotometer before return to the vessel. A photograph of the apparatus can be seen in Fig. 4.6. On-line analysis of the adsorbate concentration was performed using a Perkin Elmer Lambda 12 UV-VIS spectrophotometer, controlled by UVWinlab software, fitted with a 160 $\mu$ l quartz silica optical micro flow cell. The fluid was extracted from the flask through a 10 $\mu$ m stainless steel solvent inlet filter and circulated using a Watson Marlow 505S peristaltic pump. The pump was operated at 60rpm which corresponded to a flow rate of 30ml/min or a response time of ten seconds for the system. The vessel was agitated with a 4-bladed stainless steel agitator, at 350 $\pm$ 5rpm and temperature controlled at 25°C $\pm$ 1°C. The time taken to reach complete equilibrium was roughly 20 days. To expedite experimental determinations, it was decided to carry out pseudo-equilibrium contacts over eleven hours or 24 hours. A photograph of the batch vessel can be seen in Fig. 4.7. The detection of the pollutants was achieved at the chromophore peaks observed by a UV scan of each solution from a wavelength of 400nm to 190nm. The detection wavelengths were 269.4, 279.7, 273.2 and 273.5 for phenol, 2-chlorophenol, 3-chlorophenol and 4-chlorophenol respectively.

The sensitivity and stability of the analytical system was determined by measuring the signal noise level and the long term drift. Initial trials suggested a stability of about 0.002 absorbance units, equivalent to a change in phenol concentration of 0.13mg/l. The cause of the drift was due to changes in optical density of the reference cell over the 11-hour period and so the reference cell was removed. This action reduced the drift, in an eleven hour period, to 0.0001 absorbance units, or a 6.3 $\mu$ g/l concentration difference in a phenol solution. The degree of noise was reduced by optimising the 'response' time of the instrument to two seconds.

Fig. 4.6. Photograph of Batch Adsorption Experimental Apparatus.

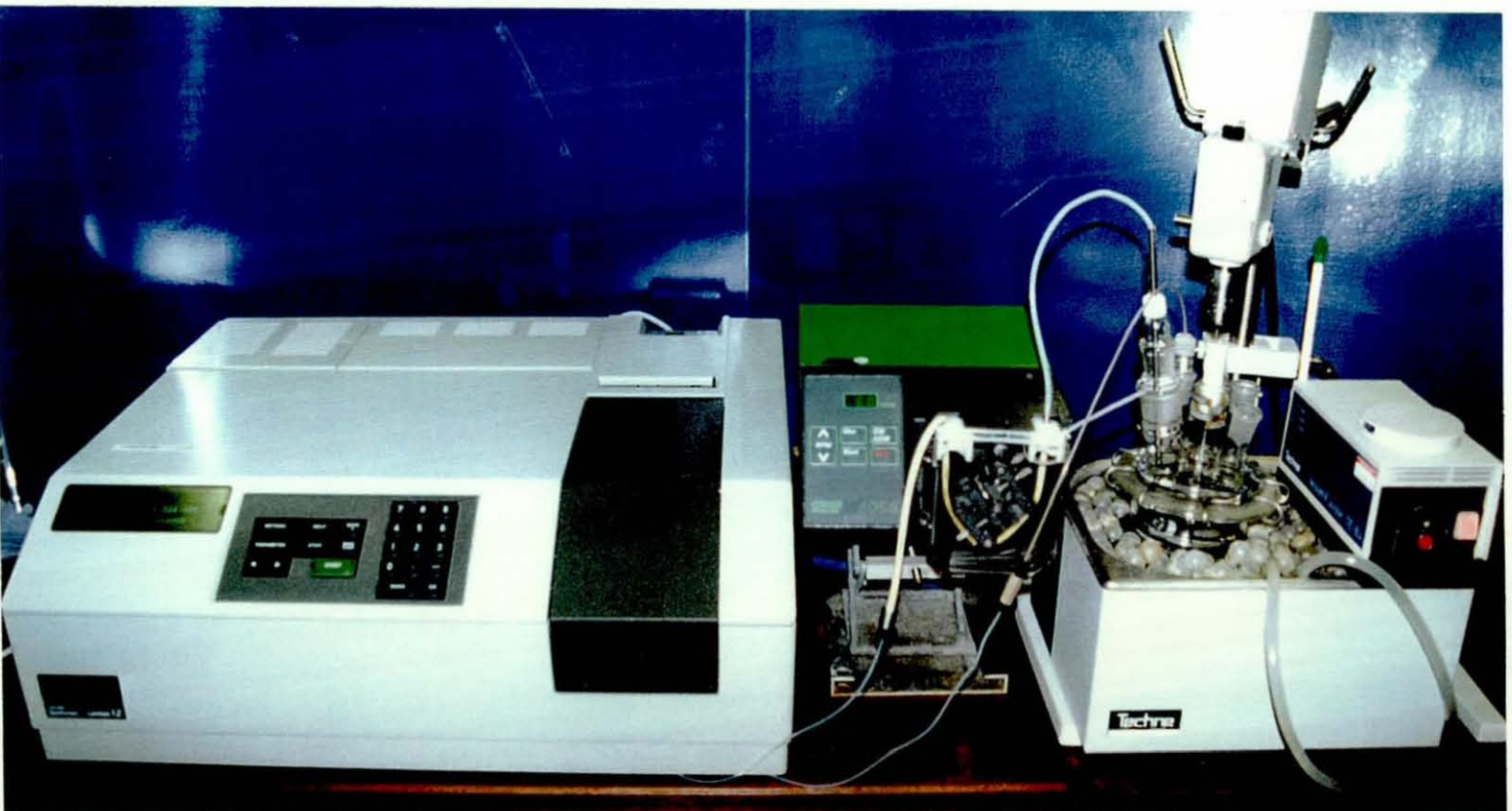
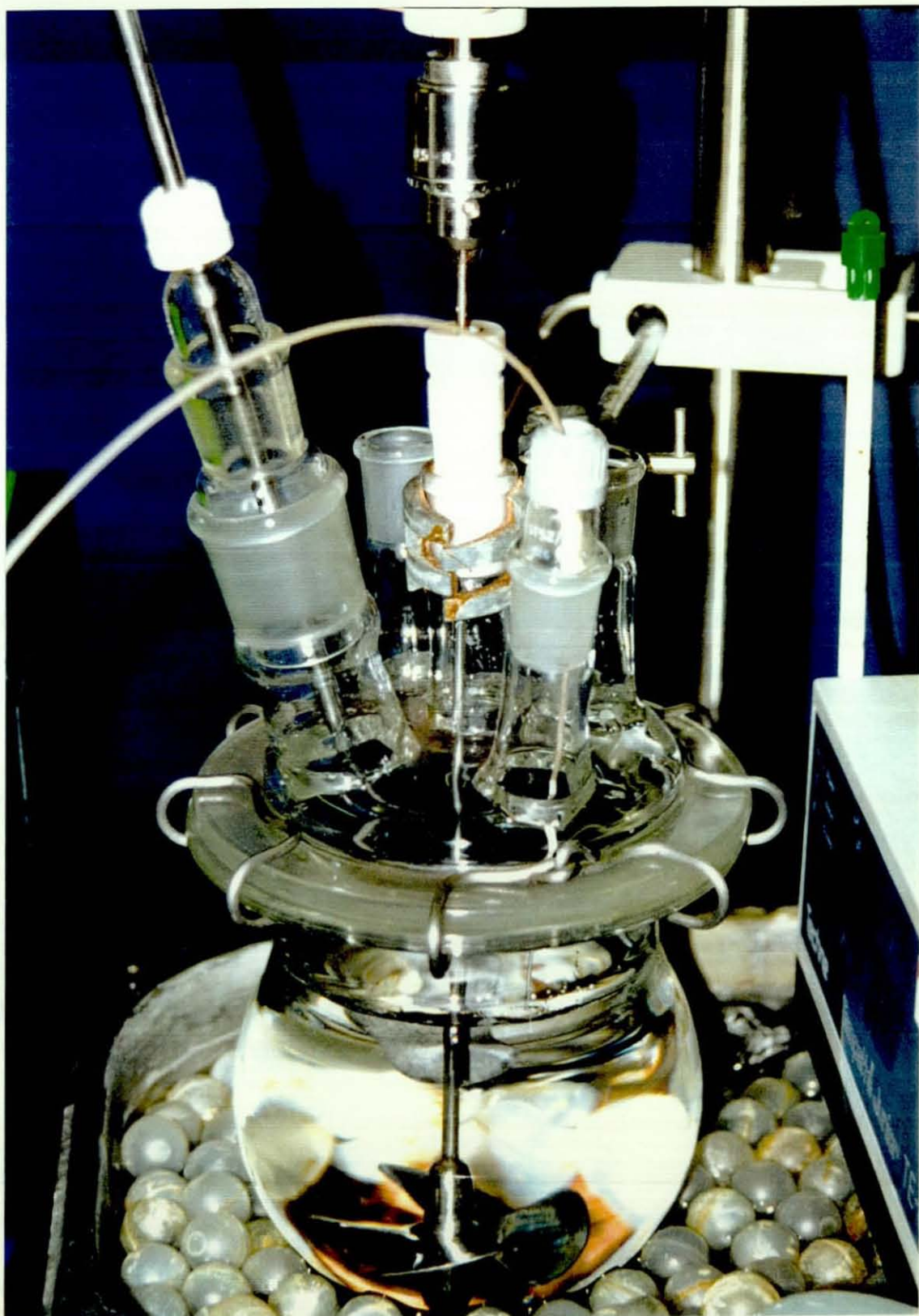




Fig. 4.7. Photograph of Batch Adsorption Reactor.



The high pressure drop in the solvent inlet filter initially selected caused air bubbles to be formed after a few days of operation, shown by spikes in the UV data. To overcome this problem a filter containing a large surface area ( $28\text{cm}^2$ ), connected using 1/4-28UNF chromatography fittings, was used. The liquid holdup of the filter was reduced by the manufacture of a new PTFE top, which occupied the internal space of the filter.

The brittleness of activated carbon and polymeric sorbents required investigations into different types of agitator to prevent mechanical damage to the sorbents. A flat bladed PTFE impellor caused significant damage to the polymeric sorbents at agitation speeds of 300rpm. Different agitators were tried before the selection of a four-bladed impellor that can be seen in Fig. 4.7.

The adsorbents used in the batch experiments were conditioned by soaking them in water overnight. Columns of 10mm diameter, with fused sintered glass discs inserted in the bottom section, were manufactured to allow the adsorbents to be washed before injection into the adsorption vessel. The washing was achieved by placing the column in a rubber bung connected to a vacuum. The adsorbent was then transferred to the adsorption vessel by the attachment of a 50ml syringe, filled with 30ml of adsorbate solution extracted from the vessel, enabling the adsorbent to be washed into the container.

### ***Equilibrium and kinetic sorption studies***

Samples of 10-1500mg of MN-100, MN-150, MN-200 and F-400 in the size range 500-600 $\mu\text{m}$  were contacted with 1l aqueous solution containing phenol, 2-chlorophenol, 3-chlorophenol and 4-chlorophenol respectively, at a concentration of 50.0mg/l. The experiments were ended at a pseudo equilibrium time of eleven hours.

### ***Effect of the agitation rate on the kinetics of removal for phenol***

500mg samples of MN-200 in the size range 500-600 $\mu\text{m}$  were contacted with 1l solutions of phenol at a concentration of 50mg/l. Agitation speeds of 0, 50, 100, 150, 250, 300, 350, 450, 550 and 750rpm were used.

***Effect of the adsorbent particle size on the kinetics and capacity for phenol***

300mg samples of MN-100, MN-150 and MN-200 in the size ranges 300-400, 400-500, 500-600, 600-700, 700-800, 800-900, and 900-1000 $\mu$ m were contacted with 1l solutions of phenol at a concentration of 50mg/l. The experiment duration was 23 hours.

***Effect of the adsorption temperature on the kinetics and capacity for phenol***

300mg samples of MN-100, MN-150 and MN-200 in the size range 500-600 $\mu$ m were contacted with 1l solutions of phenol at a concentration of 50mg/l. The solution temperature was adjusted to 15, 20, 30, 40, 50, 60, 70, 80°C using a chiller unit and a thermostatically controlled water bath. The solutions were preheated or cooled before the analysis. The experiment duration was 23 hours.

## SECTION 4.4 RESULTS AND DISCUSSION

### Adsorption Isotherms

Two isotherm models, namely the Langmuir and Freundlich, were correlated to the experimental data. The experimental data is shown in Figs. 4.8-11 and the calculated model coefficients are presented in Tables 4.4 and 4.5 together with the correlation coefficient.

**Table 4.4.** Freundlich and correlation coefficients.

|        | Phenol |       |       | 2-chlorophenol |       |       | 3-chlorophenol |       |       | 4-chlorophenol |       |       |
|--------|--------|-------|-------|----------------|-------|-------|----------------|-------|-------|----------------|-------|-------|
|        | $K$    | $1/n$ | $R^2$ | $K$            | $1/n$ | $R^2$ | $K$            | $1/n$ | $R^2$ | $K$            | $1/n$ | $R^2$ |
| MN-100 | 0.986  | 0.541 | 0.999 | 2.075          | 0.405 | 0.995 | 2.202          | 0.388 | 0.998 | 2.272          | 0.418 | 0.998 |
| MN-150 | 1.146  | 0.527 | 0.999 | 2.177          | 0.453 | 0.997 | 1.954          | 0.357 | 1.000 | 1.989          | 0.369 | 0.999 |
| MN-200 | 1.073  | 0.537 | 0.999 | 2.392          | 0.442 | 0.996 | 2.379          | 0.387 | 0.999 | 2.337          | 0.401 | 0.999 |
| F-400  | 2.063  | 0.263 | 0.997 | -              | -     | -     | -              | -     | -     | 2.928          | 0.193 | 0.997 |

\* Constants based on units of  $q$  (mmol/g) and units of  $c$  (mmol/l)

**Table 4.5.** Langmuir and correlation coefficients.

|        | Phenol    |      |       | 2-chlorophenol |      |       | 3-chlorophenol |      |       | 4-chlorophenol |       |       |
|--------|-----------|------|-------|----------------|------|-------|----------------|------|-------|----------------|-------|-------|
|        | $q_{max}$ | $b$  | $R^2$ | $q_{max}$      | $b$  | $R^2$ | $q_{max}$      | $b$  | $R^2$ | $q_{max}$      | $b$   | $R^2$ |
| MN-100 | 0.771     | 5.7  | 1.000 | 0.978          | 33.5 | 1.000 | 1.121          | 31.8 | 1.000 | 1.094          | 32.3  | 1.000 |
| MN-150 | 0.908     | 5.9  | 1.000 | 0.987          | 28.7 | 1.000 | 1.184          | 25.7 | 1.000 | 1.124          | 30.7  | 1.000 |
| MN-200 | 0.922     | 4.9  | 1.000 | 1.060          | 29.7 | 1.000 | 1.355          | 24.4 | 1.000 | 1.270          | 26.6  | 1.000 |
| F-400  | 1.215     | 71.0 | 1.000 | -              | -    | -     | -              | -    | -     | 1.695          | 509.4 | 0.997 |

\* Constants based on unit of  $q$  (mmol/g) and units of  $c$  (mmol/l)

The Freundlich model correlates well with the experimental data, except at very high surface coverage shown by the 's' shape in the isotherm. The 's' shape, which is more prominent in the isotherms for the chlorinated phenols, is typical of a type II isotherm suggesting that bulk packing of the adsorbate molecules occurs. The Langmuir model assumes monolayer coverage of the

Fig. 4.8. Phenol sorption isotherms for MN-100, MN-150, MN-200 and F-400 at 25±1°C.

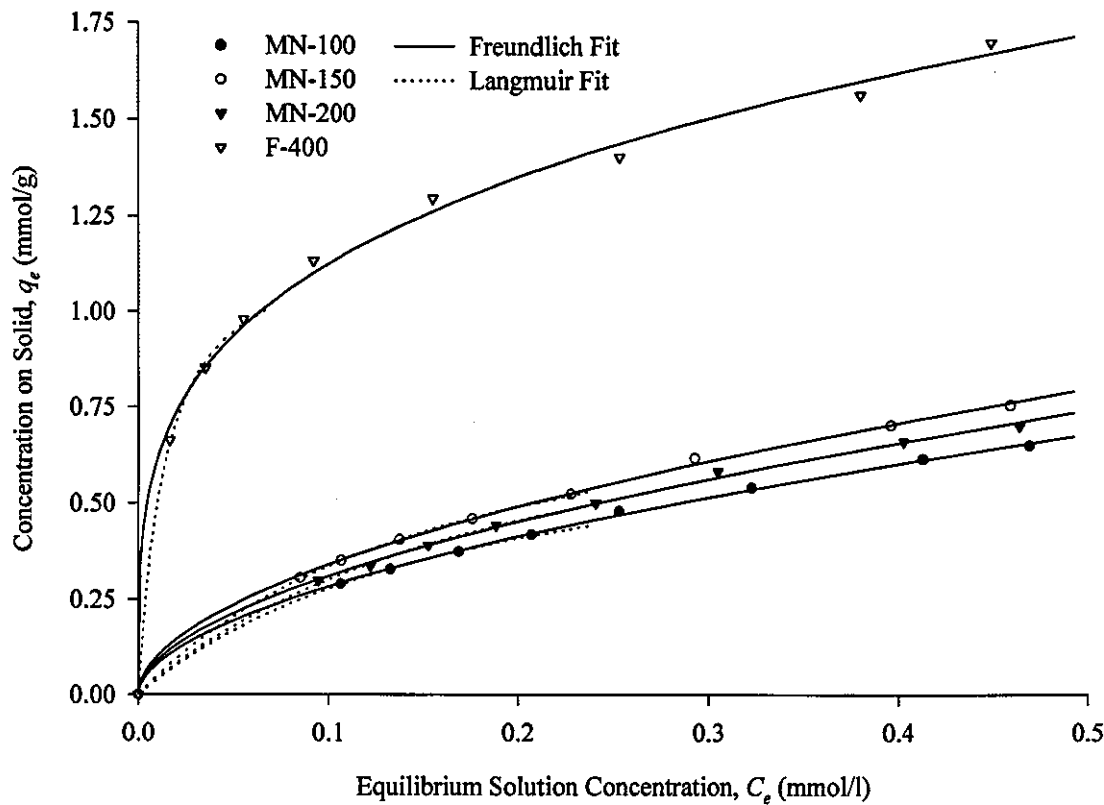


Fig. 4.9. 4-chlorophenol sorption isotherms for MN-100, MN-150 and MN-200 at 25±1°C.

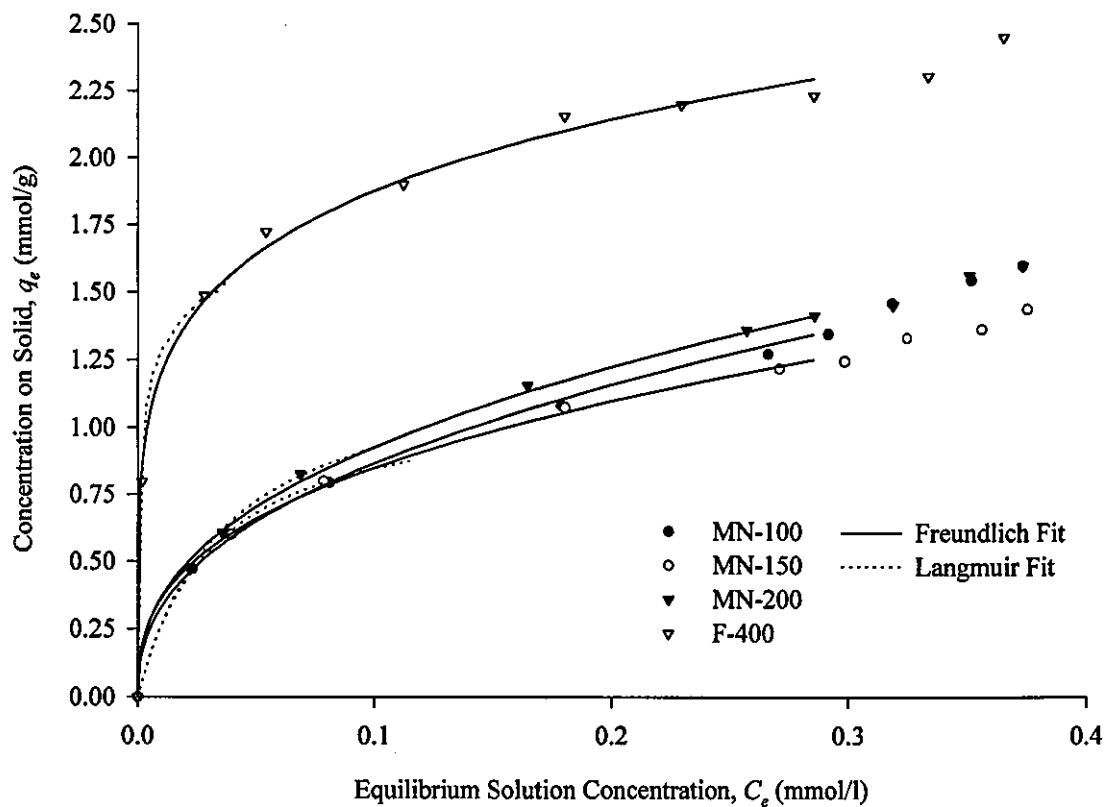


Fig. 4.10. 2-chlorophenol sorption isotherms for MN-100, MN-150 and MN-200 at 25±1°C.

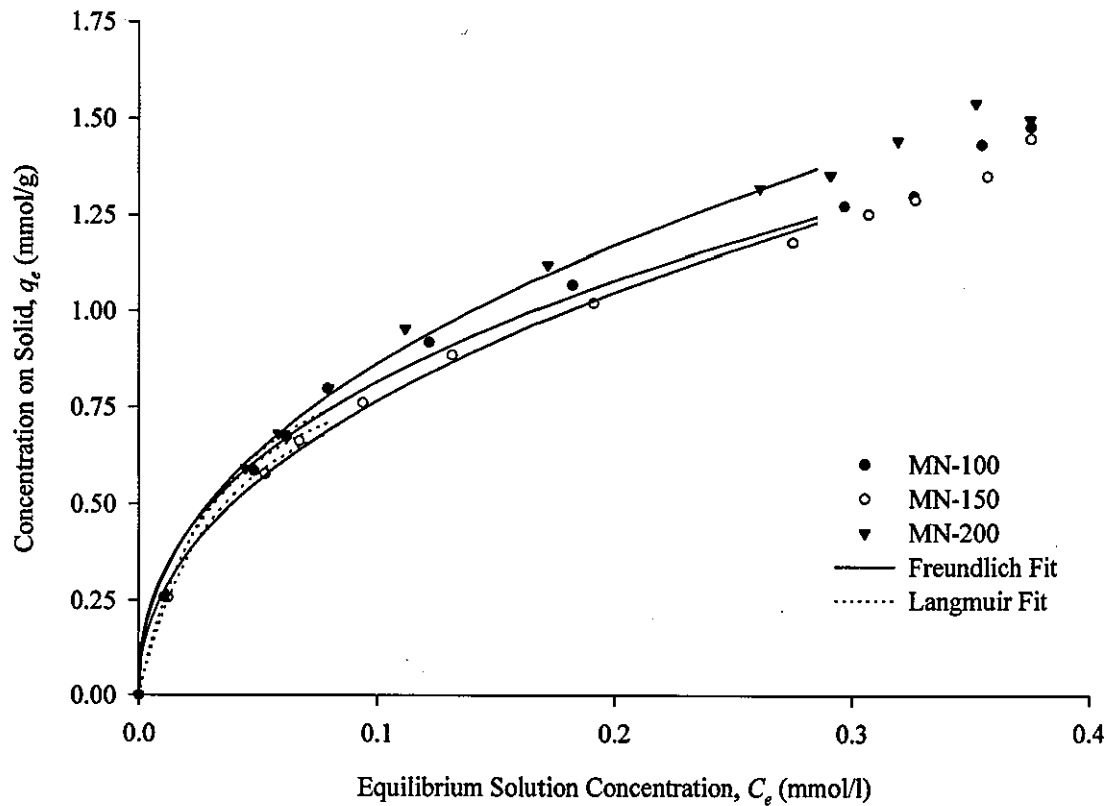
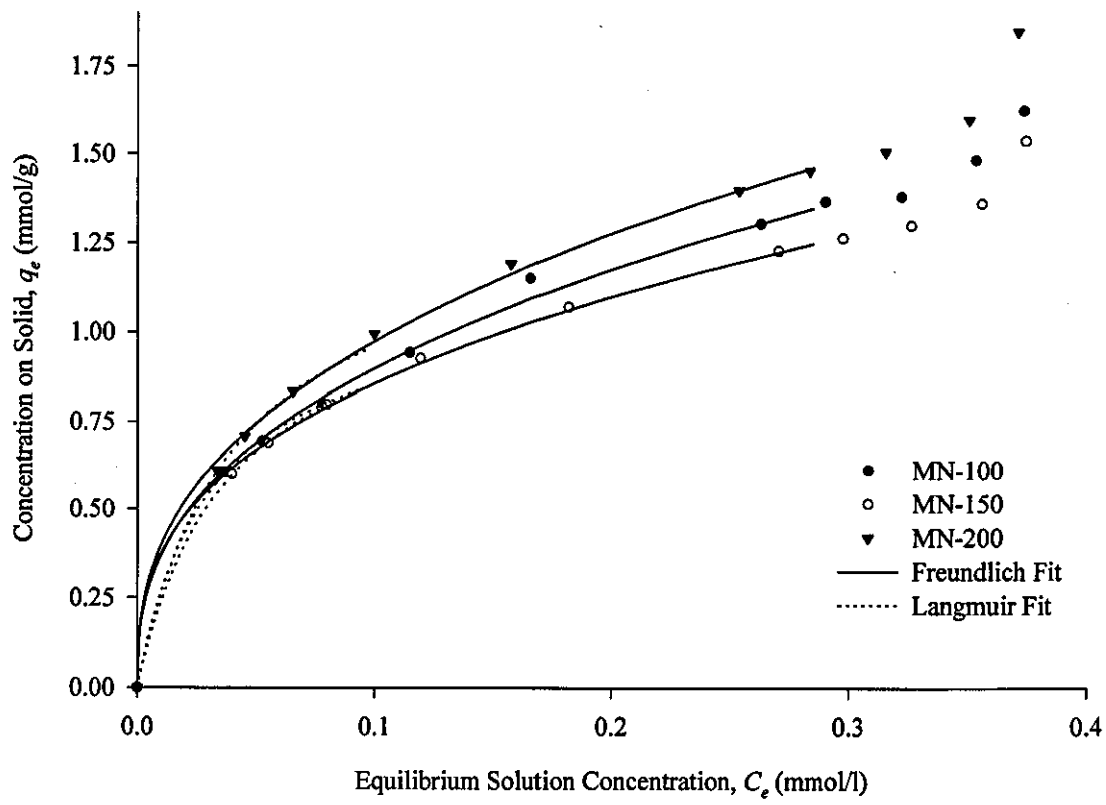


Fig. 4.11. 3-chlorophenol sorption isotherms for MN-100, MN-150, MN-200 and F-400 at 25±1°C.



surface and therefore it agrees closely with the data while the monolayer is being completed but deviates significantly at higher concentrations on the solid, indicated by a significant curve in a plot of  $1/q_e$  against  $1/c_e$ . The shapes of the isotherms are similar for all three polymers suggesting that the interaction energy between the adsorbent and the adsorbate molecules are approximately the same. Detailed analysis of the Freundlich  $1/n$  value does not show a clear trend. The strength of the adsorbate/adsorbent bond is mainly governed by the surface functionality of the polymers. FT-IR and XPS analysis of the polymers indicated the presence of carbonyl and ether groups. Coughlin *et al.* [35] suggested that the presence of chemisorbed oxygen considerably reduced the adsorption of phenol particularly in dilute solutions. Bansal *et al.* [42] argued that the presence of oxygen resulted in the irreversible binding of phenol by the interactions of  $\pi$  electrons of the benzene ring system with the partial positive charge on the carbonyl carbon atoms. Mattson *et al.* [36] suggested the formation of a donor-acceptor complex between the phenol and the adsorbent surface.

The surface charge of the polymer at a pH of dilute concentrations of phenols, pH 6, indicates that MN-200 will have a negatively charged surface compared with the positive charged surface of MN-100 and MN-150 caused by the tertiary amine. Amine functional groups may enable the adsorption of the acidic phenol by an ion exchange mechanism. A noticeable difference in the mechanism of adsorption, if ion exchange was predominant, would be expected between the behaviour of MN-100 and MN-150 compared with MN-200. However, no such trend is apparent by inspection of the  $1/n$  values. Pontius [43] observed that adsorption of phenol on a weak base phenol-formaldehyde resin took place on the functional group, in the free base form, at pH 5. At pH values below five acid was adsorbed by the resin. However, phenol has a  $pK_a$  of 9.89 which suggests that the molecule will only be anionic at pH values greater than eight. Hence, ion exchange of the phenol molecule with the weakly basic groups can not occur.

The bond strength of the chlorophenols is much greater than that for phenol indicated by lower values of  $1/n$ . However, no trend is apparent when comparing the strength of adsorption of the different chlorophenols. The  $pK_a$  of the adsorbates is unlikely to affect the adsorption capacity and mechanism of adsorption since the values are 2 pH units greater than the pH of the solutions. Hence, all the adsorbates are likely to exist in an undissociated form.

The Freundlich constant  $K$  is primarily related to the capacity of the adsorbent which is governed by the physical properties of the adsorbent. The capacity for phenol is much less than that for the chlorophenols due to the more hydrophilic nature of the adsorbate indicated by its lower octanol water partition coefficient and a higher solubility in water, see Table 4.6.

**Table 4.6. Physical properties of phenols.**

|                | Molecular weight | Molecular Diffusivity<br>(cm <sup>2</sup> /s)* | pK <sub>a</sub> | Solubility<br>in H <sub>2</sub> O<br>(g/l) | log k <sub>ow</sub> | Approximate molecular dimensions [44] |            |
|----------------|------------------|------------------------------------------------|-----------------|--------------------------------------------|---------------------|---------------------------------------|------------|
|                |                  |                                                |                 |                                            |                     | Width (Å)                             | Length (Å) |
| Phenol         | 94.11            | 1.1×10 <sup>-5</sup>                           | 9.89            | 87                                         | 1.50                | 7.0                                   | 7.6        |
| 2-chlorophenol | 128.56           | 9.6×10 <sup>-6</sup>                           | 8.52            | 22                                         | 2.15                | 7.6                                   | 7.9        |
| 3-chlorophenol | 128.56           | 9.6×10 <sup>-6</sup>                           | 9.12            | 22                                         | 2.50                | 7.6                                   | 8.2        |
| 4-chlorophenol | 128.56           | 9.6×10 <sup>-6</sup>                           | 9.41            | 27                                         | 2.39                | 6.9                                   | 8.5        |

Data extracted from the CRC Handbook of Chemistry and Physical, D.R.Lide, 74th Edition, The Chemical Rubber Co, 1993

\* Data calculated using Wilke and Chang correlation at 25°C. [45][46]

k<sub>ow</sub> Octanol-Water Partition Coefficient

The oxygen and nitrogen containing functionality of the polymers causes them to be slightly hydrophilic. If the predominant mechanism of adsorption is hydrophobic interactions, the octanol-water partition coefficient of the adsorbates should govern the capacity of the adsorbents. The results show that the capacity of the polymers for 4-chlorophenol is greater than the other chlorophenols. However, 4-chlorophenol is more hydrophilic than 3-chlorophenol which would suggest that other parameters are probably controlling the adsorption.

The effect of the functional groups can be investigated by studying the isotherms of MN-100 and MN-200, since the pore structure should be similar. The adsorption capacity of all the adsorbates is reduced by the amine functionality of MN-100, with phenol being affected the least and 4-chlorophenol affected the most. The order, phenol<2-chlorophenol<3-chlorophenol<4-chlorophenol, suggests that the molecular size of the adsorbates may control the degree of adsorption due to size exclusion in the micropores. The pores in MN-100 are smaller than those in MN-200 and have a much narrower size distribution causing molecules to be excluded to a



greater extent. A similar argument explains the enhanced adsorption of MN-150 in comparison with MN-100 for phenol and 2-chlorophenol compared with 3-chlorophenol and 4-chlorophenol. The higher surface area of MN-200 and the larger pore size distribution lead to a higher adsorption capacity for the chlorophenols than the other two polymers. However, the capacity of MN-150 for phenol exceeded that of MN-200 which may be due to the small phenol molecule being able to diffuse into the smaller micropores in MN-150, the larger chlorophenols may be excluded. The effective mean pore size, based on all the pore geometries, indicates that the adsorbate molecules are larger than some of the micropores. Size exclusion may be confirmed by considering the surface area calculated based upon the adsorption of phenol. The specific surface area,  $S$  ( $\text{m}^2/\text{g}$ ), of the polymer can be approximated from the Langmuir constant  $q_{\max}$ , which relates to the solute concentration at monolayer coverage, using the equation:

$$S = N q_{\max} A \quad (5)$$

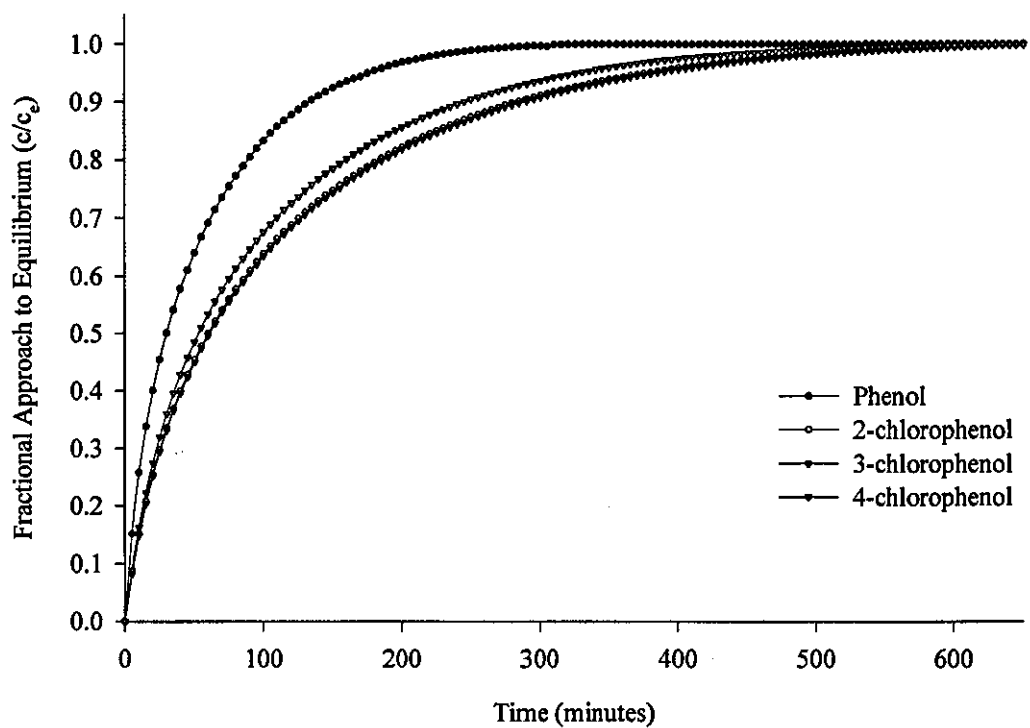
where  $N$  is the Avogadro number and  $A$  is the surface area ( $\text{m}^2$ ) of the adsorbate molecule. A value of  $52.2\text{\AA}^2$  for parallel orientation of the phenol molecule on the adsorbent surface was presented by Puri [47]. Based upon this molecular size, the specific surface area of MN-100, MN-150, MN-200 and F-400 is 242, 285, 290 and  $382\text{m}^2/\text{g}$  respectively. Nitrogen Langmuir surface areas were in the order of  $1000\text{m}^2/\text{g}$  confirming significant size exclusion.

The capacity of F-400 for all the phenols is much greater than that of the polymers. The results also demonstrate the enhanced uptake and interaction of the chlorophenol compared with phenol. The  $1/n$  coefficients are significantly lower than those for the polymers which indicate that the adsorbates are bound by a stronger adsorbent-adsorbate bond.

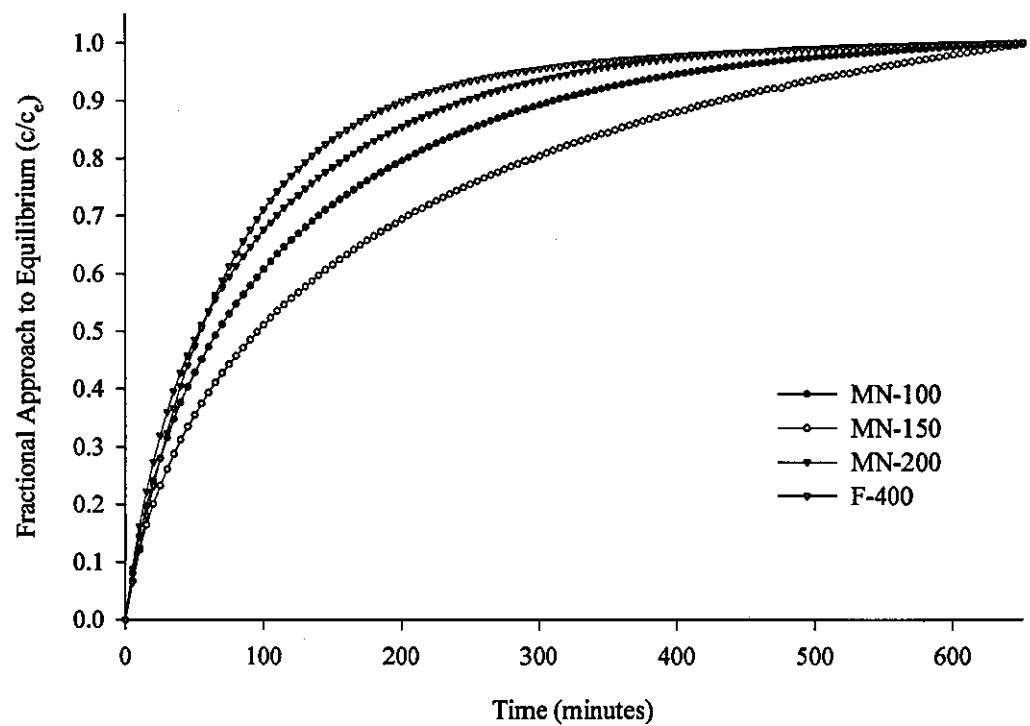
### *Adsorption Kinetics*

Figs. 4.12 and 4.13 illustrate the different adsorption rates of the phenols on the adsorbents at a constant particle size, agitation rate and temperature. The adsorption kinetics for phenol are much greater than that for the chlorophenols, which is predominately due to its larger

**Fig. 4.12.** Fractional approach to equilibrium curves for MN-200 adsorbing phenol, 2-chlorophenol, 3-chlorophenol and 4-chlorophenol. 200mg of adsorbent (500-600 $\mu$ m), 350rpm, 25°C,  $C_o=50$ mg/l.

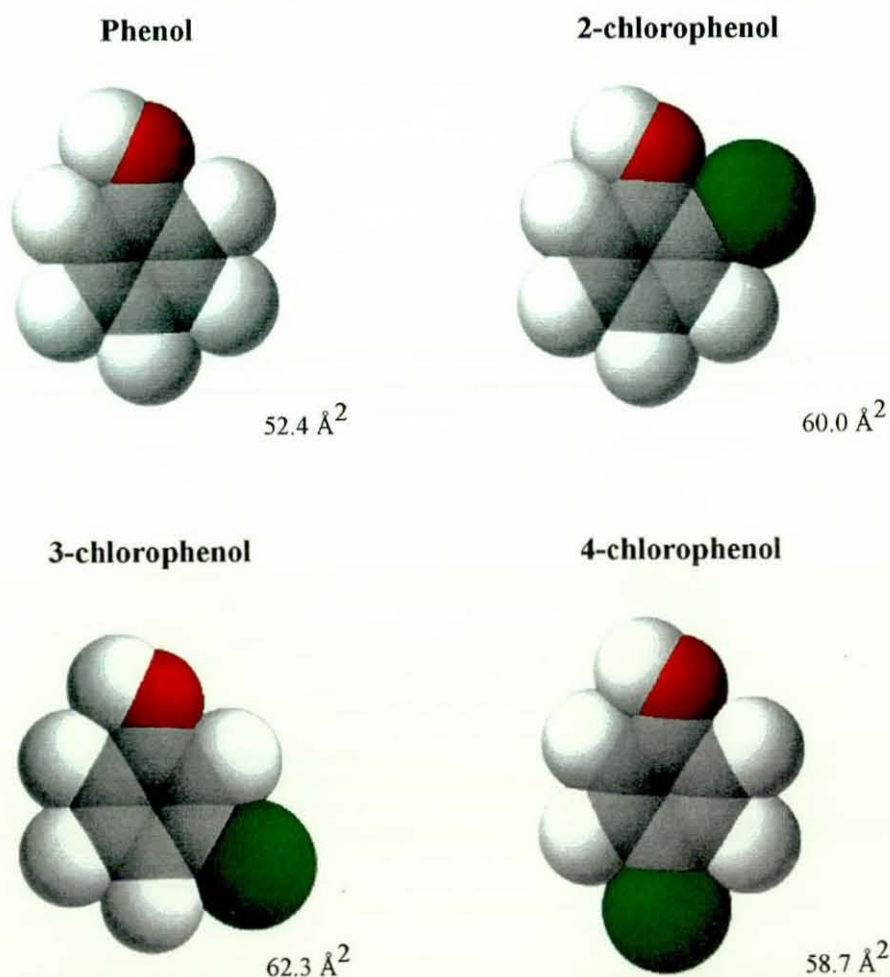


**Fig. 4.13.** Fractional approach to equilibrium curves for MN-100, MN-150, MN-200 and F-400 adsorbing phenol. 200mg of adsorbent (500-600 $\mu$ m), 350rpm, 25°C,  $C_o=50$ mg/l.



molecular diffusivity, see Table 4.6. However, since the Wilke and Chang correlation only considers the molecular volume of the compounds, by summing the atomic volumes of the individual elements, there is no difference in the calculated molecular diffusivity for the chlorophenols. Experimentally derived diffusivities often vary by up to 10% and so they cannot be used for comparison. However, the uptake rates correlate well with the approximate molecular dimensions of the adsorbates. Fig. 4.14 illustrates the shape of the different molecules.

Fig. 4.14. Molecular structure of phenol, 2-chlorophenol, 3-chlorophenol and 4-chlorophenol.



The molecular cross sectional area of 2-chlorophenol is smaller than that of 3-chlorophenol which is demonstrated by the slightly faster adsorption rate. The uptake rate of 4-chlorophenol is quicker which can be attributed to its smaller cross sectional area. The molecule, dependent on its orientation, is also narrower than the other chlorophenols allowing it to enter the smaller

micropores.

The uptake rate for the adsorbents can be explained by differences in the pore size distribution of the materials. F-400 has the fastest kinetics followed by MN-200, MN-100 and MN-150. The adsorption process for the polymers and carbon may be described as the adsorbate passing across the external liquid film followed by diffusion and adsorption in the macropores and micropores. The external film diffusion is rapid and often only controls the kinetics in the first few minutes. Relatively rapid diffusion and adsorption occurs in the macropores followed by the slow approach to equilibrium in the micropores.

The diffusion of the adsorbates into the micropores is controlled by the size of the pore and the strength of the interaction between the adsorbate and adsorbent. High interaction energies will reduce the diffusion since the molecules are prevented from hopping from one site to another. The mean micropore size of the adsorbents follows the order  $\text{MN-200} > \text{MN-100} > \text{MN-150} > \text{F-400}$ . Also, the low Freundlich  $1/n$  coefficients for F-400 compared to the polymers suggest that the micropore diffusion rate will be slower. Hence, the faster uptake rate of F-400, after about 30 minutes, is probably due to the mesoporous nature of F-400. The mesopores enhance the kinetics by acting as transport pores to the micropores. The slower kinetics of MN-150 are attributed to the smaller mean size of the micro/macropores compared to the other polymers.

The isotherm kinetic data has been correlated to the homogeneous surface diffusion model to obtain values for the external film resistance,  $k_f$ , and the surface diffusion coefficient,  $D_s$ . The model applied to the data assumes that the kinetics will be controlled by a mechanism of film transport through the external hydrodynamic boundary layer coupled with intra particle surface transport, motivated by an unsteady state solid phase concentration gradient. The HSDM assumes the adsorbent is a homogenous spherical particle and that the surface flux can be described by Fick's Law. Pore diffusion is neglected since the surface diffusion flux is many times greater than the pore diffusion flux for strongly adsorbed species.

A number of investigators have proposed methodologies to solve the nonlinear equations of the HSDM. A simplified solution technique presented by D. Roy *et al* [11, 12], which used the

orthogonal collocation method to discretize the partial differential equations of the HSDM to ordinary differential equations with initial conditions, has been used in this study. A summary of the input parameters for the model is presented on pages 84 and 85. Analysis of the Biot number indicated that the external film resistance was negligible compared to the surface diffusion. A sensitivity analysis for different  $k_f$  values indicated that the solution technique of minimising the sum of the square of the errors between the theoretical and experimental solution concentrations would be inadequate. This is due to the small number of data points in the early stages of the experiments compared to the overall experimental duration. However, when the objective function of the model depends upon a single parameter a very simple one-dimensional search method can be used while keeping the other parameter constant. The values of  $k_f$  are approximated using the equation:

$$k_f = - \frac{V}{A C_o} \cdot \left( \frac{dC}{dt} \right)_{t=0} \quad (6)$$

where V is the volume of the solution,  $C_o$  is the initial concentration and A is the external surface area of the adsorbent.  $dC/dt$  was calculated by determining the gradient of the concentration decay curve in the time range of 0-3 minutes. This technique has been used extensively in the literature. Table 4.7 presents the average coefficients for the different adsorbents and adsorbates.

**Table 4.7.** Average external mass transfer coefficients for MN-100, MN-150, MN-200, and F-400 sorbing phenol, 2-chlorophenol, 3-chlorophenol and 4-chlorophenol. 25°C, 350rpm, 500-600µm particles,  $C_o=50\text{mg/l}$ .

|                | External Mass Transfer Coefficient $k_f$ (cm/s) |                       |                       |                       |
|----------------|-------------------------------------------------|-----------------------|-----------------------|-----------------------|
|                | MN-100                                          | MN-150                | MN-200                | F-400                 |
| Phenol         | $5.25 \times 10^{-3}$                           | $4.55 \times 10^{-3}$ | $6.20 \times 10^{-3}$ | $8.95 \times 10^{-3}$ |
| 2-chlorophenol | $7.44 \times 10^{-3}$                           | $6.23 \times 10^{-3}$ | $8.03 \times 10^{-3}$ | -                     |
| 3-chlorophenol | $7.50 \times 10^{-3}$                           | $6.53 \times 10^{-3}$ | $8.34 \times 10^{-3}$ | -                     |
| 4-chlorophenol | $7.54 \times 10^{-3}$                           | $6.45 \times 10^{-3}$ | $8.30 \times 10^{-3}$ | $8.65 \times 10^{-3}$ |

The external mass transfer coefficients are not dependent on the mass of adsorbent used in the kinetic experiments and so the values of  $k_f$  presented in Table 4.7 are based on the average of all the individual coefficients. External mass transfer coefficients for spherical beads with a smooth

exterior surface should have a fixed value for a given set of experimental conditions since  $k_f$  in the context of film theory, may be described by the equation:

$$k_f = \frac{D_{AB}}{\delta} \quad (7)$$

where  $D_{AB}$  molecular diffusivity of the adsorbate in solution ( $L^2 T^{-1}$ )  
 $\delta$  conceptual thickness of the hydrodynamic boundary layer (L)

However, the coefficients for the polymers and carbon vary significantly, based on the same adsorbate. This may be due to differences in the external surface topography and the shape of the particles since these parameters will affect the thickness of the hydrodynamic boundary layer. The carbon has the roughest surface and an irregular particle shape which correspond to its high value of  $k_f$ . However, analysis of the scanning electron micrographs for MN-100 and MN-200 are virtually identical and so no explanation can be given for the differences. The lower values for MN-150 can be attributed to the smoother external surface created by the smaller macropores. The polymers film transfer coefficients are higher for the chlorophenols compared to phenol. However, the molecular diffusivity of chlorophenol is smaller than that for phenol. The  $k_f$  values for F-400 correlate with the molecular diffusivity of the adsorbates.

Table 4.8 presents the surface diffusivities for the sorption of phenol, 2-chlorophenol, 3-chlorophenol and 4-chlorophenol.

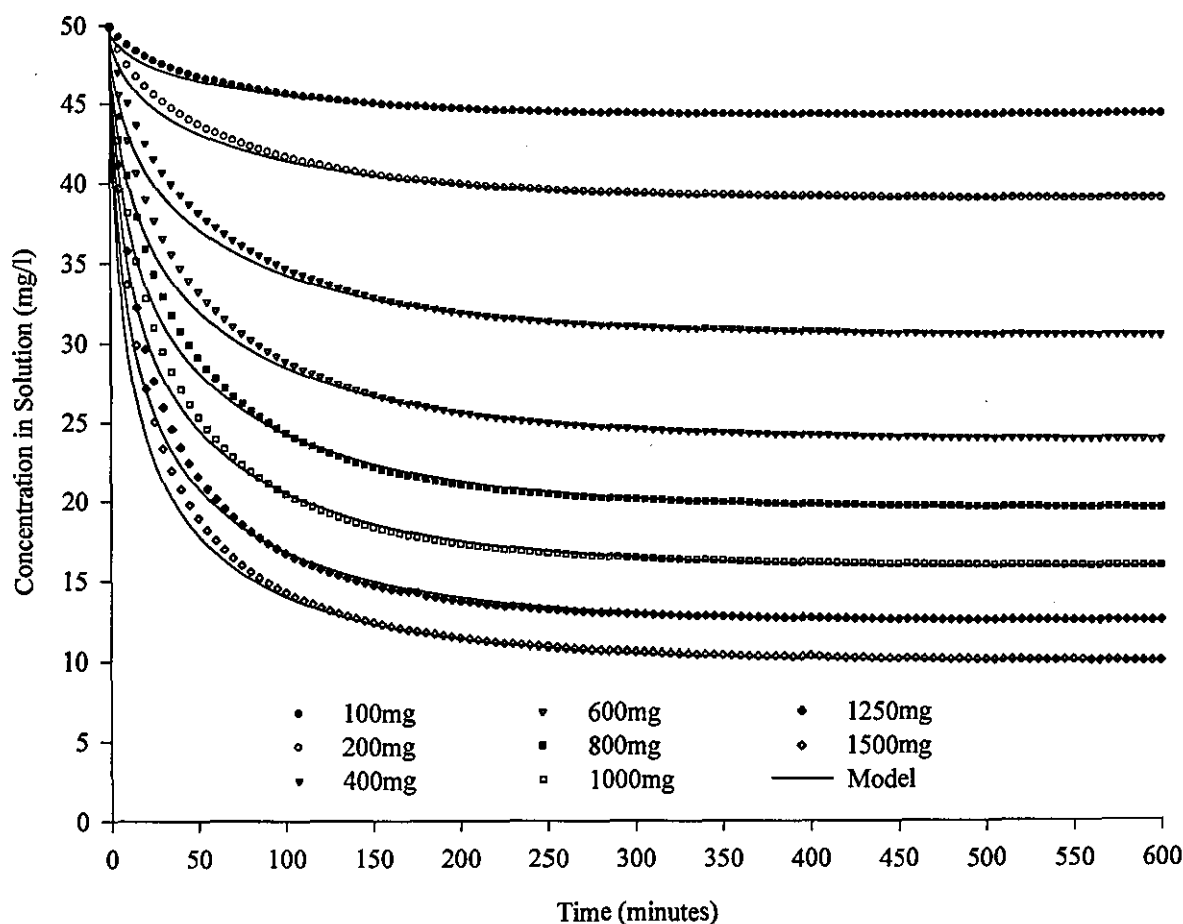
**Table 4.8. Surface Diffusivities for MN-100, MN-150, MN-200 and F-400 sorbing phenol and ortho, meta, para substituted chlorophenols. 25°C, 350rpm, 500-600µm particles,  $C_0=50\text{mg/l}$ .**

| Adsorbate      | Surface Diffusivity $D_s$ ( $\text{cm}^2/\text{s}$ ) $\times 10^9$ |        |        |        |
|----------------|--------------------------------------------------------------------|--------|--------|--------|
|                | MN-100                                                             | MN-150 | MN-200 | F-400  |
| Phenol         | 9.51                                                               | 5.82   | 10.35  | (8.60) |
| 2-chlorophenol | 5.25                                                               | 2.82   | 5.73   | -      |
| 3-chlorophenol | 4.76                                                               | 3.00   | 5.33   | -      |
| 4-chlorophenol | 4.69                                                               | 3.30   | 6.51   | (9.98) |

Data in brackets indicates a poor correlation between the experimental and theoretical decay curves.

In surface diffusion the adsorbate molecules may be visualised as migrating along the surface when an adsorption site is available, assuming that they have sufficient energy to leave the sites they are currently occupying. The data indicates that the diffusion rate of the chlorophenols is slower than that for phenol, which is as expected since the electronegative chlorine atom enhances the adsorbent/adsorbate interaction energy. MN-100 and MN-200 have similar values of  $D_s$ , which suggests that the amine functional groups on MN-100 do not interact considerably with the adsorbates used under the defined experimental conditions. The lower surface diffusion coefficients for MN-150 are probably attributable to the small mean micropore size of the polymer compared to MN-100 and MN-200, since the concentration of surface functional groups is very similar to that of MN-100. Fig. 4.15 presents the experimental kinetics data for MN-200 adsorbing phenol compared to the model prediction.

Fig. 4.15. Comparison of experimental and theoretical concentration decay curves for MN-200 adsorbing phenol. 25°C, 350rpm.



The model predicts the latter stages of the concentration decay extremely well. However, there is a significant overestimation of the kinetics in the early stages of the experiment. This may be due to slow macropore diffusion, which is not taken into account in the HSDM. Al-Duri and McKay [18] briefly described the mathematical difficulties in models that combine film, pore and surface diffusion.

Significant deviation between the theoretical and experimental decay curves for F-400 were observed which prevented accurate determination of the surface diffusion coefficient. The model under-predicted the initial uptake rates and over-predicted the latter rates. Vliet *et al* [23] presented a value of  $1.24 \times 10^{-9} \text{ cm}^2/\text{s}$  for F-400 at a stirrer speed of 1200rpm and a particle size fraction of 300-420 $\mu\text{m}$ . The value, when compared to that of the polymers used in this study, indicated that the adsorbent/adsorbate interactions are greater for the carbon, which is also confirmed by the lower value of the Freundlich  $1/n$  coefficient.

Table 4.9 presents the external film and surface diffusivity coefficients based upon different particle sizes for MN-100, MN-150 and MN-200 sorbing phenol.

**Table 4.9.** Effect of particle size on the external film and surface diffusivity coefficients for MN-100, MN-150 and MN-200 sorbing phenol. 25°C, 350 rpm,  $C_0=50\text{mg/l}$ .

| Particle<br>Diameter  | MN-100            |                            | MN-150            |                            | MN-200            |                            |
|-----------------------|-------------------|----------------------------|-------------------|----------------------------|-------------------|----------------------------|
|                       | $k_f \times 10^3$ | $D_s \times 10^9$          | $k_f \times 10^3$ | $D_s \times 10^9$          | $k_f \times 10^3$ | $D_s \times 10^9$          |
|                       | (cm/s)            | ( $\text{cm}^2/\text{s}$ ) | (cm/s)            | ( $\text{cm}^2/\text{s}$ ) | (cm/s)            | ( $\text{cm}^2/\text{s}$ ) |
| 53-75 $\mu\text{m}$   | 6.40              | 8.50                       | 6.47              | 5.62                       | 6.79              | 1.28                       |
| 300-400 $\mu\text{m}$ | 5.07              | 8.68                       | 4.42              | 5.72                       | 6.61              | 1.18                       |
| 400-500 $\mu\text{m}$ | 5.45              | 8.56                       | 5.21              | 6.12                       | 7.49              | 1.37                       |
| 500-600 $\mu\text{m}$ | 5.89              | 9.90                       | 4.83              | 5.30                       | 6.66              | 1.27                       |
| 600-700 $\mu\text{m}$ | 6.17              | 9.92                       | 5.38              | 5.81                       | 7.00              | 1.41                       |
| 700-800 $\mu\text{m}$ | 6.23              | 8.48                       | 5.20              | 5.96                       | 6.72              | 1.33                       |
| 800-900 $\mu\text{m}$ | 6.59              | 9.63                       | 5.04              | 5.70                       | 6.40              | 1.11                       |

The data illustrates no clear trends in the external or intra particle mass transfer coefficients. The



coefficients seem to be independent of particle size. The average results correlate to the parameters found in the isotherm kinetics experiments for phenol.

The effect of temperature on the adsorption equilibria and kinetics for the polymer was investigated using phenol. Due to the equilibrium changing with temperature it was not possible to use the HSDM to calculate the mass transfer coefficients since the model requires the Freundlich coefficients. The Vermeulen equation, shown below, was used to enable an approximate overall rate constant ( $k$ ) to be determined so that the effect of temperature could be investigated.

$$F(t) = \left[ 1 - \exp \left( \frac{-D_{eff} t \pi^2}{r_o^2} \right) \right]^{0.5} \quad (8)$$

where  $F(t)$  is the fractional approach to equilibrium,  $D_{eff}$  is the effective diffusivity ( $m^2/s$ ),  $t$  is time (secs) and  $r_o$  (m) is the particle radius assuming spherical geometry. The overall rate constant  $k$  is defined as  $D_{eff}\pi^2/r_o^2$ .

An Arrhenius type relationship is observed in the data indicated by the straight line obtained on a plot of  $\ln k$  versus  $1/T$ . Fig. 4.16 presents the Arrhenius plot for the three polymers. Fig. 4.17 demonstrates the effect of temperature on the equilibrium concentration ( $C_o=50mg/l$ ).

Fig. 4.16. Arrhenius plots for MN-100, MN-150 and MN-200 sorbing phenol.

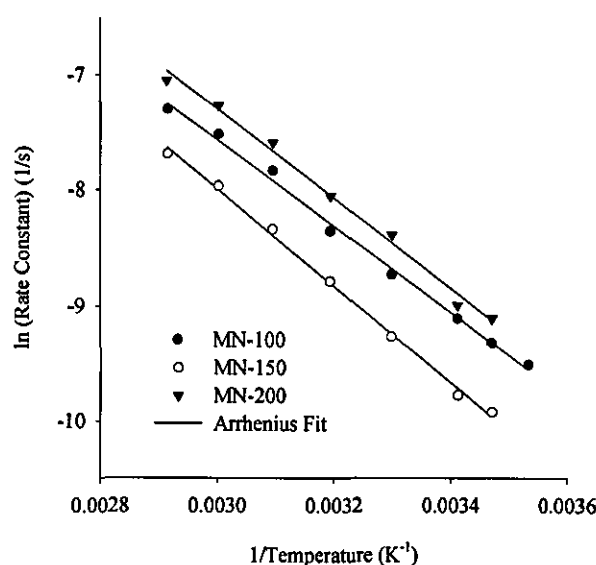
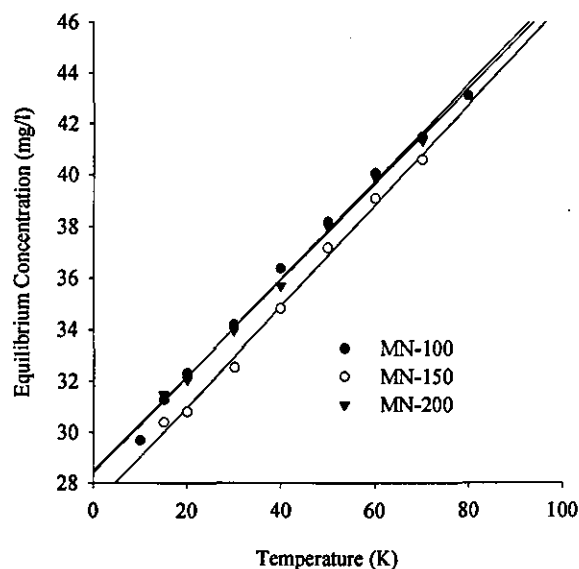


Fig. 4.17. Effect of temperature on the equilibrium conc. for MN-100, MN-150 and MN-200.



The activation energies, calculated from the gradient of the Arrhenius plots, are 30.9, 34.75, and 32.3 kJ/mol for MN-100, MN-150 and MN-200 respectively. These low values suggest that attractive forces between the adsorbent and adsorbates are predominately physical in nature, i.e. van der Waals forces.

The effect of agitation rate on the external mass transfer coefficients is presented in Table 4.10. As the agitation speed is increased the boundary layer thickness surrounding the adsorbent is reduced, resulting in an increase in the external mass transfer coefficient. The effect is more dramatic at lower agitation speeds.

**Table 4.10.** External mass transfer coefficients for MN-200 using different agitation speeds. 25°C, 500-600 µm particles,  $C_0=50$  mg/L.

| Agitation Speed (rpm)    | 0     | 50   | 150  | 250  | 300  | 350  | 450  | 550  | 750  |
|--------------------------|-------|------|------|------|------|------|------|------|------|
| $k_f \times 10^3$ (cm/s) | 0.958 | 4.74 | 6.32 | 7.21 | 7.57 | 7.87 | 8.41 | 8.86 | 9.60 |

## SECTION 4.5 CONCLUSIONS

Adsorption isotherms and kinetics have been studied for the adsorbents using phenol, 2-chlorophenol, 3-chlorophenol and 4-chlorophenol. The capacity of F-400 for phenol and 4-chlorophenol is significantly greater than that of the polymers which may be due to the delocalised electrons in the carbon forming strong interactions with the  $\pi$  electrons in the phenols. The electronegative effects of the chlorine atoms enhance the strength of the dispersion forces which result in the polymers and carbon having a greater capacity for the chlorophenols. No clear trends in the capacity of the adsorbents can be seen for the ortho, meta and para chlorophenols. The differences in the molecular size of the chlorophenols may control the uptake since size exclusion of the adsorbates is taking place in the microporous structure of the adsorbents. The functional groups on the polymers do not appear to affect the adsorption of the phenols at the experimental pH.

The adsorption kinetics of phenol are much faster than the chlorophenols, due to its larger

molecular diffusivity and the weaker interaction with the adsorbents surface. F-400 had the fastest kinetics followed by MN-200, MN-100 and MN-150 which was accounted for by differences in the pore size distributions of the adsorbents. The homogeneous surface diffusion model was used to estimate the surface diffusion coefficients. However, the model over predicted the rate of adsorption in the time range of 5-100mins which may be due to slow macro-meso pore diffusion or time delays in the concentration determination.

**SECTION 4.6 REFERENCES**

- [1] R.T. Morrison and R.N. Boyd, Organic Chemistry Sixth Edition, Prentice Hall International, Inc, (1992), p28-29.
- [2] C.H. Giles, T.H. MacEwan, S.N. Nakhwa and D. Smith, Studies in Adsorption. Part XI.\* A System of Classification of Solution Adsorption Isotherms, and its Use in Diagnosis of Adsorption Mechanisms and in Measurement of Specific Surface Areas of Solids., Journal of the Chemical Society, Part III, (1960), p3973-3993.
- [3] T. Karanfil, J.E. Kilduff and W.J. Weber (Jr.), The Role of Surface Characteristics on the Uptake of Organic Macromolecules by GAC., presented at Carbon '97, 23rd Biennial Conference on Carbon 18-23 July 1997, Extended Abstracts and Program, 1, p32-33.
- [4] G. Halsey and H.S. Taylor, The Adsorption of Hydrogen on Tungsten Powders., The Journal of Chemical Physics, 15, (9), (1947), p624-631.
- [5] B. Al-Duri and G. McKay, Comparison in Theory and Application of Several Mathematical Models to Predict Kinetics of Single Component Batch Adsorption Systems., Process Safety and Environmental Protection: Transactions of the Institution of Chemical Engineers, Part B, 68, (4), (1990), p254-268.
- [6] D.M. Ruthven, Principles of Adsorption and Adsorption Processes., John Wiley & Sons, (1984), Chapter 4.
- [7] D.W. Hand, J.C. Crittenden and W.E. Thacker, User-Oriented Batch Reactor Solutions to the Homogeneous Surface Diffusion Model., Journal of Environmental Engineering Division, ASCE, 109, (1), (1983), p82-101.
- [8] T.W. Weber and R.K. Chakravorti, Pore and Solid Diffusion Models for Fixed-Bed Adsorbers., AIChE Journal, 20, (2), p1974, 228-238.
- [9] B.R. Kim, R.A. Schmitz, V.L. Snoeyink, and G.W. Tauxe, Analysis of Models for Dichloroamine Removal by Activated Carbon in Batch and Packed-bed Reactors Using Quasilinearization and Orthogonal Collocation Methods., Water Research, 12, (1978), p317-326.
- [10] U.K. Traegner and M.T. Suidan, Evaluation of Surface and Film Diffusion Coefficients for Carbon Adsorption., Water Research, 23, (3), (1989), p267-273.
- [11] D. Roy, G-T. Wang and D.D. Adrian, Simplified Calculation Procedure for Carbon Adsorption Model, Water Environment Research, 65, (6), (1993), p781-787.
- [12] D. Roy, G-T. Wang and D.D. Adrian, A Simplified Solution Technique for Carbon Adsorption Model, Water Research, 27, (6), (1993), p1033-1040.

- [13] R.G. Peel, A. Benedek and C.M. Crowe, A Branched Pore Kinetic Model for Activated Carbon Adsorption., *AIChE Journal*, 27, (1), (1981), p26-32.
- [14] G. McKay, S. McKee and H.R.J. Walters, Solid-Liquid Adsorption Based External Mass Transfer, Macropore and Micropore Diffusion., *Chemical Engineering Science*, 42, (5), (1987), p1145-1151.
- [15] G. McKay, Mass Transfer Processes During the Adsorption of Solutes in Aqueous Solutions in Batch and Fixed Bed Adsorbers., *Chemical Engineering Research & Design*, 62, (4), (1984), p235-246.
- [16] G. McKay, M.J. Bino and A. Altememi, A External Mass Transfer During the Adsorption of Various Pollutants Onto Activated Carbon., *Water Research*, 20, (4), (1986), p435-442.
- [17] G. McKay and M.J. Bino, Adsorption of Pollutants From Waste-water Onto Activated Carbon based on External Mass-transfer and Pore Diffusion, *Water Research*, 22, (3), (1988), p79-286.
- [18] G. McKay and B. Al-Duri, Study of the Mechanism of Pore Diffusion in Batch Adsorption Systems., *Journal of Chemical Technology and Biotechnology*, 48, (3), (1990), p269-285.
- [19] B. Al-Duri and G. McKay, Prediction of Binary-system for Kinetics of Batch Adsorption Using Basic-dyes Onto Activated Carbon., *Chemical Engineering Science*, 46, (1), (1991), p193-204.
- [20] B. Al-Duri and G. McKay, Pore Diffusion - Dependence of the Effective Diffusivity on the initial Sorbate Concentration in Single and Multi-solute Batch Adsorption Systems., *Journal of Chemical Technology and Biotechnology*, 55, (3), (1992), p245-250.
- [21] H.J. Kim, S.S. Lee, J.E. Sohn, E. Furuya, Y. Takeuchi, K.E. Noll and S. Yamashita, Adsorption of Phenols Onto Macroreticular Resin Particles., *Korean Journal of Chemical Engineering*, 13, (4), (1996), p399-403.
- [22] A. Itaya, N. Kato and J. Yamamoto, Liquid Phase Adsorption Equilibrium of Phenol and its Derivatives on Macroreticular Adsorbents., *Journal of Chemical Engineering of Japan*, 17, (4), (1984), p389-395.
- [23] B.M. van Vliet, W.J. Weber (Jr) and H. Hozumi, Modelling and Prediction of Specific Compound Adsorption by Activated Carbon and Synthetic Adsorbents., *Water Research*, 14, (1980), p1719-1728.
- [24] C. Costa and A. Rodrigues, Intraparticle Diffusion of Phenol in Macroreticular Adsorbents: Modelling and Experimental Study of Batch and CSTR Adsorbers., *Chemical Engineering Science*, 40, (6), (1985), p983-993.

- [25] R.T. Huang, T.L. Chen and H.S. Weng, Adsorption of o-cresol and Benzoic Acid in an Adsorber Packed With an Ion-exchange Resin: A Comparative Study of Diffusional Models, *Separation Science and Technology*, 29, (15), (1994), p2019-2033.
- [26] R.B. Gauntlett, A Comparison Between Ion-exchange Resins and Activated Carbon for the Removal of Organics from Water., Water Research Centre, Treatment Division, Technical Report TR 10, April, (1975), p1-27.
- [27] L.R. Radovic, discussed at the 23rd Biennial Conference on Carbon, PennState University, Pennsylvania. (E-mail Irr3@psu.edu)
- [28] A. Seidel, E. Tzscheuschler, K.H. Radeke and D. Gelbin, Adsorption Equilibria of Aqueous Phenol and Indole Solutions on Activated Carbons., *Chemical Engineering Science*, 40, (2), (1985), p215-222.
- [29] A. Seidel and D. Gelbin, On Applying the Ideal Adsorbed Solution Theory on Multi-component Adsorption Equilibria of Dissolved Organic Components on Activated Carbon., *Chemical Engineering Science*, 43, (1), (1988), p79-89.
- [30] R. Johansson and I. Neretnieks, Adsorption on Activated Carbon in Countercurrent flow. An experimental study., *Chemical Engineering Science*, 35, (1980), p979-986.
- [31] M.K.N. Yenkie and G.S. Natarajan, Adsorption Equilibrium Studies of Some Aqueous Aromatic Pollutants on Granular Activated Carbon Samples., *Separation Science and Technology*, 26, (5), (1991), p661-674.
- [32] G.A. Sorial, M.T. Suidan, R.D. Vidic and S.W. Maloney, Competitive Adsorption of Phenols on GAC I: Adsorption Equilibrium., *Journal of Environmental Engineering*, 119, (6), (1993), p1026-1043.
- [33] R.D. Vidic, M.T. Suidan, U.K. Traegner and G.F. Nakhla, Adsorption Isotherms. Illusive Capacity and Role of Oxygen., *Water Research*, 24, (10), (1990), p1187-1195.
- [34] G. McKay, M.J. Bino and A.R. Altamemi, Adsorption of Various Pollutants From Aqueous Solutions on to Activated Carbon., *Water Research*, 19, (4), (1985), p491-495.
- [35] R.W. Coughlin, R.S. Ezra and R.N. Tan, Influence of Chemisorbed Oxygen in Adsorption onto Carbon from Aqueous Solution., *Journal of Colloid Interface Science*, 28, (3/4), (1968), p386-396.
- [36] J.S. Mattson, H.B. Mark (Jr), M.D. Malbin, W.J. Weber (Jr) and J.C. Crittenden., Surface Chemistry of Active Carbon: Specific Adsorption of Phenol., *Journal of Colloid and Interface Science*, 31, (1), (1969), p116-130.
- [37] J. Ma, G. Li and N.J.D. Graham, Study of the Factors Affecting the Removal of Phenolic Compounds from Water by PAC, *Water Supply*, 14, (2), (1996), p209-221.

- [38] H. Oda, M. Kishida and C. Yokokawa, Adsorption of Benzoic Acid and Phenol from Aqueous Solution by Activated Carbons-Effect of Surface Acidity., Carbon, 19, (4), (1981), p243-248.
- [39] H. Oda and C. Yokokawa, Adsorption of Aromatic Amines and O-substituted Derivatives of Phenol From Organic Solutions by Activated Carbons - Effect of Surface Acidity., Carbon, 21, (5), (1983), p485-489.
- [40] R.D. Vidic, M.T. Suidan, Effect of Dissolved Oxygen on Phenols Breakthrough from GAC Adsorbers., Water Science and Technology, 26, (5), (1992), p1185-1193.
- [41] P. Magne and P.L. Walker (Jr), Phenol Adsorption on Activated Carbons: Application to the Regeneration of Activated Carbons Polluted with Phenol., Carbon, 24, (2), (1986), p101-107.
- [42] R.C. Bansal and T.L. Dhami, Surface Characteristics and Behaviour of Polymer Carbons-IV., Carbon, 18, (1980), p137-145.
- [43] F.W. Pontius, Water Quality and Treatment A Handbook of Community Water Supplies, American Water Works Association, McGraw-Hill, London, (1992), p865
- [44] Chemical Database Service at Daresbury
- [45] C.R. Wilke and P. Chang, Correlation of Diffusion Coefficients in Dilute Solutions., AIChE Journal, 1, (2), (1955), p264-270.
- [46] C.R. Wilke, Estimation of Liquid Diffusion Coefficients, Chemical Engineering Progress, 45, (3), (1949), p218-224.
- [47] B.R. Puri, in Activated Carbon Adsorption of Organics from Aqueous Phase, Vol. 1., I.H. Suffet and M.J. McGuire, (eds)., Ann Arbor Science, Michigan, (1980), p353.

## CHAPTER 5

### PESTICIDES ADSORPTION

#### SECTION 5.1 INTRODUCTION

Water intended for human consumption in the United Kingdom must comply with the Water Act 1991, which incorporates the relevant requirements of the EC Drinking Water Directive (80/778/EEC). The EU and national standard for any individual pesticide in drinking water at the point of supply is  $0.1\mu\text{g/l}$  or  $0.1\text{ppb}$  (parts per billion), with a maximum of  $0.5\mu\text{g/l}$  for all detected compounds [1]. These limits have set a demanding target for water companies and have initiated more extensive use of granular activated carbon (GAC) beds.

In 1988, the Cincinnati Water works authority installed a large GAC treatment facility to remove synthetic organic chemicals [2]. The installation was designed to treat  $662\text{ Ml/d}$  using a total of  $6925\text{m}^3$  of GAC, based upon a carbon usage rate of  $22,700\text{kg/day}$ . Six storage tanks, each with a capacity of  $480\text{m}^3$ , were used to store spent carbon prior to regeneration on-site. The regeneration cost of activated carbon is approximately 80% of the raw material cost (£1000/tonne). Hence, the total annual expenditure on regenerating carbon, for a plant with similar capacity to the Cincinnati facility, would be £6.6 million per year or £0.027/ $\text{m}^3$  of water treated.

The presence of natural organic matter (NOM) in drinking water supplies results in premature breakthrough of the pesticides, probably caused by the NOM blocking access to the micropores. This results in a reduction in the life of the carbon bed to about three to six months, compared with a typical life of up to two years for taste and odour removal [3]. Hence, more frequent regeneration of the adsorbed species is required, increasing the cost of the treatment process.

A number of authors have investigated new materials in an attempt to reduce the overall costs of GAC treatment. Hopman *et al* [4] have investigated activated carbon fibres, containing only



micropores, for the selective adsorption of pesticides. The narrow pore size distribution allowed the pesticides to adsorb but size excluded the NOM. Numerous investigations have been undertaken on cheaper regeneration technologies for carbon, such as solvent regeneration. However, all of these studies suggested that they were not economically feasible.

The widespread use and complex chemistry of some pesticides cause drinking water levels to frequently exceed the UK legal limit. The six most frequently detected pesticides in 1991 and 1992 were atrazine, simazine, diuron, isoproturon, chlorotoluron, and mecoprop [5]. The average concentrations of the pesticides in drinking water supplies in 1993 were about  $0.03\mu\text{g/l}$  or less, although some sites exceeded  $0.1\mu\text{g/l}$  for long periods while others were below the limit of detection.

This chapter investigates the adsorption of atrazine, simazine, diuron isoproturon and chlorotoluron in single-component and multi-component solutions onto Macronet polymers and F-400 activated carbon. The influence of humic acid and fulvic acid on the adsorption of the pesticides is also discussed.

## SECTION 5.2 BACKGROUND INFORMATION AND LITERATURE REVIEW.

### *Pesticides*

Pesticides are used extensively to control different types of weeds, insects and other pests in a wide variety of agricultural and urban settings. However, these pesticides which provide increased crop production and other advantages also contaminate the hydrological system. In 1990, the most frequently detected pesticides in UK drinking water supplies were atrazine, simazine, isoproturon and mecoprop. Recently the occurrences of atrazine and simazine have declined, due to a moratorium on the use of atrazine for non-agricultural purposes (1993). However, diuron is now more frequently determined. Table 5.1 presents the concentrations of the pesticides determined in all surface and ground water for 1993 [6] and the concentrations found in UK drinking water for the years 1992 and 1993 [7].

**Table 5.1. Concentration of pesticides in drinking water sources and supplies in 1993 ( $\mu\text{g/l}$ ).**

| Pesticide     | Surface Water [6] |      | Ground Water [6] |      | Drinking Water [7] |           |
|---------------|-------------------|------|------------------|------|--------------------|-----------|
|               | Average           | Max. | Average          | Max. | 1992 Max.          | 1993 Max. |
| Atrazine      | 0.06              | 10.8 | 0.04             | 0.63 | 1.0                | 5.5       |
| Simazine      | 0.04              | 3.62 | 0.01             | 1.23 | 56.3               | 0.73      |
| Isoproturon   | 0.03              | 4.73 | 0.007            | 0.19 | 0.64               | 1.42      |
| Diuron        | 0.15              | 19.1 | 0.03             | 0.98 | 3.4                | 2.3       |
| Chlorotoluron | 0.04              | 13.6 | 0.03             | 1.9  | 0.78               | 0.34      |

The average concentration of the pesticides in source waters is generally below the legal limit of  $0.1\mu\text{g/l}$ . However, the seasonal variations in the usage of pesticides result in concentrations that significantly exceed the limit, resulting in the source not being used for drinking water production. The maximum concentration of pesticides determined in drinking water significantly exceeds the legal limit necessitating more extensive use of GAC. Table 5.2 presents the usage data for five of the most frequently detected pesticides [8].

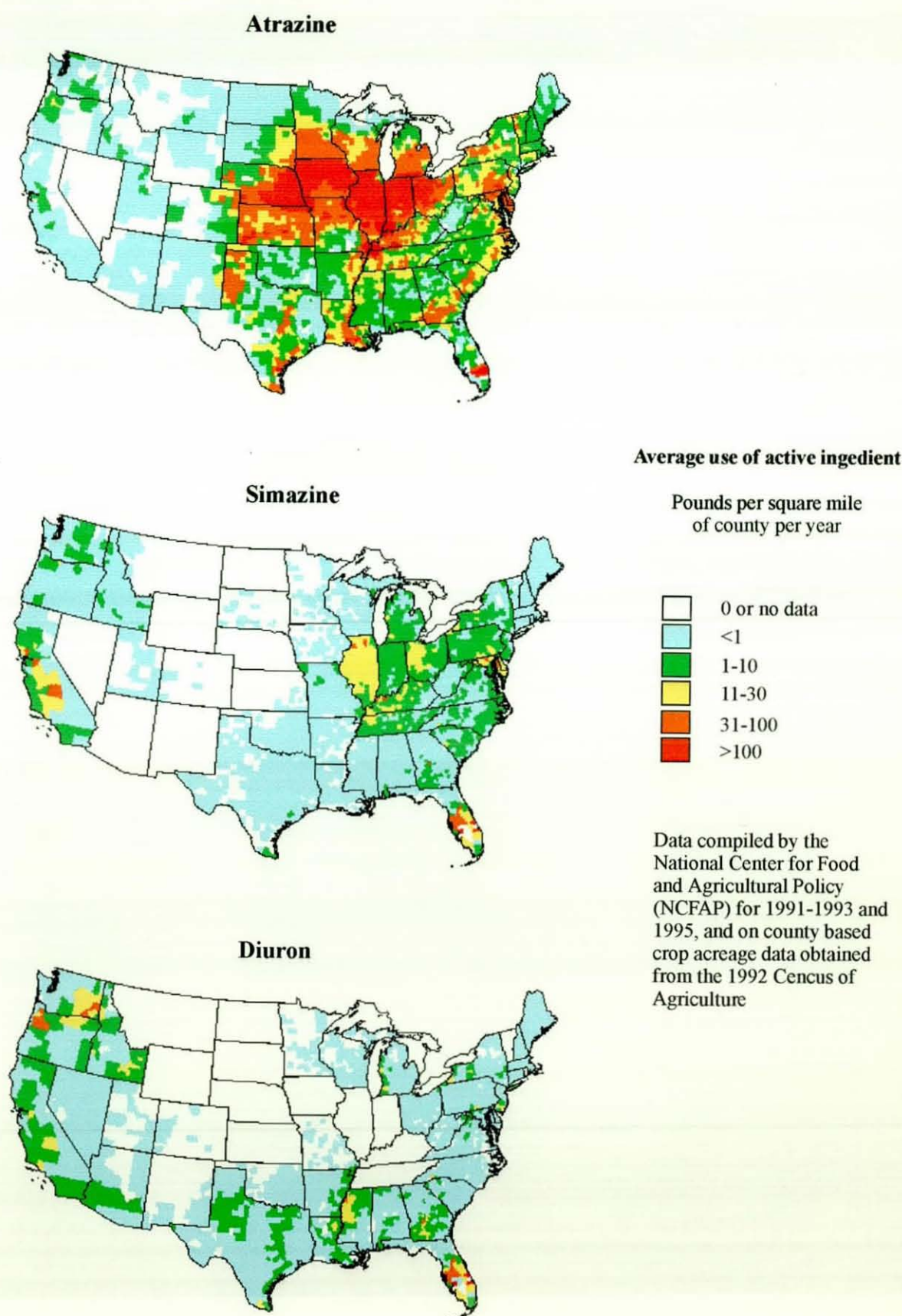
**Table 5.2. Usage data for frequently detected pesticides.**

| Pesticide     | Non agricultural use<br>(tonnes/year in 1989) | Agricultural use<br>(tonnes/year in 1990) | Class of Compound           |
|---------------|-----------------------------------------------|-------------------------------------------|-----------------------------|
| Atrazine      | 135                                           | 41                                        | 1,3,5 triazine herbicide*   |
| Simazine      | 79                                            | 139                                       | 1,3,5 triazine herbicide*   |
| Isoproturon   | -                                             | 3119                                      | Substituted urea herbicide* |
| Diuron        | -                                             | -                                         | Substituted urea herbicide* |
| Chlorotoluron | -                                             | 688                                       | Substituted urea herbicide* |

\* Herbicides are photosynthetic electron transport inhibitors

Pesticide usage in the United States of America far exceeds that of the UK. National use of pesticides has grown from 86,000 tonnes of active ingredient in 1964 to about 500,000 tonnes in 1993. Fig. 5.1 illustrates the annual application of atrazine, simazine and diuron in the US (1992) [9].

Fig. 5.1. Annual use of atrazine, simazine and diuron in 1992 [9].



The concentration of atrazine in rain was recorded to be  $2.25\mu\text{g/l}$  in the vicinity of Wye River, Maryland, USA, in May 1982 [10]. The USGS report into national water quality and assessment, pesticide national synthesis project, estimated that up to 75% of all pesticides evaporate into the atmosphere [11]. The maximum concentration limit (MCL) in drinking water for atrazine and simazine is 3 and  $4\mu\text{g/l}$  respectively. The MCL is a health based standard that has a built-in safety factor of 1,000-fold.

In November 1994 the US Environmental Protection Agency (EPA) initiated a special review of atrazine and simazine due to concerns regarding the residuals found in food and drinking water [12]. The outcome of the review is expected in late 1997. However, there is significant opposition to any restrictions on the use of the pesticides.

### *Natural Organic Matter*

Natural organic matter (NOM) is the term used to describe the complex matrix of organic compounds present in natural waters. Of particular importance to water purification using adsorption are humic substances. Humic substances are a series of relatively high molecular-weight compounds, yellow to black coloured, formed by secondary synthesis reactions. They are often fractionated into humic acid, dark-coloured organic material that is insoluble in dilute acid, and fulvic acid which is soluble in both alkali and acid. Some of the chemical properties of humic and fulvic acid are summarised in Table 5.3. Numerous techniques have been applied to the fractionation and characterisation of humic substances including titration, spectrometry, mass spectrometry etc. An excellent review of humus chemistry is provided in the book by Stevenson [13].

The molecular size and chemistry of humic and fulvic acid significantly affect their ability to be adsorbed. Humic acids are generally large molecules, equivalent to spherical particles with diameters of  $60\text{-}100\text{\AA}$  whereas fulvic acids generally have a molecular size of  $20\text{-}30\text{\AA}$  [13]. At high sample concentrations, low pH, and high amounts of neutral electrolytes, humic and fulvic acids behave like rigid "spherocolloids". In contrast, flexible linear colloids are observed at low sample concentration, neutral pH, or low ionic strengths. The large molecular size will generally

prevent the substances from entering the micropores of adsorbents. However, many granular

**Table 5.3. Chemical characteristics of humic and fulvic acid [13].**

| Characteristic         | Humic Acid     | Fulvic Acid |
|------------------------|----------------|-------------|
| Typical MW (Daltons)   | 50,000-100,000 | 500-2,000   |
| C %                    | 57.2           | 49.5        |
| H %                    | 4.4            | 4.5         |
| N %                    | 2.4            | 0.8         |
| Total acidity (meq/g)  | 8.1            | 12.4        |
| Carboxyl -COOH (meq/g) | 4.8            | 9.1         |
| Phenolic -OH (meq/g)   | 3.3            | 3.3         |
| Ketonic -C=O (meq/g)   | 2.2            | -           |
| Quinoid C=O (meq/g)    | 2.1            | -           |
| Ash %                  | 7.9            | 2.0         |

activated carbons possess mesopores (20-100Å), to quicken their adsorption kinetics, in which humic and fulvic acids can be adsorbed. The large colloidal substances tend to block the access to the micropores, thereby preventing the pesticides from being adsorbed. The highly acidic functionality of humic and fulvic acids means that they often exist as negatively charged molecules at the pH of natural waters. The  $pK_a$  of soil humic acid depends on the ionic strength of the background. At an ionic strength of 0.001M the average  $pK_a$  is 5.7, whereas at a strength of 0.1M the  $pK_a$  decreases to nearer 4.7. The point of zero charge on activated carbons can vary between 2 and 8. Hence, for negatively charged surfaces, humic and fulvic acid will be repelled. Although humic and fulvic acids are hydrophilic in nature they can contain areas that are hydrophobic. Hence, many pesticides bind to the humic substances either through hydrophobic interactions or ion exchange and coordination.

The concentrations of humic and fulvic substances in natural waters are generally in the low parts per million range which is 1000 times greater than the pesticide concentrations.

## Adsorption

To the author's knowledge, no data concerning the adsorption of atrazine, simazine, isoproturon, diuron, chlorotoluron and natural organic matter has been presented on Hypersol-Macronet polymers. Polymers have been applied in solid phase extraction of pesticides and NOM for the development of analytical methods. However, these trials normally only extract 500ml of solution and so are not representative of the work in this study. Recovery of fulvic acid, by investigators attempting to characterise the material, has been successfully performed using the macroporous resin XAD 8 [13]. To enable adsorption, the solution pH is reduced to 2. Regeneration is achieved by increasing the pH to nearer 7, where the fulvic acid molecules become ionised and thus desorb. A number of studies that compared the adsorption of organic pollutants in natural waters have been discussed in previous chapters [1.1-2]. A brief review of adsorption of the selected pesticides and NOM onto activated carbons is presented below.

A wide variety of methodologies have been investigated to assess the performance of new adsorbents, with respect to their adsorption capacity and kinetics. Table 5.4 provides a summary of some of the methodologies used to evaluate the performance of granular activated carbon.

**Table 5.4. GAC performance evaluation methodologies in comparison to field scale columns [14].**

| Methodologies       | Capacity | Kinetics | Length or EBCT | Particle size | Operation time | Model needed |
|---------------------|----------|----------|----------------|---------------|----------------|--------------|
| Pilot columns       | yes      | yes      | equal          | equal         | equal          | no           |
| Isotherms           | yes      | no       | -              | smaller       | smaller        | yes          |
| Batch Reactor       | no       | yes      | -              | smaller       | smaller        | yes          |
| Short fixed beds    | no       | yes      | smaller        | equal         | smaller        | yes          |
| Mini-columns        | yes      | no       | smaller        | smaller       | smaller        | yes          |
| Small-scale columns | yes      | yes      | smaller        | smaller       | smaller        | no           |

Pilot columns provide an accurate and reliable prediction of breakthrough behaviour in full scale columns. However, the extended times and cost of the trials have led a number of researchers to develop tests that obtain data in a fraction of the time, often in the laboratory. In 1982, Frick [15] presented the idea of scaling down full-scale adsorber parameters, by dimensional analysis,

to enable the rapid determination of a GACs performance. Crittenden and coworkers developed the idea which resulted in the rapid small scale column test [16]. The RSSCT has been recommended by the American Water Works Association as a protocol for the selection of a GAC [14].

The scaling equations are derived on the basis of the dispersed flow, pore-surface diffusion model (DFPSDM), containing the dimensionless groups; surface solute distribution parameter, pore solute distribution parameter, Stanton number, pore diffusion modulus, surface diffusion modulus and the Peclet number. The scaling equations are derived by setting the dimensionless groups of a small-scale column equal to those of the large-scale adsorber, since the six independent dimensionless groups should remain constant. Initial equations proposed by Crittenden assumed that the value of the surface diffusion coefficient remained constant. However, correlations were also presented in later publications for cases of non-constant diffusivities [17,18]. A summary of the equations can be seen in Appendix 2. Due to the reduced time for adsorption, the RSSCT cannot assess the possibilities of biodegradation or simulate accurately the effect of changes in the condition and concentration of the feed water.

Hopman *et al* [19] used the RSSCT to evaluate the breakthrough of a multi-component solution containing six substituted urea herbicides including isoproturon, chlorotoluron and diuron. Breakthrough of the herbicides, to  $0.1\mu\text{g/l}$ , occurred after 130 litres of solution had passed through one gramme of carbon (1/g) compared to 215 and 325l/g for chlorotoluron and diuron respectively. The selectivity was directly related to the hydrophobicity of the pesticides measured by the octanol water partition coefficient. Solid phase concentrations, at the breakthrough moment, were 106 and  $130\mu\text{g/g}$  for isoproturon and chlorotoluron respectively. Hopman [20] also conducted isotherm tests on ROW 0.8 S activated carbon for a variety of pesticides in ultrapure water. Simazine had an adsorption capacity of  $36\text{mg/g}$  at an equilibrium concentration of  $1\mu\text{g/l}$ .

Matsui [21] presented RSSCT data, assuming constant diffusivity, for the multi-component adsorption of simazine, diazinon and napropamid at concentrations of 106, 110 and  $108\mu\text{g/l}$  respectively. The mini-column had a bed depth of 10mm and a diameter of 15mm, resulting in

a bed volume of 1.76ml (22-26 $\mu$ m F-400). Breakthrough of all the pesticides, to 5 $\mu$ g/l, occurred at 400,000 bed volumes. The presence of humic acid, at a concentration corresponding to a UV absorbance of 0.107/cm detected at 254nm, caused breakthrough to occur at 20,000BV's. Mazet *et al* [22] investigated the influence of heat and chemical treatment on F-400 activated carbon for the adsorption of atrazine. Heat treatment of the carbon, which reduced the concentration of oxygenated functional groups, increased the capacity for atrazine adsorption by 60%. Ayele *et al* [23] investigated the adsorption of four triazine herbicides, including atrazine and simazine, onto powdered F-400. They observed that the capacity of the carbon for simazine was greater than that for atrazine. Langmuir capacities of between 1.1 and 1.5mmol/g were obtained, based on initial solution concentrations of 10-20mg/l. Adams [24] investigated the adsorption of triazine herbicides and their metabolites using powdered F-200. They observed that the adsorption capacity of the carbon for the metabolites was generally lower than for the starting material, due to the compounds increased solubility in water. Qi *et al* [25] determined the adsorption capacity and kinetics for the adsorption of atrazine onto WPH powdered activated carbon produced by the Calgon Carbon corporation. The surface diffusion coefficient, calculated using the homogeneous surface diffusion model, was  $7.9 \times 10^{-11} \text{ cm}^2/\text{min}$ . The pure water Freundlich isotherm parameters,  $1/n$  and  $K$ , were 0.335 and 797 ( $\mu\text{mole/g})(\text{L}/\mu\text{mole})^{1/n}$  respectively. Speth *et al* [26] observed similar capacities of  $1/n = 0.291$  and  $K = 858$  for pulverised F-400.

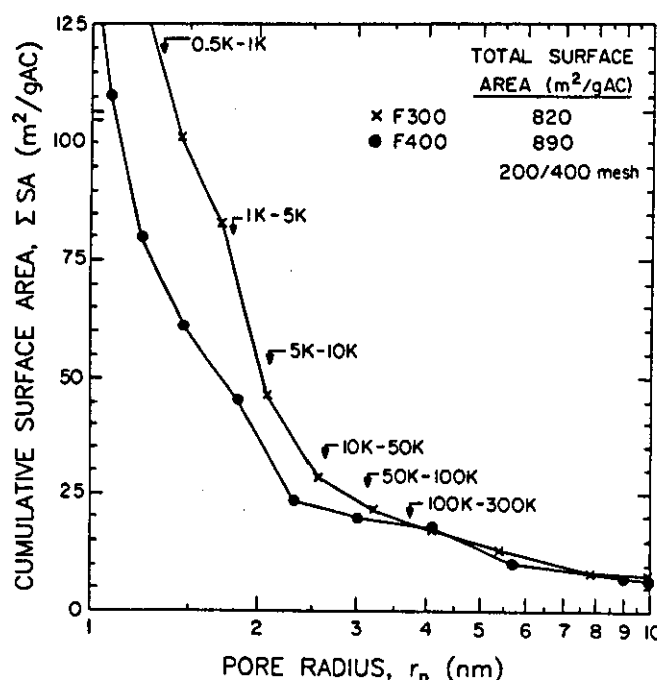
Bernazeau *et al* [27] investigated the competitive adsorption of atrazine with natural organic matter on F-400. They observed that the atrazine capacity decreased from 0.6mg/g to 0.2mg/g (for  $c_e = 0.1 \mu\text{g/l}$ ) when the concentration of natural organic matter increased from 2 to 8mg/l.

The RSSCT has also been widely applied to the adsorption of humic acid to determine capacity and kinetics parameters. Lee *et al* [28] used the HSDM to determine the surface diffusion coefficients for the adsorption of humic and fulvic acid using F-400. Analysis of the batch kinetic data gave values of  $6.0 \times 10^{-12}$  and  $2.7 \times 10^{-11} \text{ cm}^2/\text{s}$  for commercial humic and fulvic acid respectively. Summers *et al* [29] investigated the size exclusion and electrostatic interactions of humic substances on F-400 and four other activated carbons. The adsorption performance generally showed a 3 to 10-fold increase when the concentration of NaCl was increase from 0



to 0.1M NaCl. The behaviour was explained by the humic macromolecule changing size with the background electrolyte concentration. At low ionic strengths the functional groups become dissociated which causes an expansion of the macromolecule due to the mutual repulsion of like charges. As the ionic strength is increased, the counter ions in solution suppress the double layer forces, allowing the molecule to coil and reduce its effective size. They correlated the available surface area of F-300 and F-400 with the approximate size of different molecular weight fractions of humic and fulvic acid. Fig. 5.2 presents the data.

**Fig. 5.2.** Surface area distribution of the F300 and F400 activated carbons, showing available surface area for different commercial humic acid mass fractions [29].



Lafrance *et al* [30] investigated the adsorption of humic substances, in the presence of sodium salts, for F-400. They also observed that the increase in capacity was due to the neutralisation of the negative charges on the humate molecules and carbons surface functional groups, thus reducing the electrostatic repulsion. Newcombe [31] investigated the adsorption of the fulvic acid fraction, since humic acids were generally removed by conventional water treatment processes of coagulation, settling and sand filtration. He observed Langmuir type isotherms suggesting that F-300 had a high affinity for fulvic acid. At low surface concentrations he concluded that the molecules were adsorbed by ion pair formation between the carboxyl groups

of the humic material and positive groups on the surface of the carbon. The adsorption performance of activated carbon fibres for the removal of humic substances has been presented by a number of authors [32-34]. The fibres have a large capacity for small organic species. However, humic acid was size excluded from the micropores.

Frederick *et al* [35] correlated the adsorption of calcium on F-400 by pre-loading the carbon with NOM. A linear relationship was observed between the NOM loading and calcium uptake. During the thermal regeneration of the carbon calcium tends to catalyse burn off resulting in a reduction of the carbon mass and surface area. Karanfil *et al* [36] suggested that surface oxidation of F-400 reduced the uptake of NOM. Heat treatment of the carbon surface did not increase the uptake suggesting that the low degree of oxygen functionality did not interfere with the removal.

Crittenden *et al* [37] attempted to model the adsorption of humic acid onto F-400 by breaking the NOM into five fictitious components. The Freundlich isotherm equation was used to describe the single component equilibrium of the individual fictive components. The ideal adsorbed solution theory (IAST) was applied to describe the competitive interactions between the components. They found that neither the HSDM nor the pore diffusion model could be used to predict NOM pilot column data using batch determined intraparticle diffusivities and isotherm parameters. Pore diffusion controlled the mass transfer rate for the pilot column. Smith [38] also use the IAST to model the adsorption of NOM onto F-400.

Bulloch *et al* [39] presented a model to predict the influence of NOM on the adsorption of synthetic organic compounds (SOC). They used the pore and surface diffusion model (PSDM), which includes the effects of external mass transfer and intraparticle mass transfer due to both pore and surface diffusion, to model the breakthrough. The Polanyi potential theory was used to predict single solute isotherms for some of the SOC's with the competitive interactions estimated using the IAST. Crittenden and coworkers have presented many studies on the application of the IAST for the multi-component of adsorption organic species onto F-400 [40-42]. Five basic equations are used in the model, which after mathematical manipulation result in an expression which calculates the equilibrium state in an isotherm bottle if  $K, 1/n$ , (the single

solute Freundlich parameters, assuming that the Freundlich isotherm can describe the equilibrium relationship over the full concentration range), the initial concentration of each solute and carbon dose are known. However, for a solution containing  $N$  components,  $N$  non-linear simultaneous equations with  $N$  unknowns must be solved. The Newton-Raphson equation is often applied.

The Hanson Flacker modified Polanyi theory has been applied by the Calgon Carbon corporation to predict the isothermal loading and carbon use rate for both single component and multi-component systems [43]. For single component predictions the model's accuracy is within 20%. Several other multi-component isotherm models have been presented in the literature including the Polanyi model derived by Rosene and Manes [44]. However, the IAST, originally proposed by Myers and Prausnitz [45] for gas mixtures and later developed by Radke and Prausnitz [46] for dilute liquid systems, has the most thermodynamically accepted foundation. Numerous authors have investigated the IAST theories for a wide variety of systems [47,48].

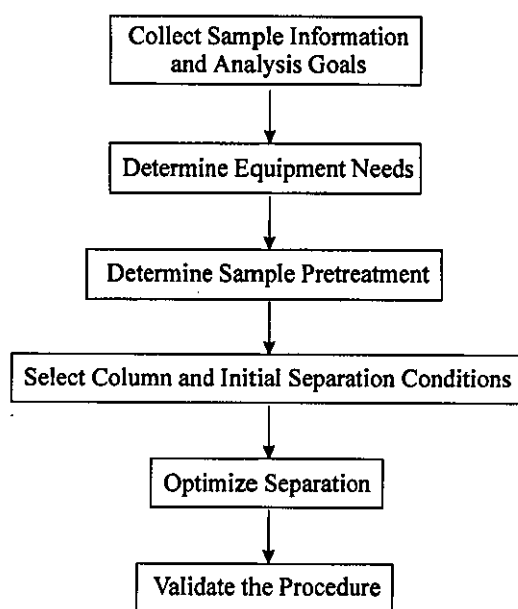
## SECTION 5.3 ANALYSIS METHOD DEVELOPMENT

### *HPLC and Solid Phase Extraction Method Development*

The information below provides a brief summary of the HPLC method development procedure to enable the determination of atrazine, simazine, isoproturon, diuron and chlorotoluron.

The stages involved in HPLC method development can be summarised by the flow sheet shown in Fig. 5.3.

**Fig. 5.3. Stages of Method Development.**



The analysis goal was to determine the concentration of atrazine, simazine, isoproturon, chlorotoluron and diuron in water at levels of 0.1ppb or below. Initially the water would be ultrapure. However, the method also had to be suitable for water contaminated with humic or fulvic acid. The complex nature of the water required the use of a diode array detector which allowed for quantification of pesticides in solution. A HP 1100 series HPLC system, consisting of a binary pump, autosampler, column thermostat and diode array detector, was used for the analysis.

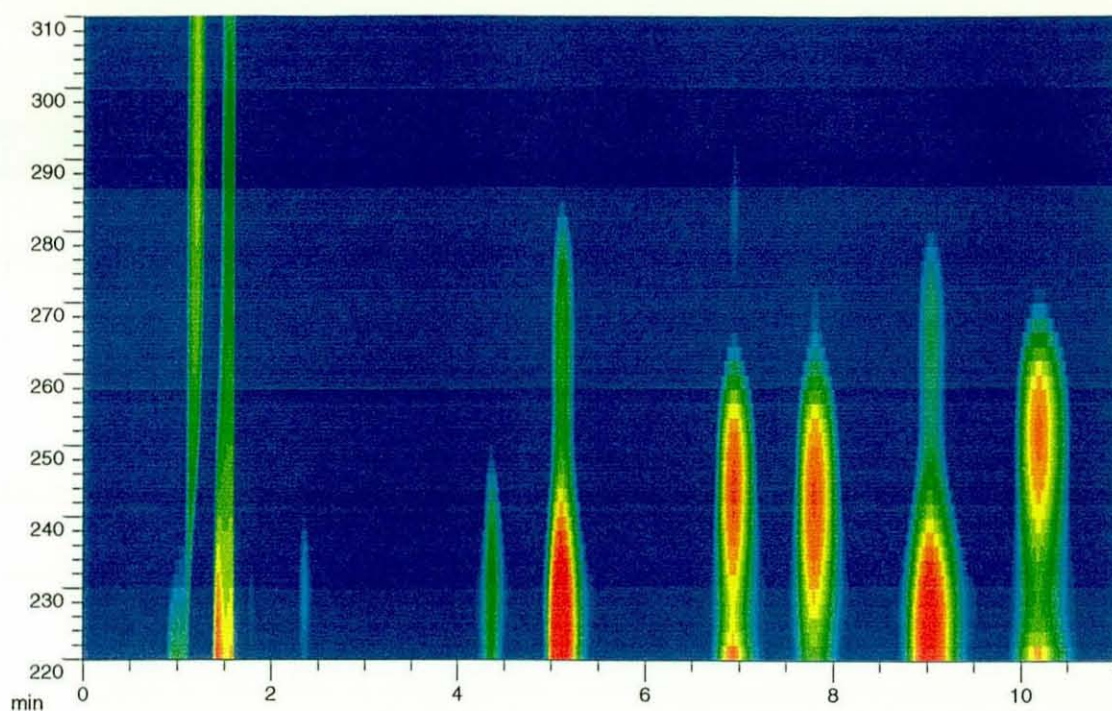
A study of the physical and chemical properties of the pesticides suggested that separation could be achieved by reverse phase chromatography using a C18 column. A Genesis C18 column (4 $\mu$ m, 150 $\times$ 3.0mm) combined with a 1cm Genesis guard column, supplied by Jones Chromatography, was selected for the analysis.

A gradient elution over 20 minutes, starting from 5% MeOH/95% H<sub>2</sub>O to 100% MeOH, suggested that an isocratic elution of the compounds could be achieved. The solvent composition was then optimised for the methanol/water isocratic elution. An equivalent strength acetonitrile/water and then a tetrahydrofuran/water mobile phase were tried. The next three injections were performed using organic phases containing 50% mixtures of each solvent. Analysis of the chromatograms suggested that the acetonitrile/THF organic phase would provide an optimum separation. The relative percentage of THF to acetonitrile was varied until a compromise between the sensitivity and resolution was achieved. A number of different buffers were investigated for the water phase at a variety of pH values. The temperature for chromatography was varied from 20°C up to 60°C to optimise the separation. A flow rate of 0.8ml/min was selected, since pressure drops greater than 150bar would reduce column life.

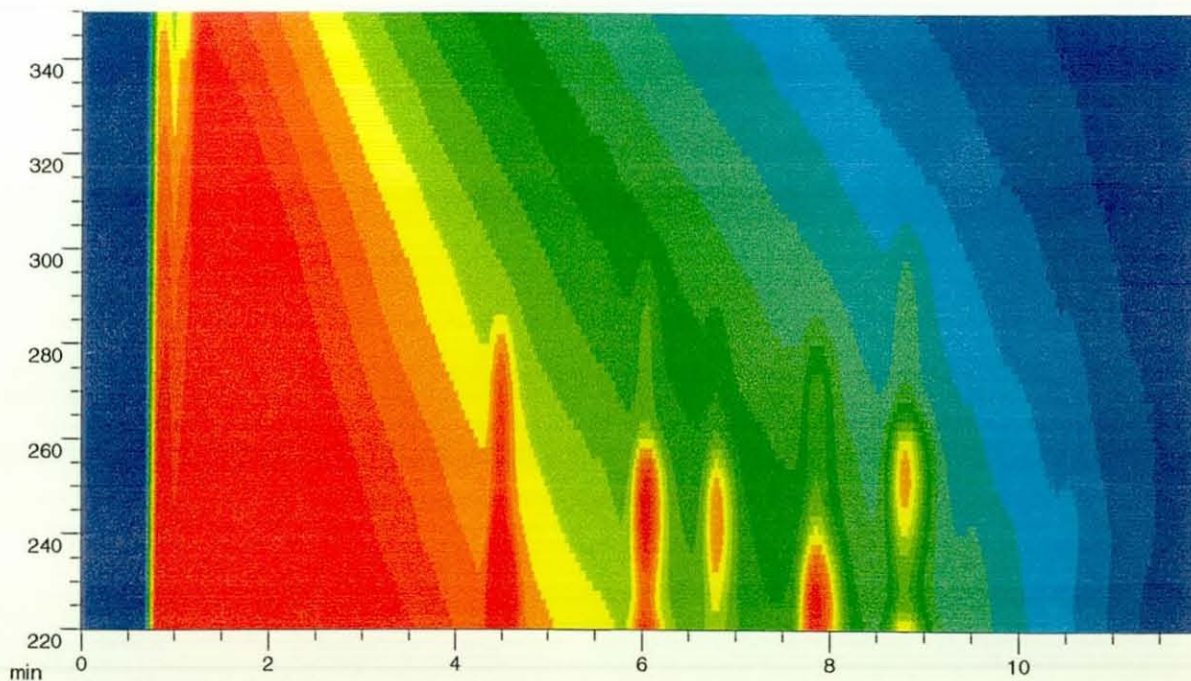
Fig. 5.4 presents the isoabsorbance plot for the optimised HPLC separation. The isoabsorbance plot is equivalent to a contour map of heights for the time versus wavelength axes and enables easy identification of co-eluting or interfering peaks. Optimum wavelengths for the detection of pesticides were 230nm for atrazine and simazine and 244nm for diuron, isoproturon and chlorotoluron. These wavelengths correspond to the maxima in the compounds UV spectra.

The interference of fulvic acid on the identification of the pesticides can be seen in Fig. 5.5. Fulvic acid contains a complex mix of organic compounds which absorb strongly in the UV region. Separation of the fulvic acid and the pesticides is achieved due to their more hydrophilic nature, which causes elution in the early stages of the chromatogram. However, the concentrations of fulvic acid are approximately 1000 times higher than those of the pesticides and interferences are caused by the tailing elution of the fulvics. The interference reduces the level at which the pesticides can be detected due to the variable baseline.

**Fig. 5.4.** Isoabsorbance plot for HPLC analysis of a pure pesticides mix.



**Fig. 5.5.** Isoabsorbance plot for HPLC analysis of a fulvic acid and pesticides mix. (No guard column).



Height: 0 ---> 70

Scale is log

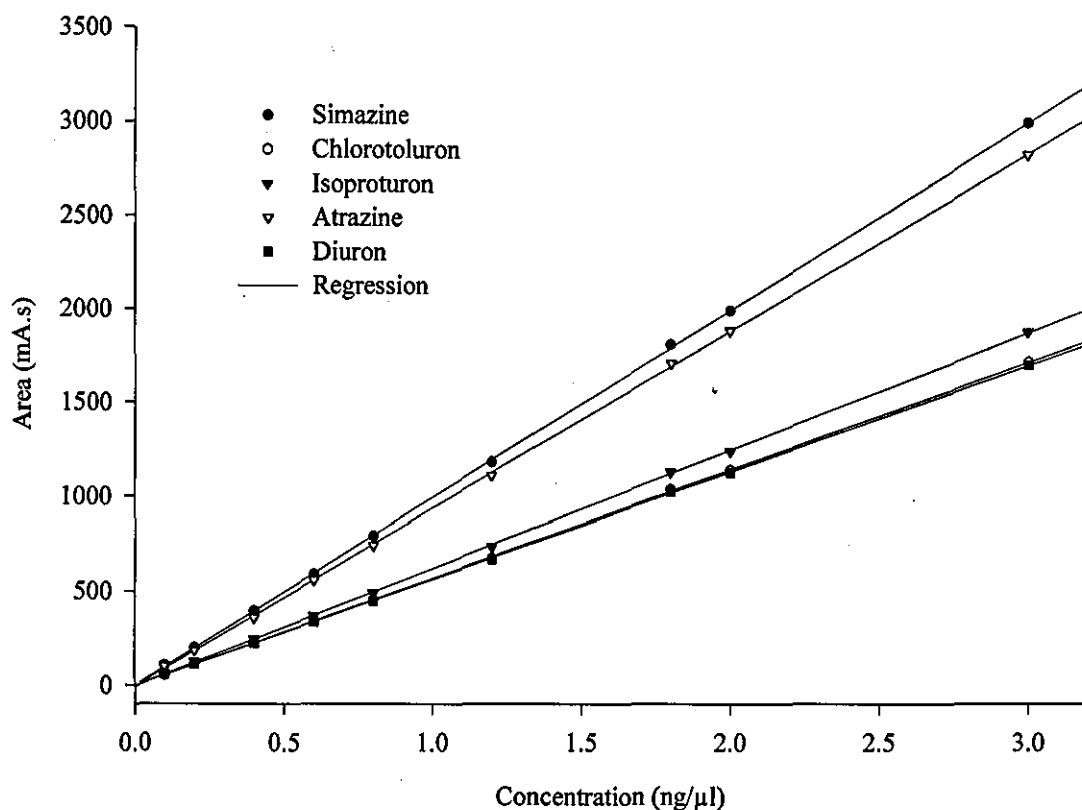


The final method used an isocratic elution using 29% of the organic phase, 60/40 acetonitrile/THF, and 71% water phase, 10mmol  $\text{KH}_2\text{PO}_4$  Buffer at pH 4.5. Detection was achieved at 230nm for the triazines and 244nm for the other pesticides using a slit width of 4nm. The 3mm column required a flow rate of 0.8ml/min which generated a pressure drop of 130bar. An injection volume of 100 $\mu\text{l}$  was used to maximise the response. The column thermostat was set at a temperature of 40°C.

Validation of the chromatographic method was then performed which included testing the specificity, linearity, accuracy, sensitivity, precision and ruggedness of the method.

The method is linear over the range 0-6ng/ $\mu\text{l}$  with correlation coefficients of 1.000 for all of the pesticides. The calibration graph, produced by multiple injections of different concentrations of external standard, can be see in Fig. 5.6. If low concentrations, less than 0.1ppb, are to be detected accurately a new calibration needs to be completed using the range 0-0.15ng/ $\mu\text{l}$ .

Fig. 5.6. HPLC calibration graph for Atrazine, Simazine, Isoproturon, Chlorotoluron and Diuron.



Before the other validation stages, it was necessary to conduct the solid phase extraction method development. This enabled the extraction procedure and HPLC analysis to be included in the validation. Table 5.5 summarises the solid phase extraction (SPE) procedure used for the analysis

**Table 5.5. Procedure for solid phase extraction.**

|                |                                                                                                                                                                                                                                                               |
|----------------|---------------------------------------------------------------------------------------------------------------------------------------------------------------------------------------------------------------------------------------------------------------|
| Conditioning   | 200mg, C8, non end capped 3ml SPE columns were conditioned by passing 3ml of HPLC grade methanol followed by 3ml of 2% MeOH in water under gravity.                                                                                                           |
| Extraction     | 500ml samples of solution were passed through the columns at a flow rate of 3ml/min. If the samples contained large particulate material a 10µm stainless steel filter was inserted in the column.                                                            |
| Drying         | The columns were dried using nitrogen for 10 minutes. If the 10µm filters were used in the extraction, the particulate were washed out of the column and the filters removed prior to the drying stage.                                                       |
| Elution        | 3ml of 10% formic acid in acetonitrile was passed through the column under gravity and the eluent collected in 7ml vials. The columns were then blown dry with nitrogen and the solvent evaporated to dryness using a stream of nitrogen or the freeze dryer. |
| Reconstitution | 500µl of 29% 40/60 THF/acetonitrile, 71% 10mmol $\text{KH}_2\text{PO}_4$ buffer at pH 4.5, was added to the vials to redissolve the analytes. The vials were shaken and their contents transferred to HPLC vials.                                             |

A 10 port manifold with PTFE valves, supplied by Jones Chromatography, was used for the solid phase extraction (SPE). The manifold is normally connected to a vacuum pump, with the flow rate through the columns being controlled by a needle valve, which increases or reduces the vacuum. The vacuum pump technique caused significant differences in the flow rates through the SPE columns which affected the recovery efficiencies. The system was improved by replacing the vacuum pump with a 0-100ml/min diaphragm metering pump, and removing the pressure indicator to prevent leaks. Prior to the extraction, the glass tank was filled with three litres of water. The new technique allowed accurate control of the flow rate through the columns.

C8 rather than C18 SPE columns were selected to enable easier recovery of the pesticides, since the slightly more hydrophilic C8 columns would have weaker binding energies enabling easier



recovery of the hydrophobic pesticides. 200mg 3ml columns were suitable for the 500ml samples since the concentrations to be analysed were extremely low. Initial extractions suggested recovery efficiencies of approximately 70% which may have been caused by breakthrough of the SPE columns or compounds being retained on the silica. Experiments were performed with one column on top of the other which suggested that breakthrough was occurring. This was attributed to inadequate wetting of the C8 silica which was overcome by using a methanol/water wash in the condition stage rather than just water. A flow rate change of 3 to 4ml/min had no effect on the breakthrough. Recovery efficiencies were improved to 75% which suggested that the pesticides were being retained by the silica. The columns were then eluted with successive 3ml washes of acetonitrile which improved the recovery efficiencies. Formic acid and triethylamine, at a concentration of 10%, were added to the acetonitrile to see if the recovery efficiencies could be improved. The 10% formic acid/acetonitrile mix enabled total recovery in 3ml. Elution curves indicated that the pesticides were desorbed in approximately 1.5ml. However, 3ml was selected for the elution quantity to guarantee total recovery.

The concentrations expected for analysis were in the range 0-5ppb and so the method was validated up to 150% of the anticipated range. The reproducibility of the method was tested by conducting 38 separate determinations of 0.1ppb of each pesticide in ultrapure water. Table 5.6 summarises the results.

**Table 5.6.** Means, relative standard deviations and recoveries for the determination of simazine, chlorotoluron, isoproturon, atrazine and diuron at a concentration of 0.1µg/l.

|               | Mean (µg/l)   | RSD        | Recovery |
|---------------|---------------|------------|----------|
| Simazine      | 0.104         | 4.1        | 106      |
| Chlorotoluron | 0.101 (0.103) | 2.9 (16.5) | 96 (103) |
| Isoproturon   | 0.105 (0.083) | 3.5 (20.5) | 98 (83)  |
| Atrazine      | 0.100         | 4.3        | 98       |
| Diuron        | 0.103 (0.103) | 3.3 (27.2) | 99 (103) |

Figures in brackets are those presented by the Drinking Water Inspectorate Guidelines [49]. RSD=Relative standard deviation

Fig. 5.7 presents the recovery of each compound with the mean indicated by a solid line and the standard deviation shown by the dotted lines.

**Fig. 5.7.** Recovery efficiency of pesticides at a concentration of 0.1ppb.

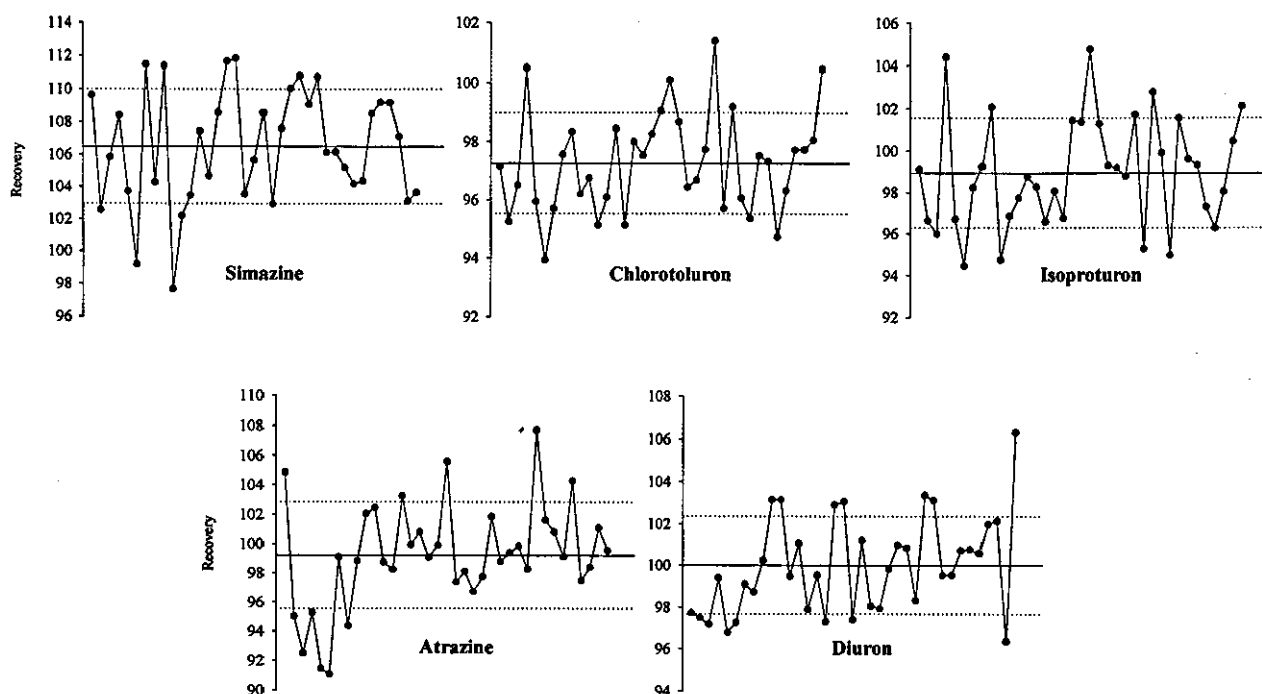


Table 5.7 presents the recovery efficiencies for the analysis of pesticides in the range 1-8 $\mu$ g/l based on four determinations for each concentration. The recovery efficiencies of chlorotoluron, isoproturon, atrazine and diuron are not affected by increasing the concentration of the pesticides to 8ppb. However, a slight reduction is observed for simazine. Simazine is an early-eluting compound and so it is probably breaking through the SPE column. This hypothesis was confirmed by using the double column technique mentioned previously. The effect of an increased SPE flow rate on the recovery efficiency was significant for simazine. At a flow rate of 4ml/min the recovery efficiency reduced to 85%, hence, care had to be taken in setting the flow rate when high concentrations of simazine were anticipated.

The limit of detection for each compound was determined directly by solid phase extraction and subsequent HPLC analysis of low concentrations of the pesticide mix. The analysis was

**Table 5.7.** Recovery efficiency for the determination of simazine, chlorotoluron, isoproturon, atrazine and diuron at a concentration range of 1-8 $\mu$ g/l.

| Concentration of<br>each pesticide ( $\mu$ g/l) | Recovery % |               |             |          |        |
|-------------------------------------------------|------------|---------------|-------------|----------|--------|
|                                                 | Simazine   | Chlorotoluron | Isoproturon | Atrazine | Diuron |
| 1                                               | 100.7      | 103.7         | 100.8       | 100.0    | 100.2  |
| 2                                               | 98.1       | 103.5         | 101.0       | 99.5     | 101.5  |
| 3                                               | 99.2       | 102.4         | 100.0       | 99.0     | 101.1  |
| 4                                               | 98.1       | 102.5         | 100.3       | 100.7    | 100.3  |
| 5                                               | 98.4       | 103.8         | 101.4       | 100.3    | 101.3  |
| 6                                               | 98.7       | 103.0         | 100.7       | 101.2    | 100.8  |
| 7                                               | 98.4       | 103.0         | 100.7       | 100.9    | 100.7  |
| 8                                               | 97.8       | 102.4         | 100.2       | 100.5    | 100.1  |

conducted using a column that was near end of life to ensure a representative reading was obtained. The absolute limit of detection for the pesticides was 0.003 $\mu$ g/l or 3 parts per trillion (ppt). The limit of determination, which is defined as the minimum level of analyte which can reliably be determined, for the pesticides are presented in Table 5.8. The values were based on the lowest concentration that the HPLC could quantify as the pesticide, based on retention time.

**Table 5.8.** Limits of determination for analytical method.

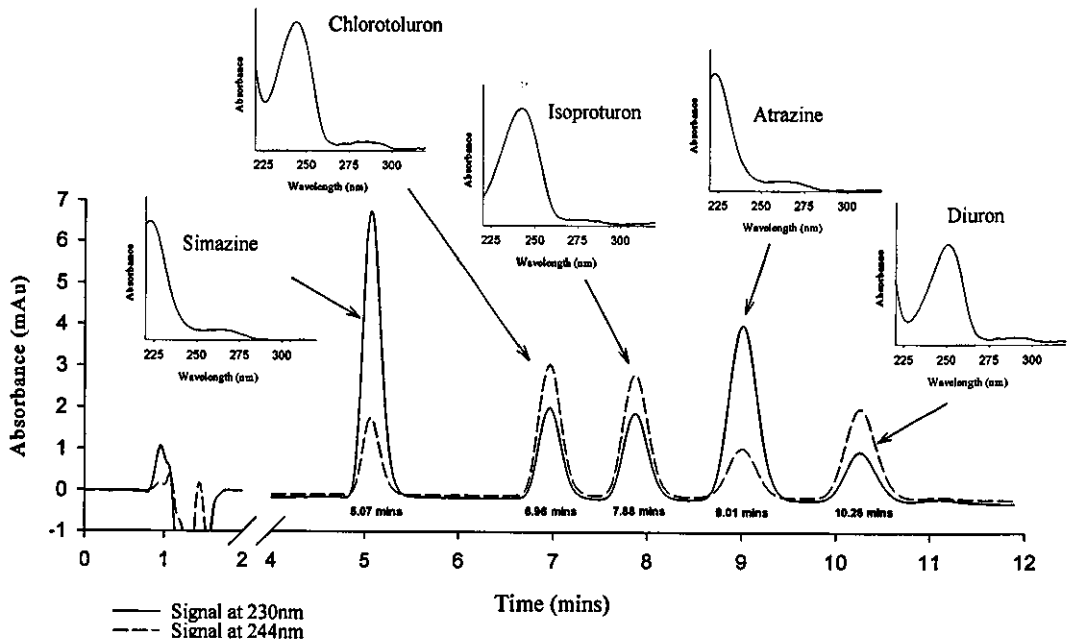
|                  | Simazine | Chlorotoluron | Isoproturon | Atrazine | Diuron |
|------------------|----------|---------------|-------------|----------|--------|
| LOD ( $\mu$ g/l) | 0.004    | 0.004         | 0.004       | 0.004    | 0.006  |

The ruggedness of the method was also validated by using columns from different batches and by a different analyst (D. J. Horner). The effect of slight variations in temperature, flow and solvent composition was studied. The HPLC pump was purged prior to analysis and the system allowed to stabilise for 1 hour before the analysis commenced. When the stabilized pressure exceeded 135bar the guard column was changed. Table 5.9 summarises the analytical method with a typical chromatogram shown in Fig. 5.8.

Table 5.9. Determination of pesticides in waters by reversed phased HPLC.

|                             |                                                                                                                                                                                                                                                                                                                                                 |
|-----------------------------|-------------------------------------------------------------------------------------------------------------------------------------------------------------------------------------------------------------------------------------------------------------------------------------------------------------------------------------------------|
| Substances determined       | Simazine, chlorotoluron, isoproturon, atrazine, diuron, and mecoprop.                                                                                                                                                                                                                                                                           |
| Type of sample              | Ultrapure water                                                                                                                                                                                                                                                                                                                                 |
| Basis of method             | The determinands are extracted by C8 solid phase extraction columns (200mg, 3ml), eluted using 10% formic acid in acetonitrile and evaporated to dryness. 25% 40/60% THF/Acetonitrile, 75% buffer is added and the extracts analysed by HPLC using UV detection. A Genesis C18 column (4µm, 150×3.0mm) and a 1cm Genesis guard column was used. |
| Range of application        | Up to 8µg/l for each pesticides. The range may be extended by dilution of the sample extract or by taking a smaller sample volume                                                                                                                                                                                                               |
| Calibration curve           | The method is linear over the range of application                                                                                                                                                                                                                                                                                              |
| Relative standard deviation | See Table 5.6.                                                                                                                                                                                                                                                                                                                                  |
| Limit of determination      | See Table 5.8.                                                                                                                                                                                                                                                                                                                                  |
| Bias                        | Extraction efficiencies are nominally 100%                                                                                                                                                                                                                                                                                                      |
| Interferences               | Any co-extracted material which has a similar retention time to the compounds of interest and which gives a detector response at a wavelength of 230nm will interfere. Analysis can be achieved with high levels of fulvic and humic acid with significant reduction in RSDs and LODs.                                                          |
| Time for analysis           | Approximately 10 samples per day                                                                                                                                                                                                                                                                                                                |

Fig. 5.8. HPLC chromatogram of pesticide mix at a concentration of 0.1µg/l.



## SECTION 5.4      EXPERIMENTAL

### *Batch Experiments*

Batch adsorption isotherms were performed by shaking 500ml amber Winchester bottles, with PTFE liners, in a Gallenkamp incubator shaker. The shaker was set to 150rpm and thermostatically controlled at  $26 \pm 1^\circ\text{C}$ . Initial solution concentrations of 1, 5, 10, 15, 20, 35, 50, 75 and 100  $\mu\text{g/l}$  were prepared by pipetting different quantities of each pesticide, at concentration of 10mg/l, into ultrapure water in the bottles. The total volume of solution in each bottle was 500ml. A Sartorius, model BP 210D, analytical balance was used to weigh out 2.50mg quantities of each adsorbent onto foil dishes. The adsorbent was washed into the bottles using 5ml of solution extracted from the bottle. The bottles were agitated vigorously before shaking for 72 hours. The solutions were analysed using the procedure outlined in section 5.3. The pH of the solutions were analysed before and after shaking.

Pesticide solutions were prepared by dissolving 30mg of pesticide in two litres of ultrapure water contained in 2.5 litre amber Winchester bottles. The solutions were placed in an ultrasonic bath for 15 minutes. Difficulties in dissolving the compounds necessitated filtration of the concentrated pesticide solutions, using Millipore solvent filtration apparatus. Anopore ceramic filters, with a pore diameter of 0.1  $\mu\text{m}$ , were used. The solutions were then diluted using ultrapure water to 10mg/l, determined by HPLC analysis. Pesticide mix solutions were prepared by mixing equal quantities of the individual pesticides, thus creating a 10mg/l solution containing 2mg/l of each pesticide.

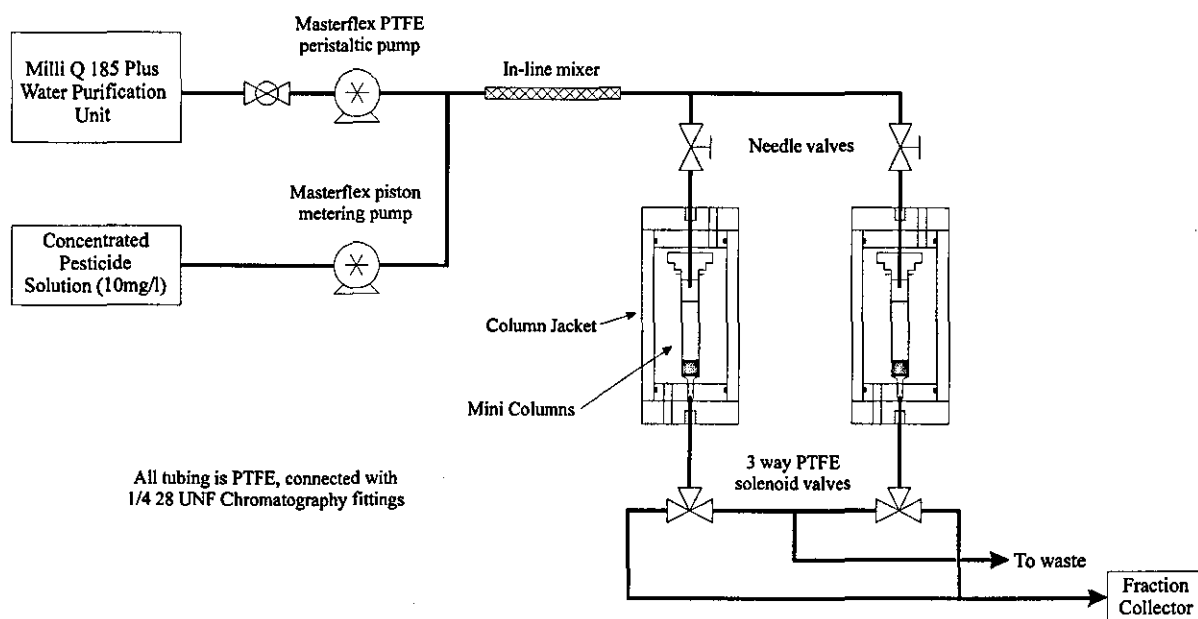
Single component isotherms were performed for MN-200 sorbing simazine, chlorotoluron, isoproturon, atrazine and diuron. Multi-component isotherms using all the pesticides were completed for MN-100, MN-150, MN-200 and F-400. An adsorption isotherm was performed for MN-200 sorbing the pesticide mix in the presence of a 20mg/l solution of fulvic acid. The experimental procedure is the same as that for the pesticide mix isotherms mentioned above except that a 20mg/l solution of fulvic acid was used rather than ultrapure water.

Adsorption isotherms for MN-200 sorbing humic and fulvic acid were performed at a concentration of 10 and 20mg/l respectively. The solutions were prepared by dissolving appropriate quantities of the humic and fulvic acid in 11 litres of ultrapure water. The pH of the solution was adjusted to 6.8 using 0.1M sodium hydroxide. The mass of adsorbent added to the 500ml of solution was varied from 2.5mg up to 320mg. The concentration in solution was analysed using a Perkin Elmer Lambda 12 UV-Vis spectrophotometer at a wavelength of 254nm. A matched pair of Hellma silica cuvettes were used for the analysis. The solutions were filtered, using filtration columns containing a 10 $\mu$ m stainless steel filter, prior to analysis. The pH of the solution was measure before and after the analysis.

### Mini-column Experiments

Mini-columns, with a bed volume of 0.65ml (8.7mm diameter, 11mm height) were prepared using MN-200 and F-400 in the size range 53-75 $\mu$ m (wet sieved). The adsorbents were wet packed into methanol washed polyethylene SPC columns using 10 $\mu$ m stainless steel frits as bed supports. The columns were then washed using 1 litre of ultrapure water to eliminate any fines. The experimental rig, illustrated in a simplified flow diagram (Fig. 5.9), consists of three sections.

Fig. 5.9. Simplified flow diagram of experimental apparatus.



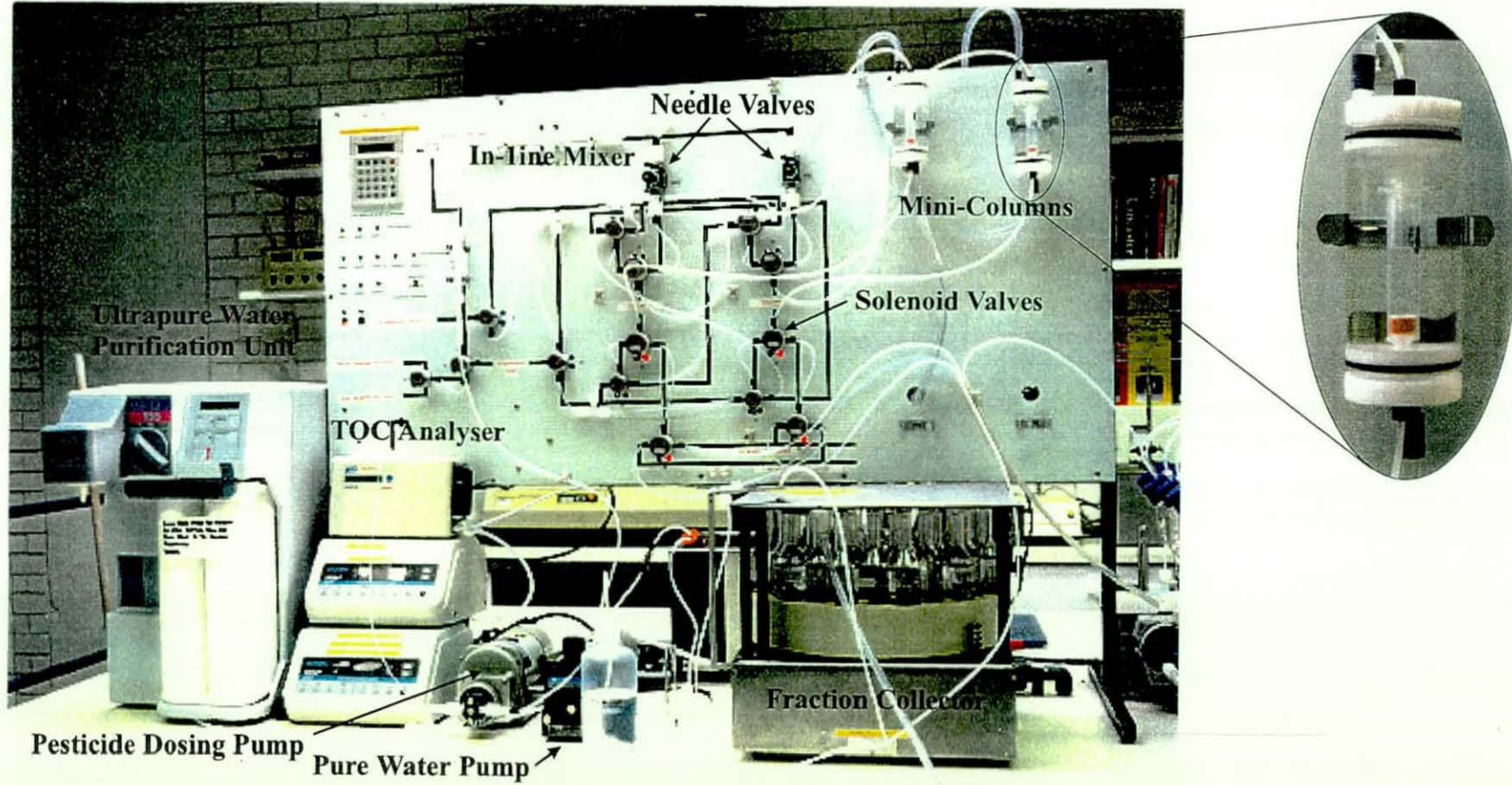
The first is the preparation of spiked ultrapure water solution, followed by the adsorption onto thermostatically controlled columns, with the effluent collected in a fraction collector.

The feed solution used for the experiments was prepared on-line by dosing the concentrated pesticide solution into ultrapure water (Grade 1) produced by a MilliQ 185 Plus water purification unit. The purification unit was connected to a level controlled 30l buffer tank which was gravity fed by a 200l tank containing grade 2 water. Makeup of the level controlled grade 2 tank was achieved using a Millipore Elix 10 water purification unit. The total organic carbon (TOC) content of the ultrapure water was determined using an Anatel A10 monitor capable of measuring a TOC range of 0-200ppb with an accuracy of 2%. To prevent the MilliQ185 plus from overheating, caused by continuous recirculation of a small volume of water through the gear pump and UV chamber, the Anatel monitor was used to enable a recycle stream back to the buffer tank. The TOC analysis consisted of three cycles; flushing, photo-oxidation of a small sample and measurement of the conductivity. The ultrapure water passed through the analyser at a flow rate of approximately 500ml/min, during the flush cycle, which enabled the recirculation loop to have a volume of about 30 litres. This successfully prevented the heat generation problems and conserved significant quantities of flush water which is normally sent to drain.

A feed solution containing 20µg/l of simazine, chlorotoluron, isoproturon, atrazine and diuron was prepared on-line by dosing a flow of 0.1ml/min of a 10mg/l pesticides mix solution into a flow of 9.9ml/min ultrapure water. Both pumps used Masterflex digitally controlled drives that enabled accurate speed control. A Masterflex PTFE peristaltic pump head was used to deliver the ultrapure water with the concentrated pesticide dosed using a FMI ceramic metering pump head having a maximum stroke volume of 50µl. A stainless steel static in-line mixer was used to obtain a homogenous solution. Needle valves were used to adjust the flow through the two columns to 5ml/min. The mini columns were thermostatically controlled at  $25 \pm 1^\circ\text{C}$  using water circulated from a temperature controlled water bath. The effluent from the two columns was directed either to the fraction collector or to waste using three-way PTFE solenoid valves. All wetted parts of the experimental rig were either stainless steel, glass or PTFE. The rig contains other three-way solenoid valves that enable up-flow regeneration and washing of the beds. A

Fig. 5.10.

Photograph of column experimental apparatus.





photograph of the experimental apparatus can be seen in Fig. 5.10. The fraction collector designed by the author consisted of 48, 100ml bottles, that enabled eight 600ml samples to be collected before emptying the bottles. The collector was controlled using a Mitsubishi FXo 14 I/O programmable logic controller (PLC) connected to a data access panel that enabled alteration of the timer constants. The PLC programme, written by the author, enabled total flexibility in collection modes. Normally, the collector was set to collect six bottles in a row over a 2 hour period. To ensure a fresh sample was passed into each group of bottles, from the columns, the solution was sent to drain for 1 hour prior to the collection of each sample. The flow path of the fraction collector enabled zero dead volume. A solenoid valve inside the fraction collector bypassed the flow while the arm moved into the collection or drain position. The valves on the column rig, used to send the flow from column 1 or 2 to waste or to the fraction collector, were controlled using a Mitsubishi FX PLC. Samples from column two were collected in the first three hours followed by column one in the second three hours. This cycle was repeated until all the bottles were filled on the fraction collector. A 50 minute delay, before the collection of the first sample, enabled a thorough flush of the system.

The samples from the fraction collector were weighed into 1 litre glass bottles prior to solid phase extraction followed by HPLC analysis of the extract. The flow rates through the columns were calculated based on the weight of each sample, and the needle values adjusted if necessary.

Mini-column pesticide adsorption experiments were also performed using a 10mg/l background solution of fulvic acid. The concentration of fulvic acid in the concentrated pesticide solution was 1g/l. A virgin carbon column containing 300mg of F-400 was used for the experiment. The polymer column had undergone two regeneration cycles using ethanol and had been in operation for six months.

### ***Humic and Fulvic Acid Purification***

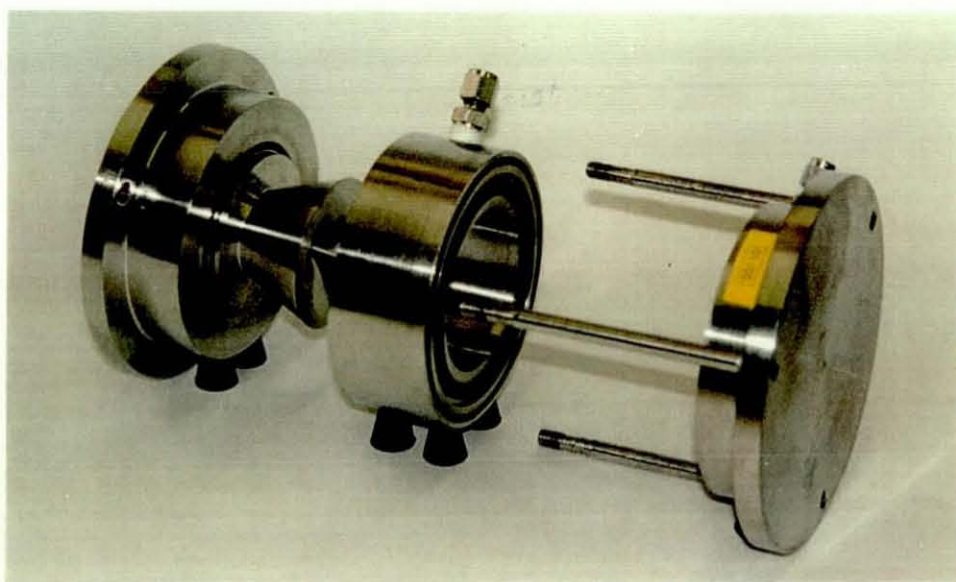
The Aldrich humic acid, sodium salt, was separated to produce humic and fulvic acid. 100g of the sodium salt were dissolved in 2.5 litres of water and filtered using a 0.12µm 90mm micro filtration membrane. The permeate was adjusted to pH 1 using concentrated hydrochloric acid.

After two hours the fulvic acid solution containing the precipitated humic acid was filtered using a Buchner flask to separate the two fractions. The precipitate was washed with 0.1M HCl and then redissolved in ultrapure water. Both the fulvic and humic acid solutions were adjusted to pH 7 using sodium hydroxide prior to rotary evaporation. The concentrated solutions were then freeze dried to obtain solid humic and fulvic acid.

### *Ultrafiltration*

The ultrafiltration equipment consisted of a stainless steel cell, that used 90mm membranes, connected to a Masterflex PTFE 0-800ml/min diaphragm pump head. The pump circulated the retentate from the feed tank through the cell and back to feed tank. A pressure control valve was installed on the return line to enable a pressure of 3 bar to be maintained. The permeate was recycled back to the feed tank. Fig. 5.11 presents a photograph of the stainless steel cell.

**Fig. 5.11.** Photograph of the ultrafiltration cell.



Ultrafiltration experiments were performed using an Amicon YC05 membrane which has a 500 Dalton molecular weight cut off. Solutions of 10mg/l pesticide mix and 20mg/l fulvic acid solution were passed separately through the filter. Samples of the permeate and retentate were taken every 10 minutes. A fulvic acid and pesticide mix was also passed through the cell with the permeate returned to a separate vessel.

***High concentration column experiments***

The apparatus used for the batch kinetics studies was modified to enable on-line monitoring of the breakthrough curve for high concentration mini-column experiments. The batch vessel was replaced by a 10 litre feed tank and the mini column placed in the circuit after the peristaltic pump. Standard Isolute column adapters were used to connect the mini-column to a male Luer adapter which connected to 1/8" PTFE tubing. The bottom of the column was connected by a stainless steel female Luer to 1/4" UNF chromatography fitting. The effluent from the column was passed through the UV spectrophotometer before going to waste.

SECTION 5.5 RESULTS AND DISCUSSION

Batch Studies

Single component adsorption isotherms for MN-200 sorbing simazine, chlorotoluron, isoproturon, atrazine and diuron can be seen in Fig. 5.12. Fig. 5.13 illustrates the adsorption isotherms for MN-100, MN-150 and MN-200 sorbing atrazine. Multi-component isotherms are presented in Figs. 5.14-16. Table 5.10 presents the Freundlich coefficients for the single and multi-component adsorption isotherms.

Table 5.10. Freundlich and correlation coefficients for the adsorption of pesticides.

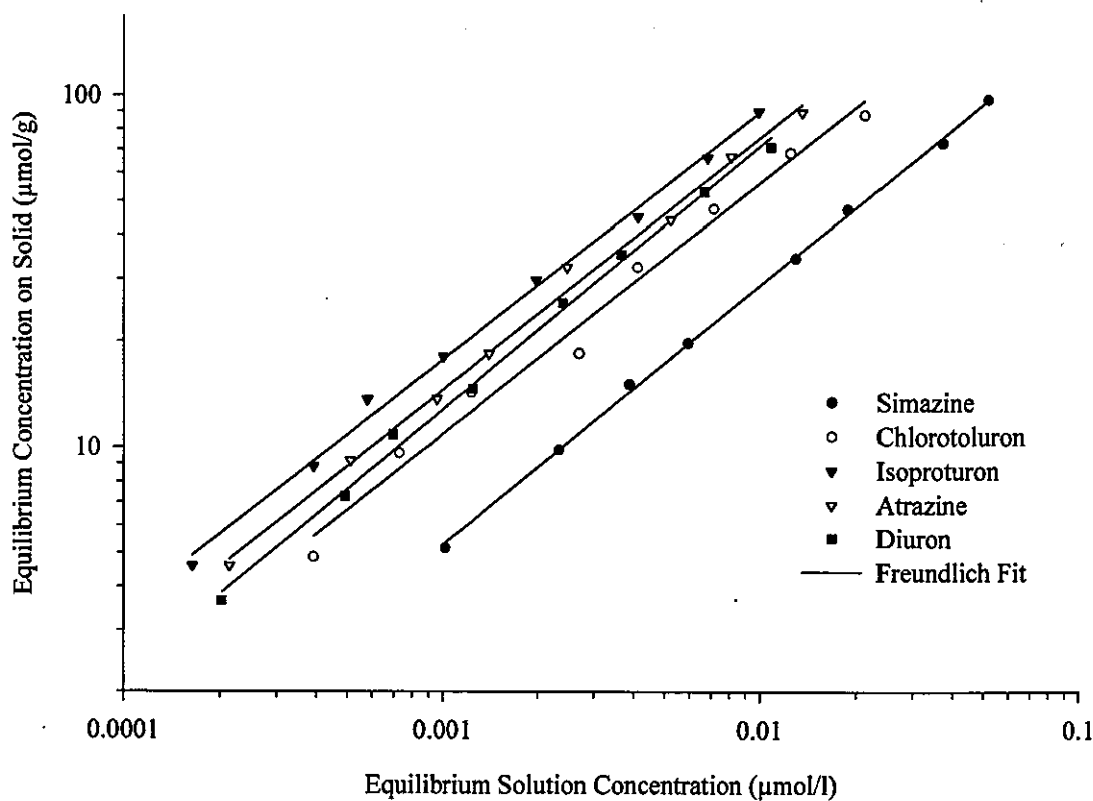
|         | Simazine |            | Chlorotoluron |            | Isoproturon |            | Atrazine |            | Diuron   |            |
|---------|----------|------------|---------------|------------|-------------|------------|----------|------------|----------|------------|
|         | <i>K</i> | <i>1/n</i> | <i>K</i>      | <i>1/n</i> | <i>K</i>    | <i>1/n</i> | <i>K</i> | <i>1/n</i> | <i>K</i> | <i>1/n</i> |
| MN-100  | 478      | 0.724      | 826           | 0.746      | 2641        | 0.825      | 4410     | 0.899      | 1852     | 0.823      |
| MN-150  | 550      | 0.718      | 1150          | 0.783      | 3288        | 0.874      | 3300     | 0.869      | 2339     | 0.844      |
| MN-200  | 440      | 0.697      | 1273          | 0.758      | 6421        | 0.893      | 3023     | 0.825      | 2374     | 0.814      |
| MN-200* | 864      | 0.738      | 1520          | 0.715      | 2323        | 0.706      | 2073     | 0.718      | 2073     | 0.718      |

|         | Correlation Coefficients |               |             |          |        |
|---------|--------------------------|---------------|-------------|----------|--------|
|         | Simazine                 | Chlorotoluron | Isoproturon | Atrazine | Diuron |
| MN-100  | 0.996                    | 0.995         | 0.990       | 0.984    | 0.990  |
| MN-150  | 0.998                    | 0.994         | 0.986       | 0.987    | 0.989  |
| MN-200  | 0.997                    | 0.996         | 0.988       | 0.990    |        |
| MN-200* | 0.999                    | 0.986         | 0.996       | 0.995    | 0.997  |

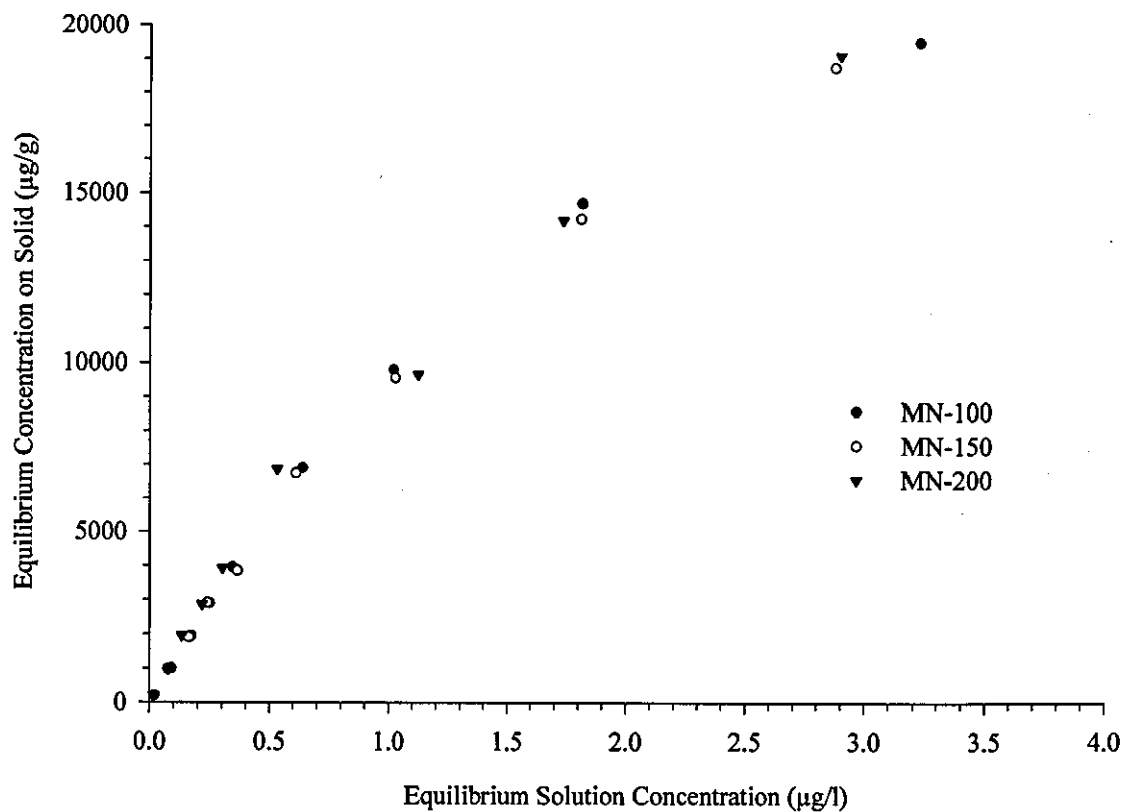
\* Coefficients for single component adsorption isotherms. Constants based on units of *q*, (μmol/g) and units of *c*, (μmol/l)

The isotherms suggest the that polymers show selectivity towards the different pesticides which follows the sequence isoproturon>atrazine>diuron>chlorotoluron>simazine. Comparison of the uptake for each pesticide indicates that the highest uptake is achieved for single component adsorption. There appears to be little difference in the uptake of the different polymers in single or multi-component adsorption. However, MN-200 consistently has a higher capacity. The

**Fig. 5.12.** Single component adsorption isotherms for MN-200 sorbing simazine, chlorotoluron, isoproturon, atrazine and diuron.



**Fig. 5.13.** Single component adsorption isotherms for MN-100, MN-150 and MN-200 sorbing atrazine



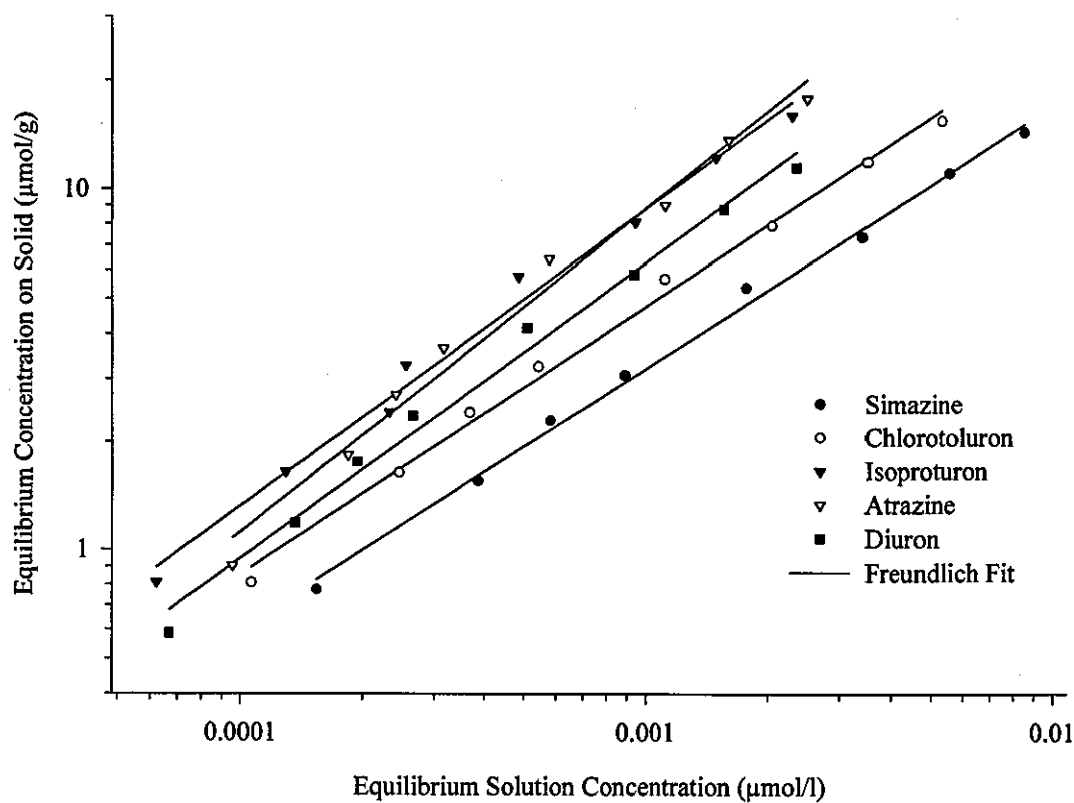
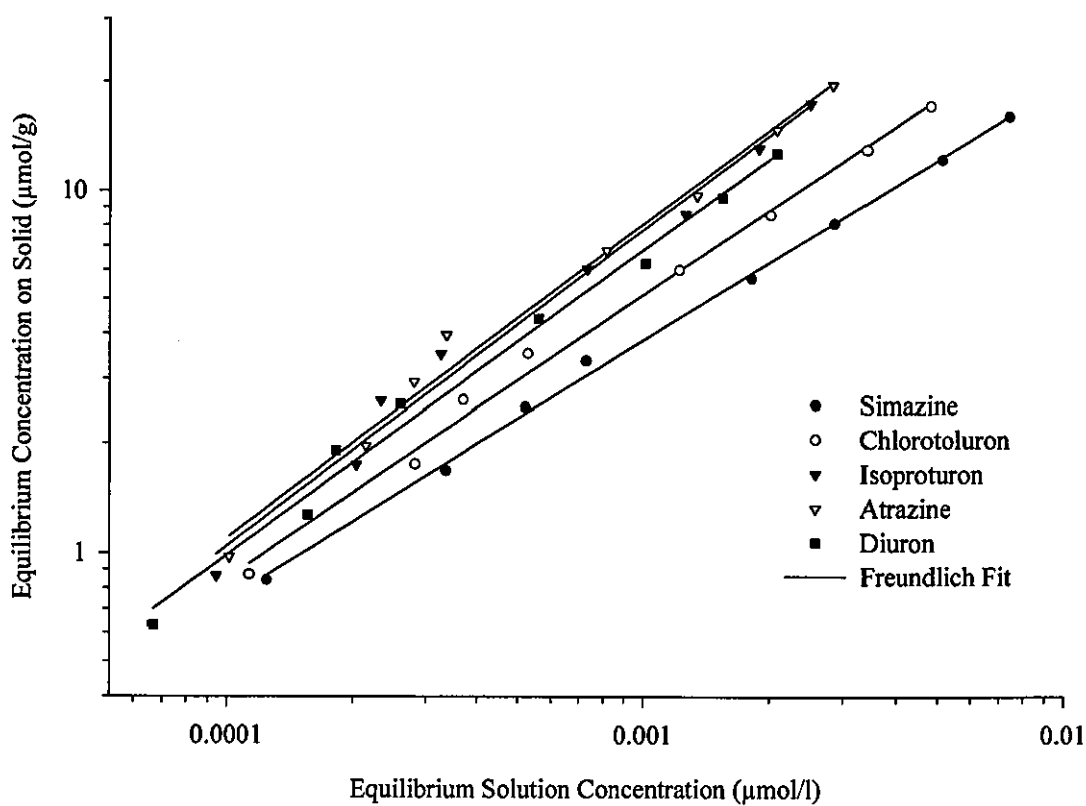
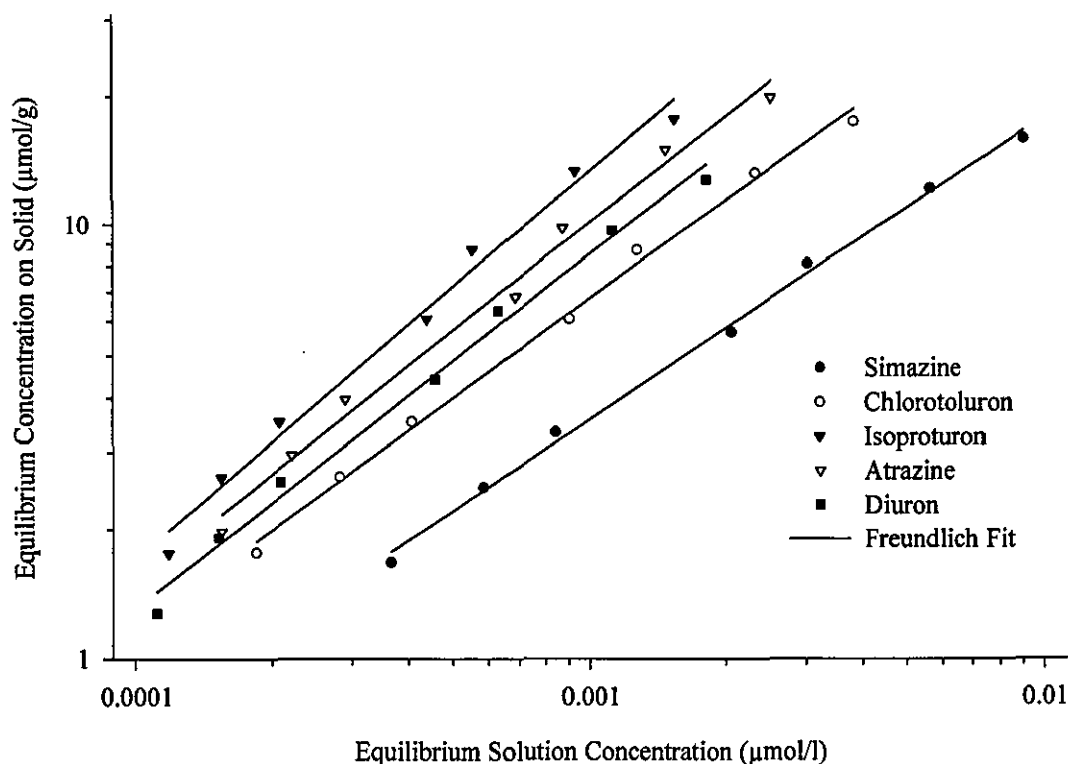
**Fig. 5.14.** Multi-component adsorption isotherms for MN-100.**Fig. 5.15.** Multi-component adsorption isotherms for MN-150.

Fig. 5.16. Multi-component adsorption isotherms for MN-200.



gradient of isotherms shown in log-log format provides the Freundlich  $1/n$  coefficient, indicative of the strength of interaction for adsorption. No clear trends in the data are observed due to the similar values. In general, it appears that isoproturon and atrazine have the lowest adsorbate-adsorbent interaction followed by diuron, chlorotoluron and simazine. Figs. 5.18 and 5.19 present the molecular structure of the pesticides modelled using a molecular modelling software package called Sybyl (Version 6.0 1992). Table 5.11 lists some of the physical properties of the pesticides.

The adsorption of pesticides may involve several mechanisms, the main ones being; 1) physical adsorption, or van der Waals forces, 2) H-bonding, 3) electrostatic attraction or chemical adsorption, and 4) coordination complexes. The octanol-water partition coefficient gives an indication of the hydrophobic-hydrophilic nature of the pesticides. If it is assumed that hydrophobic interactions dominate the adsorption process then the polymers should have the highest adsorption capacity for diuron followed by atrazine, chlorotoluron, isoproturon and simazine. The data follows this trend with two exceptions, atrazine and isoproturon. This suggests that the hydrophobic attraction is the dominant force for the sorption of diuron,

**Fig. 5.17.** Comparison of multi-component adsorption isotherms for MN-100, MN-150, MN-200 and single component isotherms for MN-200 sorbing simazine, chlorotoluron, isoproturon, atrazine and diuron.

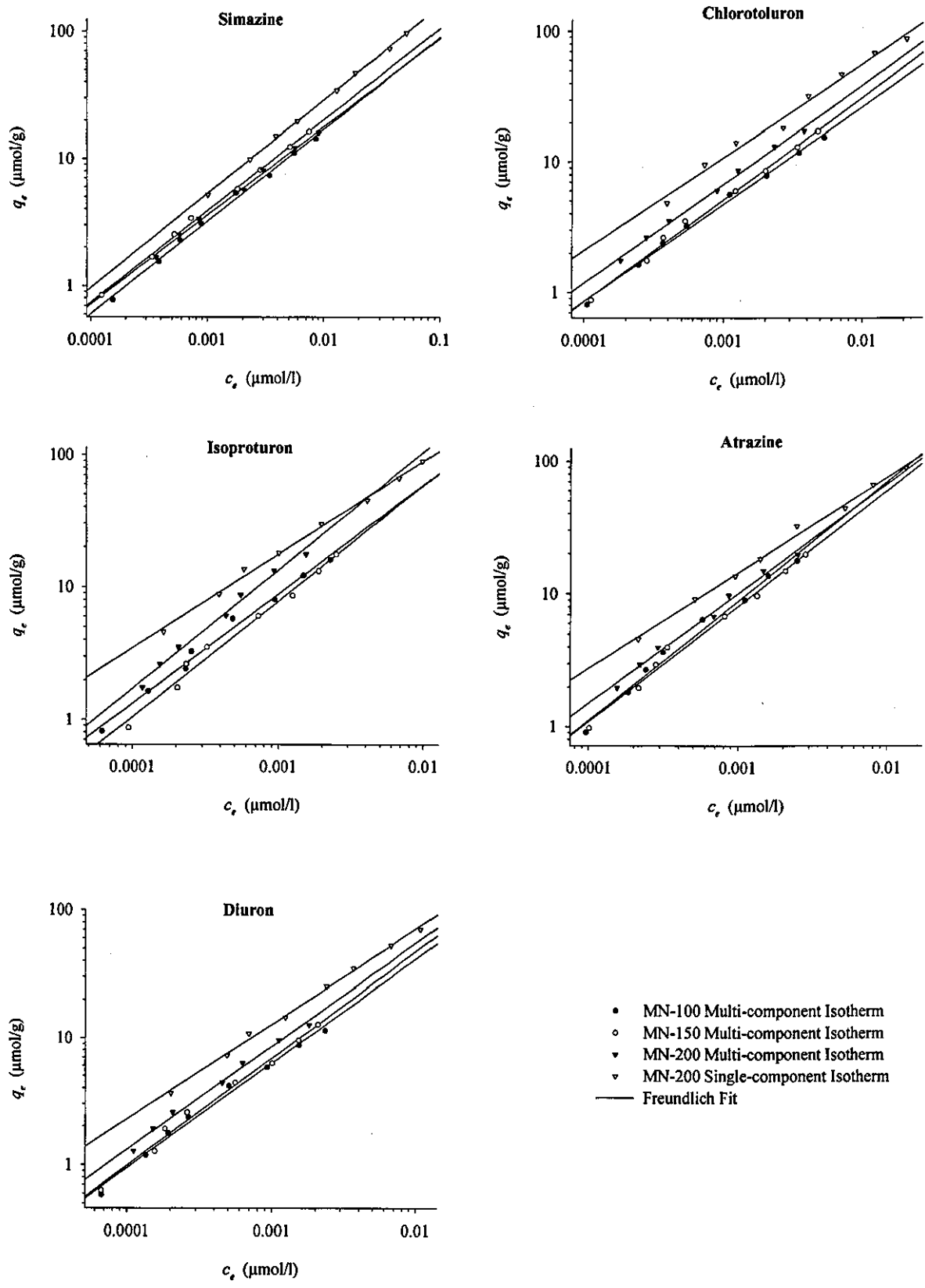
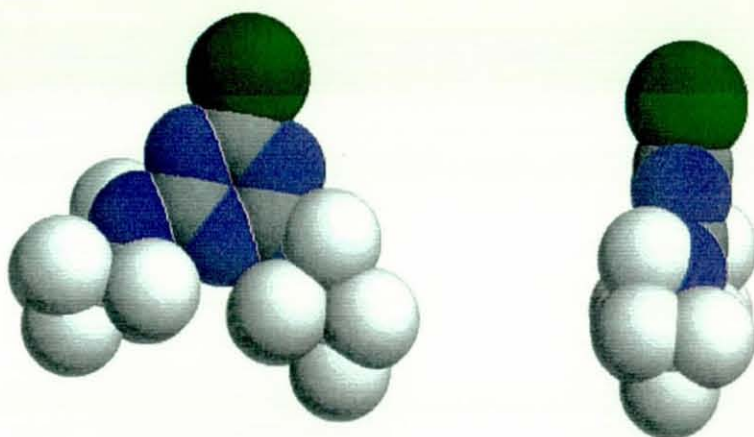


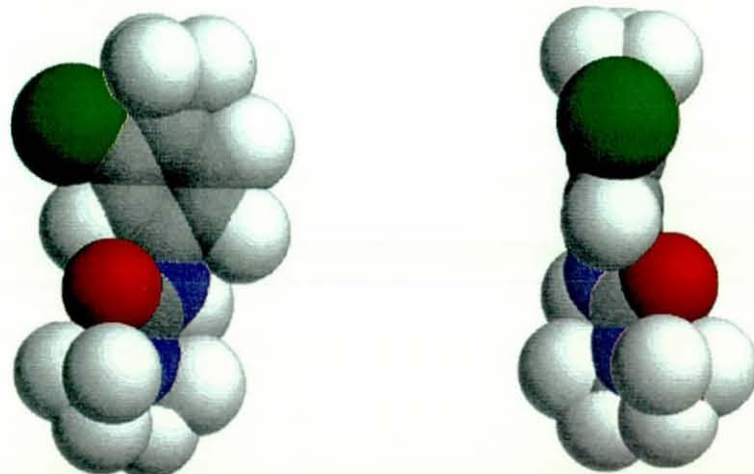


Fig. 5.18. Molecular structure of simazine, chlorotoluron and isoproturon.

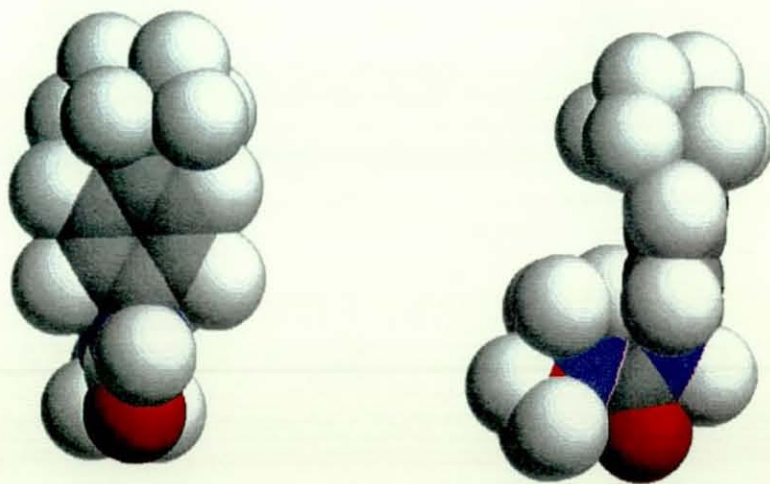
**Simazine**



**Chlorotoluron**



**Isoproturon**



Scale:

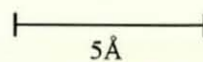
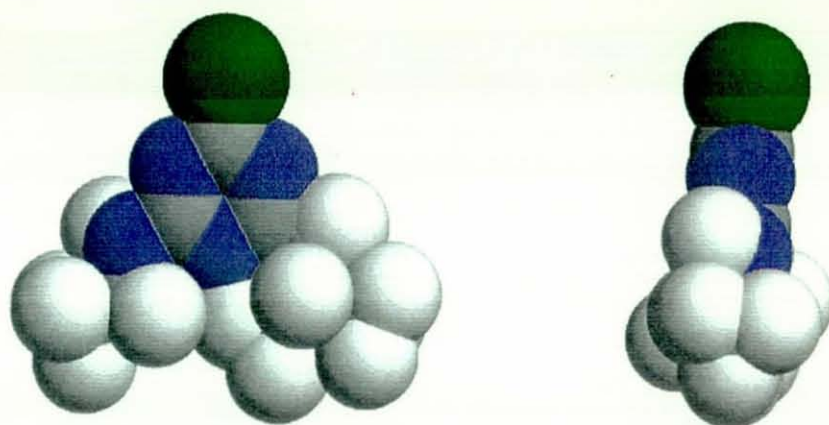
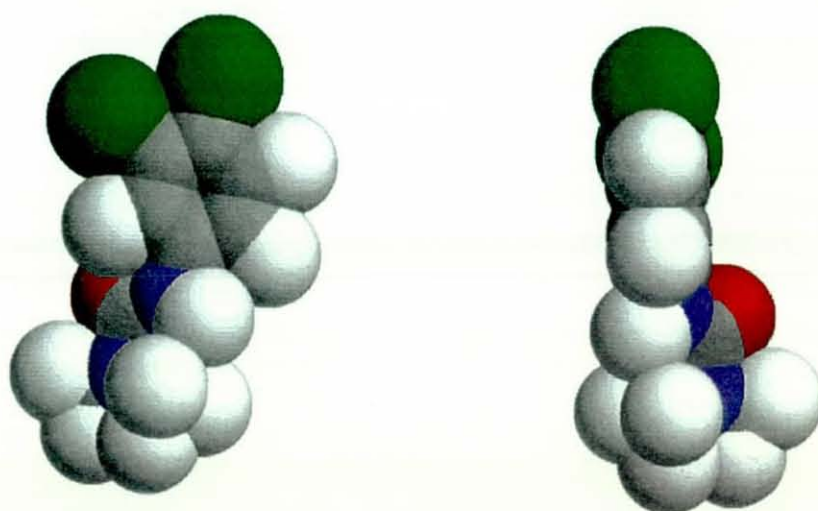


Fig. 5.19. Molecular structure of atrazine and diuron.

Atrazine



Diuron



Carbon



Chlorine



Oxygen

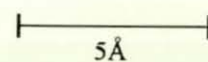


Hydrogen


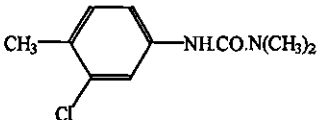
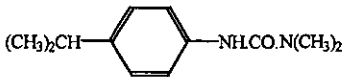
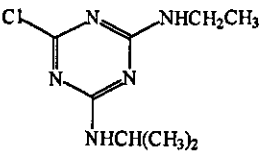
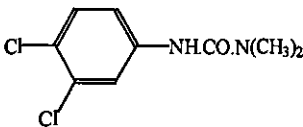


Nitrogen

Scale:



**Table 5.11. Physical properties of simazine, chlorotoluron, isoproturon, atrazine and diuron.**

|                            | Structure                                                                           | Molecular Weight | pKa  | Solubility in H <sub>2</sub> O (mg/l) | log <i>k</i> <sub>ow</sub> |
|----------------------------|-------------------------------------------------------------------------------------|------------------|------|---------------------------------------|----------------------------|
| Simazine <sup>†</sup>      |    | 201.66           | 1.62 | 6.2                                   | 2.10                       |
| Chlorotoluron <sup>‡</sup> |    | 212.69           | -    | 70                                    | 2.29                       |
| Isoproturon <sup>‡</sup>   |    | 206.29           | -    | 55                                    | 2.25                       |
| Atrazine <sup>†</sup>      |   | 215.69           | 1.70 | 33                                    | 2.68                       |
| Diuron <sup>*</sup>        |  | 233.10           | -    | 42                                    | 2.80                       |

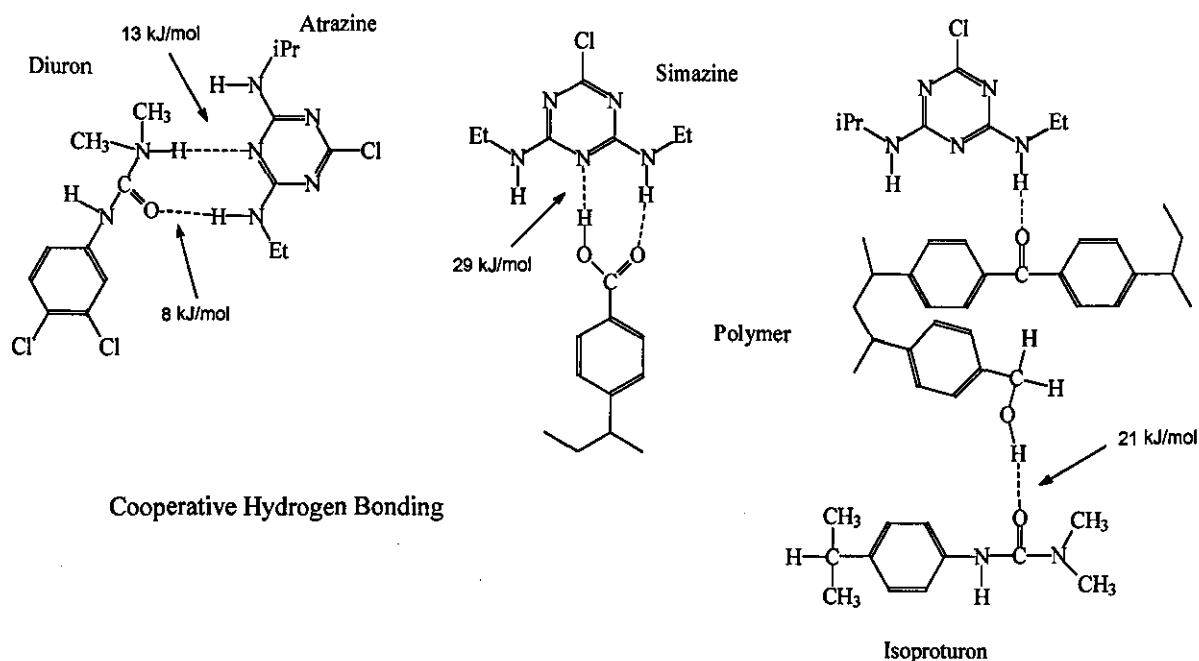
<sup>†</sup> Ciba-Geigy Corporation Data (1989)<sup>\*</sup> Dupont Corporation Data (1989)<sup>‡</sup> The UK Pesticide Guide, Revised Edition, British Crop Protection Council, 1996

chlorotoluron and simazine. Simazine has an extremely low solubility in water, often indicative of a hydrophobic molecule, which seems to contradict the *k*<sub>ow</sub> value. Analysis of the molecular structure suggests that isoproturon is the smallest adsorbate with a width comparable to that of phenol, since the substituted urea tail is flexible. The substituent groups on chlorotoluron and diuron make these molecules marginally bigger, thus restricting their access to some of the micropores in the polymers. Atrazine and simazine are also likely to suffer from size exclusion since they are the largest pesticides in this study. Hence, despite isoproturon being the second most hydrophilic molecule its small molecular size enables it to penetrate into micropores which

are not accessible by the other pesticides. However, this argument is not sustainable for atrazine since it is larger and less hydrophilic than diuron.

The delocalisation of the side-chain nitrogen lone pairs in atrazine and simazine restricts the rotation of the groups and leads to separation of charge within the atrazine molecule. A positive charge develops on the side chain nitrogens while negative charge is delocalised around the triazine rings. Welhouse *et al* [50] used  $^{15}\text{N}$ -labelled NMR to confirm that the nitrogen para to the chloride substituent carries most of the redistributed electron density and is the site where atrazine is protonated. The separation of charge suggests that atrazine can be hydrogen-bond donating, from the side-chain NH, and hydrogen-bond accepting, to the triazine N. Similar arguments can be made for the other pesticides under investigation. Strong complexation was observed by Welhouse *et al* [51,52] between atrazine and amide and carboxylic acid functional groups as a result of cooperative interactions in which both partners in the complex donate and accept hydrogen bonds. Aromatic phenol and quinone like functional groups, common on adsorbents like activated carbon, may be capable of such complexation. This complexation may enhance or reduce the adsorption in a multi-component system. Fig. 5.20 indicates some of the possible hydrogen bonding between functional groups and other pesticides.

Fig. 5.20. Possible cooperative and normal hydrogen bonding of atrazine.



The substituted urea pesticides, such as diuron, have an amide-like structure which would suggest that strong hydrogen-bond complexes with atrazine or simazine may exist. Such complexation would make the molecules significantly bigger and reduce the possibility of the pesticides hydrogen bonding with functional groups on the polymers, thus reducing their sorption. Competition for the sites from polar solvents, such as water, will significantly reduce the complexation. However, Welhouse et al suggest that in the hydrophobic domain of soil matter hydrogen bonding is an important mechanism for atrazine adsorption. The approximate dissociation energies of various hydrogen bonds are indicated in Fig. 5.20. The OH--N bond is the strongest of the group due to the electrons of the nitrogen being loosely held, in comparison to oxygen, and the more positive hydrogen of the OH group.

Chapter 3 proposed a number of oxygen containing groups on all three polymers, such as carbonyl (ketones, carboxylic acid) and hydroxyl (phenols and alcohols), as well as the amine functionality of MN-100 and MN-150. Elemental analysis of the polymers suggested that the overall concentration of oxygen plus nitrogen atoms for MN-100, MN-150 and MN-200 is 6.03, 8.13, 6.43%. Hence, the hydrogen bonding potential of the polymer does not vary significantly, which seems to be confirmed by their similar adsorption capacity and mechanism for the pesticides. The narrow mean pore size of MN-150 will oppose the slightly higher interaction energies caused by the extra nitrogen and oxygen. It was hypothesised in Chapter 3 that MN-200 contained alcohol functional groups instead of the added amine groups of MN-100 and MN-150. The strength of the OH--N hydrogen bond is greater than the other combinations and so the adsorbent-adsorbate interaction energies for MN-200 would be expected to be slightly higher. On average, this is indeed the case.

Direct titration of the polymers and carbon suggested that they contain a number of cationic functional groups such as carboxyl, phenolic and quinone type groups. The weakly basic triazine pesticides have  $pK_a$ 's around 1.7 which suggests that they would be in protonated form at pH values found in drinking water supplies. The  $pK_a$  of the main cationic functional groups on carbons and polymers range from approximately five, for carboxylic acid groups, up to nine for phenolic groups. At a pH around 6 the carboxylic acid groups may be slightly dissociated allowing for cation exchange of the triazine pesticides, since there are no stronger bases in the

solutions. However, the carboxyl titration capacity of the polymers may be an artifact of trapped HCl, generated during the crosslinking reaction. The substituted urea pesticides will only exist in protonated form at higher pH values than those found in natural waters. Also, the compounds may break apart at the amide bond before protonation. Hence, the sorption of the pesticides by an ion exchange mechanism will be minimal.

Zeta potential analysis of MN-200 suggests that it will have a negatively charged surface from pH 4.5 upwards. MN-100 and MN-150 have zero crossover points at around pH 6.5-7 and so a slight shift in pH may cause them to have a surface charge which is positive or negative. There is no net charge on the pesticides at the pH of all the solutions used in the experiments and so electrostatic interactions will not influence the sorption.

A number of batch adsorption isotherms for F-400 were attempted. However, the results were not reproducible. This was due to the removal of the pesticides from the carbon fines, trapped in the solid phase extraction cartridges, during the elution stage. Filtration to 0.1  $\mu\text{m}$  improved the results although carbon fines were still visible in the SPE cartridges. Experiments using 300-400  $\mu\text{m}$  material, which appeared to contain fewer fines still proved to be problematical.

A wide variety of adsorption capacities exist in the literature for the adsorption of pesticides. Hopman [20] quoted a value of 36mg/g for F-400 for ROW 0.8 activated carbon adsorbing simazine. The capacity in this study is 3.5mg/g at an equilibrium concentration of 1  $\mu\text{g/l}$ . Speth *et al* [26] presented Freundlich coefficients of  $1/n = 0.291$  and  $K = 858$  for atrazine adsorption onto powdered F-400. The single component adsorption capacity of MN-200 is greater than that of F-400. However, the coefficient  $K$  is strongly dependent on the value of  $1/n$  and so no direct comparisons can be made. At an equilibrium concentration of 0.01  $\mu\text{mol/l}$  the solid phase concentrations are 224  $\mu\text{mol/g}$  for F-400 compared to 76  $\mu\text{mol/g}$  for MN-200 (calculated using the Freundlich coefficients presented above). This data suggests that the capacity of carbon is approximately three times greater than MN-200 at low concentrations.

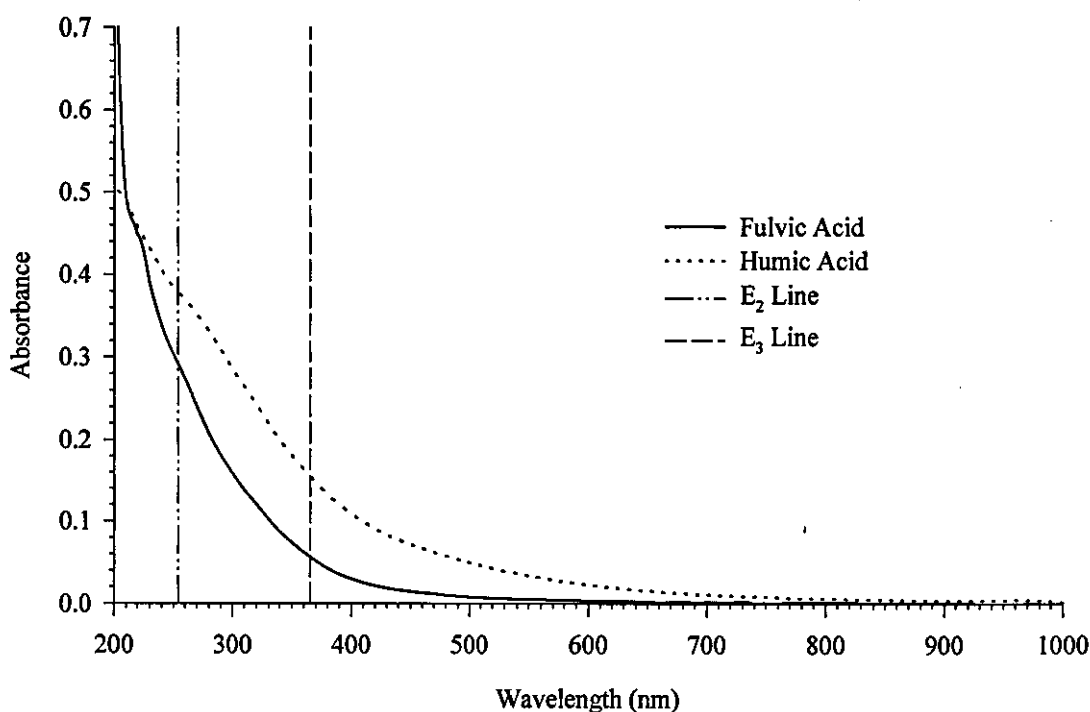
Multi-component adsorption theories were not applied to the data. The low concentrations caused a reasonable scatter in the adsorption data which creates uncertainty in the Freundlich

coefficients. Widely different values of  $K$  and  $1/n$  can be obtained, simply by eliminating one or two data points. The IAST uses the Freundlich coefficients of the single component isotherms in the calculations. The acceptable errors for each component would multiply, thus creating large errors. Even at high concentrations the IAST has an uncertainty of 20%. Any results obtained using IAST would be subject to such uncertainty that they would not be meaningful.

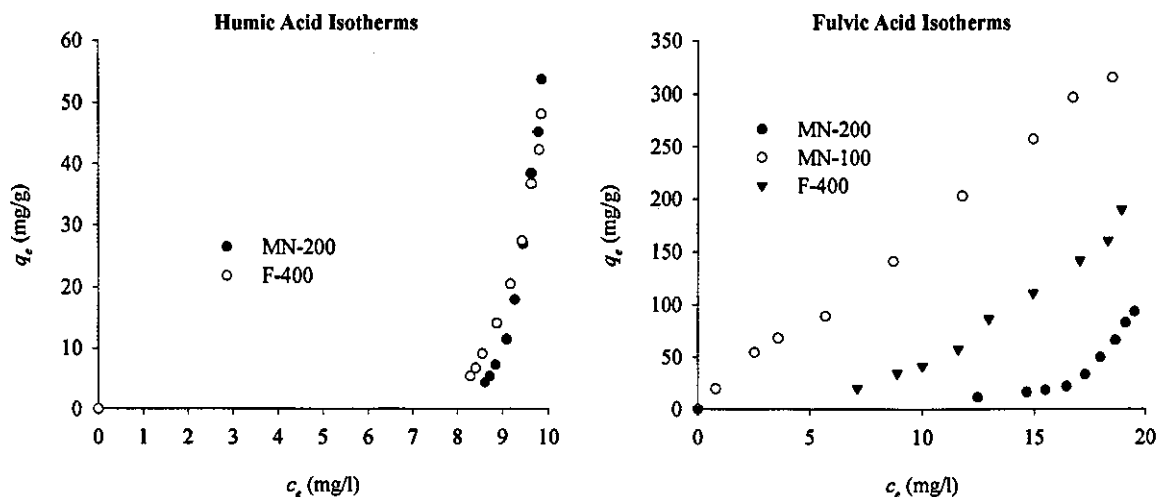
### *Humic and Fulvic Acid Adsorption*

The humic and fulvic acid fractions were obtained by separating the Aldrich humic acid sodium salt. Fig. 5.21 presents the UV-visible scan of the fractions. The spectra of humic and fulvic acid do not show well-defined maxima which is caused by the numerous chromophoric groups contained in the complex humic and fulvic acid molecules.

Fig. 5.21. UV-visible scan of humic and fulvic acid.



There are significant differences in the spectra of humic and fulvic acid which can be characterised by the  $E_2/E_3$  ratio, the absorbance at 254nm divided by the absorbance at 365nm. The  $E_2/E_3$  ratio of the humic and fulvic acids are 2.375 and 4.917 respectively. Fig. 5.22 presents the adsorption isotherms for humic and fulvic acid.

**Fig. 5.22. Adsorption isotherms for the removal of humic and fulvic acid.**

The uptake of humic acid is extremely low at high adsorbent masses which suggests that the molecules are being size excluded from the adsorbents. The humic acid adsorption capacity of F-400 is slightly higher than MN-200. This may be due to the larger accessible surface area caused by the mesopores in F-400, compared to the macropores in MN-200. There is a significant difference in the performance of MN-100, MN-200 and F-400 for the removal of fulvic acid with MN-100 having the highest capacity followed by F-400 and MN-200. Humic and fulvic acids behave as weak acid polyelectrolytes, containing a variety of oxygen functionality such as carboxylic, phenolic, carbonyl and hydroxyl. The adsorption isotherms were performed at pH 6.8 which suggests that the COOH groups on the humic and fulvic acid will be dissociated, thus causing the molecules to carry a net negative charge. The surface of MN-200 and F-400 is negatively charged at pH 6.8 which will cause electrostatic repulsion of the fulvic acid. However, the amine functionality of MN-100 reduces the repulsion and allows the fulvic acid to be removed by an ion exchange mechanism. Anion exchange of MN-100 was confirmed by the pH increase from the initial solution pH of 6.8 to an equilibrium value of 7.5. The greater capacity of F-400 for the sorption of fulvic acid, compared to MN-200 is probably due to the differences in the pore size distribution and strength of interaction of the adsorbate to the surface. F-400 contains a number of nitrogen containing functional groups [3.21] which may enable adsorption through an ion exchange mechanism.

The difference in uptake of humic acid compared with fulvic acid is probably due to differences in the size of the adsorbates. The average range of molecular weight of humic acid is of the order



of 50,000 to 100,000 Daltons, which corresponds to spherical particles with diameters of 60-100Å. A typical fulvic acid has a molecular weight range of 500 to 2000 Daltons.

Ultrafiltration was performed to enable a comparison of the molecular size of fulvic acid to that of the pesticides. The results indicated that 100% of the pesticides passed through the membrane compared to 4.6% of the fulvic acid.

The influence of a high concentration of fulvic acid on the adsorption of trace levels of pesticides for MN-200 is presented in Fig. 5.23. The fulvic acid reduces the capacity of the polymer for all the pesticides, although the influence is not appreciable. A slight reduction would also be observed if the kinetics for adsorption of the pesticides was faster than that of F-400. However, this is not the case. Thus, it may be concluded that the fulvic acid is size excluded from MN-200.

### *Mini-column Experiments*

Mini-column breakthrough curves for MN-200 sorbing simazine, chlorotoluron, atrazine, diuron and isoproturon can be seen in Fig. 5.24. The data for full breakthrough is smoothed over ten data points with only one in five data points presented. Data below 0.01µg/l is indicated as zero concentration due to the limit of detection of the HPLC analysis. The seals of the metering pump began to fail after 500,000 bed volumes had passed through the columns. Hence, the data generated after that point has been discarded. The experiment was stopped at 800,000 bed volumes which corresponds to 528l of water treated and an experiment duration of 82 days.

Breakthrough of the column, to the EU legal limit, occurs between 100,000 and 180,000 bed volumes for simazine and isoproturon respectively. The selectivity sequence is slightly different to that determined during the batch isotherm trials. Atrazine is adsorbed to a lesser extent than diuron, compared to their similar capacity previously. This may be due to the kinetic effects encountered during the batch equilibration of 5 days. During the long duration of the column experiment diuron may be able to diffuse into pores which would size exclude atrazine, hence the increased adsorption capacity. The adsorption capacity, up to 500,000 bed volumes, for simazine, chlorotoluron, atrazine, diuron, and isoproturon is 15.7, 32.7, 39.7, 44.8, 46.2mg/g

Fig. 5.23. Multi-component adsorption isotherms for MN-200 in the presence of 20mg/l fulvic acid.

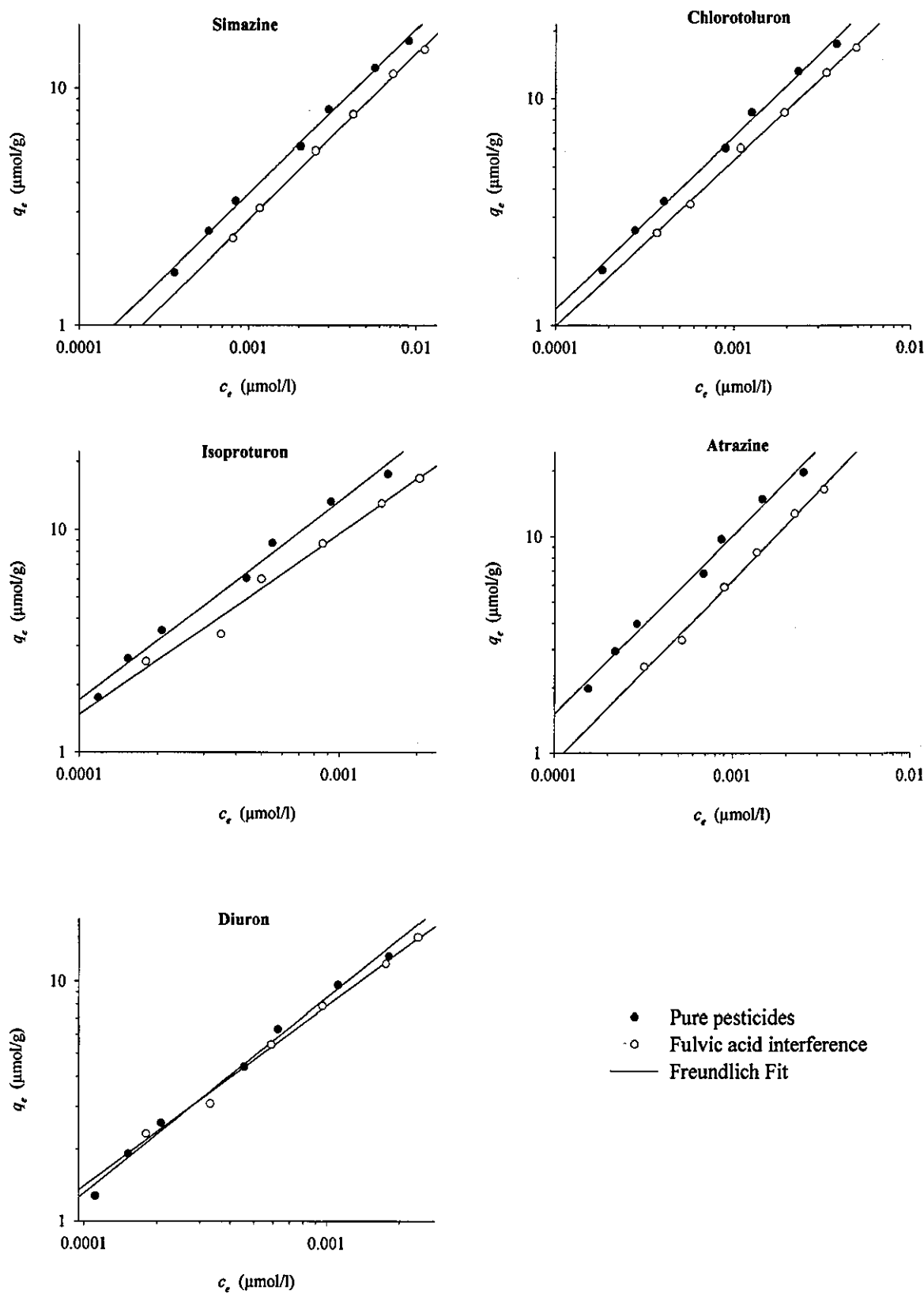
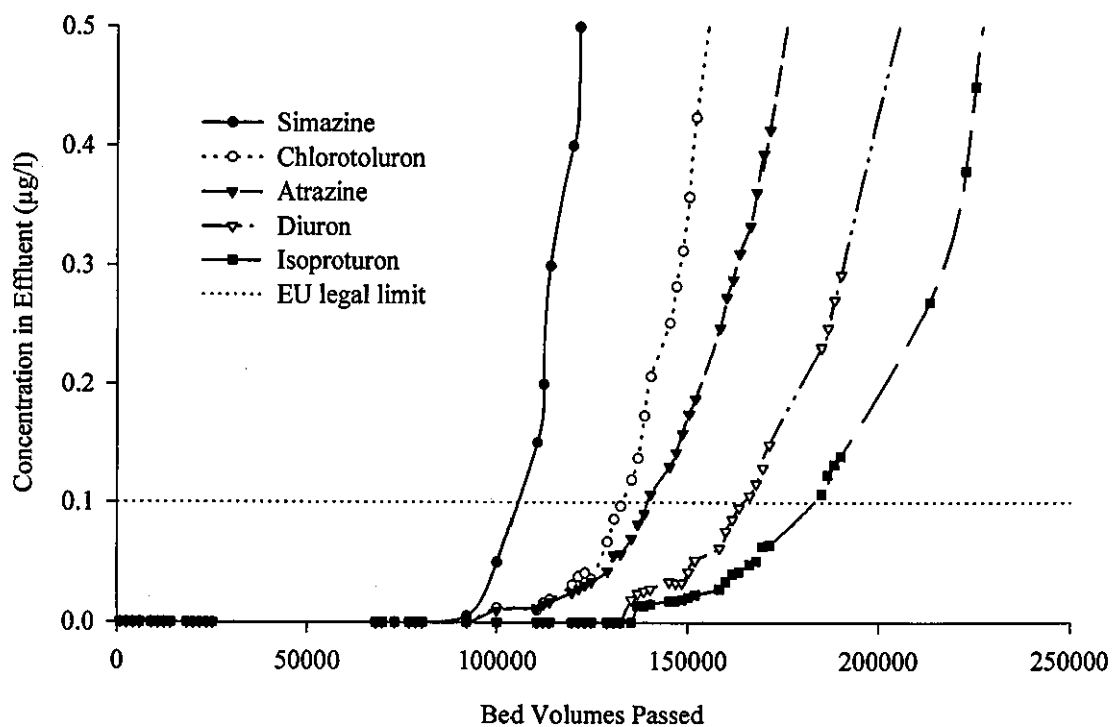
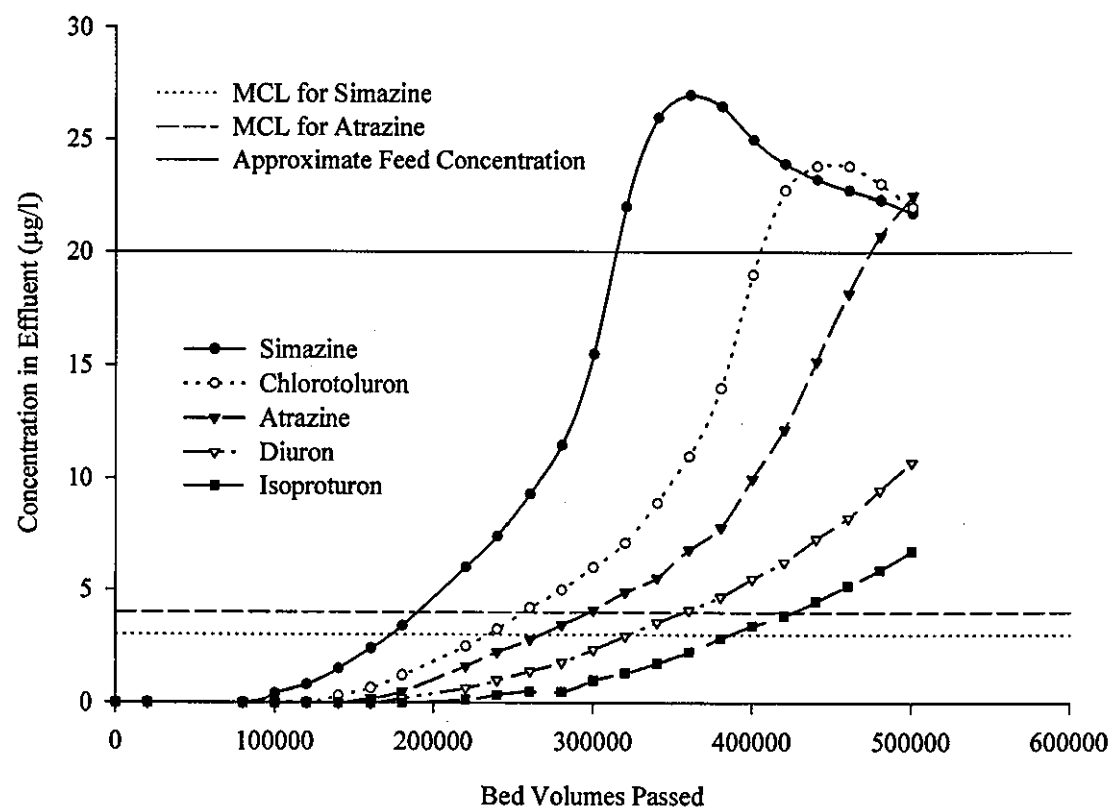


Fig. 5.24. Mini-column breakthrough curves for MN-200 sorbing simazine, chlorotoluron, atrazine, diuron and isoproturon.



respectively. Chromatographic elution is observed for the pesticides which causes the simazine concentration to reach  $28\mu\text{g/l}$ . The higher maximum contaminant limits (MCL) of the US-EPA for simazine and atrazine allow nearly 200,000 bed volumes to be treated.

The breakthrough curves are shallow in shape which suggests that the flow rate through the column was too great, thus spreading the mass transfer zone. A slower flow rate may result in a greater lifetime for the column. The concentrations used for the breakthrough curves are exceptionally high, approximately 20 times those which are found in ground and surface waters. However, the large capacity of the polymers and the limited time for trials necessitated their use.

The capacity of F-400 is considerably greater than that of MN-200 since breakthrough was not apparent even after 800,000 bed volumes. However, problems with the pumping systems and excessive pressure drop in the column prevented the continuation of the experiment.

### ***High concentration kinetic trials***

Fig. 5.25 presents some kinetic data for the adsorption of atrazine and fulvic acid. MN-100 and MN-200 have very similar kinetics for atrazine adsorption whereas the kinetics for MN-150 are considerably slower. Equilibrium appears to be achieved in approximately 2 days for the  $53\text{--}73\mu\text{m}$  polymer compared to approximately 10 days for the  $300\text{--}400\mu\text{m}$  particle size fraction. The adsorption kinetics for fulvic acid appear to be faster than those for atrazine. However, this may be due to quicker adsorption in the macropores, since the majority of the fulvic acid will be size excluded from the micropores. F-400 has faster adsorption kinetics for fulvic acid compared to that of MN-200. Fig. 5.26 presents the initial parts of the Aldrich humic acid sodium salt (humic and fulvic acid) breakthrough curves for MN-200 and F-400. F-400 has a higher capacity which may be due to faster kinetics. A reduction in the flow rate of the adsorbate solution for MN-200 to 0.3 bed volumes per minute significantly increased the amount of humic acid sodium salt removed. Hence, to minimise the humic and fulvic acid removal by the adsorbents high flow rates through the columns can be used.

Fig. 5.25. Adsorption kinetics for the sorption of atrazine and fulvic acid.

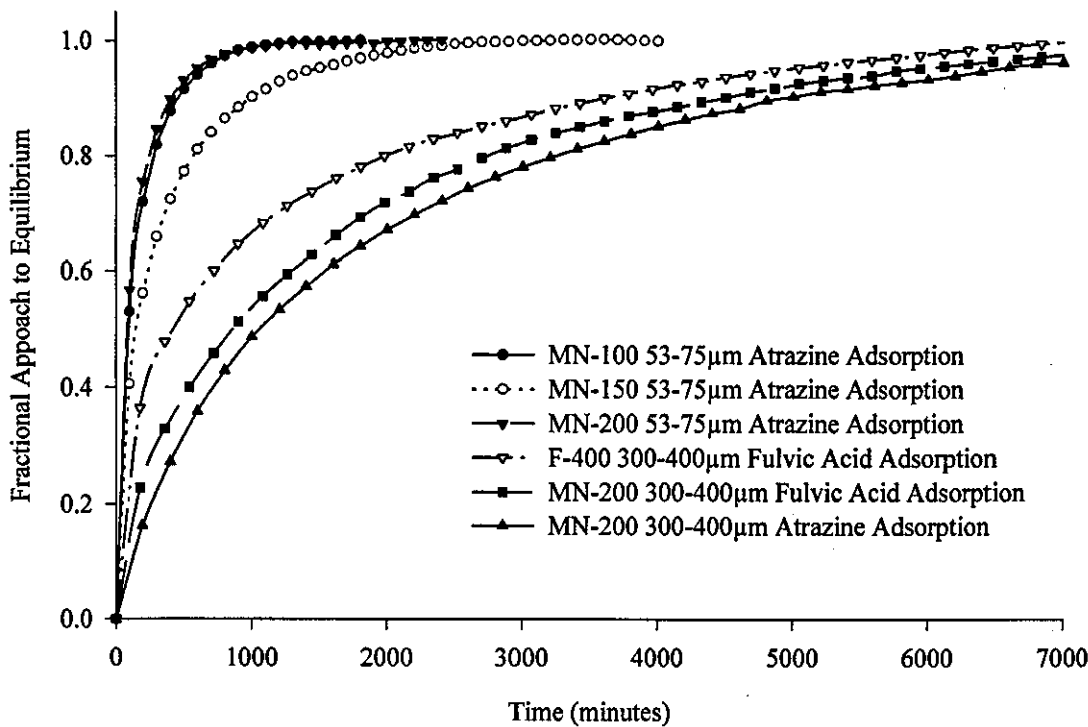
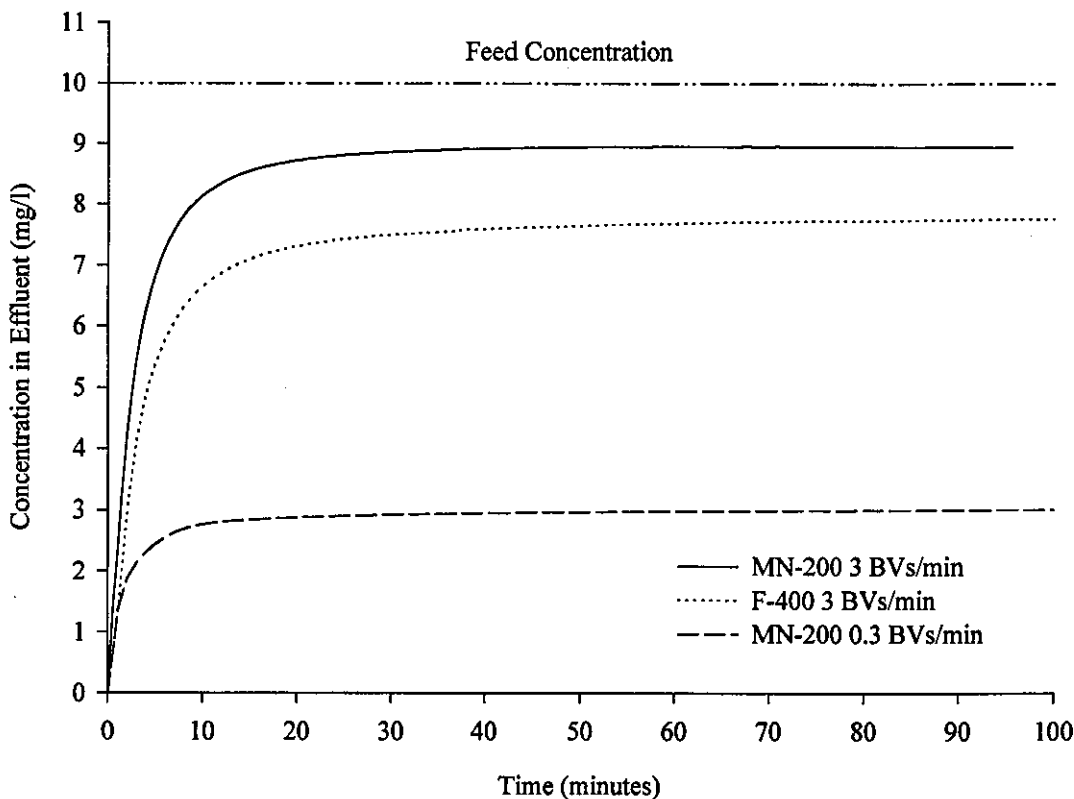


Fig. 5.26. Aldrich humic acid sodium salt breakthrough curves for MN-200 and F-400.



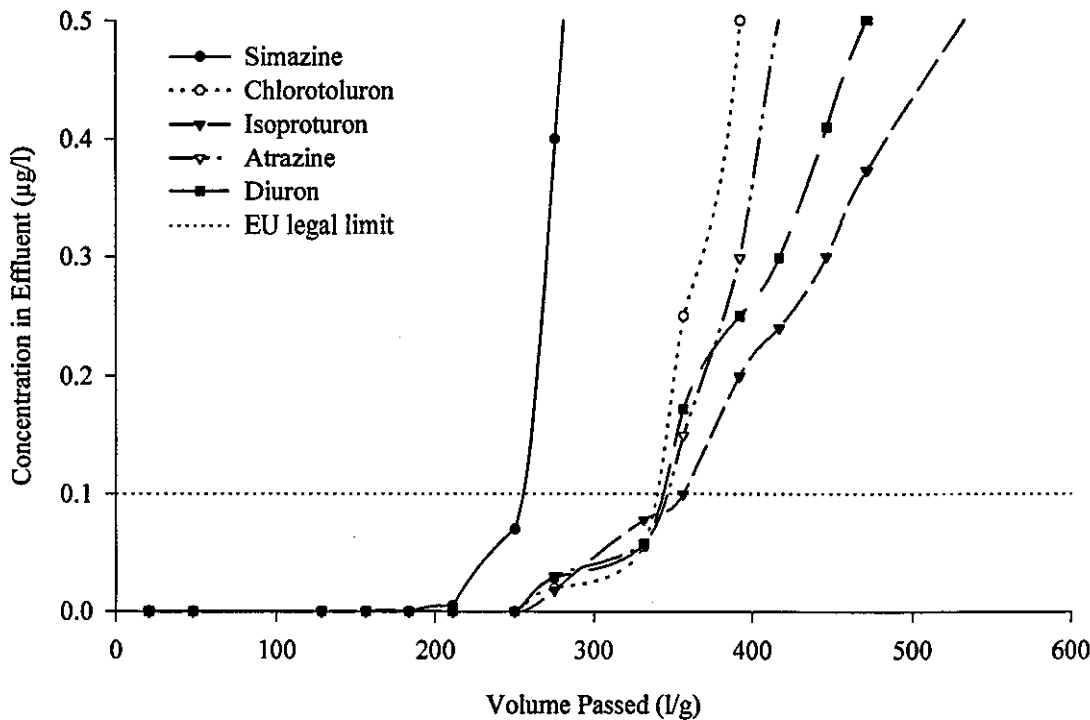
### *Influence of Fulvic acid on Mini-column breakthrough*

Figs 5.27 and 5.28 present the mini-column breakthrough curves, in the presence of fulvic acid, for regenerated MN-200 and virgin F-400 respectively. Due to a significant difference in the bulk density of the adsorbents the volume of liquid treated is normalised with respect to mass. Scatter in the data is due to fulvic acid interferences in the HPLC analysis.

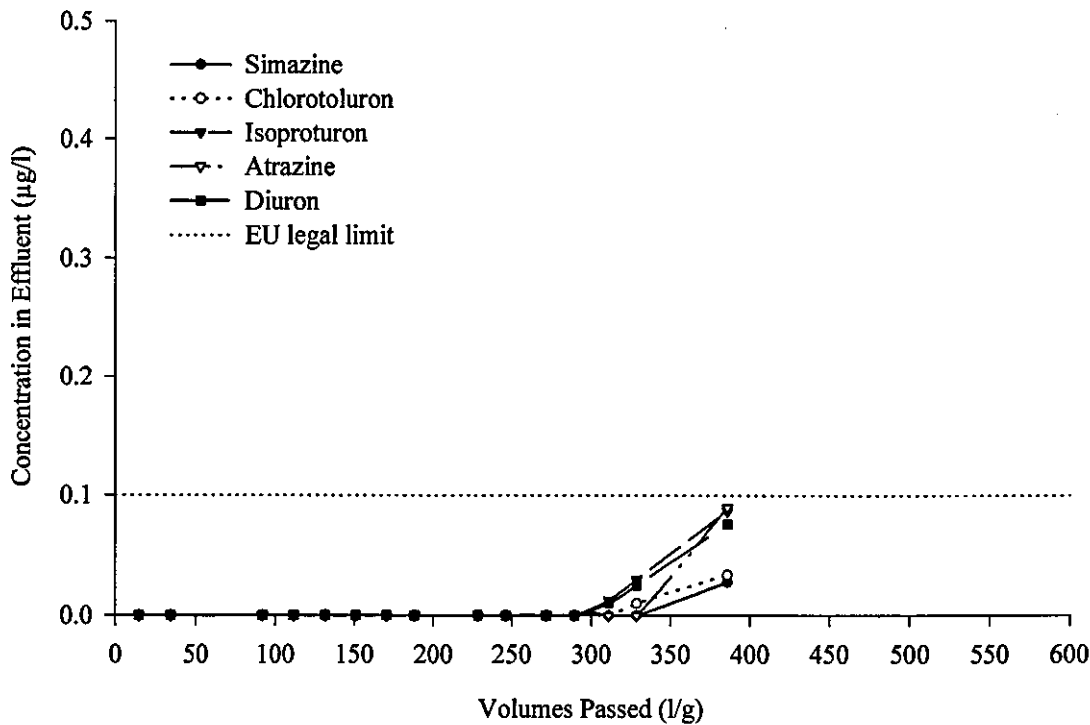
Introduction of fulvic acid into the pesticide mix feed reduced the breakthrough point for simazine to 64,000 BV's (previously 70,000 BV's). The selectivity sequence was unchanged. The 10% reduction in capacity is similar to that determined during batch competitive adsorption studies, see Fig. 5.23. The influence of fulvic acid was more pronounced for adsorption onto F-400. Breakthrough of atrazine and isoproturon, to the EU legal limit, occurred at 400l/g which corresponds to 160,000BV's (previously >800,000 BV's for adsorption in ultrapure water). Analysis of the mini-columns effluent, using a UV spectrophotometer at 254nm, suggested that F-400 was initially adsorbing 28% of the fulvic acid compared to 15% for MN-200. The fulvic acid adsorption isotherms (page 155) for MN-200 and F-400 also suggested that F-400 had the greater capacity, attributed to the mesoporous nature of the carbon. It is thought that the larger fulvic acid molecules adsorb in the mesopores, thus preventing diffusion of the pesticides into the micropore structure of the carbon. The adsorption of fulvic acid molecules onto MN-200 is believed to be due to the macroporous surface area of the polymer. The slight reduction in the adsorption capacity of the pesticides may be caused by small fulvic acid molecules adsorbing in the micropores or partial blocking of macropores.

Flame atomic adsorption spectroscopy was used to determine the amount of sodium present in the fulvic acid solution (caused by the neutralisation of HCl required to separate humic and fulvic acid). Feed solutions to the columns, pH adjusted to 6.8, contained approximately 1.4mg/l of sodium or 0.06mmol/l.

**Fig. 5.27.** Mini-column breakthrough curves for MN-200 sorbing simazine, chlorotoluron, atrazine, diuron and isoproturon in the presence of 10mg/l fulvic acid.



**Fig. 5.28.** Mini-column breakthrough curves for F-400 sorbing simazine, chlorotoluron, atrazine, diuron and isoproturon in the presence of 10mg/l fulvic acid.



## SECTION 5.6 CONCLUSIONS

The adsorption of simazine, chlorotoluron, isoproturon, atrazine and diuron in the parts per billion range has been investigated in batch and mini-column modes. The analytical technique for the pesticides comprises solid phase extraction followed by HPLC analysis of the extracts. Relative standard deviations of less than 5% were achieved for all pesticides. The polymers demonstrate different selectivity for the pesticides. Isoproturon is the most preferred followed by atrazine, diuron, chlorotoluron and simazine.

Adsorption of the pesticides appears to be controlled by hydrophobic interactions and hydrogen bonding. Size exclusion of the larger pesticides reduces their uptake. MN-100, MN-150 and MN-200 have a similar adsorption capacity for the pesticides which is probably due to the similar total degree of oxygen and nitrogen functionality of the pesticides.

MN-200 has a significantly lower adsorption capacity for fulvic acid compared to that of F-400, suggesting that the polymers will have a longer service life for real waters. MN-100 demonstrates the highest capacity for fulvic acid due to ion exchange of the anionic molecules. The adsorption capacity of MN-200 for the pesticides, in the presence of a 20mg/l solution of fulvic acid, is only slightly reduced. This is due to size exclusion of the large fulvic acid molecules, verified by ultrafiltration trials. The amount of humic and fulvic acid adsorbed during mini-column runs may be reduced by operating at high flow rates.

The adsorption capacity of F-400, for pesticides in ultrapure water, is significantly greater than that of MN-200. However, in the presence of fulvic acid a 5-fold reduction in capacity was observed for F-400 compared to a 10% reduction in capacity for MN-200. This resulted in MN-200 and F-400 having a similar adsorption capacity for all pesticides other than simazine.



**SECTION 5.7 REFERENCES**

- [1] The EC Committee, 1994, EU Environment Guide, London, (1995)
- [2] G.P. Westerhoff and R. Miller, Design of the GAC Treatment Facility at Cincinnati., Journal American Water Works Association, April, (1986), 146-155.
- [3] N.B. Smetham, Activated Carbon in Drinking Water, Southern Water Services Ltd., (1994).
- [4] R. Hopman, W.G. Siegers and J.C. Kruithof, Organic Micropollutant Removal by Activated Carbon Filter Filtration., Water Supply, 13, (3-4), (1995), p257-261.
- [5] P.K. Marsden, Drinking Water Inspectorate, private correspondence, (1995).
- [6] A. Ferguson, National Rivers Authority, Anglian Region, private correspondence, (1995).
- [7] D.B. Hampson, Department of the Environment, Water Services Division, private correspondence, (1995).
- [8] O.D. Hydes, Nitrates, Pesticides & Lead 1989/1990, Drinking Water Inspectorate, HMSO, (1992), p57.
- [9] G.P. Thelin, USGS Pesticide National Synthesis Project, (1997), Internet address: <http://water.wr.usgs.gov/pnsp/use92/index.html>
- [10] D.E. Glotfelty, G.H. Williams, H.R. Freeman and M.M. Leech, Regional Atmospheric Transport and Deposition of Pesticides in Maryland, *in* Long-range Transport of Pesticides, (D.A. Kurtz, ed.), Lewis Publishing Co., Chelsea, MI, (1990), p199-222.
- [11] G.P. Thelin, USGS Pesticide National Synthesis Project, (1997), Internet address: [http://water.wr.usgs.gov/pnsp/atmos/atmos\\_7.html](http://water.wr.usgs.gov/pnsp/atmos/atmos_7.html)
- [12] Environmental Protection Agency, Atrazine, Simazine and Cyanazine; Notice of Initiation of Special Review., Federal Register: November 23, (1994).
- [13] F.J. Stevenson, Humus Chemistry: Genesis, Composition, Reactions., Second Edition, John Wiley & Sons, Inc, (1994).
- [14] R.S. Summers, L. Cummings, J. DeMarco, D.J. Hartman, D.H. Metz, E.W. Howe, B. MacLeod and M. Simpson, Standardized Protocol for the Evaluation of GAC., American Water Works Association Research Foundation, (1992), p1-151.
- [15] B.R. Frick, Theoretische Betrachungen zu den Problemen des Scale-up von Aktivkohlefestbettadsorbern. Heft 20. Karlsruhe, Germany: Engler-Bunte-Institut,

University of Karlsruhe, (1982).

- [16] J.C. Crittenden, J.K. Berrigan (Jr), D.W. Hand, Design of Rapid Small-scale Adsorption Tests for a Constant Surface Diffusivity., *Journal of the Water Pollution Control Federation*, 58, (4), (1986), 312-319.
- [17] J.C. Crittenden, J.K. Berrigan, D.W. Hand and B. Lykins, Design of Rapid Fixed-bed Adsorption Tests for Nonconstant Diffusivities., *Journal of Environmental Engineering*, 113, (2), (1987), p243-259.
- [18] J.C. Crittenden, P.S. Reddy, H. Arora, J. Trynoski, D.W. Hand, D.L. Perram and R.S. Summers, Predicting GAC Performance with Rapid Small-scale Column Tests., *Journal American Water Works Association*, 83, (1), (1991), p77-87.
- [19] R. Hopman, M.A. Meerkerk, W.G. Siegers and J.C. Kruithof, Mini-column Tests for the Evaluation of Pesticide Removal by Adsorption., *Water Supply*, 14, (2), (1996), p49-60.
- [20] R. Hopman, M.A. Meerkerk, W.G. Siegers and J.C. Kruithof, Prediction and Optimization of Pesticide Removal by GAC-filtration., *Water Supply*, 12, (3-4), (1994), p197-207.
- [21] Y. Matsui, T. Kamei, A. Yuasa and N. Tambo, Adsorption Capacity of Organic Pesticides on Granular Activated Carbon., *Water Supply*, 14, (2), (1996), p31-41.
- [22] M. Mazet, B. Farkhani and M. Baudu, Influence of Heat or Chemical Treatment of Activated Carbon onto the Adsorption of Organic Compounds., *Water Research*, 28, (7), (1994), p1609-1617.
- [23] J. Ayele, P. Levavasseur and M. Mazet, Triazine Adsorption on Powdered Activated Carbon., *Journal of Water Supply Research and Technology-Aqua*, 45, (1), (1996), p28-34.
- [24] C.D. Adams and T.L. Watson, Treatability of s-triazine Herbicide Metabolites using Powdered Activated Carbon., *Journal of Environmental Engineering*, 122, (4), (1996), p327-330.
- [25] S. Qi, S.S. Adham, V.L. Snoeyink and B.W. Lykins (Jr), Prediction and Verification of Atrazine Adsorption by PAC., *Journal of Environmental Engineering*, 120, (1), (1994), p202-218.
- [26] T.F. Speth and R.J. Miltner, Technical note: An Evaluation of GAC for SOC's., *Journal American Water Works Association*, 82, (2), (1980), p72-75.
- [27] F. Bernazeau, V. Mandra, P. Charles, C. Anselme and J.L. Bersillon, Pesticides Removal on Activated Carbon: Competitive Adsorption with Natural Organic Matter., *Water Supply*, 14, (2), (1996), p43-48.

- [28] M.C. Lee, J.C. Crittenden, V.L. Snoeyink and M. Ari, Design of Carbon Beds to Remove Humic Substances., *Journal of Environmental Engineering*, 109, (3), (1983), p631-645.
- [29] R.S. Summers and P.V. Roberts, Activated Carbon Adsorption of Humic Substances. I. Hetero disperse Mixtures and Desorption., *Journal of Colloid and Interface Science*, 122, (2), (1988), p367-381.
- R.S. Summers and P.V. Roberts, Activated Carbon Adsorption of Humic Substances. II. Size Exclusion and Electrostatic Interactions., *Journal of Colloid and Interface Science*, 122, (2), (1988), p382-397.
- [30] P. Lafrance and M. Mazet, Adsorption of Humic Substances in the Presence of Sodium Salts., *Journal of the American Water Works Association*, 81, (4), (1989), p155-162.
- [31] G. Newcombe, Activated Carbon and Soluble Humic Substances: Adsorption, Desorption, and Surface Charge Effects., *Journal of Colloid and Interface Science*, 164, (2), (1994), p452-462.
- [32] J. Stàrek, A. Zukal and J. Rathouský, Comparison of the Adsorption of Humic Acids From Aqueous Solutions On Active Carbon and Activated Charcoal Cloths., *Carbon*, 32,(2), (1994), p207-211.
- [33] C. Brasquet, E. Subrenat and P. Le Cloirec, Adsorption of Organics in Water onto Activated Carbon Fibres: Correlation Between Adsorption Parameters and Molecular Structure., presented at Carbon '97, 23rd Biennial Conference on Carbon 18-23 July 1997, Extended Abstracts and Program, 1, p4-5.
- [34] H. Tamai, S. Kojima, M. Ikeuchi, J. Mondori, T. Kanata and H Yasuda, Preparation of Mesoporous Activated Carbon Fibres and Their Adsorption., presented at Carbon '97, 23rd Biennial Conference on Carbon 18-23 July 1997, Extended Abstracts and Program, 1, p36-37.
- [35] H. Frederick and F.S. Cannon, Calcium Accumulation by GAC in the Presence of NOM., presented at Carbon '97, 23rd Biennial Conference on Carbon 18-23 July 1997, Extended Abstracts and Program, 1, p30-31.
- [36] T. Karanfil, J.E. Kilduff and W.J. Weber (Jr), The Role of Surface Characteristics on the Uptake of Organic Macromolecules by GAC., presented at Carbon '97, 23rd Biennial Conference on Carbon 18-23 July 1997, Extended Abstracts and Program, 1, p32-33.
- [37] J.C. Crittenden, K. Vaitheeswaran, D.W. Hand, E.W. Howe, E.M. Aieta, C.H. Tate, M.J. McGuire and M.K. Davis, Removal of Dissolved Organic Carbon Using Granular Activated Carbon., *Water Research*, 27, (4), (1993), p715-721.
- [38] E.H. Smith, Bench-scale Tests and Modeling of Adsorption of Natural Organic Matter

by Activated Carbon., Water Research, 28, (8), (1994), p1693-1702.

- [39] J.L. Bulloch, D.W. Hand, J.C. Crittenden, D.R. Hokanson and M. Ulmer, Predicting the Performance of Liquid Phase Fixed-bed Granular Activated Carbon Adsorbers., presented at Carbon '97, 23rd Biennial Conference on Carbon 18-23 July 1997, Extended Abstracts and Program, 2, p76-77.
- [40] J.C. Crittenden, P. Luft and D.W. Hand, Prediction of Multicomponent Adsorption Equilibria in Background Mixtures of Unknown Composition., Water Research, 19, (12), (1985), p1537-1548.
- [41] J.C. Crittenden, P. Luft, D.W. Hand, J.L. Oravitz, S.W. Loper and M. Ari, Prediction of Multicomponent Adsorption Equilibria Using Ideal Adsorbed Solution Theory., Environmental Science and Technology, 19, (11), (1985), p1037-1043.
- [42] J.C. Crittenden, T.F. Speth, D.W. Hand, P.J. Luft and B. Lykins, Evaluating Multicomponent Competitive Adsorption in Fixed Beds., Journal of Environmental Engineering, 113, (6), (1987), p1363-1375.
- [43] S.M. Klara, A Comprehensive Performance Simulation Package For Activated Carbon and UV/Peroxide Purification Systems., presented at Carbon '97, PennState University, Pennsylvania, USA, 13-18 July 1997.
- [44] M.R. Rosene and M. Manes, Application of the Polanyi Adsorption Potential Theory to Adsorption from Solution on Activated Carbon-VII. Competitive Adsorption of Solids from Water Solution., Journal of Physics and Chemistry, 80, (1976), p953-959.  
  
M.R. Rosene, M. Özcan and M. Manes, Application of the Polanyi Adsorption Potential Theory to Adsorption from Solution on Activated Carbon-VIII. Ideal, Non-ideal and Competitive Adsorption of Some Solids from Water Solution., Journal of Physics and Chemistry, 80, (1976), p2586-2591.  
  
M.R. Rosene and M. Manes, Application of the Polanyi Adsorption Potential Theory to Adsorption from Solution on Activated Carbon-IX. Competitive adsorption of ternary solids from water solution., Journal of Physics and Chemistry, 81, (1977), p1646-1650.
- [45] A.L. Myers and J.M. Prausnitz, Thermodynamics of Mixed-gas Adsorption., AIChE Journal, 11, (1965), p121-127.
- [46] C.J. Radke and J.M. Prausnitz, Thermodynamics of Multi-solute Adsorption from Dilute Liquid Solution., AIChE Journal, 18, (4), (1972), p761-768.
- [47] E. Knettig, B.M. Thomson and S.E. Hrudey, Competitive Activated Carbon Adsorption of Phenolic Compounds., Environmental Pollution, Series B: Chemical and Physical, 12, (4), (1986), p281-299.
- [48] B. Xing, J.J. Pignatello and B. Gigliotti, Competitive Sorption Between Atrazine and

- Other Organic Compounds in Soils and Model Sorbents., *Environmental Science and Technology*, 30, (8), (1996), 2432-2440
- [49] D. Westwood, Phenylurea herbicides (urons), Dinocap, Dinoseb, Benomyl, Carbazin and Metamitron in Waters 1994, *Methods for the Examination of Waters and Associated Materials*, HMSO, (1994), p1-64.
- [50] G.J. Welhouse and W.F. Bleam, Atrazine Hydrogen-bonding Potentials., *Environmental Science & Technology*, 27, (3), (1993), p494-500.
- [51] G.J. Welhouse and W.F. Bleam, NMR Spectroscopic Investigation of Hydrogen-bonding in Atrazine., *Environmental Science & Technology*, 26, (5), (1992), p959-964.
- [52] G.J. Welhouse and W.F. Bleam, Cooperative Hydrogen-bonding of Atrazine., *Environmental Science & Technology*, 27, (3), (1993), p500-505.

## CHAPTER 6

### REGENERATION

#### SECTION 6.1 INTRODUCTION

The economics of drinking water treatment using granular activated carbon are governed by the cost of regenerating spent carbon. Regeneration, by pyrolysis of the adsorbed species, is an expensive process due to the energies required, carbon losses and the associated transport costs. A number of water utilities have installed reactivation furnaces on-site to minimise the costs. The process of thermally regenerating activated carbons is environmentally questionable due to the excessive energies required. At the Cincinnati water works regeneration facility, after burners that produce temperatures in excess of 1400°C, are used to destroy toxic byproducts [5.2]. Numerous researchers have investigated alternative regeneration technologies in an attempt to find a cheaper method. The technologies include; chemical regeneration, solvent regeneration, supercritical fluid extraction, sub critical fluid extraction, steam regeneration, microbiological regeneration and electrical regeneration.

XAD polymeric adsorbents can be regenerated by numerous simple techniques. Fox [1.2] presented commercial examples of the regeneration of phenolic compounds from XAD resins using acetone, methanol and two percent caustic soda at 80-85°C. Recovery of the solvent, such as acetone, can be achieved by distillation. This creates a closed loop process with minimal secondary wastes. Urano *et al* [1] used water to compare the regeneration efficiency of 17 organic compounds from F-400 and XAD-4. Several phenolic compounds and aniline were irreversibly adsorbed onto F-400 whereas all of the organic compounds were reversibly adsorbed on the polystyrene adsorbent.

This chapter investigates the solvent regeneration of the Macronet polymers compared to F-400 activated carbon. The literature review concentrates on the regeneration techniques applied to activated carbons since total regeneration of a variety of organic compounds from polymeric

adsorbents is demonstrated only by their use as solid phase extraction packings.

## SECTION 6.2 BACKGROUND AND LITERATURE REVIEW

A wide variety of techniques can be applied to the regeneration of adsorbents which can be divided into thermal regeneration and liquid phase desorption. The thermal reactivation of activated carbon can be divided into four process stages; drying at temperatures of up to 200°C to remove the associated water, vaporisation of volatile adsorbates and decomposition of unstable adsorbates to form volatile fragments at temperatures of 200-500°C, pyrolysis of nonvolatile adsorbates and adsorbent fragments to form carbonaceous char on the activated carbon surface at temperatures of about 500-700°C and oxidation of the char using steam and carbon dioxide at temperatures above about 700°C. The amount of carbon lost during reactivation at four facilities in the US varied between 6.9 and 12.2%, with approximately 2-3% lost due to attrition during transport [2]. For relatively volatile adsorbates, boiling points up to 120°C, direct contact steam regeneration can be used. The increase in temperature shifts the adsorption equilibrium resulting in desorption of some of the volatile material. The technique is often applied in vapour phase activated carbon processes.

Waer *et al* [2] investigated the dependency of time and temperature on the thermal regeneration of spent activated carbon. They observed that, for a coal based GAC loaded with NOM and methylene blue, total regeneration was achieved using a temperature of 850°C for 15mins. Shorter times and lower temperatures resulted in a reduction in adsorption capacity. Longer times increased the capacity for large molecules. However, a slight reduction in adsorption capacity was sometimes observed for small adsorbates. Pilard *et al* [3] studied the influence of minerals on the thermal regeneration of activated carbon. Iron, manganese, copper, aluminium, calcium, chromium, nickel and lead were all found in spent carbons. The concentration of calcium, on spent GAC at the Choisy-le-Roi water works, was nearly 40,000ppm. Pyrolysis of the adsorbed species did not reduce the mineral content of the carbon, which resulted in the regenerated carbon offering a lower surface area compared to the virgin carbon. Pilard *et al* [4] observed that acid washing of the carbon prior to thermal regeneration increased the surface area

by up to  $300\text{m}^2/\text{g}$ . The capacity of the acid washed carbon prior to thermal reactivation for atrazine, measured by the Freundlich coefficient  $K$ , was almost double that of regenerated unwashed carbon.

The regeneration of carbon using inorganic and organic solvents has been discussed extensively by Martin *et al* [5]. They investigated the regeneration efficiency of F-400 pre-loaded with aniline, phenol, benzyl alcohol, benzaldehyde and nitrobenzene. The solvents used were as follows; (acids) formic, acetic, propionic, n-butyric, iso-butyric, n-valeric, iso-valeric, n-hexanoic, phosphoric, hydrochloric (alkalis) n-propylamine, ethanolamine, n-butylamine, triethylamine, sodium hydroxide (organic solvents) benzene, acetone, methanol, ethanol, 1-propanol, 2-propanol, 1-butanol, 2-butanol, dichloroethane, chloroform, tetrachloroethane, (oxidising agents)  $\text{KMnO}_4$ ,  $\text{K}_2\text{Cr}_2\text{O}_7$ ,  $\text{NaOCl}$ . Small molecular weight organic solvents were found to be the most effective regenerants. The maximum recovery efficiencies for the different adsorbates were as follows; 100% for phenol using 2-propanol, 90.7% for aniline using methanol, 98.2% for benzyl alcohol using formic acid, 95.9% for benzaldehyde using n-propylamine and 94.3% for nitrobenzene using dichloromethane. Martin *et al* [6] also presented the recovery efficiencies of F-400 exhausted with 2-naphthol, 2-methoxyphenol, 2-chlorophenol, o-cresol and 2-nitrophenol using a variety of solvents. Efficiencies were less than 60% for 2-methoxyphenol, 2-chlorophenol, o-cresol using the regenerants examined in their first paper. The regeneration of F-400 activated carbon exhausted with humic acid has also been discussed by Martin *et al* [7]. Solvents including, acetone, methanol and ethanol provided recovery efficiencies of less than 30%; however, carboxylic acids, such as formic and acetic acid offered efficiencies of up to 178%. Newcombe *et al* [8] regenerated F-300 exhausted with dissolved organic matter using 1M sodium hydroxide at  $50^\circ\text{C}$ . No percentage removal efficiencies were presented. Chiang [9] also investigated the chemical regeneration of carbon loaded with phenolic, benzyl and naphthyl compounds. Recovery efficiencies of between 15 and 97% were observed using a variety of solvents. Rollor *et al* [10] investigated the desorption of p-chlorophenol and two-ring, four-ring and eight-ring azo dyes from five commercial activated carbons using methanol. Recovery efficiencies varied between 1 and 88% using up to 50 bed volumes of solvent. Tamon *et al* [11] observed that an electron-donating solvent, such as N,N-dimethyl-formamide should be used when ethanol regeneration was not effective. Forty



adsorbates were examined including phenolic compounds and humic acids. The recovery efficiency of two different humic acids using ethanol were 71 and 81%. Cooney *et al* [12] tried nineteen solvents for the removal of phenol from activated carbon. Acetone, dimethylformamide and methanol offered the best recoveries. After five regenerations using methanol a value of 81% of the capacity of fresh carbon was observed. McLaughlin [13] investigated the economics of solvent regeneration of activated carbons. Thermal regeneration was estimated to cost between \$0.50 to \$1.00 per pound of carbon compared to direct operating costs of \$0.01 to \$0.05 per pound for solvent regeneration (1995). Robertson *et al* [14] presented the Soxhlet extraction efficiency for the desorption of atrazine and simazine from activated carbon. Recoveries of 95% for atrazine were achieved using acetone, over a period of 16h. Polar solvents, including ethanol and methanol, offered low recoveries with only 50% of simazine extracted. Super-critical CO<sub>2</sub> fluid extraction recoveries of atrazine and simazine exceeded 90% using dynamic acetone modification (50mol%). Static acetone modification and unmodified supercritical CO<sub>2</sub> provided significantly lower extraction efficiencies. As the solid phase concentration of the triazine herbicides on the carbon reduced from 100µg/g to 1µg/g the Soxhlet extraction efficiency was reduced by approximately 25%; however, no appreciable difference was observed in the recovery efficiency using dynamic acetone modified supercritical CO<sub>2</sub>. Hawthorne [15] discusses the advantages and uses of supercritical fluid extraction for a variety of matrices and I refer the reader to the paper for further information.

Hutchinson *et al* [16] presented data for the *in situ* microbial regeneration of granular activated carbon. The mono-culture *Pseudomonas putida* was used to regenerate carbon containing phenol and a bisolute system containing phenol and p-cresol. The breakthrough performance of the columns after successive regenerations decreased due to microbial fouling of the column during bio-regeneration. Feakin *et al* [17] investigated the biodegradation of atrazine and simazine at low concentrations in surface waters. Their results suggested that inoculation of GAC filters with selected strains had potential as a biotreatment for surface waters containing s-triazine herbicides. Uhl *et al* [18] demonstrated that if a GAC adsorber is operated in series with a bioreactor much longer service-times for the carbon can be expected. This was attributed to the bioreactor reducing the biodegradable reaction products of the ozonation. Le Bec *et al* [19] developed a rapid test method for characterising the potential of bioactivity of GAC, similar to the RSSCT

developed by Crittenden. Narbaitz *et al* [20] conducted a feasibility study into the removal of phenol adsorbed on F-400 activated carbon using electrochemical regeneration. 95% regeneration efficiency was obtained, using a regeneration current of 100mA for 5 hours, in a batch reactor with a 1% NaCl solution. A gradual decline in recovery efficiency was observed after successive regenerations. However, the technique did not generate carbon fines.

## SECTION 6.3      EXPERIMENTAL

### *Trial Regeneration*

Mini-columns with a bed volume of 0.33ml were prepared by wet packing 100mg of MN-200 and 150mg of F-400 into 3ml solid phase extraction columns. 10 $\mu$ m stainless steel frits were used as bed supports. The columns were placed on the SPE manifold with a preconditioned C8 SPE cartridge underneath, to check for any leakage or breakthrough. 500ml samples containing a concentration of 10 $\mu$ g/l of atrazine or 2 $\mu$ g/l of simazine, chlorotoluron, isoproturon, atrazine and diuron were passed through the columns at 3ml/min. The columns were then dried for 10 minutes using nitrogen prior to regeneration. The C8 SPE columns were eluted using the solid phase extraction procedure detailed in Chapter 5.

A Kontron 420 HPLC pump, capable of a flow rate of 0.1-10ml/min, was used for the regeneration. Autosampler vials, 1.5ml capacity, were numbered and weighed using the Sartorius balance. Regeneration of the atrazine loaded columns was performed using HPLC grade ethanol at flow rates of 0.1, 0.55 and 2.1ml/min. Samples, with gradually increasing volumes, were collected into the vials and the vial reweighed to enable the volume of ethanol to be calculated. The ethanol was evaporated from the vials using a freeze drier and the sample reconstituted using 500 $\mu$ l of 25% 60/40 acetonitrile/THF, 75% 10mmol KH<sub>2</sub>PO<sub>4</sub> @ pH 4.5 buffer. Analysis of the extracts was performed using the HPLC method described in Chapter 5. Regeneration of columns pre-loaded with the pesticide mix was performed using HPLC grade ethanol, acetone, methanol, acetone and azeotropic ethanol at a flow rate of 0.2ml/min.

### ***Ethanol Washout***

A Waters 410 Differential Refractometer was used to study the efficiency with which the ethanol could be washed out of the mini-column using water. The detector was calibrated for 100% ethanol and 0% ethanol in water. The outlet to the solid phase extraction column was connected into the inlet port of the detector and water pumped through the column, instead of ethanol. Flow rates of 1.2 and 0.8 bed volumes per minute were used. The output was sent to a chart recorder.

### ***Regeneration of Adsorption Column***

The columns from the adsorption experiment, MN-200 and F-400, were dried using nitrogen for 10 minutes, prior to regeneration using HPLC grade ethanol at a flow rate of 0.15ml/min. Vials with a capacity of 7ml replaced the 1.5ml autosampler vials used in the trial regeneration. Gradually increasing sample volumes, from 1ml up to 6ml, were collected. After evaporation of the ethanol the samples were reconstituted to 500 $\mu$ l unless residuals of pesticide were visible in the vials. In these cases, reconstitution was performed into larger volumes of up to 200ml, which was sometimes diluted 10 times for HPLC analysis. The extracts in the 7ml vials were transferred into autosampler vials prior to HPLC analysis using the standard method. The run time was increased from 12 minutes to 30 minutes to enable strongly retained samples to be eluted. Regeneration was stopped after passing 50 ml of ethanol, 75 bed volumes.

## SECTION 6.4 RESULTS AND DISCUSSIONS

### *Trial Regeneration*

Complete regeneration of atrazine from MN-200 was achieved at all flow rates. The recovery efficiency improved as the flow rate of regenerant decreased. At 0.3BV/min only 1 bed volume was required for total regeneration, compared to 4 and 6 bed volumes for the 1.5 and 6BV/min flow rates respectively. Complete regeneration was also achieved for regeneration of the pesticide mix using the different solvents. Figs. 6.1-5 show the regeneration of MN-200 using ethanol, azeotropic ethanol, acetone, methanol and 1-propanol with a summary of the total regeneration efficiency for each solvent presented in Fig. 6.6. The regeneration of the pesticides appeared to be controlled by the adsorbates molecular size and strength of interaction with the adsorbent surface. The greater molecular size of atrazine and simazine resulted in their early elution. It is thought that the compounds are prevented from penetrating the smaller micropores, where interaction energies are stronger, resulting in faster elution. The elution curves of diuron, chlorotoluron and isoproturon are governed by the strength of interaction between the adsorbates and adsorbent surface. Diuron is the most hydrophobic pesticide resulting in the greatest interaction energy, and thus the slowest elution. Ethanol, azeotropic ethanol, methanol and 1-propanol show similar elution profiles for the pesticide mix. However, acetone is a more effective regenerant. Ethanol was chosen as the regenerant for the adsorption columns since it is believed that this solvent would be acceptable for use in the water industry. Table 6.1 provides a summary of the solubility of the pesticides in two different solvents.

**Table 6.1. Solubility of pesticides in various organic solvents.**

| Solvent  | Solubility (ppm) at 20°C |          |        |             |               |
|----------|--------------------------|----------|--------|-------------|---------------|
|          | Simazine                 | Atrazine | Diuron | Isoproturon | Chlorotoluron |
| Methanol | 400                      | 18,000   | -      | 56,000      | -             |
| Acetone  | -                        | -        | 53,000 | -           | 50,000        |

No regeneration was observed for atrazine loaded onto F-400 activated carbon using ethanol and

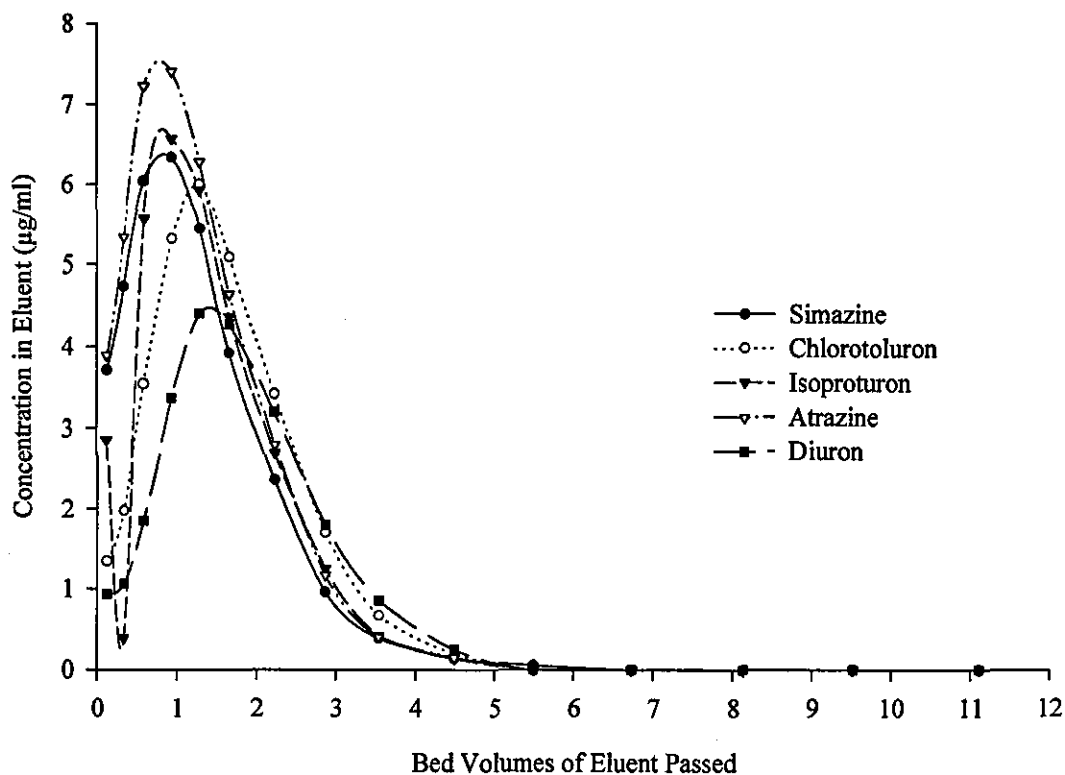
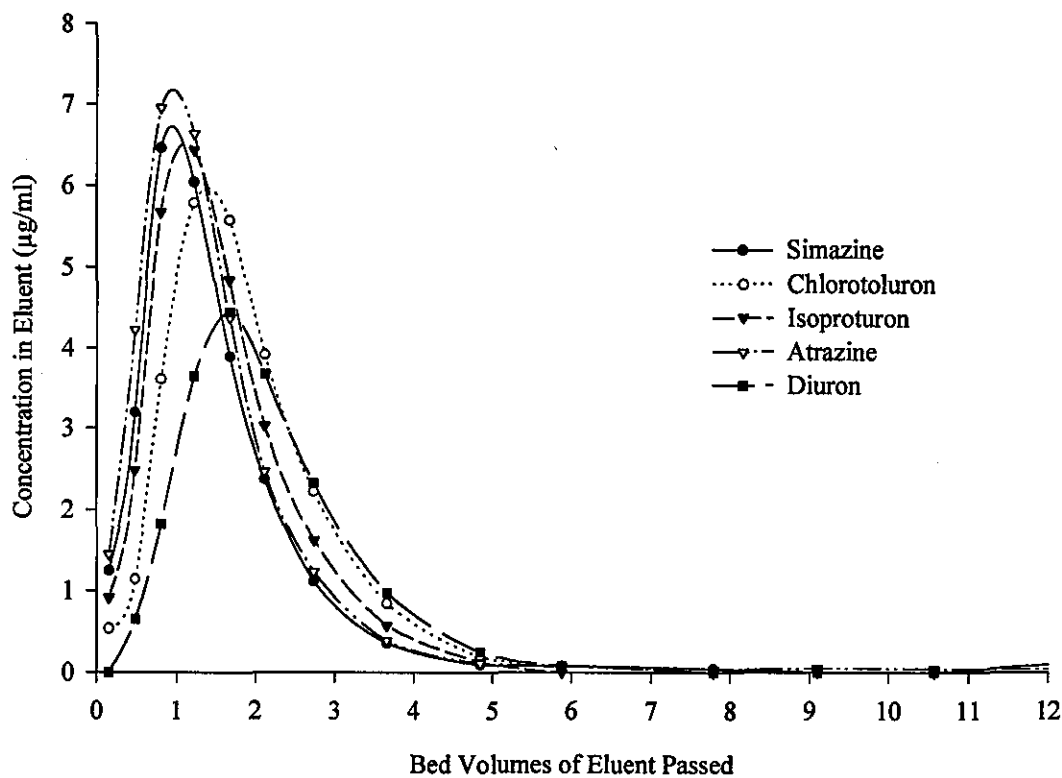
**Fig. 6.1.                      Regeneration of MN-200 using HPLC grade ethanol.****Fig. 6.2.                      Regeneration of MN-200 using azeotropic ethanol.**

Fig. 6.3.                   Regeneration of MN-200 using HPLC grade acetone.

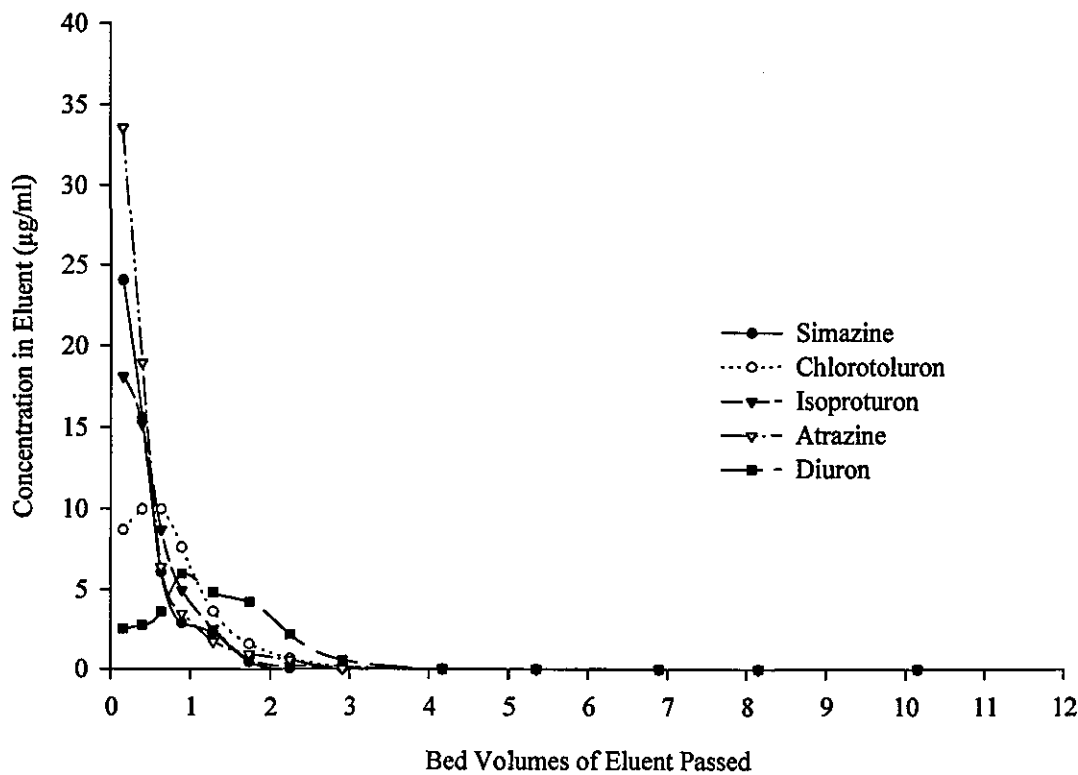


Fig. 6.4.                   Regeneration of MN-200 using HPLC grade methanol.

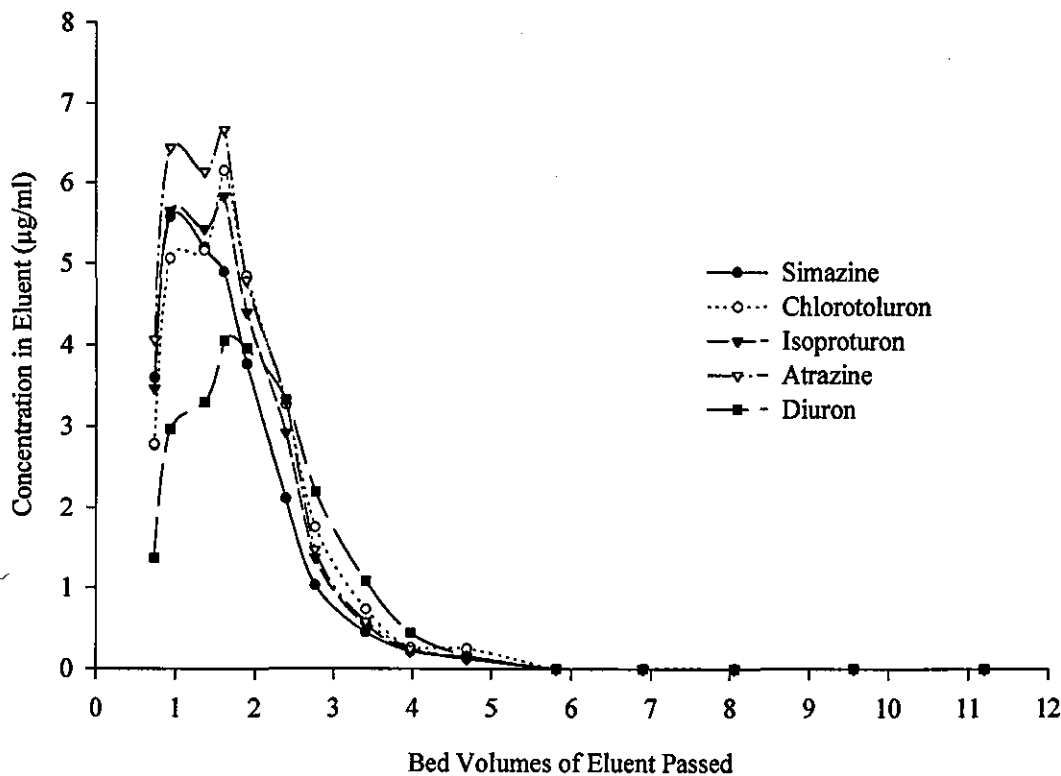


Fig. 6.5. Regeneration of MN-200 using HPLC grade 1-propanol.

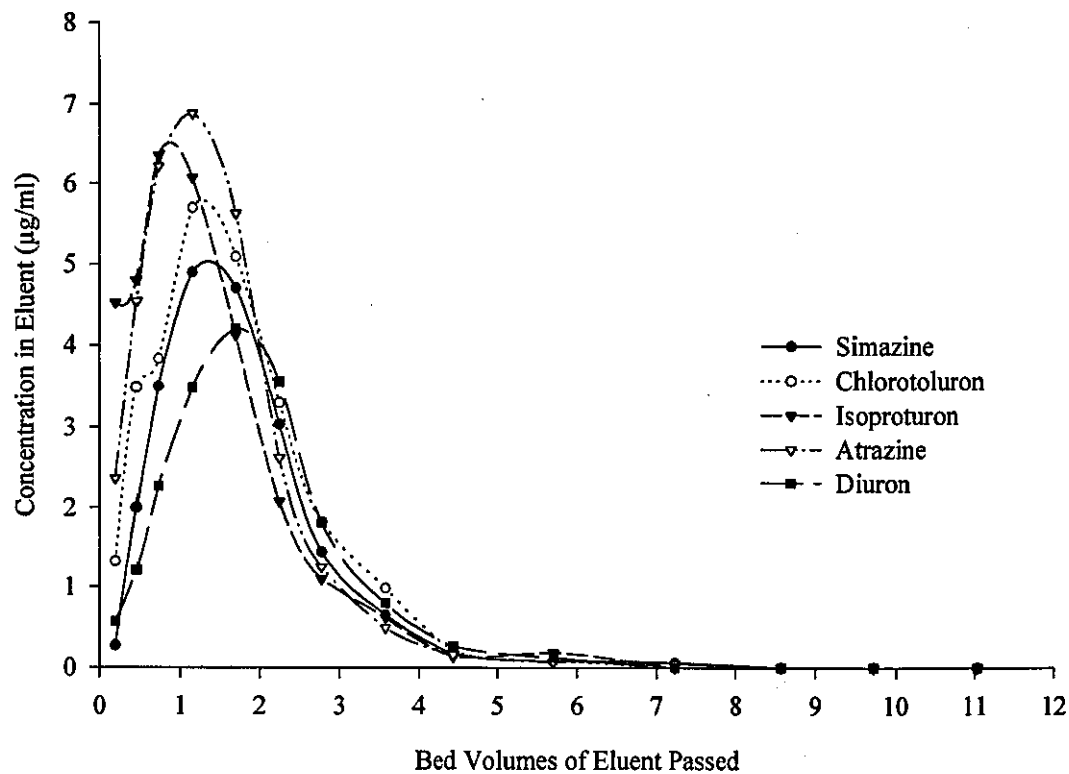
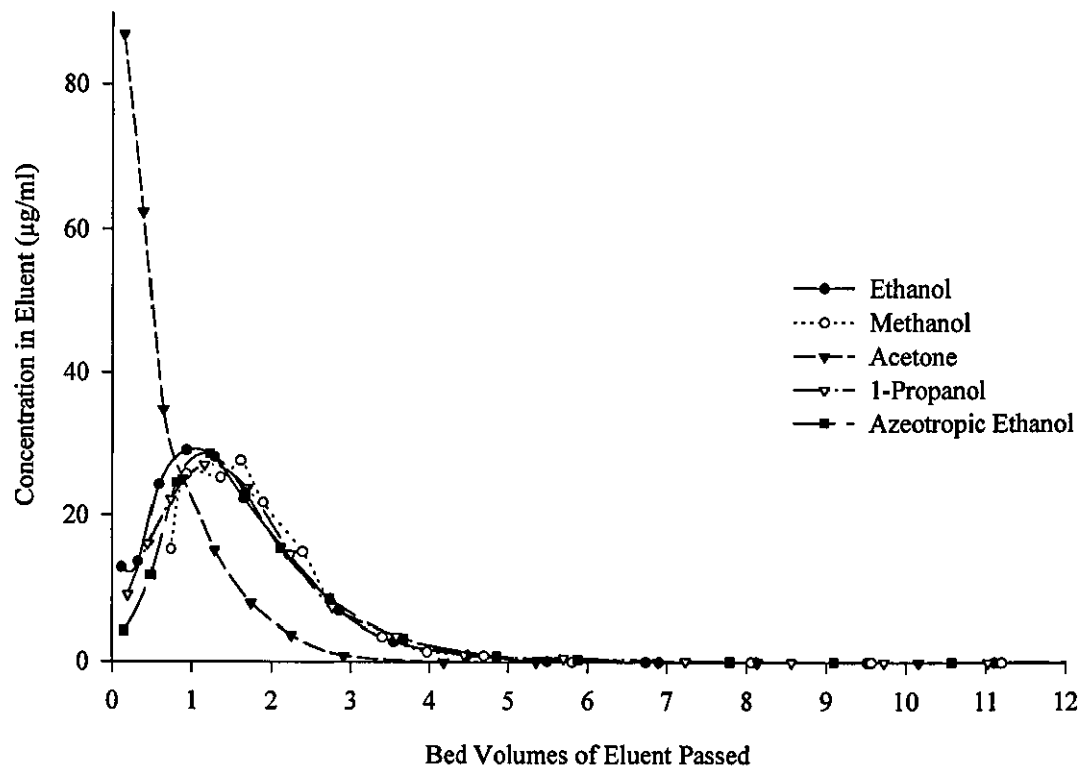


Fig. 6.6. Regeneration of MN-200 using various organic solvents.

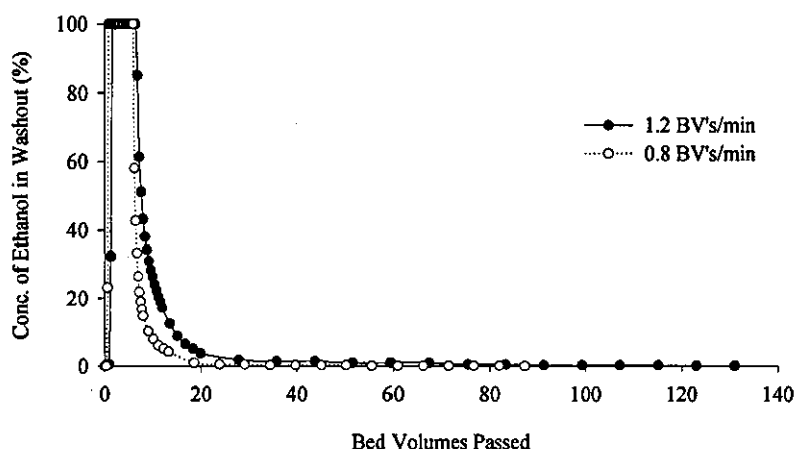


so no figure is shown. The variety of functional groups on the surface of activated carbon may allow the pesticide to be held by a combination of hydrophobic interactions between the triazine ring and the basal planes as well as hydrogen bonding of the triazine to functional groups on the edges of the planes. The interaction strength would be greater than hydrophobic bonding alone preventing the molecules from desorbing. Once these sites are full, regeneration may be possible.

### *Ethanol Washout*

Fig. 6.7 presents the ethanol wash out curves at two different flow rates for MN-200.

**Fig. 6.7.** Ethanol wash out curves for MN-200.



The curve suggests that the majority of the ethanol can be washed out in less than 20 bed volumes. Other techniques, such as steam stripping, would be more effective. However, the technique is simple and is easily performed in the laboratory. Lower flow rates reduced the overall number of bed volumes required to wash out the ethanol.

### *Adsorption columns regeneration*

Figs. 6.8 and 6.9 present the elution curves for the regeneration of the adsorption mini-columns, MN-200 and F-400. The breakthrough curves for adsorption of the pesticide mix are discussed in Chapter 5. The HPLC chromatograms for the regeneration of MN-200 are shown in Fig. 6.10. Each chromatogram represents one sample taken from the column. Table 6.2 presents the concentration of pesticides in each vial together with the bed volumes of ethanol passed.



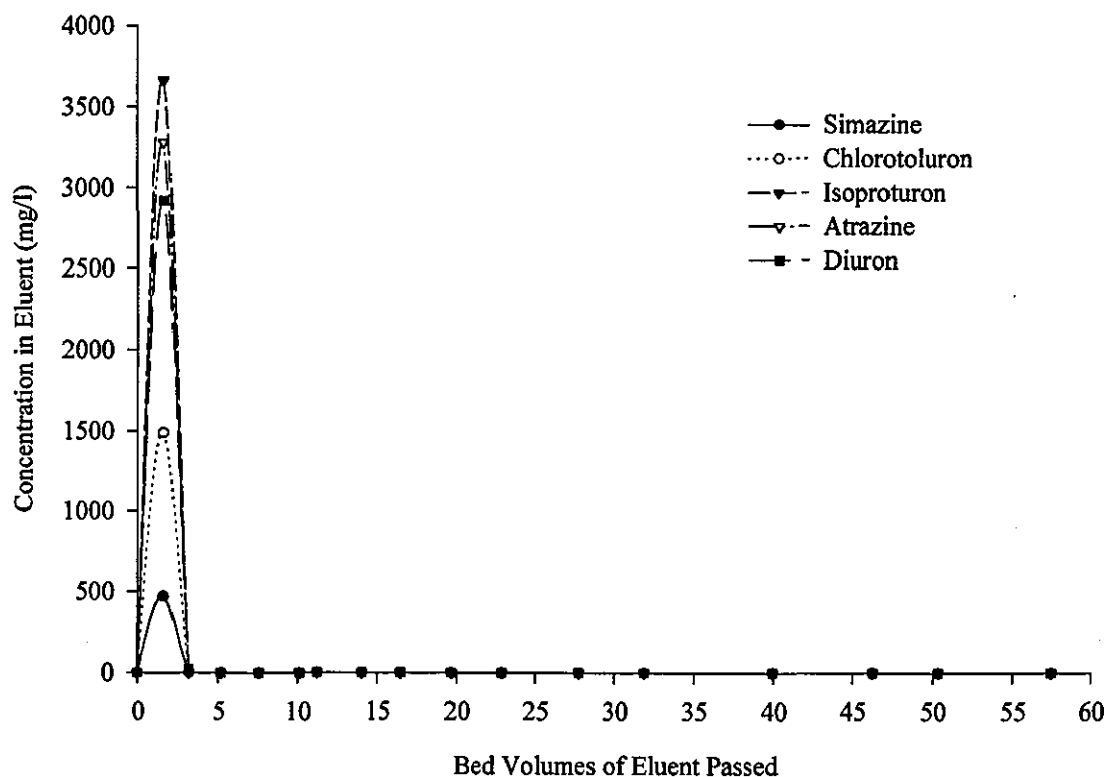
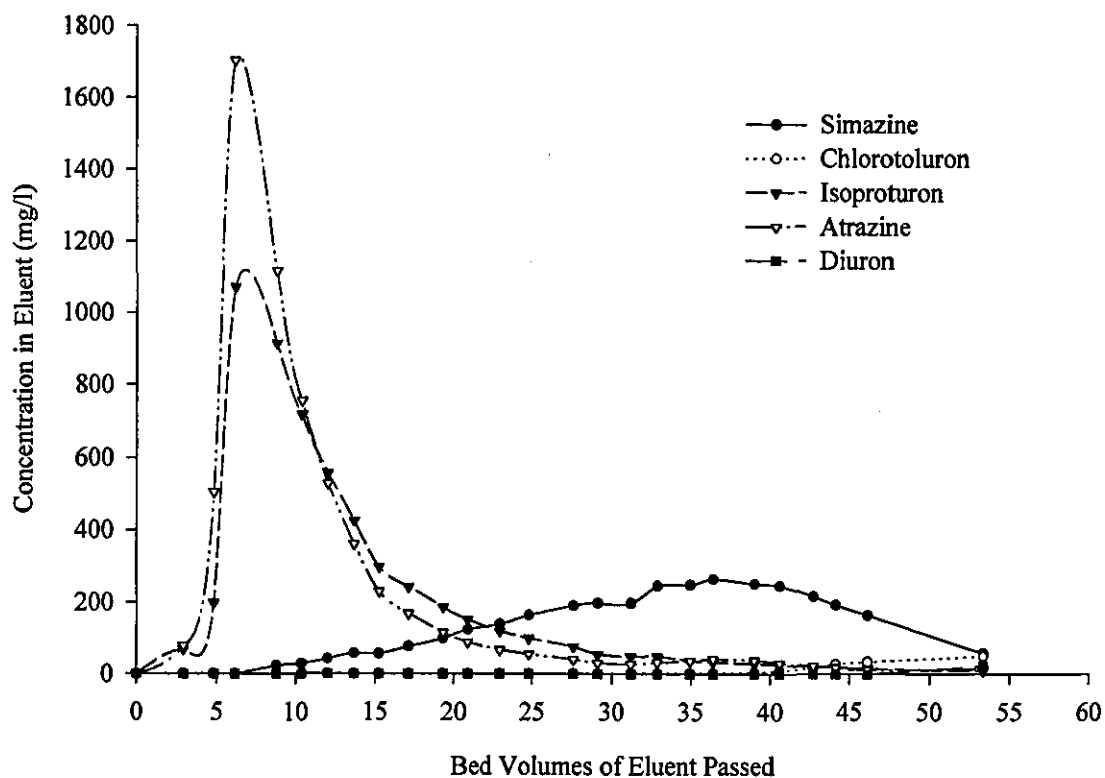
**Fig. 6.8.** Elution curves for the regeneration of the MN-200 adsorption column.**Fig. 6.9.** Elution curves for the regeneration of the F-400 adsorption column.

Fig. 6.10. HPLC chromatograms of regenerant solutions.

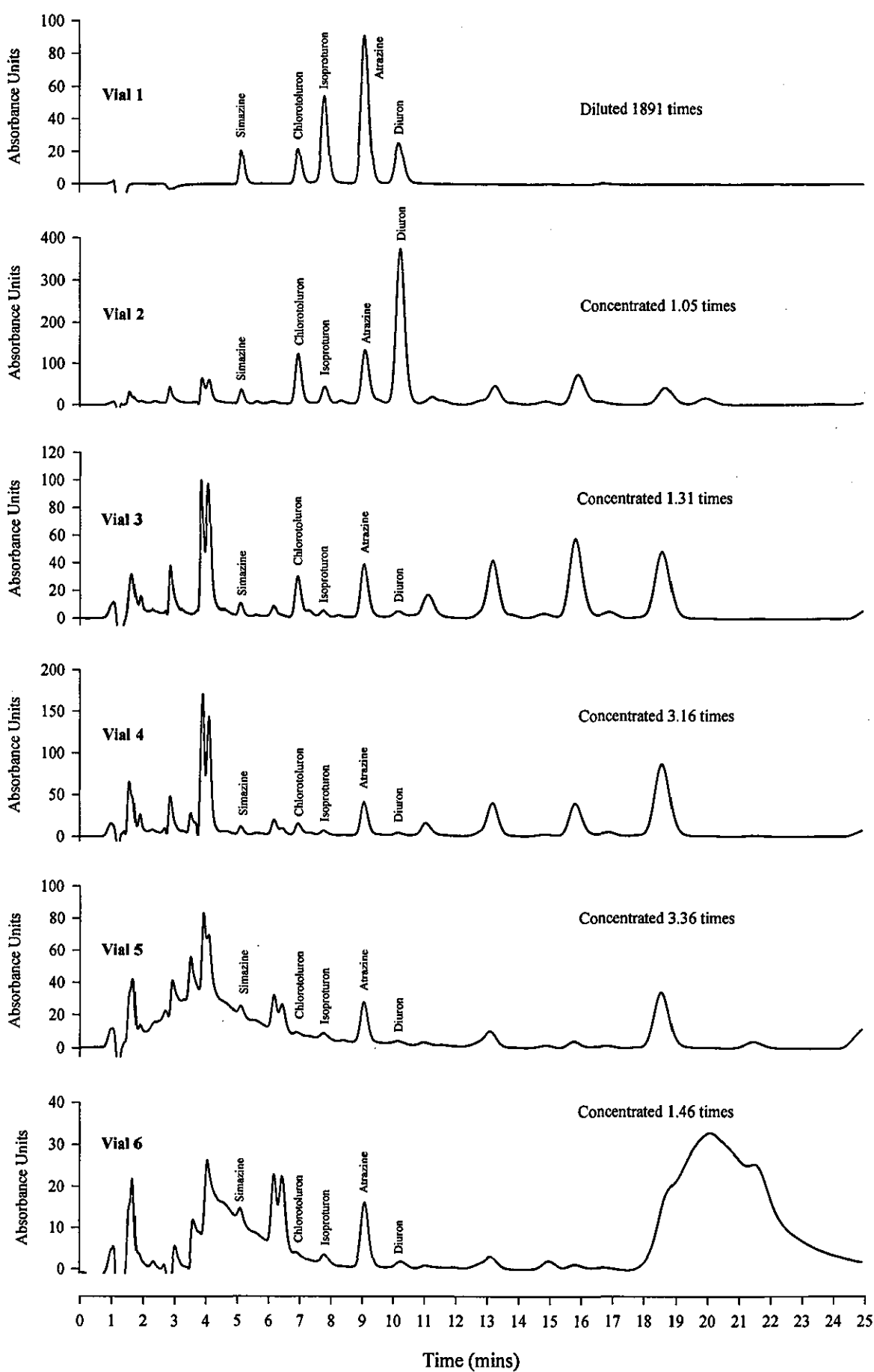


Fig. 6.10. HPLC chromatograms of regenerant solutions. Continued.

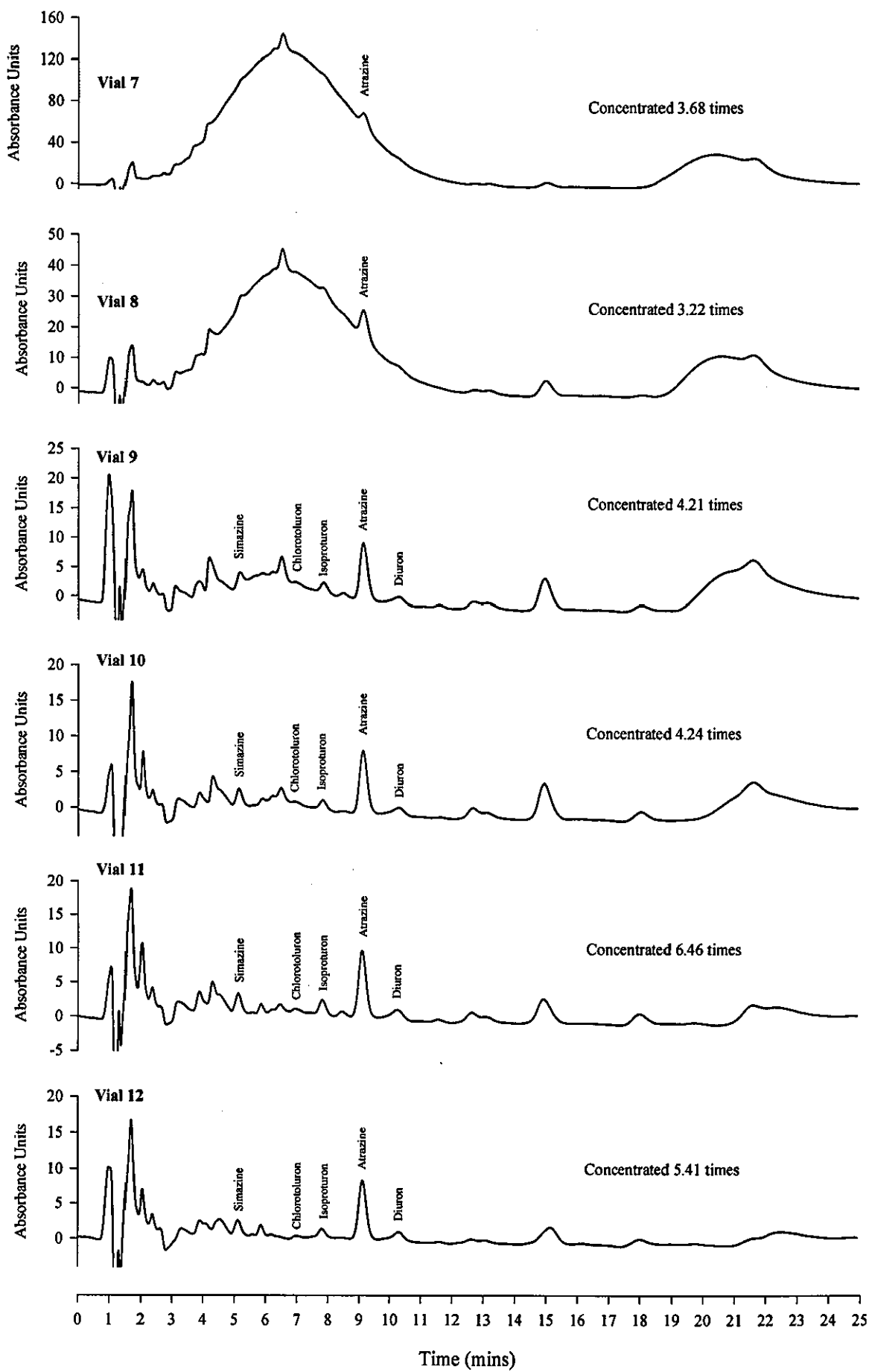


Fig. 6.10. HPLC chromatograms of regenerant solutions. Continued.

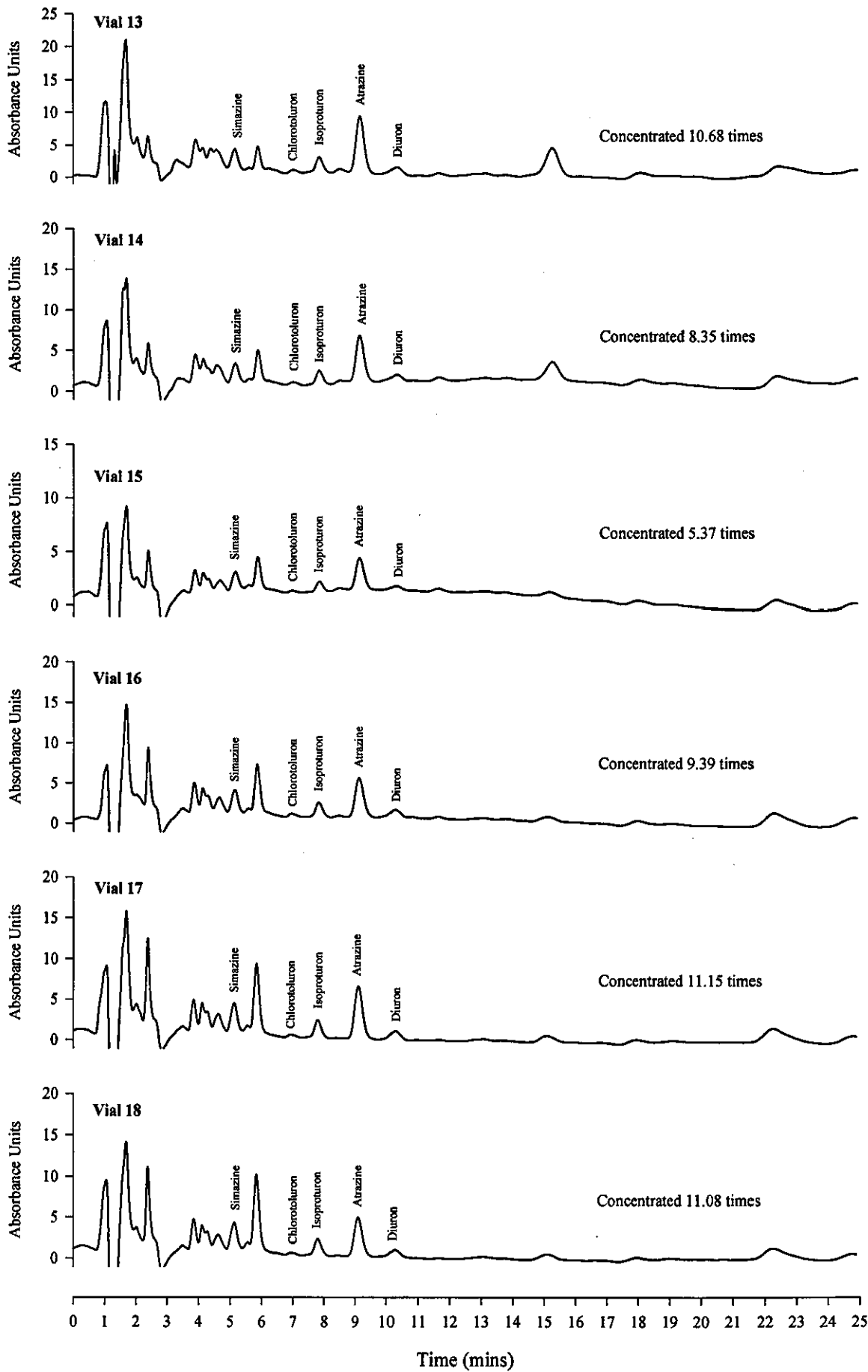


Table 6.2. Concentration of pesticides in regenerant solution for MN-200.

| Vial Number | Cumulative BVs Passed | Concentration of pesticide in regenerant ( $\mu\text{g/l}$ ) |               |             |           |           |            |
|-------------|-----------------------|--------------------------------------------------------------|---------------|-------------|-----------|-----------|------------|
|             |                       | Simazine                                                     | Chlorotoluron | Isoproturon | Atrazine  | Diuron    | Total      |
| 1           | 1.60                  | 468,000                                                      | 1,489,400     | 3,663,400   | 3,275,800 | 2,917,100 | 11,815,000 |
| 2           | 3.19                  | 359.1                                                        | 3,593         | 1,497       | 2,521     | 22,105    | 30,075     |
| 3           | 5.18                  | 75.7                                                         | 314.6         | 139.0       | 567.6     | 225.9     | 1322       |
| 4           | 7.57                  | 33.5                                                         | 58.4          | 55.6        | 234.4     | 67.4      | 449.3      |
| 5           | 10.12                 | 18.1                                                         | 13.1          | 35.4        | 140.4     | 41.1      | 248.1      |
| 6           | 11.23                 | nd                                                           | 14.6          | 49.0        | 226.6     | 67.2      | 357.4      |
| 7           | 14.02                 | nd                                                           | 5.8           | 19.5        | 90.1      | 26.7      | 142.1      |
| 8           | 16.46                 | nd                                                           | 6.6           | 22.2        | 102.8     | 30.5      | 162.2      |
| 9           | 19.66                 | 10.9                                                         | 19.2          | 14.2        | 49.3      | 18.9      | 112.5      |
| 10          | 22.87                 | 6.2                                                          | 13.6          | 11.5        | 43.6      | 16.0      | 90.9       |
| 11          | 27.76                 | 4.9                                                          | 8.9           | 10.7        | 32.1      | 13.6      | 70.2       |
| 12          | 31.86                 | 6.8                                                          | 5.1           | 9.8         | 34.7      | 13.4      | 69.8       |
| 13          | 39.86                 | 4.8                                                          | 2.9           | 6.2         | 18.1      | 8.1       | 40.0       |
| 14          | 46.27                 | 5.2                                                          | 3.5           | 7.1         | 15.0      | 23.1      | 54.0       |
| 15          | 50.35                 | 6.8                                                          | 12.3          | 20.3        | 14.0      | 42.2      | 95.5       |
| 16          | 57.46                 | 5.2                                                          | 2.9           | 5.3         | 11.3      | 17.8      | 42.5       |
| 17          | 65.91                 | 5.5                                                          | 1.9           | 3.4         | 12.2      | 5.1       | 28.1       |
| 18          | 74.30                 | 5.3                                                          | 1.7           | 3.1         | 9.5       | 44.8      | 64.4       |

nd No pesticide detected.

The regeneration of MN-200 is virtually complete after 3.15 bed volumes, since 99.95% of the total mass of pesticide recovered during the regeneration is removed in this volume. Problems with the pump for the adsorption cycle prevented the total recovery from being calculated since the mass of pesticide adsorbed could not be calculated with any accuracy. Assessment of the regeneration effectiveness was studied by repeating the adsorption cycle after the regeneration, presented later. The chromatograms show a large number of peaks which are probably due to impurities in the pesticides and the organic content of the ultrapure water. The total organic carbon content of the ultra pure water used was  $2\text{--}3\mu\text{g/l}$  which corresponds to a total mass of

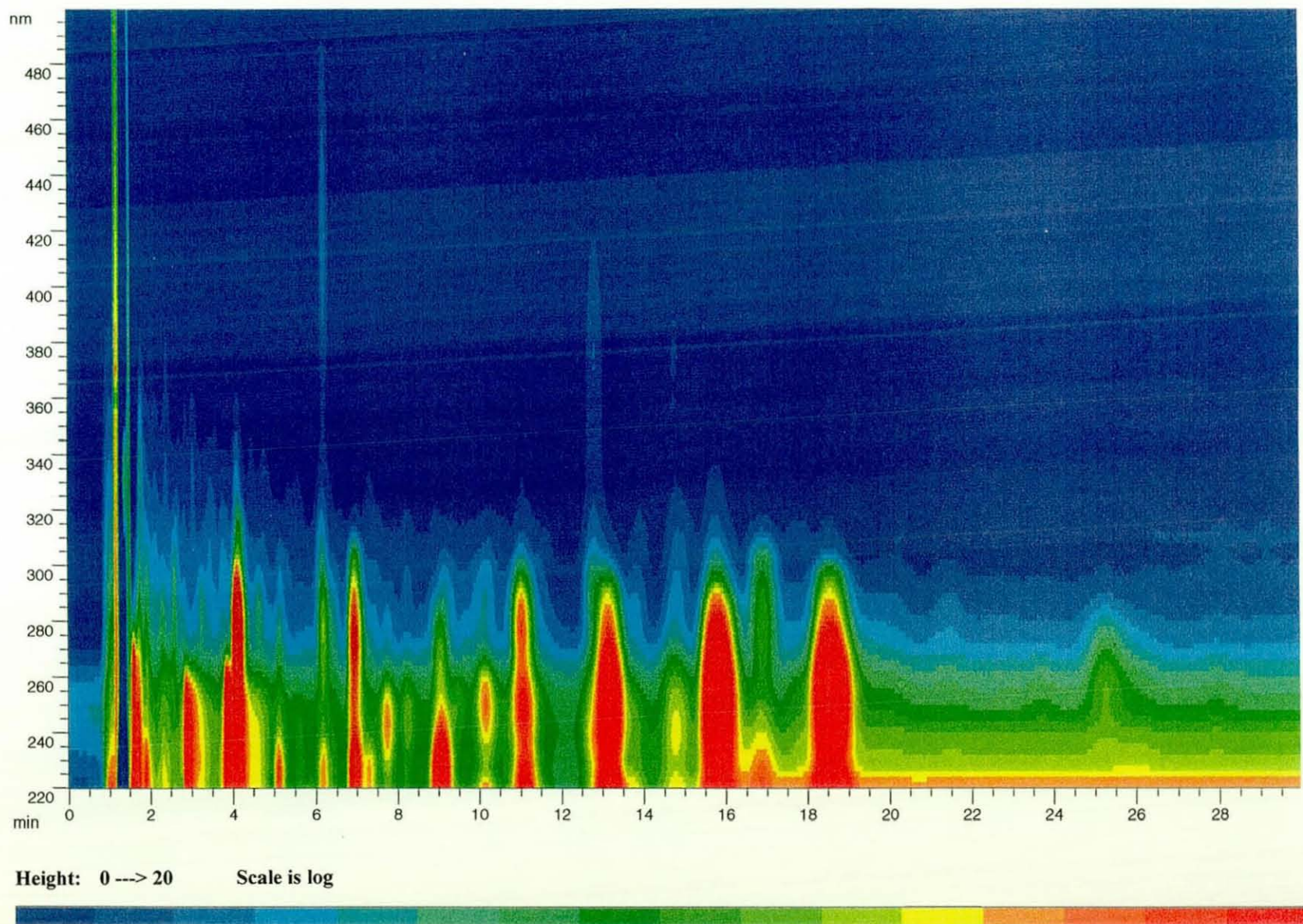
1300 $\mu$ g for the 500l of water which was passed through the column. Some peaks could also be due to degradation products of the pesticides. However, the absence of a mass spectrometer prevents quantification of the compounds. Fig. 6.11 shows the isoabsorbance plot for the analysis of vial number 3. The plot suggests that the compounds responsible for the additional peaks are not coloured, since there is little signal response after 400nm. They adsorb strongly in the UV range suggesting that they are aromatic in nature. They have retention times which are greater than those for the pesticides which suggests that they are more hydrophobic. Some compounds were retained on the HPLC column, observed when the concentration of the organic phase was increased. The solubility of the pesticides in ethanol is large which results in effective regeneration of the adsorbates physically adsorbed to the polymers. However, ethanol also dissociates to a small degree which may also enable the desorption of pesticides adsorbed by a cation exchange mechanism.

Fig. 6.9 presents the regeneration of F-400 activated carbon using ethanol with the concentrations in the regenerant solution summarised in Table 6.3. Little regeneration was observed for chlorotoluron and diuron. This is attributed to the small size of the molecule and the greater strength of interaction energy of the adsorbates with the surface. Improved regeneration may be observed by modifying the organic solvent with a low concentration of organic amine or acid. The pH shift will result in changes to the adsorbates charge and the surface charge of the adsorbent by protonation. Ionisation of functional groups of adsorbates tends to reduce the physical attraction resulting in desorption. Also, adsorbates attracted to the surface by electrostatic interactions can also be desorbed by adjusting the pH so that the carbon surface has the same charge as the adsorbate.

The elution profile follows the sequence atrazine-isoproturon-simazine-chlorotoluron-diuron which is slightly different to that of the polymers. Simazine appears to be more strongly attracted to the carbons surface resulting in a slower elution compared to MN-200. The chromatograms of the regenerant solutions, not presented, only show peaks attributable to the pesticides. This suggests that the TOC content of the ultrapure water may be irreversibly adsorbed onto the carbon, based on elution using ethanol.

Fig. 6.11.

Isoabsorbance plot for the regeneration solution in vial 3.



**Table 6.3. Concentration of pesticides in regenerant solution for F-400.**

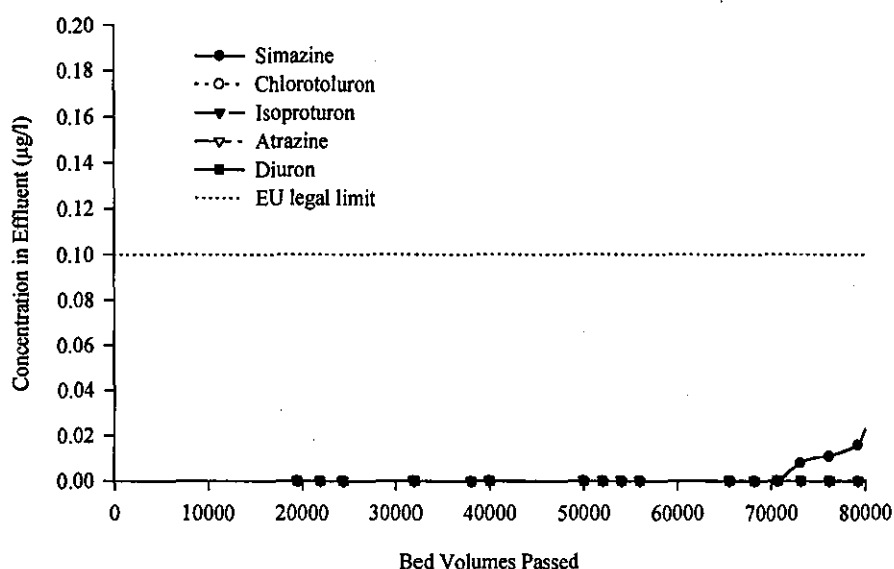
| Vial<br>Number | Cumulative<br>BVs Passed | Concentration of pesticide in regenerant (µg/l) |               |             |           |        |           |
|----------------|--------------------------|-------------------------------------------------|---------------|-------------|-----------|--------|-----------|
|                |                          | Simazine                                        | Chlorotoluron | Isoproturon | Atrazine  | Diuron | Total     |
| 1              | 2.9                      | nd                                              | nd            | 68,065      | 77,228    | nd     | 145,294   |
| 2              | 4.8                      | nd                                              | nd            | 199,189     | 504,725   | nd     | 703,914   |
| 3              | 6.2                      | nd                                              | nd            | 1,072,102   | 1,703,273 | nd     | 2,775,375 |
| 4              | 8.8                      | 22,601                                          | nd            | 914,103     | 1,117,860 | nd     | 2,054,563 |
| 5              | 10.4                     | 28,474                                          | nd            | 715,484     | 756,433   | nd     | 1,500,391 |
| 6              | 12.0                     | 41,270                                          | nd            | 555,976     | 527,376   | nd     | 1,124,622 |
| 7              | 13.7                     | 56,710                                          | nd            | 426,003     | 360,930   | nd     | 843,643   |
| 8              | 15.2                     | 56,372                                          | nd            | 297,809     | 230,100   | nd     | 584,281   |
| 9              | 17.1                     | 75,973                                          | nd            | 242,983     | 167,998   | nd     | 486,955   |
| 10             | 19.3                     | 99,084                                          | nd            | 185,603     | 115,488   | nd     | 400,175   |
| 11             | 20.9                     | 123,219                                         | nd            | 151,172     | 88,370    | nd     | 362,760   |
| 12             | 22.9                     | 138,945                                         | nd            | 119,322     | 66,846    | nd     | 325,114   |
| 13             | 24.8                     | 164,244                                         | 495           | 99,098      | 54,584    | nd     | 318,421   |
| 14             | 27.6                     | 191,028                                         | 685           | 75,369      | 39,630    | nd     | 306,712   |
| 15             | 29.1                     | 198,099                                         | 934           | 54,486      | 30,335    | nd     | 283,854   |
| 16             | 31.2                     | 197,827                                         | 966           | 48,068      | 26,521    | nd     | 273,382   |
| 17             | 32.9                     | 246,061                                         | 1,679         | 48,228      | 31,290    | nd     | 327,258   |
| 18             | 34.9                     | 249,404                                         | 1,950         | 37,270      | 36,255    | nd     | 324,878   |
| 19             | 36.4                     | 265,438                                         | 2,998         | 32,819      | 41,486    | nd     | 342,741   |
| 20             | 39.0                     | 251,956                                         | 4,655         | 28,435      | 38,088    | 912    | 324,047   |
| 21             | 40.6                     | 246,687                                         | 8,772         | 24,596      | 30,477    | nd     | 310,532   |
| 22             | 42.7                     | 216,821                                         | 16,673        | 20,687      | 21,751    | nd     | 275,932   |
| 23             | 44.1                     | 193,432                                         | 26,442        | 18,758      | 17,473    | nd     | 256,105   |
| 24             | 46.1                     | 164,536                                         | 33,479        | 15,150      | 11,162    | nd     | 224,326   |
| 25             | 53.4                     | 57,757                                          | 49,279        | 8,188       | 14,443    | 22,606 | 152,274   |

nd No pesticide detected



The adsorption-regeneration cycle was repeated on the MN-200 column, discussed previously, to assess the regeneration recovery efficiency. Fig. 6.12 presents the breakthrough curve.

**Fig. 6.12.** Mini-column breakthrough curves for MN-200 sorbing simazine, chlorotoluron, atrazine, diuron and isoproturon. Second adsorption cycle.



Initial breakthrough of simazine on the first cycle was observed at approximately 70,000BV's which is slightly less than on the second cycle, 72,000 BV's. The difference may be attributed to the ethanol removing styrene and DVB monomers trapped in the polymer, resulting in a slightly higher surface area. Regeneration of the mini-column after the second adsorption cycle suggested recovery efficiencies, on averaged, of 108%. The efficiency may be greater than 100% due to co-eluting compounds and inaccuracies in the mass balance over 120,000 bed volumes. Regeneration was 99.98% complete in 5.8 bed volumes which is marginally slower than on the first cycle. During the 5 month operation of the column the pressure drop increased dramatically. This was attributed to microbiological fouling of the column which may have caused the slower elution.

## SECTION 6.5      CONCLUSIONS

The polymers can be totally regenerated using a variety of solvents including ethanol, methanol, acetone and 1-propanol. Acetone proved to be the most effective regenerant. Regeneration of the adsorption mini-column was 99.95% complete within 3.2 bed volumes of ethanol. The first vial had a concentration of nearly 12g/l of pesticides providing an excellent concentration ratio of the pesticide in the regenerant to pesticide in the feed water of 120,000:1. The breakthrough profile of the regenerated column for the five pesticides was identical to the virgin polymer suggesting complete regeneration. A second regeneration of the mini-column confirmed total regeneration. The chromatograms of the regenerant solutions suggested that the total organic carbon (TOC) content of the ultrapure water adsorbed by the polymer could also be eluted. At low surface loadings, 25µg/g, the activated carbon could not be regenerated using ethanol. Regeneration of the mini-column indicated that limited regeneration was possible. However, less than 5% of diuron and chlorotoluron recovered after passing 55 bed volumes of ethanol. The TOC in the ultrapure water appeared to be irreversibly adsorbed onto the carbon.

**SECTION 6.6      REFERENCES**

- [1] K. Urano, H. Kano and T. Tabata, Reversibilities of the Adsorption and Desorption of Organic Compounds in Water., *Bulletin of the Chemical Society of Japan*, 57, (8), (1984), p2307-2308.
- [2] M.A. Waer, V.L. Snoeyink and K.L. Mallon, Carbon Regeneration: Dependence on Time and Temperature., *Journal American Water Works Association*, 84, (3), (1992), p82-91.
- [3] M. Pilard, G. Dagois, P. Montagnon and M. Chesneau, Influence of Minerals on the Regeneration of Activated Carbon Used in Drinking Water Treatment., *Water Supply*, 14, (2), (1996), p263-270.
- [4] M. Pilard, G. Dagois, M. Chesneau and P.J. Levy, Impact of Mineral Elements on the Regeneration Process of Activated Carbon Used in Potable Water Treatment., *Water Supply*, 13, (3-4), (1995), p1-6.
- [5] R.J. Martin and W.J. Ng, The Repeated Exhaustion and Chemical Regeneration of Activated Carbon., *Water Research*, 21, (8), (1987), p961-965.
- [6] R.J. Martin and W.J. Ng, Chemical Regeneration of Exhausted Activated Carbon-I., *Water Research*, 18, (1), (1984), p59-73.
- [7] R.J. Martin and W.J. Ng, Chemical Regeneration of Exhausted Activated Carbon-II., *Water Research*, 19, (12), (1985), p1527-1535.
- [8] G. Newcombe and M. Drikas, Chemical Regeneration of Granular Activated Carbon from an Operating Water Treatment Plant., *Water Research*, 27, (1), (1993), p161-165.
- [9] P.C. Chiang and J.S. Wu, Evaluation of Chemical and Thermal Regeneration of Activated Carbon., *Water Science and Technology*, 21, (1989), p1697-1700.
- [10] M. Rollor, M.T. Suidan, W.H. Cross and S.A. Vargo, Regeneration of Five Carbons with Methanol., *Journal of the Environmental Engineering Division, ASCE*, 108, (EE6), (1982), p1361-1377.
- [11] H. Tamon, T. Saito, M. Kishimura, M. Okazaki and R. Toei, Solvent Regeneration of Spent Activated Carbon in Wastewater Treatment., *Journal of Chemical Engineering of Japan*, 23, (4), (1990), p426-432.
- [12] D.O. Cooney, A. Nagerl and A.L. Hines, Solvent Regeneration of Activated Carbon., *Water Research*, 17, (4), (1983), p403-410.
- [13] H.S. McLaughlin, Regenerate Activated Carbon Using Organic Solvents., *Chemical Engineering Progress*, 91, (7), (1995), p45-53.

- [14] A.M. Robertson and J.N. Lester, Recovery of S-triazine Herbicides and Associated Breakdown Products From Granular Activated Carbon Using Supercritical-fluid Extraction., *Water Environment Research*, 67, (6), (1995), p899-905.
- [15] S.B. Hawthorne, Analytical-scale Supercritical Fluid Extraction., *Analytical Chemistry*, 62, (11), (1990), p633-642.
- [16] D.H. Hutchinson and C.W. Robinson, A Microbial Regeneration Process for Granular Activated Carbon. II. Regeneration Studies., *Water Research*, 24, (10), (1990), p1217-1223.
- [17] S.J. Feakin, E. Blackburn and R.G. Burns, Biodegradation of s-triazine Herbicides At Low Concentrations in Surface Waters., *Water Research*, 28, (11), (1994), p2289-2296.
- [18] W. Uhl, R. Gimbel, G. Bundermann and D. Wittich, A Two-step Process for Biodegradation and Activated Carbon Adsorption - A Means to Improve Removal of AOC and Natural Organics and to Achieve Longer Operation Times of GAC-adsorbers., *Water Supply*, 14, (2), (1996), p243-251.
- [19] R. LeBec, F. Mandon, L.J. Sorrento, L. Labouyrie and N. Merlet, Development of Rapid Tests for the Evaluation of Dynamic Adsorption and Biological Activity of Granular Activated Carbons., *Water Supply*, 14, (2), (1996), p71-84.
- [20] R.M. Narbaitz and J. Cen, Electrochemical Regeneration of Granular Activated Carbon., *Water Research*, 28, (8), (1994), p1771-1778.

## CHAPTER 7

### GENERAL CONCLUSIONS

#### SECTION 7.1 CONCLUSIONS

The objectives of this research were to evaluate the adsorption of organic species onto Hypersol Macronet™ polymers and their subsequent regeneration efficiency using organic solvents. The physical and chemical properties of the adsorbents were determined to enable hypotheses to be made regarding the mechanisms of adsorption.

Characterisation of the functional groups on the polymers was achieved by numerous techniques including; diffuse reflectance infra-red spectroscopy,  $^{13}\text{C}$  NMR spectroscopy, X-ray photoelectron spectroscopy, elemental analysis, direct titration and zeta potential analysis. The polymers contained between 5 and 6 mass percent of oxygen, with the major functional groups thought to be ketones, ethers and alcohols. The oxygen functionality appeared to enhance the adsorbate/adsorbent interaction energies by allowing hydrogen bonding.

A study of the pore size distributions of the polymers suggested a biporous nature, micropores and macropores. The mean micropore diameter for the polymers was approximately  $12\text{\AA}$ , thus allowing small adsorbates such as phenols and pesticides to be adsorbed. The mean macropore diameter was  $900\text{\AA}$  for MN-100 and MN-200 and  $532\text{\AA}$  for MN-150. The surface area contained in pores greater than  $30\text{\AA}$  was less than  $50\text{m}^2/\text{g}$  for all the polymers, or approximately 5% of their total surface area. Size exclusion of large organic molecules, such as humic and fulvic acid was observed for the polymers. This was verified by ultrafiltration experiments using a 500 Dalton membrane. All of the pesticides passed through the membrane. However, only 95.4% of the fulvic acid was retained. Analysis of the pore size distribution of F-400 suggested a proportion of mesopores may be blocked by the similarly sized natural organic matter. The mean micropore size of F-400 was smaller than the polymers.

The adsorption capacity of the polymers for phenolic compounds was dependent on the adsorbates hydrophobicity and molecular size, suggesting that hydrophobic interactions were the dominant adsorption force. Little difference was observed between the weak base resins MN-100 and MN-150 compared to MN-200, which had no added functionality. Hydrogen bonding of the phenols was expected to influence the adsorption. However, the overall degree of oxygen and nitrogen functionality was similar for the three polymers preventing quantitative findings. The electronegative chlorine atom increased the hydrophobicity of the chlorophenols resulting in greater uptake on all the polymers and carbon, compared to phenol. The substituent position, ortho, meta, and para of the chlorine atom influenced the adsorption. The effect was attributed to the different molecular size of molecules rather than the chemical properties of the molecules; the smallest molecules being adsorbed to a greater extent. The capacity of F-400 was significantly greater than the polymers for phenol and the chlorophenols. Similar degrees of functionality were present on F-400 compared to the polymers. Hence, the enhanced interaction energies, indicated by low values of the coefficient  $1/n$ , were attributed to the delocalised electrons in the basal planes of the carbon. It was also thought that the molecules may be held by a combination of  $\pi$  electrons in the basal planes with the  $\pi$  electrons of the adsorbate as well as hydrogen bonds to oxygen or nitrogen functionality on the edges of the planes.

The adsorption kinetics were governed by the pore size distribution and chemical functionality of the adsorbents. F-400 possessed the fastest kinetics attributed to the mesopores enhancing transport to the micropores. Of the polymers, MN-200 had the fastest kinetics followed by MN-100 and MN-150. The reduced kinetics of MN-100 were attributed to enhanced adsorbate-adsorbent interactions which would slow down the surface hopping of the adsorbates. This was suggested by slower surface diffusivities of the aminated resins calculated using the homogeneous surface diffusion model. The smaller mean macropore diameter of MN-150 and high degree of amine functionality resulted in slow kinetics. Differences were observed in the kinetics of adsorption for the different phenols. The chlorophenols demonstrated similar kinetics and were much slower than those of phenol. This was attributed to molecular weight and size differences. The surface diffusivity appeared to be independent of particle size. Activation energies for all three polymers were similar, approximately 30-35kJ/mol, suggesting no difference in the adsorption mechanisms.

Adsorption of the pesticides, atrazine, simazine, isoproturon, diuron and chlorotoluron was conducted in batch and mini-column modes up to concentrations of 100µg/l. Little difference was seen in the adsorption capacity of the polymers for the pesticides. Difficulties with carbon fines prevented the generation of batch adsorption isotherms for F-400 activated carbon. Breakthrough of the MN-200 mini-column, to the EU legal limit, occurred between 100,000 and 180,000 bed volumes for simazine and isoproturon respectively. Chromatographic elution of the pesticides was observed as the experiment proceeded. The F-400 mini-column did not reach breakthrough in 800,000 (adsorbent mass was 50% greater than the polymers to obtain the same bed volume). The excessive pressure drop in the column, 5bar, prevented completion of the experiment.

Trial regeneration of MN-200 and F-400 was performed on mini-columns loaded with small quantities of pesticide. Total regeneration was achieved for MN-200 in approximately 5 bed volumes; no regeneration was apparent for F-400. A variety of flow rates and solvents, including acetone, methanol, ethanol and 1-propanol, were used to optimise regeneration for MN-200. Acetone proved to be the most effective regenerant. However, ethanol was selected as the solvent for future regenerations since it was believed to be acceptable to the water industry. Sharper elution profiles were observed as the eluent flow rate decreased. Ethanol was washed out from the columns using water, in approximately 20 bed volumes, allowing the next adsorption cycle. Total regeneration of the MN-200 mini-column loaded with over 500,000 bed volumes of pesticide was achieved. Only 3.2 bed volumes of ethanol enabled 99.85% recovery, providing a concentration ratio of 120,000:1. Total regeneration was verified by conducting a second adsorption cycle after regeneration. The breakthrough point was identical to that of the virgin mini-column. Partial regeneration of F-400 did occur. However the process is not viable due to the excessive volumes of regenerant that would be required.

Adsorption capacities for humic and fulvic acid were extremely low due to size exclusion from the micropores of MN-200 and electrostatic repulsion of the negatively charged adsorbates with the negatively charged adsorbent surface, determined by zeta potential analysis. The nitrogen containing functional groups on MN-100 allowed significant uptake by an ion exchange mechanism. Sorption of fulvic acid onto F-400 was much greater than that of MN-200 due to

the nitrogen functional groups and the mesoporous nature of the carbon. Competitive adsorption, in batch and mini-columns suggested that high concentrations did not significantly reduce the uptake of the pesticides. However, the capacity of F-400 was dramatically reduced. Hence, in the presence of fulvic acid the MN-200 has a similar capacity to F-400.

## SECTION 7.2 FUTURE WORK

The present study has provided an insight into the potential of Macronet polymers for drinking water purification. However, a major research project is required to fully assess their potential.

Results obtained in this study were based on ultrapure water spiked with various pollutants including pesticides and commercial humic substances. The adsorption of the commercial fulvic acid, used in this work, may not be representative of natural organic matter found in real waters. A number of researchers have investigated adsorption of water extracted from lakes and rivers. However, the water treatment processes prior to GAC adsorption tends to either remove or breakdown humic acids into smaller molecules, similar in chemistry to fulvic acids. Thus, little benefit is obtained by transporting lake or river water. It is concluded that for realistic trials experiments require water to be taken from the treatment works prior to the GAC adsorption stage. The adsorption of organic species is also dependent on the concentration of ionic species in the feed water. This has not been assessed in the current project. However, similar problems exist in attempting to simulate real waters with respect to ionic species.

The scale of operation used in the study allowed results to be obtained in the time frame of a PhD. Pilot scale columns are required to assess the microbiological fouling of columns and their true breakthrough behaviour. The list below summarises future work which needs to be completed in the laboratory prior to pilot scale operation using real waters.

- 1 Competitive adsorption of pesticides and fulvic acid at a variety of flow rates, to assess kinetics limitations, and at different pH values. A wider variety of pesticides needs to be investigated, e.g. pesticides which are more hydrophilic in nature.



- 2 Introduce ionic species into the feed solutions to the columns. Experiments could be performed using tap water which would contain ionic and organic species.
- 3 Optimise ethanol regeneration parameters, i.e. pH and flow rate. Regeneration of columns loaded with NOM needs to be performed. Initial trials suggested that total regeneration occurs but this must be confirmed.

### SECTION 7.3      COMMERCIAL IMPLICATIONS

The adsorption capacity of the polymers for pesticides in pure water is significantly less than F-400 activated carbon. However, the adsorption performance is similar when pesticides are adsorbed in the presence of NOM since MN-200's pore structure size excludes the fulvic and humic acid molecules. Fulvic and humic acid contribute to taste and odour problems with drinking water and so another adsorbent may be required if the concentrations which pass through the column are a problem. Activated carbons such as F-100 or anion exchange resins, including the aminated Macronet polymers, could be used.

MN-200 can be regenerated fully using less than five bed volumes of ethanol. Stronger solvents reduced the number of bed volumes required. However, ethanol is believed to be an acceptable solvent for the water industry. The concentration ratio of 120,000:1 would require the use of 5m<sup>3</sup>/d of ethanol for a treatment plant producing 600,000,000 l/d (the capacity of Cincinnati's installation mentioned previously). The regenerant can be recovered by distillation/evaporation leaving a solid pesticide/NOM residue, which could be disposed of by incineration. Alternative technologies such as nano-filtration could also be considered to enable solvent recycling. Solvent regeneration can be performed on-site and does not necessitate the transfer of the adsorbent to a separate vessel. However, this may well be desirable. The polymers are resistant to a wide variety of chemicals which would allow the removal of any biological fouling. Improved regeneration efficiency can be obtained by air or nitrogen drying the adsorbent prior to regeneration. Ethanol can be stripped from the column using a variety of techniques including steam stripping or simply water washing. Depending in the consent level of ethanol in water,

water washing offers the cheapest and simplest technique. The wash water could be treated further up stream in the treatment process.

The polymers have excellent mechanical strength which opens up the possibilities of using reduced particle size adsorbent material. Activated carbons break up during operation generating carbon fines, resulting in high pressure drop in GAC columns. As the particle size is reduced the kinetics of adsorption increase dramatically. This enables the height of the adsorption column to be reduced whilst maintaining an identical breakthrough profile. The empty bed contact time for full particle size F-400 activated carbon, mean diameter of 1000 $\mu\text{m}$ , is often 15mins. If the mean particle size is reduced to 150 $\mu\text{m}$  the EBCT could range from 2mins 15secs to 20secs, depending on whether the surface diffusion coefficient remains constant as the particle size is decreased. Initial trials for the polymer suggested that the diffusion coefficient remains constant which would allow the shorter EBCT to be used. The reduction in EBCT would allow the total inventory of adsorbent to be reduced by up to 40 times. A reduction in the inventory of the polymer would necessitate more frequent regeneration, i.e. approximately every week compared to a service life of 6 months for full particle size activated carbon. However, regeneration can be completed simply and quickly. The pressure drop through the reduced particle size column should not be significantly greater than that experienced with full size activated carbon due to the lower packing density of the polymers and no fine material.

Presently, the Macronet polymers are 10-15times more expensive than F-400 activated carbon. However, if reduced particle size material is used the initial capital costs would be similar or less than those for carbon. Significant cost savings would be achieved in the regeneration since McLaughlin [6.13] demonstrated that solvent regeneration is 1-5% of the cost of thermal reactivation. The Cincinnati water works authority operated at a carbon usage rate of 22,700kg/d which equates to a regeneration cost of approximately £18,000/day or £6.5 million/year. Solvent regeneration costs would result in annual savings of over £6 million per year. No data is currently available on the number of regeneration cycles that Macronet polymers will withstand; four cycles have been completed during this study. Fox [1.2] presented cyclic adsorption data for XAD resins, similar in mechanical strength to Macronet polymers. In a two year period, the polymers were cycled 1300 times with no reduction in capacity and no broken or cracked beads.

It is believed that the Macronet polymers will behave similarly.

In conclusion, it is believed that Macronet polymer possess some significant advantages over activated carbon for drinking water purification due to their mechanical strength and ability for regeneration. Thermal reactivation of activated carbon causes significant harm to the environment due to the extreme temperatures required to pyrolyse the adsorbed species and the associated pollution with respect to the carbons transportation to the reactivation facility. Process treatment plants designed around the polymer would minimise secondary wastes, the result being a closed loop environmentally friendly treatment process. The polymers can also offer significant cost savings if their full scale operation behaves in a similar way to the limited trials undertaken in this research work.

APPENDIX 1

Fig. A1.1 presents the six main types of physisorption isotherm, with the different types of hysteresis loops illustrated in Fig. A1.2 [2,4]. Explanations of the isotherms and hysteresis loops can be found in the original reference.

Fig. A1.1. Types of physisorption isotherms.

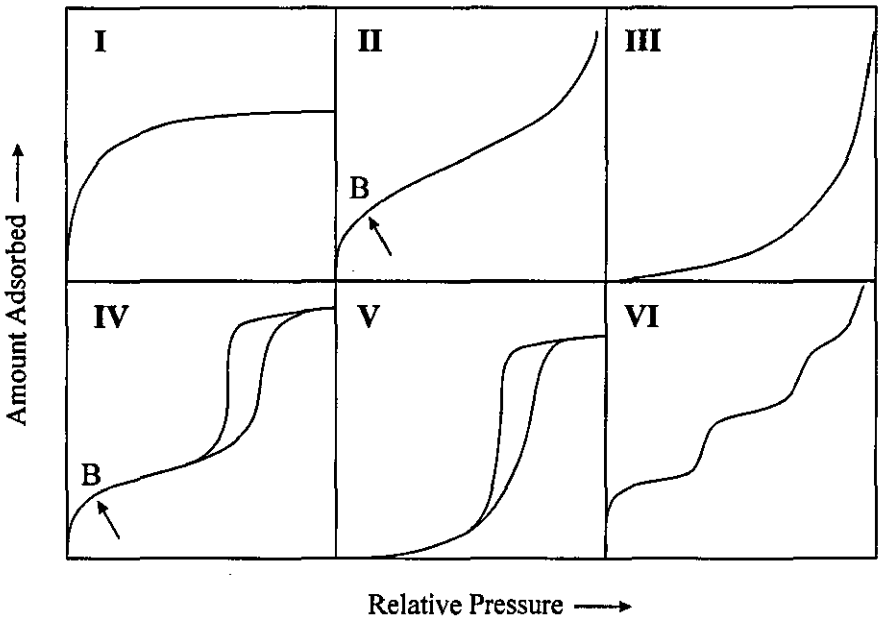
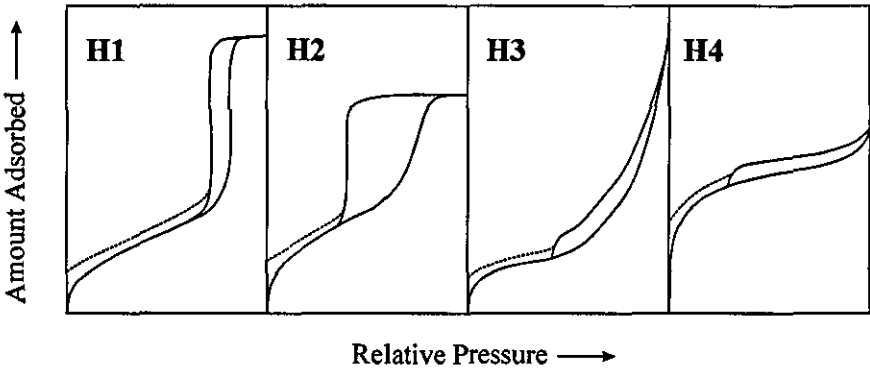


Fig. A1.2. Types of hysteresis loops.



## APPENDIX 2

The scaling equations of the rapid small scale column test are as follows:

$$EBCT_{SC} = \left( \frac{d_{SC}}{d_{LC}} \right)^{2-X} EBCT_{LC} \quad (9)$$

$$t_{SC} = \left( \frac{d_{SC}}{d_{LC}} \right)^{2-X} t_{LC} \quad (10)$$

where  $EBCT_{SC/LC}$  = empty bed contact time of small/large particle column.  
 $t_{SC/LC}$  = operation time of small/large particle column.  
 $d_{SC/LC}$  = small/large particle diameter.  
 $X$  = non-constant diffusivity factor ( $X=0 \rightarrow 1$ ).

If the surface diffusion is independent of the adsorbents particle size then the diffusivity factor is zero. However, for a number of carbons the coefficient will not remain constant. In these cases, the diffusivity factor is determined by linearising the equation:

$$D_{SC} = \left( \frac{d_{SC}}{d_{LC}} \right)^X D_{LC} \quad (11)$$

where  $D_{SC/LC}$  = diffusion coefficient in small/large particle.

Schneider demonstrated that the diffusion coefficient showed a linear relationship with particle size. For this case the value of  $X$  would be one. The Stanton and Peclet numbers only remain equal between the full scale and small scale columns if the diffusion coefficient is constant. In this case, the following equation is obtained:

$$v_{SC} = \left( \frac{d_{LC}}{d_{SC}} \right) v_{LC} \frac{Re_{SC,min}}{Re_{LC}}$$

where  $v_{SC/LC}$  = velocity in small/large particle column.  
 $Re_{S,min}$  = minimum Reynolds number in small particle column.  
 $Re_{LC}$  = Reynolds number in large-particle column.

$Re_{S,min}$  defines the minimum velocity that can be used in the operation of the RSSCT without over exaggerating the effects of dispersion and external mass transfer. A value of 0.13 is often

used for organic micropollutants such as pesticides. The length of the small particle column,  $L_{SC}$ , can then be calculated using the equation:

$$L_{SC} = v_{SC} \cdot EBCT_{SC} \quad (13)$$

